# Topological coupling between slow and fast quantum systems

Jacquelin Luneau

# THÈSE

en vue de l'obtention du grade de Docteur, délivré par

**l'École Normale Supérieure de Lyon**

**École Doctorale** N°52
**École Doctorale de Physique et Astrophysique de Lyon (PHAST)**

**Discipline : Physique**

Soutenue publiquement le 18/09/2023, par :

**Jacquelin LUNEAU**

# Topological coupling between slow and fast quantum systems

## Couplage topologique entre systèmes quantiques lents et rapides

Devant le jury composé de :

| | | | |
|---|---|---|---|
| Citro, Roberta | Professeure | Università degli Studi di Salerno | Rapporteure |
| Meyer, Julia | Professeure des universités | Université Grenoble Alpes | Rapporteure |
| Dalibard, Jean | Professeur des universités | Collège de France | Examinateur |
| Huard, Benjamin | Professeur des universités | LP ENS de Lyon | Examinateur |
| Mora, Christophe | Professeur des universités | MPQ, Université Paris Cité | Examinateur |
| Douçot, Benoît | Directeur de Recherche | LPTHE, Sorbonne Université | Examinateur |
| Carpentier, David | Directeur de Recherche | LP ENS de Lyon | Directeur de thèse |

# Remerciements

Je tiens tout d'abord à remercier chaleureusement David et Benoît. Je me sens très chanceux d'avoir pu bénéficier de votre encadrement. J'ai énormément appris avec vous, aussi bien sur le plan scientifique que sur la pratique de la recherche. Je vous en suis très reconnaissant.

Je souhaite remercier Roberta Citro, Julia Meyer, Jean Dalibard, Benjamin Huard, et Chritsophe Mora pour avoir examiné ce travail. Merci pour vos questions et commentaires très stimulants. Je remercie tout particulièrement Roberta Citro et Julia Meyer pour le temps que vous avez accordé à ce travail en acceptant d'être rapporteure de ce manuscrit.

Merci à toutes les personnes avec qui j'ai eu la chance de collaborer pendant ces trois ans : Tommaso, Clément, Pierre, Quentin, Benjamin, Yannick, Marcelo. Nos échanges ont toujours été très enrichissants.

Merci aux membres du groupe, Baptiste, Eric, et Marcelo, pour avoir fait vivre nos échanges réguliers, particulièrement durant le covid où l'isolement rendait ces moments précieux. Je remercie également Thomas E., tu as rejoins le groupe peu de temps avant que je commence ma rédactions, et tes questions et ton envie de comprendre en profondeur m'ont bien aidé à préciser ma façon de présenter le sujet. C'est un plaisir de collaborer avec toi maintenant.

Merci aux doctorants du laboratoire, grâce à qui l'ambiance est très agréable. Tout d'abord la troupe du M7.111.5 : Charles, Léo M., Geoffroy, Thomas B., Léo D., Marcelo, toujours d'une bonne humeur contagieuse. Merci également aux doctorants de physique théorique, pour ces échanges hebdomadaires enrichissants et votre camaraderie. Je tiens à remercier généralement tous les membres du laboratoire, et tout particulièrement la direction et les gestionnaires, grâce à qui nous pouvons travailler dans de très bonnes conditions.

Je remercie tous mes amis, membres de la Fanfare et de Bërk pour ces moments partagés si précieux.

À mes parents et ma sœur pour avoir toujours été à mes côtés quand j'en avais besoin, dans un soutien bienveillant.

Enfin, Anaïs. Sans toi je n'en serais pas là. Ton amour, ton intelligence, ton courage, ta bienveillance, ton soutien, ta joie, illuminent ma vie. Ce que nous construisons ensemble avec Blue et Moka, est ce qui m'est de plus précieux.

# Contents

# Introduction

The work presented in this manuscript consists in describing topological pumps within the context of slow-fast quantum systems. Let us first recall briefly the notion of topological pump before explaining the motivation of this reformulation.

## 1 Topological pumps

The experimental discovery of the quantized Hall effect by von Klitzing *et al.* in 1980 [1] is a breakthrough in the understanding of topology as an alternative to symmetries to characterize phases of matter. This experiment provides a measure of the electric conductivity of a two-dimensional electron gas at low temperature and under a magnetic field. For high values of the magnetic field, the transverse conductivity of the Hall sample is measured to be proportional to a ratio of fundamental constants $e^2/h$, with $e$ the electric charge of an electron, $h$ the Planck constant, and where the proportionality factor is measured to be an integer with a relative uncertainty lower than $10^{-9}$. Soon after this experimental discovery, Thouless, Kohmoto, Nightingale, and den Nijs [2], showed that this extreme precision was of topological origin, deriving the integer factor as a topological invariant, corresponding mathematically to a Chern number [3–5]. The understanding of the topological origin of the quantization of Hall conductivity allowed the definition of a new type of pumps, topological pumps as topological responses of a slowly driven quantum system.

### Laughlin pump

This topological property of matter was early discussed in relation with pumping phenomena. In an enlightening *gedankenexperiment*, Laughlin [6] considered a Hall sample wrapped on a cylinder and related the quantized conductivity to a transfer of charges between the edges. The Laughlin argument was extended by Halperin [7], leading to a modern interpretation of a quantum Hall pump as a pumping of charge between the edges of a Hall cylinder as an enclosed magnetic flux is smoothly increased through the cylinder [8, 9]. Seeing this external magnetic flux as a slow drive of the Hall sample, this quantum Hall pump is the first example of topological pump displaying a quantized response of a slowly driven quantum system. This has been realized recently in a synthetic atomic Hall cylinder [10].

### Thouless pumps

This quantized adiabatic pumping of a time-dependent quantum system was soon generalized beyond the quantum Hall effect to a driven one-dimensional band insulating crystal by Thouless [11]. For a suitable periodic time-dependence, exemplified by the Rice-Mele model [12], Thouless showed the appearance of a quantized steady current in the bulk of the crystal. The quantization involves the same topological invariant as the quantum Hall effect, a Chern number. Such topological pumping can be characterized by a quantized anomalous velocity for semiclassical states of non-interacting particles in an insulating band [13], recently realized experimentally using cold atoms lattices [14–17], quasicrystals [18, 19], optical waveguides [20–22], magnetically coupled mechanical resonators [23], stiffness-modulated elastic plates [24], or electromagnetic waveguides [25]. Thouless pumps are the canonical examples of topological pumps. They have been subjected to numerous studies since the seminal work of Thouless. We refer the reader to the recent review [26] for additional information.

### Topological response of flux networks

Later on, Niu, Thouless and Wu introduced the notion of generalized boundary conditions for quantum Hall states [27]. The quantum Hall topological properties are expressed as the Chern number of the ensemble of many-body groundstates over the closed manifold of phase boundary conditions. Niu and Thouless [28] introduced similar boundary conditions to study Thouless pumps in presence of many-body interaction. These boundary conditions parameters were later related by Avron *et al.* to electromotive forces through loops connecting opposite edges of the sample [29] effectively generalizing the topology of Laughlin's *gedankenexperiment* to that of a torus. This was then generalized to describe quantum transport in mesoscopic multiply connected systems, consisting of a mesoscopic piece of metal or superconductor containing holes threaded by magnetic fluxes. A topological quantization of conductances is associated to Chern numbers defined from the parametrization of the Hamiltonian by these time-dependent fluxes [30].

### Mesoscopic superconducting systems

Extensions of these pumping schemes were unveiled recently in slowly driven quantum system of effective zero spatial dimension. The first theoretical proposal was in the context of Cooper pair pumps. A Cooper pair pump [31] is a mesoscopic superconducting network of Josephson junctions whose boundaries are connected to macroscopic superconducting leads, for which control parameters such as gate voltages are externally modulated in time. Topological quantization by a Chern number of the charge transported between the leads were theoretically proposed [32, 33]. Later on, another manifestation of topological response of a slowly driven zero dimensional quantum system were discovered in multi-terminal Josephson junction [34, 35], were the drives consists in independent superconductors' phase differences. The study of topological properties of Josephson tunnel junction circuits and multi-terminal Josephson junctions is an active domain of research, see *e.g.* [36–42]. We refer to the recent review [43] concerning multi-terminal Josephson junctions.

### Topological frequency conversion

Another mechanism of topological response of a driven zero dimensional system was proposed recently, named topological frequency conversion [44]. The simplest realization was a qubit driven at two frequencies, later extended to more complex driven zero dimensional devices [45–53]. Using a Floquet description of the dynamics of the quantum system slowly and periodically driven at several frequencies, it is inferred a quantized current in an abstract space of harmonics of the drives. This current thereby effectively describes a transfer of energy between the drives.

# 2 Motivation for an alternative description of topological pumping

### What is pumping?

The above examples of topological pumps were historically described as a response of a slowly driven quantum system, *i.e.* considering its origin from an imposed external drive, see also [54, 55]. The topological property is related to a dynamical feature of the quantum system: an anomalous velocity of electrons along the cylinder in Laughlin pumps, an anomalous velocity of particles in a one dimensional periodic potential in Thouless pumps, or an anomalous velocity in an abstract space of harmonics in topological frequency converters. The above cited experimental realizations are measures of such quantized velocities.

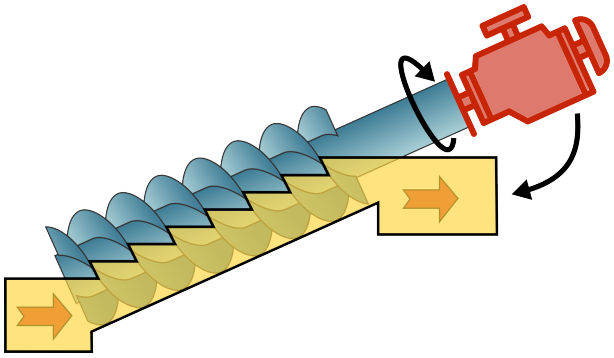

Figure 1: Archimedes screw pump (modern view).

But what is a pump? Let us consider the historical example of Archimedes' screw pump, represented on Fig. 1. It is made of three elements: an engine, a screw, and a fluid. The engine, here represented by a motor, slowly rotates the screw which, in return, induces a flow of a fluid. As such, pumping corresponds to a transfer of energy from one system (the motor) to second one (the fluid) mediated by a third one (the screw). Hence, describing pumping naturally amounts to consider the rotation of the motor and the flow of the fluid. Focusing only on the rotation of the screw provides an indirect description of pumping. In the topological pumps discussed above, the screw corresponds to the quantum system, and the rotation of the screw is the dynamics of the driven quantum system, on which the previous descriptions of pumping have focused – thereby amounting for an indirect characterization of the pumping process.

### Purpose of this thesis

The starting point of this thesis is to reconcile the description of such a topological device with that of traditional pumps, by considering the driving parameters as the slow degrees of freedom of the environment coupled to the quantum system, and focusing on their effective dynamics. The topological property is a feature of the couplings between these systems. Hence, we are led to consider a closed quantum system containing a separation of timescales, namely a slow-fast system. The coupled degrees of freedom of the environment are slower than the inner dynamics of the quantum system. When we describe the effective adiabatic dynamics of the slow degrees of freedom by taking into account the backaction of the fast subsystem onto the slow one, the topological nature of the coupling translates in an energy or charge exchange between these slow subsystems. This leads us to consider new physical phenomena in isolated quantum systems originating from a topological coupling between slow and fast quantum subsystems.

### Organization of the manuscript

This description of topological pumps within the context of slow-fast quantum systems will be introduced step by step in this manuscript, in increasing level of complexity. This manuscript is organized as follows.

- In chapter 1, we describe the adiabatic evolution of a slowly time-dependent quantum system. Since the historical descriptions of topological pumps focus on the inner dynamics of a driven system, they rely on this formalism. We introduce a notion of adiabatic states of the driven system as those leading to the slowest time-evolution of physical observables. Such a slowly driven quantum system is a particular case of a slow-fast system, where the fast subsystem is the quantum system and the slow subsystem corresponds to external classical variables inducing the time-dependence. The peculiar aspect of this description is that the dynamics of the slow variables is given *a priori*, meaning that we assume that it is unaffected by the coupling to the quantum system. There is no backaction.

- In chapter 2, we introduce slow-fast quantum systems. Physically, they correspond to the same kind of systems as those considered in the first chapter, namely a closed quantum system containing two types of degrees of freedoms, associated to a separation of timescales. The advantage of treating the drives of chapter 1 as slow degrees of freedom is in particular to describe the backaction of the fast subsystem onto the slow dynamics. Indeed, we are here looking at an effective dynamics of the slow degrees of freedom, describing states of the total system evolving only at the slow timescales. This effective dynamics involves a geometric object, a Berry curvature, carrying the topological notion of Chern number on which this manuscript is rooted. In the first two sections, we introduce the subject with the historical examples of the Born-Oppenheimer treatment of a molecule, and of the semiclassical dynamics of electrons in a crystal. In sections 2.3 and 2.4, we detail a general theory of adiabatic dynamics of such a slow-fast quantum system. The main goal is to construct a subspace of states of the total system, the adiabatic subspace, and to derive their effective slow dynamics. The determination of the adiabatic subspace follows the same method as the definition of the adiabatic states of a

slowly driven quantum system in chapter 1, whereas the technical implementation of the method differ. In particular, we provide precise conditions of validity of the adiabatic expansion.

- In chapter 3, we apply the description of chapter 2 to the case of topological coupling between slow and fast quantum systems, which allows to describe topological pumps as a slow-fast system with a quantized transfer of charge or energy between the slow degrees of freedom. This formalism enables the identification of the physical observables whose dynamics carry the topological property, namely the quantized transfer of charge or energy. We restrict ourselves to a classical description of the dynamics of the slow system. This chapter is based on the first three sections of the publication [56].

- In chapter 4, we illustrate the virtue of the formalism introduced in chapter 3 with an experimental proposal of topological coupling between microwave modes and a superconducting quantum circuit. The topological nature of the coupling induces a quantized redistribution of powers between the microwave modes. We identify the observables carrying the topological invariant. The experimental proposal is designed to allow for an experimental measure of the topological flow. This chapter is based on the last section of the publication [56].

- In chapter 5, we extend the formalism of topological coupling between slow classical degrees of freedom and a fast quantum system of chapter 3 to a full quantum description, describing quantum mechanically both slow and fast quantum systems, thus recovering the formalism of chapter 2 of adiabatic dynamics of a slow-fast quantum system. We focus on the simplest example of a two-level system, a qubit, topologically coupled to two quantum modes. In contrast with the chapter 2, we pay attention on the nature of the adiabatic states, the states evolving slowly and described by the effective adiabatic dynamics. We show that they are not naturally prepared experimentally, but that any initial state decomposes into a sum of two of such states. The topological nature of the coupling leads to a separation of these two components in phase space, leading generically to a creation of cat states. Besides, we quantify the entanglement between the qubit and the quantum modes in terms of geometric objects, and characterize the time-evolution of the quantum fluctuation of the modes. This chapter is based on the submitted article [57].

- In chapter 6, we consider the dynamics of two quantum harmonic oscillators topologically coupled to a qubit. On short timescales, we recover the adiabatic dynamics described in chapter 5, superposed by Landau-Zener processes, leading to a mechanism in which the topological pumping rates are reversed in a roughly periodic sequence. At long timescales, the topological nature of the coupling leads to chaotic behavior. This quantum chaotic behavior manifests itself in spectral properties *via* level repulsion, and by two families of eigenstates with different distributions of average value of observables.

Chapter 1

# Adiabatic time-dependent perturbation theory

Adiabatic time-dependent perturbation theory deals with the dynamics of a slowly time-dependent closed quantum system. When such a system is time-independent the eigenstates of the Hamiltonian are initial states of particular interest. They are stationary in the sense that they lead to no change in time of the statistics of measure of any physical observable.

For a time-dependent Hamiltonian, there is no longer a notion of stationary state in general. The eigenstates of the Hamiltonian are time-dependent and preparing the quantum system in an instantaneous eigenstates of the Hamiltonian does not lead in general to time-independent statistics of measure of physical observables. However, one expects the evolution of the system to remain close to eigenstates when the Hamiltonian evolves very slowly. The purpose of the adiabatic theorem of quantum mechanics is to quantify this expectation.

The notion of adiabaticity in quantum mechanics dates back to the beginning of quantum theory, with the work of Ehrenfest [58] who studied the role of adiabatic invariants in the old formulation of the correspondence between classical and quantum mechanics. His work contains the ideas behind the now common time-dependent adiabatic theory, introduced in the modern formulation of quantum mechanics by Born and Fock [59], and further precised onto the adiabatic theorem by Kato [60].

The adiabatic theorem of quantum mechanics states that when the system is prepared in an instantaneous eigenstate of the Hamiltonian then in the limit of an infinitely slow time-dependence of the Hamiltonian and under certain conditions to be precised, the system stays in an instantaneous eigenstate during the time evolution. The physical phenomena we are interested in this manuscript require to extend the results in this limit. Thus, we will start by a detailed discussion of this adiabatic theorem before developing their extensions in the reminder of this thesis.

The strategy employed in the literature consists in working with the leading corrections in this limit. We present the derivation of such corrections in Sec 1.1. This method leads to the notion of geometric phase acquired by the state-vector during the time evolution, and to the first correction to the approximation of staying in an instantaneous eigenstate.

In Sec. 1.2, we present a more personal understanding of the adiabatic time-dependent theory. We introduce a notion of adiabatic states, different from the eigenstates. These

states are defined to be those leading to the slowest time-evolution of physical observables. In this manuscript, we emphasize the physical relevance of this second strategy.

Finally, in Sec. 1.2.3 we discuss in details the conditions of validity of the adiabatic perturbative expansion and discuss Landau-Zener transitions, which are non-perturbative and non-adiabatic effects.

## 1.1 Time evolution of an instantaneous eigenstate

### 1.1.1 Result of the first order adiabatic approximation

We consider a time-dependent closed quantum system and note $H(t)$ its time-dependent Hamiltonian. The adiabatic theorem states that when prepared in an instantaneous eigenstate, the system remains in an instantaneous eigenstate in the limit of an infinitely slow variation of the Hamiltonian. We note $H(t)$ its time-dependent Hamiltonian and $|\psi_{\nu,0}(t)\rangle$ its instantaneous normalized eigenstates of eigenenergy $E_{\nu,0}(t)$

$$H(t)\,|\psi_{\nu,0}(t)\rangle = E_{\nu,0}(t)\,|\psi_{\nu,0}(t)\rangle\,. \tag{1.1}$$

The index "0" is explained in Sec. 1.2, where the eigenstates appear as the zeroth order approximation of adiabatic states. We use this notation in this section for consistency. Note that there is a large amount of arbitrariness in the definition of the instantaneous eigenstates, since the phase of the eigenstate at each time $t$ is chosen arbitrarily. A set of "continuous"[1] eigenstates $|\psi_{\nu,0}(t)\rangle$ corresponds to a choice of gauge. We assume an arbitrary smooth gauge, meaning that the time derivatives of $|\psi_{\nu,0}(t)\rangle$ are well-defined and continuous. The physical observables are always gauge independent.

Crucially, we consider the initial state in an eigenstate $\nu$

$$|\Psi(t=0)\rangle = |\psi_{\nu,0}(t=0)\rangle\,. \tag{1.2}$$

As will be explained in Sec. 1.2.3, one condition of adiabaticity is that the Hamiltonian depends smoothly on time and for all time $t$ the corresponding eigenenergy $E_{\nu,0}(t)$ is not degenerate:

$$E_{\mu,0}(t) \neq E_{\nu,0}(t) \qquad \text{for } \mu \neq \nu, \tag{1.3}$$

for all time $t$. We further detail the condition of validity of the following result in Sec. 1.2.3. As derived in Sec. 1.1.3, the time-evolution of the instantaneous eigenstates at first order in adiabatic expansion reads

$$\begin{aligned}|\Psi(t)\rangle = e^{i\gamma^d_{\nu,0}(t)+i\gamma^g_{\nu,0}(t)} &\left(|\psi_{\nu,0}(t)\rangle - i\hbar\sum_{\mu\neq\nu}\frac{\langle\psi_{\mu,0}(t)|\,\frac{\mathrm{d}}{\mathrm{d}t}\,|\psi_{\nu,0}(t)\rangle}{E_{\nu,0}(t)-E_{\mu,0}(t)}\,|\psi_{\mu,0}(t)\rangle\right)\\ &+ i\hbar\sum_{\mu\neq\nu} e^{i\gamma^d_{\mu,0}(t)+i\gamma^g_{\mu,0}(t)}\left[\frac{\langle\psi_{\mu,0}(t)|\,\frac{\mathrm{d}}{\mathrm{d}t}\,|\psi_{\nu,0}(t)\rangle}{E_{\nu,0}(t)-E_{\mu,0}(t)}\right]_{t=0}|\psi_{\mu,0}(t)\rangle\end{aligned} \tag{1.4}$$

with the dynamical phase defined by

$$\gamma^d_{\nu,0}(t) = -\frac{1}{\hbar}\int_0^t E_{\nu,0}(t')\mathrm{d}t', \tag{1.5}$$

[1] The subtle notion of parallel transport is not essential in this manuscript. It is presented in [61] and its role in physical contexts is discussed in [62].

while the geometric phase satisfies

$$\gamma^g_{\nu,0}(t) = \int_0^t \langle \psi_{\nu,0}(t')| \, i\frac{\mathrm{d}}{\mathrm{d}t'} \, |\psi_{\nu,0}(t')\rangle \, \mathrm{d}t'. \tag{1.6}$$

The denomination "geometric" phase is explained in the next section. Although the last term of Eq. (1.4) is often ignored in the literature, we explain in Sec. 1.2 that it is physically very relevant and originates from the difference between eigenstates and adiabatic states.

### 1.1.2 Limit of infinitely slow variation of the Hamiltonian and Berry phase

#### Infinitely slow limit

The adiabatic theorem deals with the limit of an infinitely slow Hamiltonian. To discuss this limit we consider that the time-dependence of the Hamiltonian originates from the dependence on the time-variation of external parameters denoted collectively $\boldsymbol{\xi} = \{\xi^1, \xi^2, \dots\} = \{\xi^\alpha\}$:

$$H(t) = H(\boldsymbol{\xi}(t)) \quad ; \quad |\psi_{\nu,0}(t)\rangle = |\psi_{\nu,0}(\boldsymbol{\xi}(t))\rangle \quad ; \quad E_{\nu,0}(t) = E_{\nu,0}(\boldsymbol{\xi}(t)). \tag{1.7}$$

In Chap. 3, these variables $\boldsymbol{\xi}$ will be treated as phase-space coordinates of a slow dynamical classical system. For now, they are considered as external parameters. The limit of an infinitely slow Hamiltonian corresponds to the limit $\dot{\xi}^\alpha \to 0$, where $\dot{\xi}^\alpha$ denotes the time derivative of $\xi^\alpha$. To discuss this limit, we isolate in the expression (1.4) the dependence on the velocities $\dot{\xi}^\alpha(t)$ from the dependence on the instantaneous value $\boldsymbol{\xi}(t)$ of the parameters:

$$\begin{aligned} |\Psi(t)\rangle = {} & e^{i\gamma^d_{\nu,0}(t)+i\gamma^g_{\nu,0}(t)} \, |\psi_{\nu,0}(\boldsymbol{\xi})\rangle \\ & - \sum_\alpha \dot{\xi}^\alpha(t) \left( \sum_{\mu\neq\nu} e^{i\gamma^d_{\nu,0}(t)+i\gamma^g_{\nu,0}(t)} \frac{\hbar A_{\mu\nu,\alpha,0}(\boldsymbol{\xi})}{E_{\nu,0}(\boldsymbol{\xi}) - E_{\mu,0}(\boldsymbol{\xi})} \, |\psi_{\mu,0}(\boldsymbol{\xi})\rangle \right) \\ & + \sum_\alpha \dot{\xi}^\alpha(t=0) \left( \sum_{\mu\neq\nu} e^{i\gamma^d_{\mu,0}(t)+i\gamma^g_{\mu,0}(t)} \left[ \frac{\hbar A_{\mu\nu,\alpha,0}(\boldsymbol{\xi})}{E_{\nu,0}(\boldsymbol{\xi}) - E_{\mu,0}(\boldsymbol{\xi})} \right]_{t=0} |\psi_{\mu,0}(\boldsymbol{\xi})\rangle \right), \end{aligned} \tag{1.8}$$

where we introduce the components of the non-abelian Berry connection

$$A_{\mu\nu,\alpha,0}(\boldsymbol{\xi}) = i \, \langle \psi_{\mu,0}(\boldsymbol{\xi}) | \partial_\alpha \psi_{\nu,0}(\boldsymbol{\xi}) \rangle \, , \tag{1.9}$$

with the notation $\partial_\alpha = \frac{\partial}{\partial \xi^\alpha}$. The Berry connection, and the Berry curvature introduced below, play a central role in the geometrical description of an ensemble of quantum states parametrized by continuous parameters. See [63] for a pedagogical introduction. We obtain the result of the adiabatic theorem: in the limit of infinitely slow time variation of the Hamiltonian, a state initially prepared in an instantaneous eigenstate remains in an instantaneous eigenstate:

$$|\Psi(t)\rangle \underset{\dot{\xi}^\alpha \to 0}{\to} e^{i\gamma^d_{\nu,0}(t)+i\gamma^g_{\nu,0}(t)} \, |\psi_{\nu,0}(\boldsymbol{\xi}(t))\rangle \, . \tag{1.10}$$

### Geometric phase

The parametrization of the Hamiltonian by external continuous variables enables also to discuss the geometric nature of the geometric phase $\gamma^g_{\nu,0}(t)$. This phase takes the form of a line integral in parameter space, such that it depends only on the path taken in this space, and not on the velocity of travel along this path:

$$\gamma^g_{\nu,0}(t) = \int_{\mathcal{P}[\boldsymbol{\xi}(0)\to\boldsymbol{\xi}(t)]} \sum_\alpha A_{\nu,\alpha,0}(\boldsymbol{\xi}) \mathrm{d}\xi^\alpha \tag{1.11}$$

where $\mathcal{P}[\boldsymbol{\xi}(0) \to \boldsymbol{\xi}(t)]$ denotes the path $\boldsymbol{\xi}(t')$ in parameter space from $\boldsymbol{\xi}(0)$ to $\boldsymbol{\xi}(t)$, and where we introduce the components of the Berry connection of eigenstates $\nu$

$$A_{\nu,\alpha,0}(\boldsymbol{\xi}) = A_{\nu\nu,\alpha,0}(\boldsymbol{\xi}) = i \left\langle \psi_{\nu,0}(\boldsymbol{\xi}) | \partial_\alpha \psi_{\nu,0}(\boldsymbol{\xi}) \right\rangle . \tag{1.12}$$

### Berry phase and Berry curvature

The Berry phase corresponds to the geometric phase associated to a cyclic trajectory in parameter space, for which $\boldsymbol{\xi}(T) = \boldsymbol{\xi}(0)$. This notion raised a lot of interest since the work of Berry [64] partly because he highlighted its gauge invariance, in the sense that it does not depend on the choice of phase made in the definition of the eigenstates $|\psi_{\nu,0}(\boldsymbol{\xi})\rangle$.

To emphasize the gauge invariance of the Berry phase, Berry introduced a way to compute it from a gauge invariant quantity, the Berry curvature, which plays a central role in this manuscript. The components of the Berry curvature are defined by

$$F_{\nu,\alpha\beta,0}(\boldsymbol{\xi}) = \partial_\alpha A_{\nu,\beta,0}(\boldsymbol{\xi}) - \partial_\beta A_{\nu,\alpha,0}(\boldsymbol{\xi}) \tag{1.13}$$

and are gauge invariant. The Berry phase associated to a closed path $\mathcal{P}[\boldsymbol{\xi}(0) \to \boldsymbol{\xi}(0)]$ can be computed by integrating the Berry curvature on any surface $\mathcal{S}$ surrounded by this path

$$\oint_{\mathcal{P}[\boldsymbol{\xi}(0)\to\boldsymbol{\xi}(0)]} \sum_\alpha A_{\nu,\alpha,0}(\boldsymbol{\xi}) \mathrm{d}\xi^\alpha = \int_{\mathcal{S}} \sum_{\alpha<\beta} F_{\nu,\alpha\beta,0}(\boldsymbol{\xi}) \mathrm{d}\xi^\alpha \wedge \mathrm{d}\xi^\beta . \tag{1.14}$$

This result is a particular case of Stokes' theorem for differential forms, see [63] for an introduction in physical contexts, and [61] for an introduction of the mathematical formalism.

## 1.1.3 Canonical method of derivation

We present here the canonical derivation of the time evolution of a slowly time dependent quantum system. This method consists in solving differential equations governing the time evolution of coefficients entering the decomposition of the state of the system on the instantaneous eigenstates of the time-dependent Hamiltonian $H(t)$. This method is partly discussed in quantum mechanics textbooks, see for example [65, 66], and [67] for a detailed discussion of its variants. This section follows more closely the first appendix of [56].

The main advantage of this method is that it leads to explicit expressions of the state-vector $|\Psi(t)\rangle$, the geometric phase, and the dynamical phase of the quantum system, such that it is useful for practical computations. Its main disadvantage is that the identification

of the small parameter for perturbation theory and its generalizations at higher orders in the perturbation theory is unclear. In this section we discuss briefly the nature of the small parameter, and we postpone a more detailed discussion to section 1.2.3. Let us stress that the notion of adiabatic states detailed in section 1.2 enables a geometric intuition of the result, and is physically relevant as will be emphasized in this manuscript.

Let us mention that the historical technique of derivation of the adiabatic theorem [60, 68] slightly differs from the one presented below. It consists in using a unitary transformation of the Hamiltonian to put it on a traditional form of perturbation theory $H_0(t) + V(t)$ where $H_0(t)$ is a Hamiltonian generating an ideal adiabatic evolution and $V(t)$ is a perturbation. It has the advantage to be clearly formulated in terms of standard time-dependent perturbation theory. This method is also very enlightening in the context of Shortcuts To Adiabaticity where the purpose is to search for a modified Hamiltonian whose exact evolution corresponds to the ideal adiabatic evolution of the unmodified Hamiltonian [69]. However, it does not provide an explicit expression of the state-vector $|\Psi(t)\rangle$, but an expression of the time evolution operator. In particular, the determination of the geometric and dynamical phases requires minors extra steps, which is probably a reason for its lack of use nowadays.

### Method

To determine the time evolution of this initial state, we decompose the state of the system $|\Psi(t)\rangle$ on the instantaneous eigenstates

$$|\Psi(t)\rangle = \sum_{\mu} a_\mu(t)\,|\psi_{\mu,0}(t)\rangle\,. \tag{1.15}$$

We aim at solving the time-dependent Schrödinger equation

$$i\hbar\frac{\mathrm{d}}{\mathrm{d}t}\,|\Psi(t)\rangle = H(t)\,|\Psi(t)\rangle \tag{1.16}$$

by solving the corresponding system of coupled differential equations for the coefficients $a_\mu(t)$, obtained by differentiating (1.15) with respect to time and projecting it onto $|\psi_{\mu,0}(t)\rangle$:

$$\dot{a}_\mu(t) = i\left[i\,\langle\psi_{\mu,0}(t)|\,\frac{\mathrm{d}}{\mathrm{d}t}\,|\psi_{\mu,0}(t)\rangle - \frac{1}{\hbar}E_{\mu,0}(t)\right]a_\mu(t) - \sum_{\sigma\neq\mu}\langle\psi_{\mu,0}(t)|\,\frac{\mathrm{d}}{\mathrm{d}t}\,|\psi_{\sigma,0}(t)\rangle\,a_\sigma(t)\,. \tag{1.17}$$

We get rid of the first term introducing the dynamical phase (1.5) and the geometric phase (1.6) by the substitution $a_\mu(t) = e^{i\gamma^d_{\mu,0}(t)+i\gamma^g_{\mu,0}(t)}\tilde{a}_\mu(t)$. After substitution and time-integration, we express (1.17) in the form

$$\tilde{a}_\mu(t) - \tilde{a}_\mu(0) = -\sum_{\sigma\neq\mu}\int_0^t \mathrm{d}t'\; e^{i\gamma^{\mathrm{Bohr}}_{\sigma\mu,0}(t')}f_{\mu\sigma}(t')\tilde{a}_\sigma(t'), \tag{1.18}$$

with

$$\gamma^{\mathrm{Bohr}}_{\sigma\mu,0}(t) = \gamma^d_{\sigma,0}(t) - \gamma^d_{\mu,0}(t) = -\frac{1}{\hbar}\int_0^t \mathrm{d}t'(E_{\sigma,0}(t') - E_{\mu,0}(t')) \tag{1.19}$$

a dynamical phase evolving at the Bohr frequency $(E_{\sigma,0} - E_{\mu,0})/\hbar$, and

$$f_{\mu\sigma}(t) = e^{i\gamma^g_{\sigma,0}(t)-i\gamma^g_{\mu,0}(t)}\,\langle\psi_{\mu,0}(t)|\,\frac{\mathrm{d}}{\mathrm{d}t}\,|\psi_{\sigma,0}(t)\rangle\,. \tag{1.20}$$

So far everything is exact. We start the perturbation expansion of (1.18) considering the exponential of the dynamical phase as a fast oscillating term, oscillating at the Bohr frequency. The strategy consists in doing successive integration by part of the exponential term, such that at each step a factor of inverse of Bohr frequency $\hbar/(E_{\sigma,0} - E_{\mu,0})$ comes out:

$$\begin{aligned}
&\int_0^t \mathrm{d}t' \; e^{i\gamma^{\mathrm{Bohr}}_{\sigma\mu,0}(t')} f_{\mu\sigma}(t')\tilde{a}_\sigma(t') \\
&\qquad = \left[ e^{i\gamma^{\mathrm{Bohr}}_{\sigma\mu,0}(t')} \frac{i\hbar}{E_{\sigma,0}(t') - E_{\mu,0}(t')} f_{\mu\sigma}(t')\tilde{a}_\sigma(t') \right]_0^t \\
&\qquad\quad - \int_0^t \mathrm{d}t' \; e^{i\gamma^{\mathrm{Bohr}}_{\sigma\mu,0}(t')} \frac{\mathrm{d}}{\mathrm{d}t'} \left( \frac{i\hbar}{E_{\sigma,0}(t') - E_{\mu,0}(t')} f_{\mu\sigma}(t')\tilde{a}_\sigma(t') \right) \qquad (1.21) \\
&\qquad = \left[ e^{i\gamma^{\mathrm{Bohr}}_{\sigma\mu,0}(t')} \frac{i\hbar}{E_{\sigma,0}(t') - E_{\mu,0}(t')} f_{\mu\sigma}(t')\tilde{a}_\sigma(t') \right]_0^t \\
&\qquad\quad - \left[ e^{i\gamma^{\mathrm{Bohr}}_{\sigma\mu,0}(t')} \frac{i\hbar}{E_{\sigma,0}(t') - E_{\mu,0}(t')} \frac{\mathrm{d}}{\mathrm{d}t'} \left( \frac{i\hbar}{E_{\sigma,0}(t') - E_{\mu,0}(t')} f_{\mu\sigma}(t')\tilde{a}_\sigma(t') \right) \right]_0^t + \dots \qquad (1.22)
\end{aligned}$$

We then have to check at each step that the terms in front of the inverse of instantaneous gap $E_{\sigma,0}(t) - E_{\mu,0}(t)$ is small compared to this gap. In particular, the coefficient $\hbar f_{\mu\sigma}(t)$ and its time derivatives have to be small compared to the instantaneous gap. To discuss this, as in the previous section, we consider that the time dependence of the Hamiltonian originates from the dependence on parameters $\boldsymbol{\xi}(t)$. The amplitude of the coefficient $\hbar f_{\mu\sigma}(t)$ then scales as the velocities $|\hbar f_{\mu\sigma}(t)| = |\sum_\alpha \hbar \dot{\xi}^\alpha A_{\mu\sigma,\alpha,0}(\boldsymbol{\xi})|$. Using the expression (1.11) of the geometric phase, we find that its time derivatives also scales as higher time derivatives of the parameters. This gives an ensemble of conditions on how slowly the parameters $\boldsymbol{\xi}(t)$ have to evolve such that the first order of the adiabatic expansion is valid.

The adiabatic expansion then consists in replacing (1.22) in (1.18), and using in the right-hand-side the lowest order result $\tilde{a}_\mu(t) = \tilde{a}_\mu(0)$. For an initial state prepared in an instantaneous eigenstates, we have $\tilde{a}_\mu(0) = \delta_{\mu\nu}$ and we recover (1.4) at first order.

### 1.1.4 Historical treatment of the infinitely slow limit

In the historical works on the adiabatic theorem is considered a change of the Hamiltonian $H(t)$ of a closed quantum system from an initial Hamiltonian $H_i = H(t = 0)$ to a final Hamiltonian $H_f = H(t = T)$ during a time $T$ [60, 68, 70]. The slowness of the time-dependence of the Hamiltonian is then controlled by the duration $T$ of the change of Hamiltonian, were the limit of infinitely slow Hamiltonian correspond to the limit $T \to \infty$. The strategy to study this limit was to use a rescaled dimensionless time $s = t/T$, such that the Schrödinger equation becomes

$$i\hbar \frac{\mathrm{d}}{\mathrm{d}s} |\Psi(s)\rangle = T H(s) |\Psi(s)\rangle \,, \qquad (1.23)$$

which is studied in the limit of large timescale $T$, among other typical timescales to be determined. A lot of mathematical subtleties arise from the singularity of such equation in the limit $T \to \infty$ [71].

The factor $1/T$ can be placed in front of $\hbar$ in Eq. (1.23). This is the reason why the adiabatic limit shares common features with the semiclassical limit, which is often discussed as the limit where $\hbar$ is much smaller than any other typical scale of action of the system.

The genuine difficulty of the adiabatic perturbation theory is the *a priori* identification of small dimensionless perturbative parameter. We know physically that we require a slow Hamiltonian, such that the corresponding small dimensionless quantity is a ratio of typical timescales, or frequency scales. There are several frequencies in the problem, such as: the instantaneous Bohr frequencies, the rate of variation of the Hamiltonian – or equivalently the rate of variation of the external variables governing its time-dependence –, or the matrix elements of the Hamiltonian divided by $\hbar$. The definition of the small dimensionless parameter from these frequency scales is not clear *a priori*.

We address this difficulty is the next section by defining a notion of adiabatic state. Translating their physical definition into a mathematical construction enables us to define *a posteriori* the dimensionless adiabatic parameter. The method to construct the adiabatic states will share a lot of common ideas with the method to derive the adiabatic dynamics of a slow-fast quantum system presented in Chap. 2.

## 1.2 Adiabatic states

In this section, we develop a personal understanding of the adiabatic approximation of a slowly time-dependent quantum system, introducing a notion of adiabatic state and a non-standard method to construct them enabling to discuss the condition of validity of the adiabatic approximation.

As discussed in the introduction of this chapter, the eigenstates of the Hamiltonian of a time-independent quantum system are physically interesting because they are stationary states: they lead to an absence of time evolution of the physical observables. Each of these stationary states is associated with an eigenenergy which enters the dynamics of non-stationary initial state. Non-stationary initial states decompose into a superposition of stationary states, and the rate of change of the physical observables are given by the Bohr frequencies set by the difference of eigenenergies of stationary states divided by the Planck constant $\hbar$.

In the time-dependent case, the instantaneous eigenstates of the time-dependent Hamiltonian are no longer stationary states in general, in the sense introduced above. In this section, rather than looking at the time evolution of an instantaneous eigenstate, we introduce the concept of adiabatic states which are constructed to have properties similar to the stationary states of a time-independent quantum system. Besides, we will emphasize in this manuscript that they are the physically relevant states to consider when dealing with a quantum system with slow and fast degrees of freedom.

### 1.2.1 Physical definition of the adiabatic states

We consider a slowly time-dependent quantum system, described by a Hamiltonian $H(t)$. We define the adiabatic states as solutions of the Schrödinger equation with the slowest time-evolution of the physical observables, at a rate of change which is of the same order of magnitude as the rate of change of the time-dependent Hamiltonian.

Similarly to the stationary states in the time-independent case, we also expect the adiabatic states to be associated with energies, such that we can define Bohr frequencies from pairs of different adiabatic states. We then expect the rate of change of the adiabatic states to be small compared to these Bohr frequencies, in order to be able to distinguish external drive from the internal quantum dynamics in the time-variation of a physical observable. With this definition, we understand that the notion of adiabatic state is relevant for rates of time-dependence of the Hamiltonian small compared to its bare Bohr frequencies.

### Slow manifold

Let us comment on the link between our definition of the adiabatic states and the notion of slow manifold, which plays a central role in physics. We consider the example of the derivation of hydrodynamic equations starting from kinetic equations for a fluid in motion. When the fluid is at equilibrium, we define thermodynamic variables, such as the density, the temperature, and the pressure. Slightly out of equilibrium, the hydrodynamic equations do not describe all the microscopic initial conditions of the fluid, but only those for which a notion of local equilibrium exists, with local thermodynamic variables which vary slowly in space and in time. The set of these initial conditions is what is called a slow manifold, and the hydrodynamic equations govern the dynamics within this slow manifold.

In quantum mechanics, the eigenstates of a time-independent Hamiltonian are the initial states for which the physical observables are at equilibrium, they do not vary in time, analogously to the thermodynamic variables of a fluid at equilibrium. For a slowly time-dependent Hamiltonian, what we define as the adiabatic states are those leading to slow evolution of the observables, analogously to the slow manifold of a fluid slightly out of equilibrium.

### Method of construction

In this manuscript, we use the following approach. We study a time-dependent quantum system for which we assume a separation of time-scales. In the limit of infinite separation, the dynamics simplifies. We will introduce a variable $\lambda$ to identify the dimensionless quantities controlling the separation of timescales. We physically expect that the dynamics simplifies in the limit of infinitely slow time-variation of the Hamiltonian. This will correspond to the limit $\lambda \to 0$. The idea is to build a perturbation theory around this limit.

More precisely, we consider a family of physical problems, parametrized by the variable $\lambda$. The limit $\lambda \to 0$ corresponds to the problem of an infinitely slow time variation of the Hamiltonian, for which the dynamics simplifies. The limit $\lambda \to 1$ corresponds to the physical problem we are studying, namely a quantum system governed by the time dependent Hamiltonian $H(t)$. The variable $\lambda$ interpolates between the limit of an infinitely slow Hamiltonian and the physical problem we are considering.

The strategy is to identify the solutions of the problems perturbatively in power series of $\lambda$. As we will explain, the conditions of validity of a formal expansion, related to the conditions of convergence of the series for $\lambda = 1$, provides the dimensionless quantity of validity of the condition of adiabaticity.

We use the same method in Chap. 2 to define the adiabatic dynamics of a slow-fast quantum system. The difference between these two chapters is the technical implementation of the method.

Besides, this method will be fruitful to determine the topological properties of adiabatic states. We come back to these aspects in Chap. 5.

#### Use of the density matrix

To consider the rate of change of a physical observable, it is not necessary to consider the rate of change of the state-vector $|\Psi(t)\rangle$. Indeed, a time-variation of a global phase of $|\Psi(t)\rangle$ does not induce any time-variation of the average value of an observable. Instead, we consider the density matrix $\rho(t) = |\Psi(t)\rangle\langle\Psi(t)|$, that encodes the rate of variation of any observable $\hat{O}$:

$$\langle\hat{O}\rangle(t) = \mathrm{Tr}\Big[\rho(t)\hat{O}\Big]. \tag{1.24}$$

The density matrix was used historically in analogy with the treatment of adiabaticity in classical Hamiltonian mechanics [72, 73].

### 1.2.2 Construction of the adiabatic states

#### Equations of definition

We note $\tilde{\rho}(t)$ the density matrix of a solution of the problem where the speed of variation of the Hamiltonian has been scaled by a factor $\lambda$, *i.e.* evolving according to $H(\lambda t)$,

$$i\hbar\frac{\mathrm{d}}{\mathrm{d}t}\tilde{\rho}(t) = [H(\lambda t), \tilde{\rho}(t)]. \tag{1.25}$$

In order to write the Schrödinger equation (1.25) on a suitable form for perturbation theory, we define $\rho(t) = \tilde{\rho}(t/\lambda)$, such that[2] Eq. (1.25) written for $\rho(t)$ gives

$$\lambda i\hbar\frac{\mathrm{d}}{\mathrm{d}t}\rho(t) = [H(t), \rho(t)]. \tag{1.26}$$

In particular, for $\lambda = 1$, $\tilde{\rho}(t) = \rho(t)$ is a dynamical solution of $H(t)$, the problem we are interested in.

For $\lambda \to 0$, a simple solution of the previous equation is $|\psi_{\nu,0}(t)\rangle\langle\psi_{\nu,0}(t)|$ for an ensemble of instantaneous eigenstates $|\psi_{\nu,0}(t)\rangle$ of $H(t)$. We suppose that some solutions $\rho_\nu(t)$ of (1.26) for finite $\lambda$ can be defined perturbatively from this $\lambda \to 0$ solution, i.e. decomposed as a power series

$$\rho_\nu(t) = \rho_{\nu,0}(t) + \lambda\rho_{\nu,1}(t) + \cdots = \sum_k \lambda^k \rho_{\nu,k}(t). \tag{1.27}$$

We define the $\nu$-th adiabatic state of the time-dependent Hamiltonian $H(t)$ as such solution for $\lambda = 1$, namely for the physical problem we are considering. We will show in

[2] The time-dependent density matrices $\tilde{\rho}(t)$ and $\rho(t)$ obviously depend on $\lambda$. We could write them $\tilde{\rho}(t;\lambda)$ and $\rho(t;\lambda)$. We do not write explicitly the dependence on $\lambda$ to lighten the notations. The dependence is manifest when we introduce the power series decomposition. The solutions of the physical problem of interest are obtained for $\lambda = 1$.

Sec. 1.2.4 that when these adiabatic states exist they are the solutions leading to the slowest time-evolution of physical observables.

Let us comment on the analogy between our method and the derivation of hydrodynamic equations from kinetic equations. In this analogy, the left hand side of Eq. (1.26) is analogous to a Liouville term, and the right hand side to a "collision term". When $\lambda \to 0$, the "collision term" dominates, such that $[H(t), \rho_{\nu,0}(t)] = 0$ (analogous to a "local equilibrium condition"). The time dependence leads to a small non-zero value to the LHS, so we need to introduce $\rho_\nu(t)$ into $\rho_{\nu,0}(t) + \lambda\rho_{\nu,1}(t)$, and so on. This is formally similar to the Chapman-Enskog perturbation theory used to derive hydrodynamic equations. The main difference is that there is no "thermalization" here, simply a condition to remain close to equilibrium states.

### Recurrence relations

Inserting the power expansion (1.27) into (1.26) provides recurrence relations between the successive orders of the expansion

$$[H(t), \rho_{\nu,k}(t)] = i\hbar\dot{\rho}_{\nu,k-1}(t), \tag{1.28}$$

where the right hand side of (1.28) vanishes for $k = 0$.

As shown below in the algorithm of determination of $\rho_\nu(t)$, we must consider a pure state condition. Usually when solving the Schrödinger equation, we do not care about this condition because we aim at solving it from an initial condition which is a pure state $\rho(t = 0) = |\psi(t = 0)\rangle \langle\psi(t = 0)|$. The time-evolution of a pure-state by the Schrödinger equation is a pure state such that the condition is automatically satisfied for all time $t$. In contrast, here we want to identify the adiabatic state $\rho_\nu(t)$ for all time $t$ at once. As shown below, the recurrence relation (1.28) does not define uniquely $\rho_\nu(t)$, but imposing the extra pure state condition $\rho_\nu(t)^2 = \rho_\nu(t)$ does. This condition leads to the recurrence relations between the different orders

$$\sum_{l=0}^{k} \rho_{\nu,l}(t)\rho_{\nu,k-l}(t) = \rho_{\nu,k}(t). \tag{1.29}$$

### Asymptotic series and condition of adiabaticity

Let us discuss the interpretation of the power series expansion (1.27). Such an expansion is an asymptotic series (also called Poincaré expansion) [71]. This means that the leading terms often provide a good approximation of the true solution $\rho_\nu(t)$. Higher corrections are relevant as long as they are small compared to the previous ones. Namely, $\sum_{k=0}^{N} \rho_{\nu,k}(t)$ provides a good estimate of the $\nu$-th adiabatic state of $H(t)$ as long as $\rho_{\nu,N}(t)$ is much smaller than the previous orders. The comparison between operators will be precised below.

In particular, for the perturbative expansion to be valid as a starting point, the first correction $\rho_{\nu,1}(t)$ has to be much smaller than the zeroth order $\rho_{\nu,0}(t)$. We will quantify the ratio between $\rho_{\nu,1}(t)$ and $\rho_{\nu,0}(t)$, and we define it as the dimensionless adiabatic parameter, which has to be small compared to 1. This dimensionless parameter is determined *a posteriori*, after the perturbative construction of the adiabatic states.

Crucially, such an expansion (1.27) cannot capture non-perturbative effects. A non perturbative quantity is a non-analytic function of $\lambda$, typically $\exp(-\alpha/\lambda)$. In mathematical terms, the equations involving $\rho_\nu(t)$ are true up to $\mathcal{O}(\lambda^\infty)$ terms. We emphasize the physical relevance of non-perturbative effects in Sec 1.2.5 by considering non-perturbative Landau-Zener transitions, useful to determine the time of validity of the adiabatic approximation.

### Algorithm of computation

We present the algorithm to compute order by order the adiabatic states, allowing to determine explicitly the conditions of validity of the perturbative expansion from the expression of the first order.

At zeroth order, the conditions (1.28) and (1.29) are expressed as

$$[H(t), \rho_{\nu,0}(t)] = 0 \tag{1.30}$$

$$\rho_{\nu,0}(t)^2 = \rho_{\nu,0}(t) \tag{1.31}$$

which are satisfied by any $\nu$-th instantaneous non degenerate eigenstate

$$\rho_{\nu,0}(t) = |\psi_{\nu,0}(t)\rangle \langle\psi_{\nu,0}(t)| \,. \tag{1.32}$$

We find that at order zero in the adiabatic expansion, the adiabatic states are provided by the instantaneous eigenstates. This is expected since the rates of change of the instantaneous eigenstates are indeed slow, of the same order of magnitude as the rate of change of the Hamiltonian. However, they are not solutions of Eq. (1.26), and the higher order terms correct this.

In the following, it is useful to express the matrix elements of the $k$-th order $\rho_{\nu,k}(t)$ in the basis of the instantaneous eigenstates $|\psi_{\mu,0}(t)\rangle$, for an arbitrary[3] gauge. The equation (1.28) gives the off-diagonal elements for which $E_{\mu,0}(t) \neq E_{\sigma,0}(t)$:

$$\langle\psi_{\mu,0}(t)| \rho_{\nu,k}(t) |\psi_{\sigma,0}(t)\rangle = i\hbar \frac{\langle\psi_{\mu,0}(t)| \dot{\rho}_{\nu,k-1}(t) |\psi_{\sigma,0}(t)\rangle}{E_{\mu,0}(t) - E_{\sigma,0}(t)} \qquad \text{for } \mu,\sigma \text{ s.t. } E_{\mu,0}(t) \neq E_{\sigma,0}(t). \tag{1.33}$$

The equation (1.29) gives the $\nu$-th diagonal element

$$\langle\psi_{\nu,0}(t)| \rho_{\nu,k}(t) |\psi_{\nu,0}(t)\rangle = -\sum_{l=1}^{k-1} \langle\psi_{\nu,0}(t)| \rho_{\nu,l}(t)\rho_{\nu,k-l}(t) |\psi_{\nu,0}(t)\rangle \,, \tag{1.34}$$

and the matrix elements on the terms different from $\nu$

$$\langle\psi_{\mu,0}(t)| \rho_{\nu,k}(t) |\psi_{\sigma,0}(t)\rangle = \sum_{l=1}^{k-1} \langle\psi_{\mu,0}(t)| \rho_{\nu,l}(t)\rho_{\nu,k-l}(t) |\psi_{\sigma,0}(t)\rangle \qquad \text{for } \mu,\sigma \neq \nu. \tag{1.35}$$

We should in particular check the compatibility between (1.33) and (1.35) for matrix elements $(\mu,\sigma)$ such that $E_{\mu,0}(t) \neq E_{\sigma,0}(t)$.

From these three equations (1.33), (1.34) and (1.35), we can compute systematically the adiabatic state order by order. In particular at first order it gives

$$\rho_{\nu,1}(t) = -i\hbar \sum_{\mu\neq\nu} |\psi_{\mu,0}(t)\rangle \frac{\langle\psi_{\mu,0}(t)| \frac{\mathrm{d}}{\mathrm{d}t} |\psi_{\nu,0}(t)\rangle}{E_{\nu,0}(t) - E_{\mu,0}(t)} \langle\psi_{\nu,0}(t)| + \text{h.c.} \tag{1.36}$$

[3] C.f. note 1 above.

### 1.2.3 Conditions of adiabaticity

As explained above, we get the quantitative conditions for the adiabatic expansion to be valid by requiring that the first order $\rho_{\nu,1}(t)$ is small compared to $\rho_{\nu,0}(t)$. Given the expression of $\rho_{\nu,0}(t)$ Eq. (1.32), we require the matrix elements of $\rho_{\nu,1}(t)$ to be small compared to 1. It leads to

$$\hbar \frac{\left|\langle\psi_{\mu,0}(t)|\, \frac{\mathrm{d}}{\mathrm{d}t}\, |\psi_{\nu,0}(t)\rangle\right|}{|E_{\nu,0}(t) - E_{\mu,0}(t)|} = \hbar \frac{\left|\langle\psi_{\mu,0}(t)|\, \frac{\mathrm{d}H}{\mathrm{d}t}(t)\, |\psi_{\nu,0}(t)\rangle\right|}{|E_{\mu,0}(t) - E_{\nu,0}(t)|^2} \ll 1 \qquad \text{for } \mu \neq \nu. \tag{1.37}$$

As such, rather than a unique parameter we obtain a family of time-dependent quantities associated to each transition $\mu \neq \nu$

$$\boxed{\varepsilon_{\mu\nu}(t) = \hbar \frac{\left|\langle\psi_{\mu,0}(t)|\, \frac{\mathrm{d}H}{\mathrm{d}t}(t)\, |\psi_{\nu,0}(t)\rangle\right|}{|E_{\mu,0}(t) - E_{\nu,0}(t)|^2}} \tag{1.38}$$

which have to be small compared to 1 for the adiabatic expansion to be relevant. We can then construct the adiabatic small parameter $\varepsilon_{\mathrm{adiab}}$ as the maximum of these quantities

$$\varepsilon_{\mathrm{adiab}} = \max_t \max_{\mu\neq\nu} \varepsilon_{\mu\nu}(t). \tag{1.39}$$

This quantity was introduced in [68] *via* a strategy different from the one discussed in this manuscript.

It is instructive to consider the case where the time-dependence of the Hamiltonian originates from the coupling to parameters $\boldsymbol{\xi}(t)$, as introduced in Sec. 1.1.2. Using $|\,\langle\psi_{\mu,0}|\, \frac{\mathrm{d}}{\mathrm{d}t}\, |\psi_{\nu,0}\rangle\,| = |\sum_\alpha \dot{\xi}^\alpha A_{\mu\nu,\alpha,0}|$, Eq. (1.37) provides conditions on how slowly the parameters have to vary for the adiabaticity to be valid. The component $A_{\mu\nu,\alpha,0}$ of the non-abelian Berry connection converts the velocity $\dot{\xi}^\alpha$ of the variable $\xi^\alpha$ into a scale of frequency which has to be small compared to the Bohr frequency. We require for all $\xi^\alpha(t)$ variables[4]

$$\boxed{\left|\dot{\xi}^\alpha(t) A_{\mu\nu,\alpha,0}(\boldsymbol{\xi}(t))\right| \ll \frac{|E_{\mu,0}(\boldsymbol{\xi}(t)) - E_{\nu,0}(\boldsymbol{\xi}(t))|}{\hbar}.} \tag{1.40}$$

If $\varepsilon_{\mu\nu}(t) \ll 1$, then the expansion is valid up to order $\rho_{\nu,N}(t)$ as long as it is small compared to the previous orders $k < N$. We obtain these conditions from the recursive expression of the matrix elements of the $k$-th order correction $\rho_{\nu,k}(t)$ given in Sec. 1.2.2. In particular, from Eq. (1.33) we obtain the condition

$$|\langle\psi_{\mu,0}(t)|\, \dot{\rho}_{\nu,k}(t)\, |\psi_{\sigma,0}(t)\rangle| \ll \frac{|E_{\mu,0}(t) - E_{\sigma,0}(t)|}{\hbar} \tag{1.41}$$

for the order $\rho_{\nu,k+1}(t)$ to be relevant. In terms of typical timescale of variations of parameters $\boldsymbol{\xi}(t)$, Eq. (1.41) translates into conditions on the higher order time derivatives of the parameters.

[4] Of course Eq. (1.37) requires the less restrictive condition $|\sum_\alpha \dot{\xi}^\alpha A_{\mu\nu,\alpha,0}| \ll |E_{\mu,0} - E_{\nu,0}|/\hbar$. Requiring Eq. (1.40) for all $\xi^\alpha$ variable is sufficient, and it is physically relevant to consider separate conditions for the velocity of each variable.

### 1.2.4 Rate of variation of observables

We introduce the energy associated to the adiabatic states, then derive the dynamics of any state to show that the adiabatic states are those leading to the slowest time-evolution of physical observables, according to their physical definition.

#### Energy of adiabatic state

The adiabatic state $\rho_\nu(t)$ defines a time-dependent energy

$$E_\nu(t) = \mathrm{Tr}[\rho_\nu(t)H(t)]. \tag{1.42}$$

At zeroth order, it reduces to the instantaneous eigenenergies $E_{\nu,0}(t)$ of the Hamiltonian. The first order correction (1.36) being purely off-diagonal, $E_\nu(t)$ also reduces to the eigenenergy $E_{\nu,0}(t)$ at first order. At higher orders, these two energies may differ.

#### Dynamics of an adiabatic state

The density matrix of the adiabatic states $\rho_\nu(t)$ are constructed to be solutions of the time-dependent Schrödinger equation. The density matrix can be written $\rho_\nu(t) = |\psi_\nu(t)\rangle \langle\psi_\nu(t)|$, with $|\psi_\nu(t)\rangle$ the adiabatic states vectors for a given choice of gauge. From the result of first order (1.36), it can be written at first order as

$$|\psi_{\nu,0}(t)\rangle - i\hbar \sum_{\mu\neq\nu} \frac{\langle\psi_{\mu,0}(t)| \frac{\mathrm{d}}{\mathrm{d}t} |\psi_{\nu,0}(t)\rangle}{E_{\nu,0}(t) - E_{\mu,0}(t)} |\psi_{\mu,0}(t)\rangle . \tag{1.43}$$

However, in general such a choice of gauge $|\psi_\nu(t)\rangle$ is not a dynamical solution, *i.e.* a solution of the time-dependent Schrödinger equation (1.16). A dynamical solution satisfies $|\Psi(t)\rangle = e^{i\theta(t)} |\psi_\nu(t)\rangle$ with $\theta(t)$ a phase factor to be determined. We obtain this phase factor by substitution of this dynamical solution in the Schrödinger equation (1.16), projection onto $|\psi_\nu(t)\rangle$, and time-integration. It leads to

$$|\Psi(t)\rangle = e^{i\gamma_\nu^d(t)+i\gamma_\nu^g(t)+i\alpha} |\psi_\nu(t)\rangle , \tag{1.44}$$

with the dynamical phase associated to the gauge-invariant energy

$$\gamma_\nu^d(t) = -\frac{1}{\hbar}\int_0^t E_\nu(t')\mathrm{d}t', \tag{1.45}$$

and with the geometric phase associated to the gauge choice

$$\gamma_\nu^g(t) = \int_0^t \langle\psi_\nu(t')| i\frac{\mathrm{d}}{\mathrm{d}t'} |\psi_\nu(t')\rangle \,\mathrm{d}t', \tag{1.46}$$

and with $\alpha$ a remaining global phase, the phase relating $|\Psi(t=0)\rangle$ to $|\psi_\nu(t=0)\rangle$.

Let us mention that we do not have to care about these phase factors if we are only interested in the dynamics originating from an initial state prepared in an adiabatic state. These phases are only necessary to consider the dynamics of generic states.

### Time evolution of an arbitrary state

If the spectrum of the Hamiltonian is never degenerate $E_{\mu,0}(t) \neq E_{\sigma,0}(t)$, for all $\sigma \neq \mu$, for all $t$, we can construct an adiabatic state from each instantaneous eigenstate. Two distinct adiabatic states are orthogonal[5], such that, at each time $t$, the adiabatic states form an orthonormal basis of the Hilbert space $\{|\psi_\nu(t)\rangle, \nu = 1, 2, \dots\}$. In a sense, we have constructed a basis of the space of solutions of the Schrödinger equation. Any initial state decomposes on this basis

$$|\Psi(t=0)\rangle = \sum_\nu a_\nu |\psi_\nu(t=0)\rangle , \tag{1.47}$$

such that the time evolution is given by

$$|\Psi(t)\rangle = \sum_\nu e^{i\gamma_\nu^d(t)} e^{i\gamma_\nu^g(t)} a_\nu |\psi_\nu(t)\rangle + \mathcal{O}(\lambda^\infty), \tag{1.48}$$

where $\mathcal{O}(\lambda^\infty)$ denotes non-perturbative effects explained in Sec. 1.2.5.

Let us compare with the result derived in Sec. 1.1. The time-evolved instantaneous eigenstate (1.4) has components oscillating at different dynamical phase rates, illustrating that the initial eigenstate $|\psi_{\nu,0}(t=0)\rangle$ is not an adiabatic state but has small components on the other adiabatic states $|\psi_\mu(t=0)\rangle$, for $\mu \neq \nu$.

### Rate of variation of observables

Let us now study the speed of evolution of the expectation values (1.24), in order to derive explicit conditions for the adiabatic states to be those leading to the slowest evolution of the physical observables.

From Eq. (1.48), we obtain

$$\langle \hat{O} \rangle(t) = \sum_\nu |a_\nu|^2 \langle \psi_\nu(t)| \hat{O} |\psi_\nu(t)\rangle + \sum_{\mu\neq\nu} e^{i\gamma_{\mu\nu}^{\mathrm{Bohr}}(t)} a_\nu a_\mu^* e^{-i\gamma_\mu^g(t)} \langle \psi_\mu(t)| \hat{O} |\psi_\nu(t)\rangle e^{i\gamma_\nu^g(t)} \tag{1.49}$$

with the "Bohr phase factor"

$$\gamma_{\mu\nu}^{\mathrm{Bohr}}(t) = \gamma_\mu^d(t) - \gamma_\nu^d(t) = -\frac{1}{\hbar}\int_0^t (E_\mu(t') - E_\nu(t'))\, \mathrm{d}t'. \tag{1.50}$$

In the time evolution of an observable $\hat{O}$ in an arbitrary state (1.49), the first term corresponds to time-evolution in adiabatic states, and the second term correspond to the effect of the non-adiabaticity of the initial state. We thus require the second term to vary much faster than the first one.

The rate of variation of a physical observable $\hat{O}$ in $\rho_\nu(t)$ is controlled by $\dot{\rho}_\nu(t)$. We estimate it with an operator norm, such as the Frobenius norm

$$||\dot{\rho}_\nu(t)||_F^2 = \mathrm{Tr}\left[\dot{\rho}_\nu(t)^\dagger \dot{\rho}_\nu(t)\right] = \sum_{\mu\neq\nu} \left| \langle \psi_\mu(t)| \frac{\mathrm{d}}{\mathrm{d}t} |\psi_\nu(t)\rangle \right|^2 . \tag{1.51}$$

[5] See [74]. In this reference, the authors discuss the commutation of two adiabatic projectors $\hat{\Pi}_\nu$ and $\hat{\Pi}_\mu$ associated to two different eigenenergies, in the context of slow-fast quantum systems introduced in Chap. 2. The density matrix $\rho_\nu(t)$ of the adiabatic state can be written as the Weyl symbol of such adiabatic projector, such that the commutation between $\hat{\Pi}_\nu$ and $\hat{\Pi}_\mu$ for $\mu \neq \nu$ is equivalent to the orthogonality between $|\psi_\nu(t)\rangle$ and $|\psi_\mu(t)\rangle$ for all time $t$. The notions of adiabatic projector and Weyl symbol are discussed in Chap. 2.

In Eq. (1.49), the rate of variation of $e^{i\gamma_\nu^g(t)}\,|\psi_\nu(t)\rangle$ identifies with the rate of variation of the density matrix $\rho_\nu(t)$. Indeed, from (1.46), we get

$$\left\|\frac{\mathrm{d}}{\mathrm{d}t}\left(e^{i\gamma_\nu^g(t)}\,|\psi_\nu(t)\rangle\right)\right\|^2 = \sum_\mu \left|\langle\psi_\mu(t)|\,\frac{\mathrm{d}}{\mathrm{d}t}\left(e^{i\gamma_\nu^g(t)}\,|\psi_\nu(t)\rangle\right)\right|^2 \tag{1.52}$$

$$= \sum_{\mu\neq\nu}\left|\langle\psi_\mu(t)|\,\frac{\mathrm{d}}{\mathrm{d}t}\,|\psi_\nu(t)\rangle\right|^2 = ||\dot\rho_\nu(t)||_F^2. \tag{1.53}$$

Hence, the first term of (1.49) varies much slower than the second term as long as $\rho_\nu(t)$ varies much slower than the Bohr phase factor. We can then write the condition as

$$\boxed{\left|\langle\psi_\mu(t)|\,\frac{\mathrm{d}}{\mathrm{d}t}\,|\psi_\nu(t)\rangle\right| \ll \left|\dot\gamma_{\mu\nu}^{\mathrm{Bohr}}(t)\right| = \frac{|E_\mu(t)-E_\nu(t)|}{\hbar} \qquad \text{for } \mu\neq\nu.} \tag{1.54}$$

These conditions have to be satisfied such that the adiabatic states are the slowest states. In particular, at lowest order, we recover the condition of validity of the perturbative expansion discussed in Sec. 1.2.3.

### 1.2.5 Landau-Zener non-perturbative transitions

We obtained in Sec. 1.2.3 the time-dependent quantities $\varepsilon_{\mu\nu}(t)$ which have to be small compared to 1 for the adiabatic expansion to be valid. If those are small initially, a first estimate of the validity of the time-dependent solution amounts to evaluate the time $t$ when the $\varepsilon_{\mu\nu}(t)$ become of order 1.

We can refine the time of validity of the adiabatic approximation by considering temporal fluctuations of the $\varepsilon_{\mu\nu}(t)$, evaluating the collision times $t_{\mathrm{col}}$ at which an adiabatic parameter $\varepsilon_{\mu\nu}(t)$ becomes temporarily larger. This typically occurs when the time-dependent gap $|E_{\nu,0}(t)-E_{\mu,0}(t)|$ of the Hamiltonian reaches a minimum. For small gaps, Landau-Zener transition take place [75,76], which are transitions between adiabatic states $|\psi_\nu(t)\rangle$ and $|\psi_\mu(t)\rangle$. The probability of transition between the two adiabatic states is proportional to $\exp(-\pi/(4\varepsilon_{\mu\nu}(t_{\mathrm{col}})))$ [75,76]. It is evaluated by a linearization of the time-dependence of the Hamiltonian around the time of collision $t_{\mathrm{col}}$. In this formula, we identify a characteristic time of the collision $\tau_{\mu\nu}^{\mathrm{col}} = |E_{\mu,0}-E_{\nu,0}|/\left|\langle\psi_{\mu,0}|\,\frac{\mathrm{d}H}{\mathrm{d}t}\,|\psi_{\nu,0}\rangle\right|$, which converts into an energy broadening $\delta E = \hbar/\tau_{\mu\nu}^{\mathrm{col}}$. Transitions occur when this broadening is comparable with the gap $E_{\mu,0}(t_{\mathrm{col}})-E_{\nu,0}(t_{\mathrm{col}})$, and the parameter $\varepsilon_{\mu\nu}(t_{\mathrm{col}})$, which controls the validity of the adiabatic approximation, identifies with this ratio $\varepsilon_{\mu\nu}(t_{\mathrm{col}}) = \delta E/|E_{\mu,0}-E_{\nu,0}|$.

The Landau-Zener probability is not perturbative in $\varepsilon_{\mu\nu}(t)$. This gives an estimation of the non-perturbative contributions denoted $\mathcal{O}(\lambda^\infty)$ in the time-evolved state (1.48) as

$$|\langle\psi_\mu(t_+)|\,U(t_+,t_-)\,|\psi_\nu(t_-)\rangle|^2 \simeq \exp\left(-\frac{\pi}{4\varepsilon_{\mu\nu}(t_{\mathrm{col}})}\right) \tag{1.55}$$

with the limits of the collision interval $t_\pm = t_{\mathrm{col}} \pm \tau_{\mu\nu}^{\mathrm{col}}/2$, and $U(t_+,t_-)$ the time-evolution operator between these two times. The Landau-Zener collision is a transition process between two adiabatic subspaces.

Note that in the works of Zener [75] and Landau [76], the time-dependence of the Hamiltonian is linearized around the collision time, and the collision are considered between $t_\pm = \pm\infty$. Moreover, they do not consider transition amplitude between adiabatic states but between their zeroth order approximation, the eigenstates $|\psi_{\nu,0}(-\infty)\rangle$ and $|\psi_{\mu,0}(+\infty)\rangle$. For a Hamiltonian depending linearly on time, the adiabatic states identify with the eigenstates in the limit $t \to \pm\infty$, such that we recover Eq. (1.55).

This analysis is particularly useful when we consider a series of similar Landau-Zener transitions separated by a typical mean free time $\tau_{\rm mft}$, for example when the spectrum reaches similar gap minima associated to a typical adiabatic collision parameter. It is then possible to determine the characteristic time of validity of the adiabatic approximation $\tau_{\rm adiab}$ by constraining the cumulative transition probability to be sizable, *e.g.* of order 0.1, such that we get

$$\tau_{\rm adiab} \approx 0.1\ \tau_{\rm mft}\ \exp\left(\frac{\pi}{4\varepsilon_{\mu\nu}(t_{\rm col})}\right). \tag{1.56}$$

Note that for the above analysis to be consistent, the collision time $\tau^{\rm col}_{\mu\nu}$ must be smaller than the mean free time $\tau_{\rm mft}$. Since we focus on aperiodic evolution, we also neglected the effect of relative phases accumulated between the transitions [77].

### 1.2.6 Comment on the denominations

In this manuscript, we denote by "adiabatic" all quantities that express in perturbative expansion of the perturbative parameter $\lambda$. In particular, the first order correction (1.36) of the adiabatic density matrix $\rho_\nu(t)$ is called an "adiabatic effect".

We denote all the quantities which are not perturbative in $\lambda$ as "non-adiabatic", such as the Landau-Zener transition probability.

Sometimes in the literature (see *e.g.* [55]), the denomination "non-adiabatic" is used to refer to any effects originating from corrections to the limit of infinitely slow variation of the Hamiltonian, such as the first order correction (1.36).

## 1.3 Conclusion of chapter

In this chapter, we discussed the perturbation theory of a slowly time-dependent quantum system. We first discussed in Sec. 1.1 the canonical derivation of the time evolution of an instantaneous eigenstate. The adiabatic theorem states that when the quantum system is prepared in an instantaneous eigenstate, then, in the limit of an infinitely slow time dependence of the Hamiltonian, the quantum system remains in an instantaneous eigenstate. We identified the difficulty of the adiabatic perturbation theory, the *a priori* determination of perturbative dimensionless parameter.

We addressed this aspect in Sec. 1.2, by defining a notion of adiabatic state as the dynamical solutions leading to the slowest time-evolution of the physical observables. We construct their density matrix perturbatively, in an adiabatic small quantity which is determined *a posteriori*, requiring that the perturbative expansion is valid.

In the next chapter, we discuss the adiabatic dynamics of a slow-fast quantum system. It corresponds to a closed quantum system with two types of degrees of freedom with

a separation of characteristic dynamical timescales. The external drive imposing a time dependence of the Hamiltonian of a quantum system is replaced by a coupling to a second "slow" dynamical quantum system. We will quantify what we mean by a "slow" dynamical quantum system by defining a notion of adiabatic subspace, following the same method as the one discussed in Sec. 1.2.1 to define adiabatic states. The technical tools to implement this method will be different, in order to keep track of the back-action of the fast subsystem onto the slow one.

Chapter 2

# Slow-fast quantum systems

Slow-fast quantum system are closed quantum system whose dynamics contains a separation of characteristic timescales, or frequency scales. The total system splits in two types of degrees of freedom, the slow and the fast ones, associated to the corresponding timescales. The "adiabatic elimination" consists in deriving an effective dynamics of the slow degrees of freedom accounting for the back action of the fast degrees of freedom. This chapter is an introduction to slow-fast quantum systems, and to the geometrical properties entering the effective dynamics of the slow degrees of freedom. Different examples of possible slow-fast quantum systems with their corresponding slow and fast subsystems are given in Table 2.1.

In Sec. 2.1 we discuss the historical example of a slow-fast quantum system, a molecule. The Born-Oppenheimer method introduces the main ideas of the adiabatic theory of a slow-fast quantum system, in particular a notion of effective subspace. In Sec. 2.2, we discuss the historical example of an electron in a crystal. This example introduces the effective equations of motion within the effective subspace involving the Berry curvature. We will then detail a general theory of adiabatic dynamics of a slow-fast quantum system. The method to construct this adiabatic dynamics is the same as the one introduced in Chap. 1 to define the adiabatic states of a slowly driven quantum system. The technical tools used to implement this method are different. We introduce these tools in Sec. 2.3. We present this theory and its conditions of validity in Sec. 2.4.

### Comment on the notations

In Chap. 1, we considered a slowly time-dependent quantum system. We noted $H(t)$ its time-dependent Hamiltonian, $|\psi_{\nu,0}(t)\rangle$ its instantaneous eigenstates, and $|\psi_\nu(t)\rangle$ its perturbatively constructed adiabatic states.

In this chapter, we are led to consider a Hamiltonian $H(\mathbf{x},\mathbf{p})$ of the fast subsystem depending on phase space variables of the slow subsystem $(\mathbf{x},\mathbf{p})$. We use the notation $|\psi_\nu(\mathbf{x},\mathbf{p})\rangle$ for its eigenstates instead of the notation $|\psi_{\nu,0}(\mathbf{x},\mathbf{p})\rangle$ of Chap. 1. No confusion is possible in this chapter given that, in general, there is no notion of adiabatic states of the fast subsystem, but only a notion of adiabatic states of the total system. We will introduce a notion of adiabatic projector of the total system, which defines the adiabatic states of the total system. Its lowest order (Weyl symbol[1]) is noted

[1]The Weyl symbol of an operator is defined in Sec. 2.3.3.

$\Pi_{\nu,0}(\mathbf{x},\mathbf{p}) = |\psi_\nu(\mathbf{x},\mathbf{p})\rangle\langle\psi_\nu(\mathbf{x},\mathbf{p})|$. The (Weyl symbol of the) adiabatic projector at all orders is noted $\Pi_\nu(\mathbf{x},\mathbf{p})$.

| Total system | Slow degrees of freedom | Fast degrees of freedom |
|---|---|---|
| Molecules | Nuclei positions | Electrons positions |
| Electron in a crystal | Position on Bravais lattice | Dynamics inside unit cell |
| Metals | Phonons | Electrons |
| Frustrated magnets | Collective zero energy modes | Gapped magnon excitations |
| Mesoscopic superconductors | Collective modes | Bogoliubov quasi-particles |
| Superconducting tunnel junctions | Collective modes | Andreev bound states |
| Relativistic spinor | Position and spin | Particle – antiparticle degree of freedom |
| Circuit QED | Cavity electromagnetic modes | Superconducting qubit |

Table 2.1: Examples of slow-fast quantum systems.

## 2.1 Historical Born-Oppenheimer problem

We present the canonical example of a molecule as a slow-fast quantum system using the approach of the Born-Oppenheimer approximation. This method contains the main ideas needed to discuss the geometrical aspects in slow-fast quantum systems.

### 2.1.1 Molecules as canonical slow-fast quantum systems

A molecule is a canonical example of quantum system with slow and fast degrees of freedom. The nuclei being much heavier than the electrons, we expect them to be much slower. We describe a molecule by the positions of the nuclei and the positions of the electrons, ignoring the spin for simplicity. Then the Hilbert space of the total system splits in

$$\mathcal{H}_{\text{tot}} = \mathcal{H}_{\text{nuclei}} \otimes \mathcal{H}_{\text{electrons}}. \tag{2.1}$$

We note collectively $\mathbf{R} = \{R_i\}$ the position coordinates of all the nuclei, and $\mathbf{P}$ their conjugated momenta. We note similarly $\mathbf{r}$ the position coordinates of the electrons and $\mathbf{p}$ the conjugated momenta. To simplify the notations, we assume that all the atoms are of the same element such that all the nuclei have the same mass $M$, and we note $m$ the mass of an electron. The total Hamiltonian of the molecule reads

$$\hat{H}_{\text{tot}} = \sum_i \frac{\hat{P}_i^2}{2M} + \sum_j \frac{\hat{p}_j^2}{2m} + V(\hat{\mathbf{R}},\hat{\mathbf{r}}) \tag{2.2}$$

where $V(\hat{\mathbf{R}},\hat{\mathbf{r}})$ is the potential Coulomb energy of interaction between the nuclei, between the nuclei and the electrons, and between the electrons. The historical work of Born and

Oppenheimer [78] consists in deriving the spectrum of the molecule using perturbation theory in the small ratio $m/M$. However, what is now referred as the Born-Oppenheimer approximation [68,79] is a different method to diagonalize the Hamiltonian of the molecule using important ideas on which this manuscript is rooted.

### 2.1.2 Born-Oppenheimer ansatz and effective Hamiltonian

The starting point of the Born-Oppenheimer approximation amounts to neglect the kinetic energy of the nuclei in the Hamiltonian of the molecule (2.2), in the limit where the mass of the nuclei is larger than the mass of the electrons. The Hamiltonian simplifies into

$$\hat{H} = \sum_j \frac{\hat{p}_j^2}{2m_e} + V(\hat{\mathbf{R}}, \hat{\mathbf{r}}) \tag{2.3}$$

which commutes with the position operators of the nuclei $\hat{\mathbf{R}}$. As such, we can co-diagonalize $\hat{H}$ and the position operators of the nuclei

$$\hat{H} \;\; |\mathbf{R}\rangle \otimes |\psi_\nu(\mathbf{R})\rangle = E_\nu(\mathbf{R}) \;\; |\mathbf{R}\rangle \otimes |\psi_\nu(\mathbf{R})\rangle \tag{2.4}$$

where $|\psi_\nu(\mathbf{R})\rangle \in \mathcal{H}_{\text{electrons}}$ are electronic states. They are the normalized eigenstates of the electronic operator $H(\mathbf{R})$ for fixed positions $\mathbf{R}$ of the nuclei. When we use this form of eigenstates of the molecule, we consider the positions of the nuclei as conserved quantities meaning that they do not change during the dynamics, so we indeed treat the nuclei as infinitely slow.

Then we aim at determining the eigenstates of the molecule treating the kinetic energy of the nuclei as a perturbation. We will use a variational ansatz for this purpose. Let us motivate this ansatz. A small perturbation modify two eigenstates close in energy, for which $E_\nu(\mathbf{R}) - E_{\nu'}(\mathbf{R}')$ is of the order of the perturbation. Moreover, the perturbation is written in terms of the momenta operators of the nuclei, which are local in position. Hence, the perturbation can only alter pairs of eigenstates for which $\mathbf{R} \simeq \mathbf{R}'$. The energy $E_\nu(\mathbf{R})$ being continuous with respect to $\mathbf{R}$ we have $E_\nu(\mathbf{R}) \simeq E_\nu(\mathbf{R}')$ for $\mathbf{R}' \simeq \mathbf{R}$, such that the whole family of states $|\mathbf{R}\rangle \otimes |\psi_\nu(\mathbf{R})\rangle$ for all $\mathbf{R}$ at a fixed $\nu$ is affected by the perturbation. If the energy differences between electronic states of different families $\nu' \neq \nu$ around the same position $E_\nu(\mathbf{R}) - E_{\nu'}(\mathbf{R})$ are sufficiently large, then an eigenstate of the total Hamiltonian (2.2) will decompose mostly onto a simple family of eigenstates $|\mathbf{R}\rangle \otimes |\psi_\nu(\mathbf{R})\rangle$. We thus expect a suitable ansatz for the eigenstates of the total Hamiltonian (2.2) to be

$$|\Psi_{\text{tot}}\rangle = \int \mathrm{d}\mathbf{R} \;\; \chi(\mathbf{R}) \;\; |\mathbf{R}\rangle \otimes |\psi_\nu(\mathbf{R})\rangle \tag{2.5}$$

with a complex function $\chi(\mathbf{R})$ to determine.

Using the variational method with respect to $\chi(\mathbf{R})$ [68,80], we obtain an approximate eigenstate of the total Hamiltonian of energy $E$ for a function $\chi(\mathbf{R})$ satisfying

$$\left[\sum_i \left( \frac{(-i\hbar\partial_{R_i} - \hbar A_{\nu,R_i}(\mathbf{R}))^2}{2M} + \frac{\hbar^2}{2M} g_{\nu,R_i R_i}(\mathbf{R}) \right) + E_\nu(\mathbf{R}) \right] \chi(\mathbf{R}) = E \;\chi(\mathbf{R}), \tag{2.6}$$

with the Mead-Berry connection

$$A_{\nu,R_i}(\mathbf{R}) = i \,\langle \psi_\nu(\mathbf{R}) | \partial_{R_i} \psi_\nu(\mathbf{R}) \rangle \,, \tag{2.7}$$

and the quantum metric

$$g_{\nu,R_iR_i} = \mathrm{Re}\,\langle \partial_{R_i}\psi_\nu | \left(1 - |\psi_\nu\rangle \langle \psi_\nu|\right) |\partial_{R_i}\psi_\nu\rangle\,. \tag{2.8}$$

Let us mention an alternative method to obtain Eq. (2.6), which is more explicit and frequently used. We can decompose generically the total state $|\Psi_{\rm tot}\rangle$ on the basis $\{|\mathbf{R}\rangle\otimes|\psi_\nu(\mathbf{R})\rangle\}_{\mathbf{R},\nu}$ of the total Hilbert space using a family of functions $\chi_\nu(\mathbf{R})$, rather than restrict the decomposition (2.5) on one family $\nu$. Then the time-independent Schrödinger equation leads to coupled differential equations between the $\chi_\nu(\mathbf{R})$. Ignoring the couplings between $\chi_\nu(\mathbf{R})$ and $\chi_{\mu\neq\nu}(\mathbf{R})$ corresponds to the Born-Huang approximation [79] and leads to Eq. (2.6).

### 2.1.3 Born-Oppenheimer method

We summarize the important steps of the Born-Oppenheimer method, which are at the basis of the general adiabatic theory of slow-fast quantum systems exposed in Sec. 2.4. This is often referred as the "adiabatic elimination" because this amounts to eliminate the fast degrees of freedom and to focus only on the slow ones, with the intuition that the state of the fast system is determined by the state of the slow system. In that case it is sufficient to focus on the slow system in order to infer all the information we want on the total system. This is a reduction of the number of degrees of freedom.

The adiabatic elimination can be summarized by the following steps:

1. Identify the slow and fast degrees of freedom.

2. Freeze the slow variables.

3. Parametrize the states of the total system by the states of the slow system.

4. Unfreeze the slow variables.

**Step 1: Identify the slow and fast degrees of freedom.**

This step is immediate when we study a molecule. The fast degrees of freedom are the electrons positions and the slow degrees of freedom are the nuclei positions. This provides the splitting of Hilbert space (2.1).

**Step 2: Freeze the slow variables.**

For the Born-Oppenheimer problem, we freeze the slow variables by considering the case of infinitely massive nuclei, ignoring their kinetic energy in the Hamiltonian. Then the positions of the nuclei are frozen in the sense that they are constants of motion: the remaining Hamiltonian $\hat{H}$ commutes with the positions $\hat{\mathbf{R}}$. The eigenstates of the frozen Hamiltonian are eigenstates of the positions of the slow variables, of the form $|\mathbf{R}\rangle \otimes |\psi_\nu(\mathbf{R})\rangle$.

**Step 3: Parametrize the states of the total system by the states of the slow system.**

The diagonalization of the frozen Hamiltonian gives a decomposition of the total Hilbert into a direct sum of subspaces $\mathcal{H}_{\nu,0}$, which we will call the Born-Oppenheimer subspaces

$$\mathcal{H}_{\text{tot}} = \mathcal{H}_{\text{nuclei}} \otimes \mathcal{H}_{\text{electrons}} = \bigoplus_{\nu} \mathcal{H}_{\nu,0} \tag{2.9}$$

such that intuitively within each subspace $\nu$, we can parametrize the states of the total system by a state of the nuclei lying in $\mathcal{H}_{\text{nuclei}}$. The subscript "0" is used to distinguish the Born-Oppenheimer subspace $\mathcal{H}_{\nu,0}$ from the adiabatic subspace $\mathcal{H}_{\nu}$ detailed in Sec. 2.4. This mapping appears in the decomposition (2.5) of the total state: if we interpret the function $\chi(\mathbf{R})$ as a wavefunction of the nuclei, then every state of $\mathcal{H}_{\nu,0}$ is associated to a state in $\mathcal{H}_{\text{nuclei}}$. We have an approximate isomorphism between $\mathcal{H}_{\nu,0}$ and $\mathcal{H}_{\text{nuclei}}$. In the end of the chapter, we will quantify through the relation (2.108) to which extent the two spaces fail to be exactly isomorphic.

Let us comment this approximate isomorphism by introducing briefly the notion of vector bundle[2]. For each position $\mathbf{R}$ of the nuclei, the $\nu$-th electronic eigenstate $|\psi_\nu(\mathbf{R})\rangle$ defines a one dimensional subspace of $\mathcal{H}_{\text{electrons}}$, noted $\mathbb{C}\,|\psi_\nu(\mathbf{R})\rangle = \{z\,|\psi_\nu(\mathbf{R})\rangle \ ; \ z \in \mathbb{C}\}$. The collection of all of these subspaces for $\mathbf{R}$ lying in the configuration space of the nuclei defines a line bundle over this configuration space. If the configuration space of the slow subsystem is compact, then this line bundle can have a non-trivial topology. In such a case, the isomorphism between the Hilbert space of the slow system and the Born-Oppenheimer subspace $\mathcal{H}_{\nu,0}$ is not guarantied [82–84]. The non-trivial topology of line-bundles plays a central role in this thesis.

The notion of Born-Oppenheimer subspace, and the notion of adiabatic subspace that we will define in Sec. 2.4, are fundamental in this manuscript. They are defined by an orthogonal projector onto this subspace. In the case of Born-Oppenheimer treatment of a molecule, the Born-Oppenheimer projector $\hat{\Pi}_{\nu,0}$ takes the form

$$\hat{\Pi}_{\nu,0} = \int \mathrm{d}\mathbf{R} \ \ |\mathbf{R}\rangle\langle\mathbf{R}| \otimes |\psi_\nu(\mathbf{R})\rangle\langle\psi_\nu(\mathbf{R})| \,. \tag{2.10}$$

**Step 4: Unfreeze the slow variables.**

For a molecule, this corresponds to taking into account the kinetic energy of the nuclei, such that the positions $\mathbf{R}$ of the nuclei are no longer conserved quantities. This step is implemented in different ways in various approaches. The Born-Oppenheimer treatment of a molecule assumes that an eigenstate decomposes within a subspace $\mathcal{H}_{\nu,0}$ and uses a variational method. In the wavepacket approach of the semiclassical dynamics of an electron in a crystal discussed in Sec. 2.2, the state of the electron is assumed to lie within such a subspace $\mathcal{H}_{\nu,0}$ and equations of motion governing the center of the wavepacket are derived from a Lagrangian approach. In the general theory introduced in Sec. 2.4, we rather construct a deformed version of the Born-Oppenheimer subspace $\mathcal{H}_{\nu,0}$, the adiabatic subspace $\mathcal{H}_{\nu}$, which is stable[3] by the dynamics and derive equations governing the evolution of the state within this subspace.

[2] We refer to [61, 81] for an introduction to the mathematical formalism of vector bundles.

[3] The adiabatic subspace is stable up to non-perturbative effects, in a sense precised in Sec. 2.4.

Each of these steps contain different types of difficulties depending on the physical system we consider, which are discussed in this chapter.

### 2.1.4 Role of Mead-Berry connection

#### Interpretation of the function $\chi(\mathbf{R})$

The role of the Mead-Berry connection (2.7) in Eq. (2.6) enlighten an important aspect of step 3 of the adiabatic elimination: the parametrization of the states of the total system in the subspace $\mathcal{H}_{\nu,0}$ by a state of the slow system (the nuclei) in $\mathcal{H}_{\text{nuclei}}$. If we interpret the wavefunction $\chi(\mathbf{R})$ used in the decomposition (2.5) as the wavefunction of the nuclei, then the representation of their momenta $\hat{\mathbf{P}}$ differs from a canonical spatial representation.

To explain this, we recall that the electronic states $|\psi_\nu(\mathbf{R})\rangle$ are defined as eigenstates of the Hamiltonian $H(\mathbf{R})$. This leads to a gauge freedom in the parametrization, where a gauge transformation reads

$$|\psi_\nu(\mathbf{R})\rangle \to |\psi'_\nu(\mathbf{R})\rangle = e^{i\alpha(\mathbf{R})}\,|\psi_\nu(\mathbf{R})\rangle\,, \tag{2.11}$$

$$\chi(\mathbf{R}) \to \chi'(\mathbf{R}) = e^{-i\alpha(\mathbf{R})}\chi(\mathbf{R}), \tag{2.12}$$

and a corresponding transformation of $A_{\nu,R_i}(\mathbf{R})$ as

$$A_{\nu,R_i}(\mathbf{R}) \to A'_{\nu,R_i}(\mathbf{R}) = A_{\nu,R_i}(\mathbf{R}) - \frac{\partial\alpha}{\partial R_i}(\mathbf{R}). \tag{2.13}$$

As such, the modulus square of the function $\chi(\mathbf{R})$ is gauge independent and corresponds indeed to a probability density of position of the nuclei, *i.e.* for an observable $f(\hat{\mathbf{R}})$ depending only on the nuclei positions we have

$$\langle\Psi_{\text{tot}}|\, f(\hat{\mathbf{R}})\,|\Psi_{\text{tot}}\rangle = \int \mathrm{d}\mathbf{R}\ |\chi(\mathbf{R})|^2 f(\mathbf{R}). \tag{2.14}$$

However, the function $\chi(\mathbf{R})$ is not sufficient to get information on the momenta $\hat{P}_i$: the connection components $A_{\nu,R_i}(\mathbf{R})$ are also required,

$$\langle\Psi_{\text{tot}}|\,\hat{P}_i\,|\Psi_{\text{tot}}\rangle = \int \mathrm{d}\mathbf{R}\ \chi(\mathbf{R})^*\left(-i\hbar\partial_{R_i} - \hbar A_{\nu,R_i}(\mathbf{R})\right)\chi(\mathbf{R}), \tag{2.15}$$

which is indeed gauge invariant.

#### Role of connection and curvature

In the early works on the Born-Oppenheimer approximation, the connection $A_{\nu,R_i}(\mathbf{R})$ was often not considered in (2.6), either as an approximation or assuming that a suitable gauge transformation could make it vanish possibly at the cost of considering multivalued electronic eigenstates $|\psi_\nu(\mathbf{R})\rangle$ and multivalued wavefunction $\chi(\mathbf{R})$ [85, 86]. The role of the connection has been identified following the seminal work of Mead and Truhlar [86]. We refer to the review of Mead [87] for discussions of the literature.

For our purpose, we are interested in the case where the curvature of this connection does not vanish[4]

$$F_{\nu,R_iR_j}(\mathbf{R}) = \partial_{R_i}A_{\nu,R_j}(\mathbf{R}) - \partial_{R_j}A_{\nu,R_i}(\mathbf{R}) \neq 0. \tag{2.16}$$

[4]It can vanish locally, for some $\mathbf{R}$, but not globally, not for all $\mathbf{R}$.

The curvature being gauge invariant, in this case there cannot be any gauge transformation for which the connection vanish globally. This connection acts as a vector potential and the Berry curvature as the corresponding effective magnetic field. Then, if we use a correspondence principle from the effective Hamiltonian (2.6) (despite the delicate interpretation of the function $\chi(\mathbf{R})$ explained above), we get classical equations of motion for the nuclei containing an effective Lorentz force originating from this effective magnetic field [80, 88].

The experimental signatures of the geometric phase associated to the Mead-Berry connection were studied in the spectra of molecules [81, 87]. Spectral signatures of topological properties of the fiber bundle of the Born-Oppenheimer decomposition were also studied [82–84]. In this manuscript, we are mainly interested in dynamical signatures. For a review on the different theoretical treatments of the dynamics of electrons and nuclei in molecular systems within the chemical physics community, we refer to [89]. These works do not focus on the geometrical aspects entering effective dynamics.

## 2.2 Semiclassical dynamics of electrons in a crystal

In this section, we discuss the semiclassical dynamics of electrons in a crystal. This is an historical example of slow-fast quantum system for which the Berry curvature was understood to play an important role in the equations of motion of the slow variables. It is also the first example where the Berry curvature depends on compact variables, the Bloch momenta, necessary to define a topological Chen number.

### 2.2.1 Decomposition into slow and fast degrees of freedom

We consider a single electron in a crystal in $d$ dimensions and describe this system as a slow-fast quantum system. We introduce the Bloch theorem as a tool to identify the slow variables of step 1 of the adiabatic elimination introduced in Sec. 2.1.3. This discussion does not only apply to an electron in a crystal but also to any wave in a periodic medium.

We saw in Sec. 2.1 on the Born-Oppenheimer treatment of a molecule that the positions of the nuclei are the slow variables because, in the limit of infinite mass of the nuclei, they are conserved quantities which means that they do not have any dynamics. We follow this strategy to identify the slow degrees of freedom for an electron in a crystal. The Bloch theorem states that the crystal momentum is a good quantum number, *i.e.* a conserved quantity, for a particle in a periodic potential. We thus define a degree of freedom associated to the crystal momentum, with a splitting of the total Hilbert space similar to the splitting (2.1).

#### Splitting of the Hilbert space

The state of the electron $|\Psi\rangle$ is given by a wavefunction $\Psi(\mathbf{x})$ depending on the real space position $\mathbf{x} \in \mathbb{R}^d$

$$|\Psi\rangle = \int_{\mathbb{R}^d} \mathrm{d}\mathbf{x}\ \Psi(\mathbf{x})\ |\mathbf{x}\rangle\,. \tag{2.17}$$

The dynamics of the electron in a periodic potential is given by a Hamiltonian

$$\hat{H} = \frac{\hat{\mathbf{p}}^2}{2m} + V(\hat{\mathbf{x}}) \tag{2.18}$$

where the momentum operator $\hat{\mathbf{p}}$ is $-i\hbar\nabla_{\mathbf{x}}$ in position representation, namely $\langle \mathbf{x}| \hat{p}_i |\Psi\rangle = -i\hbar\partial_{x_i}\Psi(\mathbf{x})$. The potential has the translation symmetry of a Bravais lattice $\Gamma$. We label by $\mathbf{R} \in \Gamma$ the discrete set of Bravais lattice translations which we identify to the discrete set of positions of unit-cells by fixing an origin of space. We have for all $\mathbf{x} \in \mathbb{R}^d$ and $\mathbf{R} \in \Gamma$

$$V(\mathbf{x} + \mathbf{R}) = V(\mathbf{x}). \tag{2.19}$$

We introduce the discrete and compact variables used in the description of an electron in a periodic medium. This discussion is useful to discuss other types of compact variables [90] which will be considered in this manuscript. A position $\mathbf{x}$ in real space is given by a value of unit cell $\mathbf{R}$ and a position $\mathbf{r}$ inside the unit-cell via the unique decomposition $\mathbf{x} = \mathbf{R} + \mathbf{r}$. To consider separately the Bravais lattice position $\mathbf{R} \in \Gamma$ and the position inside the unit-cell $\mathbf{r}$, we define $\Psi(\mathbf{R}, \mathbf{r}) = \Psi(\mathbf{R} + \mathbf{r})$, where we have the subtle periodic conditions

$$(\mathbf{R}, \mathbf{r} + \mathbf{a}) \equiv (\mathbf{R} + \mathbf{a}, \mathbf{r}) \tag{2.20}$$

for $\mathbf{R}, \mathbf{a} \in \Gamma$ and for $\mathbf{r}$ on the boundary of unit cell[5]. Defining $|\mathbf{R}\rangle \otimes |\mathbf{r}\rangle = |\mathbf{R} + \mathbf{r}\rangle$ with the same periodic conditions, we have decomposed the Hilbert space in a discrete degree of freedom $\mathbf{R} \in \Gamma$, and a continuous and compact degree of freedom $\mathbf{r} \in \mathbb{R}^d/\Gamma$

$$\mathcal{H}_{\text{tot}} \simeq \mathcal{H}_{\text{Bravais-lattice}} \otimes \mathcal{H}_{\text{unit-cell}} \tag{2.21}$$

with

$$|\Psi\rangle = \sum_{\mathbf{R}\in\Gamma} \int_{\text{unit-cell}} \mathrm{d}\mathbf{r}\ \Psi(\mathbf{R}, \mathbf{r})\ |\mathbf{R}\rangle \otimes |\mathbf{r}\rangle\,. \tag{2.22}$$

### Discrete and compact variables

We now introduce the Bloch momentum, which is the compact conserved quantity of an electron in a periodic potential. This discussion of compact variables conjugated to discrete variables will also be useful when discussing quantum modes.

The reciprocal lattice $\Gamma^\star$ is made of vectors $\mathbf{G} \in \mathbb{R}^d$ such that $\mathbf{G} \cdot \mathbf{R} \in 2\pi\mathbb{Z}$ for all lattice vectors $\mathbf{R} \in \Gamma$. The Bloch momentum $\mathbf{k}$ lying in the first Brillouin zone $\mathbb{R}^d/\Gamma^\star$ is the momentum of the electron defined up to a reciprocal lattice vector. We can define it in the same way as the position with the unique decomposition $\mathbf{p} = \hbar(\mathbf{G} + \mathbf{k})$ for $\mathbf{p} \in \mathbb{R}^d$, $\mathbf{G} \in \Gamma^\star$ and $\mathbf{k} \in \mathbb{R}^d/\Gamma^\star$. We introduce a compact basis of $\mathcal{H}_{\text{Bravais-lattice}}$ made of $|\mathbf{k}\rangle$ states, Fourier transform of the discrete basis of $|\mathbf{R}\rangle$ states

$$|\mathbf{k}\rangle = \sqrt{\frac{V_{\text{cell}}}{(2\pi)^d}} \sum_{\mathbf{R}\in\Gamma} e^{i\mathbf{k}\cdot\mathbf{R}}\ |\mathbf{R}\rangle \tag{2.23}$$

with $V_{\text{cell}}$ the volume of the unit cell. This is an orthonormal basis of $\mathcal{H}_{\text{unit-cell}}$ when $\mathbf{k} \in$ BZ,

$$\langle \mathbf{k}'|\mathbf{k}\rangle = \delta(\mathbf{k} - \mathbf{k}') \qquad ; \qquad \int_{\text{BZ}} \mathrm{d}\mathbf{k}\, |\mathbf{k}\rangle\langle\mathbf{k}| = \mathbf{1}_{\mathcal{H}_{\text{Bravais-lattice}}}. \tag{2.24}$$

[5] This is due to the embedding $\begin{array}{ccc} \Gamma \times \text{Unit-Cell} & \to & \mathbb{R}^d \\ (\mathbf{R}, \mathbf{r}) & \mapsto & \mathbf{R} + \mathbf{r} \end{array}$.

In short, $\mathcal{H}_{\text{Bravais-lattice}}$ has a discrete basis of states $|\mathbf{R}\rangle$ of position on the Bravais lattice $\mathbf{R} \in \Gamma$, and a compact and continuous basis of states $|\mathbf{k}\rangle$ of crystal momentum $\mathbf{k} \in \mathbb{R}^d/\Gamma^\star$. Similarly, $\mathcal{H}_{\text{unit-cell}}$ has a compact and continuous basis of states $|\mathbf{r}\rangle$ of position in the unit cell $\mathbf{r} \in \mathbb{R}^d/\Gamma$, and a discrete basis of states $|\mathbf{G}\rangle$ of reciprocal lattice vectors $\mathbf{G} \in \Gamma^\star$, even though the latter is rarely used. The Bloch theorem states that the Bloch momentum is a conserved quantity for the Hamiltonian (2.18) associated to the discrete translational symmetry by the Bravais lattice. Similarly, the position of the nuclei is a conserved quantity for a molecule if we ignore the kinetic energy of the nuclei.

However, contrary to the case of a molecule, we usually do not introduce an operator $\hat{\mathbf{k}}$ corresponding to the Bloch momentum acting on $\mathcal{H}_{\text{Bravais-lattice}}$, even if we could by defining (2.23) as its eigenstate associated to the eigenvalue $\mathbf{k}$ such that it corresponds to the periodic operator conjugated to the discrete operator $\hat{\mathbf{R}}$ [90], $[\hat{R}_i, \hat{k}_j] = i\delta_{ij}\mathbf{1}_{\mathcal{H}_{\text{Bravais-lattice}}}$.

### Bloch basis

In the study of an electron in a crystal, it is convenient is to introduce a basis of Bloch states of the total Hilbert space $\mathcal{H}_{\text{tot}}$. This is a basis which has a simple expression in the representation of Bloch momenta and position inside the unit cell. A simple basis is made of $|\mathbf{k}\rangle \otimes |\mathbf{r}\rangle$ with $\mathbf{k} \in \text{BZ}$ and $\mathbf{r} \in \mathbb{R}^d/\Gamma$. However, as discussed below, the position operator of the electron $\hat{\mathbf{x}}$ does not have a convenient expression in this basis. A choice of Bloch basis is characterized by a function $\alpha(\mathbf{k}, \mathbf{r})$, where we define the states $|\mathbf{k}, \mathbf{r}\rangle \in \mathcal{H}_{\text{tot}}$ as

$$|\mathbf{k}, \mathbf{r}\rangle = e^{i\alpha(\mathbf{k},\mathbf{r})} |\mathbf{k}\rangle \otimes |\mathbf{r}\rangle = \sqrt{\frac{V_{\text{cell}}}{(2\pi)^d}} \sum_{\mathbf{R}\in\Gamma} e^{i\mathbf{k}\cdot\mathbf{R}} e^{i\alpha(\mathbf{k},\mathbf{r})} |\mathbf{R}\rangle \otimes |\mathbf{r}\rangle . \tag{2.25}$$

The choice of function $\alpha(\mathbf{k}, \mathbf{r})$ corresponds to a choice of convention of Fourier transform, or geometrically to a choice of trivialization of the Bloch bundle [62] which is not canonical. This ensemble of states is a basis of the total Hilbert space when $\mathbf{k} \in \text{BZ}$ and $\mathbf{r} \in$ unit-cell

$$\langle \mathbf{k}', \mathbf{r}' | \mathbf{k}, \mathbf{r} \rangle = \delta(\mathbf{k} - \mathbf{k}')\delta(\mathbf{r} - \mathbf{r}') \qquad ; \qquad \int_{\text{BZ}} \mathrm{d}\mathbf{k} \int_{\text{unit-cell}} \mathrm{d}\mathbf{r} \ |\mathbf{k}, \mathbf{r}\rangle \langle \mathbf{k}, \mathbf{r}| = \mathbf{1}_{\mathcal{H}_{\text{tot}}}. \tag{2.26}$$

A Bloch state $|\mathbf{k}, u\rangle$ is characterized by a crystal momentum $\mathbf{k} \in \text{BZ}$ and a state $|u\rangle \in \mathcal{H}_{\text{unit-cell}}$ which is given by a periodic function satisfying $u(\mathbf{x} + \mathbf{a}) = u(\mathbf{x})$. It is defined by

$$|\mathbf{k}, u\rangle = \int_{\text{unit-cell}} \mathrm{d}\mathbf{r} \ u(\mathbf{r}) \ |\mathbf{k}, \mathbf{r}\rangle = \int_{\mathbb{R}^d} \mathrm{d}\mathbf{x} \ e^{i\mathbf{k}\cdot\mathbf{R} + i\alpha(\mathbf{k},\mathbf{r})} u(\mathbf{r}) \, |\mathbf{x}\rangle , \tag{2.27}$$

where in the last expression, $\mathbf{R}$ and $\mathbf{r}$ are defined from the unique decomposition $\mathbf{x} = \mathbf{R}+\mathbf{r}$.

Note that the Bloch base states $|\mathbf{k}, \mathbf{r}\rangle$ are separable for the decomposition (2.21) of the total Hilbert space but in general a Bloch state $|\mathbf{k}, u\rangle$ defined from a state $|u\rangle \in \mathcal{H}_{\text{unit-cell}}$ is not separable unless $\alpha(\mathbf{k}, \mathbf{r}) = a(\mathbf{k})b(\mathbf{r})$. A choice which would seem practical is to consider $\alpha(\mathbf{k}, \mathbf{r}) = 0$. This would be the case in the discussion of the Born-Oppenheimer treatment of a molecule, where $\mathbf{k}$ would be replaced by the momentum $\mathbf{P}$ of the nuclei and $\mathbf{r}$ by the position of the electron. This will be also the case in Chap. 5 where we consider the dynamics of quantum modes topologically coupled to a qubit, where $\mathbf{k}$ will be replaced by the phase $\boldsymbol{\phi}$ of the modes and $|\mathbf{r}\rangle$ by base states of the qubit Hilbert space.

However, this is not a practical choice in the case of an electron in a crystal. The reason is that we are interested in the position operator $\hat{\mathbf{x}}$ which acts on $\mathcal{H}_{\text{tot}}$ and not

solely on $\mathcal{H}_{\text{Bravais-lattice}}$, so a separable basis has no reason to be particularly suited. The use of the Bloch theorem gives an "almost" canonical choice [62]

$$\alpha(\mathbf{k}, \mathbf{r}) = \mathbf{k} \cdot \mathbf{r}, \tag{2.28}$$

such that the state (2.27) is a common eigenstate of the all operators of translation by lattice vectors $\mathbf{R} \in \Gamma$. We describe this choice in the following paragraph.

### Choice of Bloch basis from Bloch theorem

The Bloch theorem states that the eigenstates $|\psi_{\nu,\mathbf{k}}\rangle$ of the total Hamiltonian are labelled by $\mathbf{k} \in \text{BZ}$ and by a band index $\nu$ such that their wavefunction has the form

$$\psi_{\nu,\mathbf{k}}(\mathbf{x}) = e^{i\mathbf{k}\cdot\mathbf{x}} u_\nu(\mathbf{k}, \mathbf{x}) \tag{2.29}$$

with a periodic Bloch function $u_\nu(\mathbf{k}, \mathbf{x} + \mathbf{R}) = u_\nu(\mathbf{k}, \mathbf{x})$. This means that the eigenstates $|\psi_{\nu,\mathbf{k}}\rangle \in \mathcal{H}_{\text{tot}}$ are common eigenstates of the Hamiltonian $\hat{H}$ and all the operators $e^{-\frac{i}{\hbar}\hat{\mathbf{p}}\cdot\mathbf{R}}$ of translations in real space by lattice vectors $\mathbf{R} \in \Gamma$:

$$e^{-\frac{i}{\hbar}\hat{\mathbf{p}}\cdot\mathbf{R}} |\psi_{\nu,\mathbf{k}}\rangle = e^{-i\mathbf{k}\cdot\mathbf{R}} |\psi_{\nu,\mathbf{k}}\rangle , \tag{2.30}$$

$$\hat{H} |\psi_{\nu,\mathbf{k}}\rangle = E_\nu(\mathbf{k}) |\psi_{\nu,\mathbf{k}}\rangle . \tag{2.31}$$

We check that to write $|\psi_{\nu,\mathbf{k}}\rangle$ under the form (2.27), we have to consider $\alpha(\mathbf{k}, \mathbf{r}) = \mathbf{k} \cdot \mathbf{r}$

$$|\psi_{\nu,\mathbf{k}}\rangle = |\mathbf{k}, u_\nu(\mathbf{k})\rangle \qquad \text{if } \alpha(\mathbf{k}, \mathbf{r}) = \mathbf{k} \cdot \mathbf{r}. \tag{2.32}$$

This choice gives a natural expression of the Bloch basis in the real space basis $|\mathbf{x}\rangle$ of $\mathcal{H}_{\text{tot}}$, with $\mathbf{x} \in \mathbb{R}^d$

$$|\mathbf{k}, \mathbf{r}\rangle = \sqrt{\frac{V_{\text{cell}}}{(2\pi)^d}} \sum_{\mathbf{R}\in\Gamma} e^{i\mathbf{k}\cdot\mathbf{R}} e^{i\alpha(\mathbf{k},\mathbf{r})} |\mathbf{R}\rangle \otimes |\mathbf{r}\rangle \tag{2.33}$$

$$= \sqrt{\frac{V_{\text{cell}}}{(2\pi)^d}} \sum_{\mathbf{R}\in\Gamma} e^{i\mathbf{k}\cdot(\mathbf{r}+\mathbf{R})} |\mathbf{r} + \mathbf{R}\rangle \qquad \text{if } \alpha(\mathbf{k}, \mathbf{r}) = \mathbf{k} \cdot \mathbf{r}. \tag{2.34}$$

This is the reason why these states diagonalize the translations by lattice vectors.

### Projected observables and covariant derivative

Let us explain that the previous choice of Bloch basis is useful to manipulate the position operator $\hat{\mathbf{x}}$. We consider a wavepacket projected in a band $\nu$

$$|\Psi\rangle = \int_{\text{BZ}} \mathrm{d}\mathbf{k}\ \chi(\mathbf{k})\ |\psi_{\nu,\mathbf{k}}\rangle . \tag{2.35}$$

In this case, as already noticed by Blount in the beginning of the formalism of band theory [91] and then highlighted by King-Smith and Vanderbilt studying electric polarization [92] the action of the projected position operator on such projected state corresponds to a covariant derivative with respect to the connection

$$A_{\nu,i}(\mathbf{k}) = i \langle u_\nu(\mathbf{k}) | \partial_{k_i} u_\nu(\mathbf{k}) \rangle = i \int_{\text{unit-cell}} \mathrm{d}\mathbf{r}\ u_\nu(\mathbf{k}, \mathbf{r})^* \frac{\partial u_\nu}{\partial k_i}(\mathbf{k}, \mathbf{r}), \tag{2.36}$$

*i.e.*

$$\langle\Psi|\,\hat{x}_i\,|\Psi\rangle = \int_{\mathrm{BZ}} \mathrm{d}\mathbf{k}\ \chi^*(\mathbf{k})\left(i\frac{\partial}{\partial k_i} + A_{\nu,i}(\mathbf{k})\right)\chi(\mathbf{k}) \qquad \text{if } \alpha(\mathbf{k},\mathbf{r}) = \mathbf{k}\cdot\mathbf{r}. \tag{2.37}$$

This is also the reason why such convention is well suited when we consider a tight-binding Hamiltonian, where we replace the unit cell positions $|\mathbf{r}\rangle$ by orbital degrees of freedom $|j\rangle$ localized around $\mathbf{r}_j$ on the unit-cell, such that we should consider $\alpha(\mathbf{k}, j) = \mathbf{k}\cdot\mathbf{r}_j$ to have a similar expression of the position operator $\hat{\mathbf{x}}$ [62, 63, 93]. But if we are interested in other observables, other conventions can be more convenient.

### 2.2.2 Semiclassical dynamics of center of wavepacket

The Bloch theorem provides a splitting of the Hilbert space of an electron in a crystal into band subspaces $\mathcal{H}_{\nu,0}$

$$\mathcal{H}_{\mathrm{tot}} = \bigoplus_{\nu} \mathcal{H}_{\nu,0} \tag{2.38}$$

where the projector on each band $\nu$ is defined by

$$\hat{\Pi}_{\nu,0} = \int_{\mathrm{BZ}} \mathrm{d}\mathbf{k}\ \ |\psi_{\nu,\mathbf{k}}\rangle\langle\psi_{\nu,\mathbf{k}}|\,. \tag{2.39}$$

This is a spectral decomposition of the total Hilbert space, in the sense that each subspace $\mathcal{H}_{\nu,0}$ is stable under the dynamics of the translation invariant $\hat{H}$ (2.18). This is in contrast to the Born-Oppenheimer subspaces introduced in Sec. 2.1 which are not stable under the dynamics of the total Hamiltonian of the molecule but only under the dynamics of the Hamiltonian (2.3) where we ignore the mass of the nuclei. So step 2 of adiabatic elimination, the freezing of the slow variables, is already done if we consider an unperturbed crystal.

If the electron is also coupled to a weak and slowly varying in space classical electromagnetic field, then the translational symmetry by the Bravais lattice vectors is broken, and the Bloch momentum is no longer a conserved quantity. By Peierls substitution [94], the Hamiltonian reads

$$\hat{H}_{\mathrm{tot}} = \frac{1}{2m}\left(\hat{\mathbf{p}} + e\boldsymbol{\mathcal{A}}(\hat{\mathbf{x}})\right)^2 + V(\hat{\mathbf{x}}) - e\phi(\hat{\mathbf{x}}) \tag{2.40}$$

with $\boldsymbol{\mathcal{A}}(\mathbf{x})$ the electromagnetic vector potential and $\phi(\mathbf{x})$ the electromagnetic scalar potential.

The Bravais lattice translational symmetry of the Hamiltonian $\hat{H}$ (2.18) is broken in the perturbed Hamiltonian $\hat{H}_{\mathrm{tot}}$. We use respectively the notations $\hat{H}_{\mathrm{tot}}$ and $\hat{H}$ to keep the parallel with respectively the total Hamiltonian $\hat{H}_{\mathrm{tot}}$ of the molecule (2.2) and the Hamiltonian $\hat{H}$ (2.3) of the molecule without the kinetic energy of the nuclei, under which the position of the nuclei is conserved ($\hat{H}$ is symmetric by nuclei momenta translations).

We are now interested in the semiclassical dynamics of the electron. Historically, one of the strategies to derive the equations of motion governing the center of an electronic wavepacket was to construct an effective Hamiltonian and to use the correspondence principle [94]. This is similar to the correspondence principle mentioned in Sec. 2.1.4 to derive effective equations of motion for the nuclei position in the Born-Oppenheimer treatment of a molecule.

We do not discuss the vast literature on this subject but rather present the theory based on electronic wavepackets projected into a band because this theory highlights the role of the Berry curvature in the dynamics. It is rooted in the works of Chang, Niu, and Sundaram [95–97], and is detailed in the review [13]. We do not enter into the technical details of this theory but rather explain the main strategy, the difficulties and the limitations.

A core assumption of this approach consists in focusing on electronic wavepacket projected into a band of the unperturbed Hamiltonian $\hat{H}$ and localized in phase space

$$|\Psi\rangle = \int_{\mathrm{BZ}} \mathrm{d}\mathbf{k}\ \chi(\mathbf{k})\ \ |\psi_{\nu,\mathbf{k}}\rangle \tag{2.41}$$

which is similar to considering a Born-Oppenheimer state in Eq. (2.5). The center of the wavepacket in crystal momentum is $\mathbf{k}_c = \int_{\mathrm{BZ}} \mathrm{d}\mathbf{k}\ \mathbf{k}|\chi(\mathbf{k})|^2$, and the center in real space is $\mathbf{x}_c = \langle\Psi|\,\hat{\mathbf{x}}\,|\Psi\rangle$. In order to determine the time-evolution of the center of the wavepacket, the total Hamiltonian is linearized around it. A subtlety of this linearization is that the unperturbed Hamiltonian $\hat{H}$ – from which we define the Bloch eigenstates – is defined from a linearization in position of the total Hamiltonian $\hat{H}_{\mathrm{tot}}$ around the center of the wavepacket $\mathbf{x}_c$. As such, the Bloch eigenstates $|\psi_{\nu,\mathbf{k}}\rangle$ depend on $\mathbf{x}_c$, and also enter the definition of $\mathbf{x}_c$ *via* $\mathbf{x}_c = \langle\Psi|\,\hat{\mathbf{x}}\,|\Psi\rangle$. This leads to a self-consistent definition of the center of the wavepacket. The strategy is then to consider $\mathbf{x}_c$ and $\mathbf{k}_c$ as classical dynamical variables and determine their equation of motion. Niu *et al.* introduced a Lagrangian governing the dynamics of $\mathbf{x}_c$ and $\mathbf{k}_c$

$$L(\mathbf{x}_c, \dot{\mathbf{x}}_c, \mathbf{k}_c, \dot{\mathbf{k}}_c) = \langle\Psi|\left(i\hbar\partial_t - \hat{H}_{\mathrm{tot}}\right)|\Psi\rangle\,. \tag{2.42}$$

The linearization of the total Hamiltonian induces a term in the Lagrangian involving the average value of the position operator $\hat{\mathbf{x}}$ which, as given by Eq. (2.37), depends on the connection (2.36), such that the corresponding equations of motion involve the Berry curvature. We do not detail the derivation of the equations of motion from the Lagrangian. They read [13]

$$\dot{\mathbf{r}}_c = \frac{1}{\hbar}\nabla_{\mathbf{k}_c} E_{\nu,m} - \dot{\mathbf{k}}_c \times \mathbf{F}_\nu, \tag{2.43a}$$

$$\hbar\dot{\mathbf{k}}_c = -e\mathbf{E} - e\dot{\mathbf{r}}_c \times \mathbf{B}. \tag{2.43b}$$

These equations involve the electric field $\mathbf{E}(\mathbf{x}_c) = -\nabla_{\mathbf{x}}\phi(\mathbf{x}_c)$, the magnetic field $\mathbf{B}(\mathbf{x}_c) = \nabla_{\mathbf{x}} \times \boldsymbol{\mathcal{A}}(\mathbf{x}_c)$, the Berry curvature written as a 3-dimensional vector

$$\mathbf{F}_\nu(\mathbf{k}_c) = \nabla_{\mathbf{k}} \times \mathbf{A}_\nu(\mathbf{k}_c) \tag{2.44}$$

where the connection is written as a 3-dimensional vector $\mathbf{A}_\nu$ whose components are given by Eq. (2.36), and a modified band energy

$$E_{\nu,m}(\mathbf{k}_c) = E_\nu(\mathbf{k}_c) - \mathbf{B}\cdot\mathbf{m}_\nu(\mathbf{k}_c) \tag{2.45}$$

with the orbital magnetic moment of Bloch electrons

$$\mathbf{m}_\nu(\mathbf{k}) = -i\frac{e}{2\hbar}\left[\langle\nabla_{\mathbf{k}}u_\nu(\mathbf{k})| \times \left(E_\nu(\mathbf{k}) - H(\mathbf{k})\right)|\nabla_{\mathbf{k}}u_\nu(\mathbf{k})\rangle\right] \tag{2.46}$$

with the Bloch Hamiltonian $H(\mathbf{k}) = \exp(-i\mathbf{k}\cdot\hat{\mathbf{x}})\hat{H}\exp(i\mathbf{k}\cdot\hat{\mathbf{x}})$.

In the first historical studies of the semiclassical dynamics of an electron in a crystal, the role of the Berry curvature was not highlighted in the equations of motion [98]. The semiclassical dynamics of an electron was understood by considering only a group velocity $\nabla_{\mathbf{k}} E_\nu/\hbar$.

In one dimension, the Berry curvature and magnetic field vanishes, such that for a uniform electric field Eq. (2.43b) leads to a linear increase in time of the crystal momentum, which corresponds to a periodic motion through the one dimensional Brillouin zone. The energy being periodic in momentum, this translates *via* Eq. (2.43a) into periodic oscillations in real space, named Bloch oscillations [99, 100], at a period $h/(ea|\mathbf{E}|)$ with $a$ the size of the lattice unit cell.

In this manuscript, we are mostly interested in the role of the Berry curvature in the equations of motion. In the absence of a magnetic field $\mathbf{B} = 0$, the Berry curvature leads to a contribution to the velocity $\dot{\mathbf{r}}_c$ transverse to the electric field $e\mathbf{E} \times \mathbf{F}_\nu/\hbar$ called the anomalous velocity. It was discovered earlier by Karplus and Luttinger in the study of the Hall effect in ferromagnets [91, 101].

In terms of slow-fast quantum system, there is an important difference between the semiclassical dynamics of an electron in a crystal and the Born-Oppenheimer treatment of a molecule. Eq. (2.43) are equations governing the center of the electron wavepacket $\mathbf{x}_c$ and $\mathbf{k}_c$. They do not correspond to observables of the slow subsystem of the decomposition Eq. (2.21), because $\mathbf{x}_c$ is a position in real space, so an observable of the total system $\mathcal{H}_{\text{tot}}$, and not the Bravais lattice position $\mathbf{R}$. In contrast, in the Born-Oppenheimer method, the effective equations are written in terms of the slow degrees of freedom only, namely the positions of the nuclei.

### 2.2.3 Experimental signatures

This semiclassical theory of electron dynamics in a crystal ignores incoherent scattering of the electron on impurities. As such, it is valid to describe the dynamics of the electron on timescales shorter than its scattering time. Historically the observation of Bloch oscillations in semiconductors was very difficult because the scattering time of electrons is usually shorter than the Bloch period $h/(ea|\mathbf{E}|)$. This difficulty was overcome experimentally using semiconductor superlattices to increase the lattice spacing $a$ and thus reduce the Bloch period [102].

The use of the semiclassical dynamics of a wavepacket to measure experimentally the Berry curvature in cold atom experiments was proposed theoretically in 2012 and 2013 [103, 104]. It was then realized experimentally with ultracold fermions in an optical lattice implementation of the Haldane model [105], and with ultracold bosons in an implementation of Hofstadter bands [106]. Such local Hall deflection in ultracold atoms platform were observed in anomalous Floquet topological systems [107, 108]. Similar role of the Berry curvature in the dynamics of excitons was proposed theoretically [109] and observed experimentally [110] in 2017. Measurements of the Berry curvature *via* the anomalous velocity were realized in photonic systems in 2017 [111], and in polariton systems in 2020 [112]. The anomalous Hall drift along a synthetic dimension made of magnetic sublevels of an atom was observed experimentally in 2020 [113].

### 2.2.4 Adiabaticity beyond semiclassical wavepacket states

The theory of semiclassical dynamics of electronic wavepackets uses both a semiclassical approximation and an adiabatic approximation. The adiabatic approximation is related to the assumption that the state (2.41) of the electron stays projected in a band $\mathcal{H}_{\nu,0}$, whereas the semiclassical approximation is the assumption that the wavepacket is localized in phase space such that it can be characterized by its average value of position and crystal momentum.

In this theory, it is not clear how to quantify separately the conditions of validity of both approximations. In particular, the condition of adiabaticity is less restrictive than the semiclassical approximation. The use of the effective equations of motion enables us to describe the dynamics of a larger class of initial states containing but not restricted to semiclassical wavepacket states. We discuss this point in the next section and in Chap. 5.

## 2.3 Framework of adiabatic perturbation theory

In Sec. 2.4, we will detail the general theory of adiabatic dynamics of a slow-fast quantum system. We will present this theory according to the method we used in the first chapter to define and construct the adiabatic states of a slowly driven quantum system, detailed in Sec. 1.2.1. The technical tools to implement this method in the context of slow-fast quantum system are different from those of the first chapter.

In Sec. 2.3.1, we recall our strategy introduced in the first chapter, which involves a variable $\lambda$ interpolating between a physical problem where the dynamics simplifies and the physical problem we are interested in. In Sec. 2.3.2, we argue that this variable should be introduced *via* the commutator of the slow variables. In Sec. 2.3.3, we introduce the Wigner-Weyl representation, which is a phase space representation of quantum mechanics well suited for perturbation theory in the variable introduced in Sec. 2.3.2. Finally, in Sec. 2.3.4, we discuss related approaches of the literature using this phase space representation, and their main differences with our approach.

### 2.3.1 Adiabatic perturbative expansion

We recall our approach to study slow-fast systems. We study a quantum mechanical system for which we suppose a separation of time-scales controlled by dimensionless quantities, which are not known *a priori*. In the limit where these quantities go to zero, the dynamics simplifies. To identify these quantities, we introduce a smooth extrapolation controlled by a variable $\lambda$, where the limit $\lambda \to 0$ corresponds to the limit where the dynamics simplifies, and the limit $\lambda \to 1$ corresponds to the physical problem we are considering. The goal is to construct observables of interest perturbatively in $\lambda$.

The central object which we will determine perturbatively is a projector $\hat{\Pi}_\nu$ acting on the total system, which we call the adiabatic projector. It is defined by an asymptotic series in $\lambda$

$$\hat{\Pi}_\nu = \hat{\Pi}_{\nu,0} + \lambda\hat{\Pi}_{\nu,1} + \lambda^2\hat{\Pi}_{\nu,2} + \cdots = \sum_k \lambda^k \hat{\Pi}_{\nu,k}. \tag{2.47}$$

We recall the meaning of such asymptotic series:

(i) For the expansion to be relevant, the first order correction $\hat{\Pi}_{\nu,1}$ has to be small compared to the lowest order $\hat{\Pi}_{\nu,0}$. We will explain how we compare two operators.

(ii) The leading terms often provide a good approximation of the solution $\hat{\Pi}_\nu$. In other words, $\sum_{k=0}^{N} \hat{\Pi}_{\nu,k}$ provides a good estimation of the adiabatic projector of the problem as long as $\hat{\Pi}_{\nu,N}$ is much smaller than the previous orders.

(iii) The series cannot capture non-perturbative effects[6] in $\lambda$, denoted $\mathcal{O}(\lambda^\infty)$.

The dimensionless quantities controlling the separation of timescales of the quantum system are identified from the condition (i). We will determine them quantitatively in Sec. 2.4.4. In particular, we precise the notion of "slowness" of the slow subsystem, and we obtain new conditions in terms of gauge covariant tensors which were not discussed previously in the literature.

### 2.3.2 Role of the commutator of the slow variables

In this section, we introduce the variable $\lambda$ of the adiabatic perturbation theory from the commutator of the slow observables. Let us motivate this by extending the Born-Oppenheimer treatment of a molecule to other physical systems. The Born-Oppenheimer treatment of a molecule uses the core property that the electrons couple only to the position of the nuclei and not to their momentum. As such, when we ignore the kinetic energy of the nuclei, the corresponding Hamiltonian $\hat{H}$ (2.3) depends only on the positions of the nuclei, which are commuting operators. In other words, $\hat{H}$ is invariant by translation of the nuclei momenta. We can then diagonalize $\hat{H}$ and the positions $\hat{\mathbf{R}}$ at the same time. The corresponding eigenstates $|\mathbf{R}\rangle \otimes |\psi_\nu(\mathbf{R})\rangle$ are obtained by a diagonalization of the Hamiltonian of the electron with fixed nuclei positions $H(\mathbf{R})$. Similarly, in the case of an electron in a crystal, in absence of electromagnetic fields, the Hamiltonian is invariant under translation by Bravais lattice vectors, and the eigenstates of the Hamiltonian are also eigenstates of Bloch momenta. In the following, we consider a more general situation where the fast quantum system couples to non-commuting observables of the slow quantum system, such that no symmetry preserves the slow-fast decomposition.

#### Notations

We consider a quantum system made of two subsystems, the slow and the fast subsystem. The total Hilbert space splits into

$$\mathcal{H}_{\text{tot}} = \mathcal{H}_{\text{slow}} \otimes \mathcal{H}_{\text{fast}}. \tag{2.48}$$

The slow subsystem is composed of $N$ degrees of freedom corresponding to conjugated operators $\hat{x}_i$, $\hat{p}_i$, $i = 1, \dots, N$, noted collectively $\hat{\mathbf{x}}$ and $\hat{\mathbf{p}}$. In the case of a molecule, they correspond respectively to the positions and momenta of the nuclei $\mathbf{R}$ and $\mathbf{P}$, whereas

[6] We recall that a typical non-perturbative term in $\lambda$ has the form $\exp(-\alpha/\lambda)$. They are physically relevant, like the tunnel effect or the Landau-Zener transitions of a time-dependent quantum system discussed in Sec. 1.2.5.

for an electron in a crystal they correspond respectively to the position on Bravais lattice and Bloch momentum $\mathbf{R}$ and $\mathbf{k}$.

We note $\hat{H}_{\text{tot}}$ the Hamiltonian of the total system. We can decompose the Hamiltonian $\hat{H}_{\text{tot}}$ of the total system into

$$\hat{H}_{\text{tot}} = \hat{H}_{\text{slow}} + \hat{H}, \tag{2.49}$$

where $\hat{H}_{\text{slow}}$ is the bare Hamiltonian of the slow subsystem, acting solely on $\mathcal{H}_{\text{slow}}$, whereas $\hat{H}$ contains the bare Hamiltonian of the fast subsystem as well as coupling between the two subsystems. In the following, $\hat{H}$ is called the fast Hamiltonian.

The decomposition (2.49) is physically natural, but is not essential for the theory. The fast timescales will be derived from $\hat{H}$ only, but the slow timescales will be derived from the total Hamiltonian $\hat{H}_{\text{tot}}$ and not solely from $\hat{H}_{\text{slow}}$. In short, what is key is not to determine the decomposition (2.49), but rather to identify in the total Hamiltonian the observables $\hat{\mathbf{x}}$ and $\hat{\mathbf{p}}$ which we physically expect to be slow.

In the following, we write the operators acting on the slow subsystem $\mathcal{H}_{\text{slow}}$ with hats, such as $\hat{x}_i$. We also write the operators acting on both subsystems with hats, such as the Hamiltonian $\hat{H}$ of a molecule without the kinetic energy of the nuclei of Eq. (2.3). On the other hand, operators acting solely on the fast subsystem are written without hat, such as the operator $H(\mathbf{R})$ acting on the electrons with fixed position of the nuclei introduced in Sec. 2.1.2. This convention is useful to distinguish easily between operators and Weyl symbols in the following.

### Perturbative variable $\lambda$

In the case of a molecule or of an electron in a crystal, $\hat{H}$ depends only on commuting observables of the slow subsystem: respectively the positions $\hat{\mathbf{R}}$ of the nuclei or the Bloch momenta $\hat{\mathbf{k}}$. To diagonalize $\hat{H}$ we can freeze the slow variables and diagonalize the remaining Hamiltonian of the fast system for each value of the slow variables, leading respectively to the electronic eigenstates $|\psi_\nu(\mathbf{R})\rangle$ for the molecule and the unit-cell periodic Bloch states $|u_\nu(\mathbf{k})\rangle$ for the electron in a crystal. This corresponds to the Step 2 of the Born-Oppenheimer method discussed in Sec. 2.1.2.

In the general case where $\hat{H}$ depends on both $\hat{\mathbf{x}}$ and $\hat{\mathbf{p}}$, it is not possible to freeze all the slow variables because $\hat{x}_i$ and $\hat{p}_i$ do not commute. The intuitive strategy is to build a perturbative theory whose perturbative parameter corresponds to this commutator. Intuitively, the lowest order of this approximation corresponds to commuting $\hat{\mathbf{x}}$ and $\hat{\mathbf{p}}$ such that we freeze them and diagonalize the remaining Hamiltonian acting on the fast subsystem.

Besides, the physical intuition about the ideal adiabatic limit is that all slow variables involved in the total Hamiltonian are constants of motion. So we have to consider their commutator with the total Hamiltonian $\hat{H}_{\text{tot}}$, and not only with $\hat{H}$. Phrased differently, in Heisenberg representation, the time variation of these observables is given by their commutator with the total Hamiltonian. One way to recover the limit of infinitely slow observables is then to rescale their commutator.

We thus introduce a family of physical problems indexed by the variable $\lambda$, given by the Hilbert space and Hamiltonian introduced above. For each problem, the operators of the slow subsystem satisfy

$$[\hat{x}_i, \hat{p}_j] = \lambda i\hbar\delta_{ij}\mathbf{1}. \tag{2.50}$$

As such, the $\lambda \to 0$ limit corresponds to a problem where all the observables of the slow subsystem commute with the total Hamiltonian, so they are conserved quantity: they do not change with respect to time. So this limit corresponds indeed to the limit of an infinitely slow subsystem.

Let us comment on the physical dimension of the commutator of the slow observables. In the case of an electron in a crystal, the operators of the slow subsystem are the Bravais lattice position $\hat{\mathbf{R}}$ and the Bloch momenta $\hat{\mathbf{k}}$ introduced in Sec. 2.2.1. Their commutator does not involve $\hbar$. To build a perturbation theory in this case, the variable $\lambda$ is introduced as

$$[\hat{R}_i, \hat{k}_j] = \lambda i \delta_{ij} \mathbf{1}. \tag{2.51}$$

Similarly, if the slow subsystem is made of quantum electromagnetic modes, $\hat{x}_i$ and $\hat{p}_i$ can correspond to quadratures of the field, which can be adimensionalized, such that their commutator is $i\mathbf{1}$. In this case, the starting point is also a commutation relation with the variable $\lambda$ and no factor $\hbar$. In the following, we consider that the commutator of the conjugated observables of the slow subsystem involves $\hbar$ through (2.50). Namely, $x_i$ and $p_i$ have the dimension of classically conjugated physical observables.

### 2.3.3 Wigner-Weyl phase space representation

We want to construct a perturbation theory in $\lambda$ introduced in Eq. (2.50). A suited technical tool to perform computation in perturbative series in the scale of commutators is the Wigner-Weyl representation. We present in this section the most useful technical aspects of this representation and refer to the Appendix 2.A for further technical details.

Different aspects of this representation were first introduced by Wigner [114], Weyl [115], Baker [116], Moyal [117], and Bopp [118], as well as Blount [91] in the context of band theory. For pedagogical introductions of these notions, we refer the reader to [119–121].

#### Weyl symbol

The Wigner-Weyl representation is a phase space representation of quantum mechanics. In this representation, an operator $\hat{A}$ acting on the total system $\mathcal{H}_{\text{tot}}$ is represented by a function of operators $A(\mathbf{x}, \mathbf{p})$. For each point $(\mathbf{x}, \mathbf{p})$ in the phase space of the slow system, $A(\mathbf{x}, \mathbf{p})$ is an operator acting on the fast subsystem $\mathcal{H}_{\text{fast}}$. $A(\mathbf{x}, \mathbf{p})$ is called the Weyl symbol, or symbol, of the operator $\hat{A}$.

We consider that the slow variables have a continuous and infinite domain $\mathbf{x}, \mathbf{p} \in \mathbb{R}^N$. This is the case for the position and momentum of the nuclei of a molecule, and for quadratures of a quantum electromagnetic mode. We discuss below the case of discrete and compact variables like the Bravais lattice position and Bloch momenta.

The symbol $A(\mathbf{x}, \mathbf{p})$ of the operator $\hat{A}$ and is defined by

$$A(\mathbf{x}, \mathbf{p}) = \int \mathrm{d}\mathbf{y} \ \exp\left(-i \frac{\mathbf{p} \cdot \mathbf{y}}{\lambda \hbar}\right) \left\langle \mathbf{x} + \frac{\mathbf{y}}{2} \middle| \hat{A} \middle| \mathbf{x} - \frac{\mathbf{y}}{2} \right\rangle. \tag{2.52}$$

Note that if the operator $\hat{A}$ acts on the slow subsystem $\mathcal{H}_{\text{slow}}$ only, then $A(\mathbf{x}, \mathbf{p})$ is a scalar. In general, $A(\mathbf{x}, \mathbf{p})$ is an operator acting on $\mathcal{H}_{\text{fast}}$.

Conversely, the expression of the operator $\hat{A}$ from its symbol $A(\mathbf{x}, \mathbf{p})$ is given by

$$\langle \mathbf{x}_1 | \hat{A} | \mathbf{x}_2 \rangle = \frac{1}{(\lambda 2\pi\hbar)^N} \int \mathrm{d}\mathbf{p} \ \exp\left(i \frac{\mathbf{p} \cdot (\mathbf{x}_1 - \mathbf{x}_2)}{\lambda \hbar}\right) A\left(\frac{\mathbf{x}_1 + \mathbf{x}_2}{2}, \mathbf{p}\right). \tag{2.53}$$

The factor $\lambda\hbar$ in the exponential corresponds to the factor of the commutator (2.50).

A useful expression is the trace of an operator $\hat{A}$, given by the phase space integral of the trace of its symbol $A(\mathbf{x},\mathbf{p})$

$$\mathrm{Tr}_{\mathcal{H}_{\mathrm{tot}}}\left(\hat{A}\right) = \frac{1}{(\lambda 2\pi\hbar)^N}\int \mathrm{d}\mathbf{x}\mathrm{d}\mathbf{p}\ \ \mathrm{Tr}_{\mathcal{H}_{\mathrm{fast}}}\left(A(\mathbf{x},\mathbf{p})\right). \tag{2.54}$$

### Product of observables – Moyal product

The main reason for the usefulness of this representation within the adiabatic perturbation theory is the natural expansion in $\lambda$ of the symbol of a product of observables.

Noting $\hat{C} = \hat{A}\hat{B}$ the product of two observables, the symbol $C(\mathbf{x},\mathbf{p})$ of this product is given by a non-commutative product of the symbols $A(\mathbf{x},\mathbf{p})$ and $B(\mathbf{x},\mathbf{p})$, called the Moyal product or $\star$-product, and often written $(A\star B)(\mathbf{x},\mathbf{p})$. It is given by

$$C(\mathbf{x},\mathbf{p}) = (A\star B)(\mathbf{x},\mathbf{p}) \tag{2.55}$$

$$= A(\mathbf{x},\mathbf{p})\ \exp\left[\lambda\frac{i\hbar}{2}\sum_{i=1}^{N}\left(\frac{\overleftarrow{\partial}}{\partial x_i}\frac{\overrightarrow{\partial}}{\partial p_i} - \frac{\overleftarrow{\partial}}{\partial p_i}\frac{\overrightarrow{\partial}}{\partial x_i}\right)\right]\ B(\mathbf{x},\mathbf{p}) \tag{2.56}$$

$$= A(\mathbf{x},\mathbf{p})B(\mathbf{x},\mathbf{p}) + \lambda\frac{i\hbar}{2}\sum_{i=1}^{N}\left(\frac{\partial A}{\partial x_i}\frac{\partial B}{\partial p_i} - \frac{\partial A}{\partial p_i}\frac{\partial B}{\partial x_i}\right)(\mathbf{x},\mathbf{p}) + \mathcal{O}(\lambda^2). \tag{2.57}$$

We provide the expression of the expansion of the Moyal product at all order in $\lambda$ in the appendix 2.A, explaining the condensed notation (2.56). The Weyl symbol of the operators $\hat{x}_i$ and respectively $\hat{p}_i$ are naturally given by the functions $(\mathbf{x},\mathbf{p}) \mapsto x_i\mathbf{1}_{\mathcal{H}_{\mathrm{fast}}}$ and respectively $(\mathbf{x},\mathbf{p}) \mapsto p_i\mathbf{1}_{\mathcal{H}_{\mathrm{fast}}}$. As such, from the expression of the Moyal product, the Weyl symbol of their commutator is naturally given by the constant function $\lambda i\hbar\mathbf{1}_{\mathcal{H}_{\mathrm{fast}}}$.

### Wigner function

The Wigner function is a rescaled Weyl symbol of a density matrix, which plays a role of quasi-density in phase space, in the sense explained below.

We consider a state of the total system $|\Psi\rangle \in \mathcal{H}_{\mathrm{tot}}$. We note $\rho(\mathbf{x},\mathbf{p})$ the Weyl symbol of its density matrix $\hat{\rho} = |\Psi\rangle\langle\Psi|$

$$\hat{\rho} = |\Psi\rangle\langle\Psi| \quad \underset{\text{Weyl symbol}}{\longrightarrow} \quad \rho(\mathbf{x},\mathbf{p}). \tag{2.58}$$

The Wigner function of the slow subsystem is the scalar function

$$w(\mathbf{x},\mathbf{p}) = \frac{1}{(\lambda 2\pi\hbar)^N}\ \mathrm{Tr}_{\mathcal{H}_{\mathrm{fast}}}[\rho(\mathbf{x},\mathbf{p})]. \tag{2.59}$$

For an observable $\hat{a}$ of the slow subsystem, *i.e.* an operator acting on $\mathcal{H}_{\mathrm{slow}}$ only, its Weyl symbol $a(\mathbf{x},\mathbf{p})$ is a scalar function. The average of the observable $\hat{a}$ in the state $|\Psi\rangle$ is then given by

$$\langle\Psi|\,\hat{a}\,|\Psi\rangle = \int \mathrm{d}\mathbf{x}\mathrm{d}\mathbf{p}\ w(\mathbf{x},\mathbf{p})a(\mathbf{x},\mathbf{p}). \tag{2.60}$$

As such, the normalization of the Wigner function by the factor $(\lambda 2\pi\hbar)^N$ enables us to interpret it as a phase space quasi-density[7]. The Wigner function is a quasi-density and not a proper phase-space density because it can take negative values.

[7] Eq. (2.60) is not an immediate consequence of the trace relation (2.54). We expect from Eq. (2.54) to

#### Case of discrete and compact variables

In Eq. (2.52) and Eq. (2.53), the integrals are over $\mathbb{R}^N$ because we consider slow variables of continuous and infinite domain $\mathbf{x}, \mathbf{p} \in \mathbb{R}^N$. Blount introduced a similar Wigner-Weyl representation in the case of electron in a crystal [91, 122] which he called "mixed representation". In this case $\mathbf{x}$ is replaced by the Bravais lattice position $\mathbf{R}$ and $\mathbf{p}$ by the Bloch momentum[8] $\mathbf{k}$. The formulas do not involve $\hbar$ in this case, because $\mathbf{k} \cdot \mathbf{R}$ is dimensionless. The integrals over $\mathbf{k}$ are done over the Brillouin zone, and the integral over $\mathbf{p}$ are replaced by discrete sum for $\mathbf{R}$ lying on the Bravais lattice. Note that Blount does not introduce a dimensionless perturbative variable $\lambda$. He identifies the order of perturbative expansion in Eq. (2.56) as the order of phase space derivative. For more technical discussions on the Wigner-Weyl formalism for lattice models, we refer to [123].

### 2.3.4 Other introductions of a perturbative parameter

In the literature, a "small parameter" $\epsilon$ is often used saying that it controls the separation of timescales between the slow and the fast quantum system, and that its physical meaning depends on the context. The Wigner-Weyl formalism is then used to study the limit $\epsilon \to 0$. We cite [124], which provides in particular a discussion of the literature. We discuss briefly different ways which are often employed to introduce this parameter, and then explain the main difference of our approach.

#### Semiclassical approximations

The perturbative variable $\lambda$ is introduced in factor of $\hbar$ in Eq. (2.50), because we want to consider the limit of small commutators of the slow variables. In the first chapter, to define the adiabatic states of a slowly time-dependent quantum system, we also introduced the parameter $\lambda$ in factor of $\hbar$ in Eq. (1.26). It originated from the fact that we considered the dynamics under the Hamiltonian $H(\lambda t)$.

The fact that $\lambda$ can be introduced as a factor of $\hbar$ explains why in many works the adiabatic approximations are discussed as semiclassical approximations. We cite for example [74].

#### Quantization of adiabatic invariants

An adiabatic small parameter $\epsilon$ was used historically in classical mechanics, with a classical Hamiltonian depending on two pairs of conjugated variables $(q, p)$ and $(Q, P)$ by

$$H_{\text{tot}}(\epsilon q, p; Q, P) \tag{2.61}$$

where the limit $\epsilon \to 0$ leads to $p$ being a classical conserved quantity. The degree of freedom $(q, p)$ can be seen as the slow degree of freedom, and $(Q, P)$ as the fast degree of

have a Moyal product between the Wigner function $w(\mathbf{x}, \mathbf{p})$ and the symbol $a(\mathbf{x}, \mathbf{p})$ in the integral. The result (2.60) shows that the leading term $w(\mathbf{x}, \mathbf{p})a(\mathbf{x}, \mathbf{p})$ in the expansion in $\lambda$ is the only non-vanishing one after integration.

[8] The fast subsystem then correspond to $\mathcal{H}_{\text{unit-cell}}$, as discussed in Sec. 2.2.1. Blount does not discuss directly operators acting on this subspace. Instead, he uses a band representation, with band indices. This just means that he expresses these operators in the Bloch basis $|u_\nu(\mathbf{k})\rangle$ of Eq. (2.32).

freedom. The quantization of such classical system proceeds by introducing a Hamiltonian

$$H_{\mathrm{tot}}(\epsilon q, -i\hbar\partial_q; Q, -i\hbar\partial_Q). \tag{2.62}$$

The study of such problem can be traced back to the Solvay Congress in 1911. We cite the work of Karasev [125] which aim at comparing the adiabatic limit and semiclassical limit by comparing $\epsilon$ and $\hbar$, in a sense which has to be precised.

### Coupled wave equations and multicomponent WKB approximation

A small parameter $\epsilon$ is also often introduced when discussing multicomponent classical wave equations. We recover wave equations from a slow-fast quantum system using the position representation of the slow variables. A state of the slow subsystem is represented by a wavefunction $\psi(\mathbf{x})$. A possible representation of the operators $\hat{\mathbf{x}}$ and $\hat{\mathbf{p}}$ satisfying the commutation relation (2.50) is

$$(\hat{x}_i\psi)(\mathbf{x}) = x_i\psi(\mathbf{x}) \tag{2.63}$$

$$(\hat{p}_i\psi)(\mathbf{x}) = \lambda(-i\hbar)\frac{\partial\psi}{\partial x_i}(\mathbf{x}). \tag{2.64}$$

In this case, the degrees of freedom of the fast subsystem are captured by a multicomponent wave field $\psi_\alpha(\mathbf{x})$. Within a quantum mechanical language, we introduce a basis $|e_\alpha\rangle$ of $\mathcal{H}_{\mathrm{fast}}$ and for a state of the total system $|\Psi\rangle \in \mathcal{H}_{\mathrm{tot}}$, the field components read $\psi_\alpha(\mathbf{x}) = (\langle\mathbf{x}| \otimes \langle e_\alpha|)\,|\Psi\rangle$. The Hamiltonian $\hat{H}_{\mathrm{tot}}$ is then represented by a matrix of differential operators acting on the wave vector field $\psi_\alpha(\mathbf{x})$

$$H_{\mathrm{tot}}(\mathbf{x}, -\lambda i\hbar\nabla_{\mathbf{x}}). \tag{2.65}$$

The multi-component WKB approximation is a method to determine the eigenstates of a Hamiltonian written similarly, $H(\mathbf{x}, -i\epsilon\nabla_{\mathbf{x}})$, in the limit $\epsilon \to 0$. Littlejohn and Flynn [126] revealed the role of Berry phases and Berry curvature in this theory. In WKB theory, the eigenstates are constructed from a classical Hamiltonian description. Littlejohn and Flynn showed that this classical Hamiltonian description is affected by the Berry curvature and by a modified energy, in a similar way than the semiclassical equations of motion of an electronic wavepacket in the later theory of Niu *et al.*, see Eq. (2.45) in Eq. (2.43a).

### Scale of phase space variation of an observable

The perturbation theory based on Wigner-Weyl calculus is also well suited when we deal with observables which are slowly varying in phase space. Indeed, as explicitly written in appendix 2.A, a term of a given order in $\lambda$ is of the same order of the number of phase space derivative of symbols.

This is relevant in the context of an electron in a crystal, where we deal with perturbative electromagnetic potentials slowly varying in space. Blount discussed the notion of order of perturbation theory in this way [91]. In general, the Wigner-Weyl representation is relevant for any wave equations with slowly varying parameters [126]. We refer to the PhD thesis of Nicolas Perez for applications in the context of topological waves in geophysics [127].

#### Distinct formalisms

Other approaches have been developed to study the adiabatic or semiclassical theory of slow-fast quantum systems. For example, Kuratsuji and Iida developed a path integral approach in the late '80s [128–132]. See also [133] for a Lagrangian approach in the context of the Born-Oppenheimer treatment of a molecule. In this manuscript, we focus on Hamiltonian approaches.

Gosselin *et al.* developed Hamiltonian approaches motivated by the study of the electron dynamics of a crystal [134–137]. Their approaches do not use phase space representation, but contains ideas similar to the previous works of Littlejohn and Flynn [126], and of Emmrich and Weinstein [74]. We do not discuss the approach of Gosselin *et al.* in this manuscript.

#### Main difference of our approach

In the different approaches discussed above, $\epsilon$ is considered as a small parameter and computations are done in the limit $\epsilon \to 0$. In our case, we use a variable $\lambda$ to interpolate between a problem of infinitely slow subsystem and the problem we are interested in, which enables us to determine the conditions of validity of the adiabatic expansion *via* the condition (i) of Sec. 2.3.1. This condition is not stated explicitly in the literature which I have considered. We will provide an explicit form of this condition in the following.

## 2.4 Adiabatic theory of a slow-fast quantum system

In this section, we detail a general adiabatic theory of a slow-fast quantum system. For a general slow-fast quantum system introduced in Sec. 2.3.2, the goal is to construct a family of states of the total system evolving slowly, and to evaluate their dynamics. This is the idea of a slow manifold mentioned in Sec. 1.2.1 of the first chapter.

The family of states is defined from a projector, called the adiabatic projector. We introduce it in Sec. 2.4.1. The evaluation of the dynamics of this family of states is discussed in Sec. 2.4.2. These two subsections are partly based on the work of Emmrich and Weinstein [74], and of Stiepan and Teufel [124]. In these works, the authors do not talk about a slow manifold. Their goal is to construct a family of states of the total system which is stable by the dynamics, and to evaluate the effective dynamics within this subspace. We provide our personal understanding of these results.

In Sec. 2.4.3, we provide an explicit expression of the adiabatic projector at first order. This enables us to discuss quantitatively the conditions of validity of the theory in Sec. 2.4.4. These two subsections describe an original work.

### 2.4.1 Adiabatic projector and adiabatic subspace

#### Adiabatic projector

The adiabatic projector $\hat{\Pi}_\nu$ defines the family of initial states for which the adiabatic dynamics is valid. This is the slow manifold, constructed perturbatively in the parameter $\lambda$, where the limit $\lambda \to 0$ corresponds to the problem of infinitely slow subsystem. We thus assume that it can be expressed as an asymptotic series of $\lambda$, given by Eq. (2.47).

The adiabatic projector $\hat{\Pi}_\nu$ is defined as an orthonormal projector into an almost-invariant subspace, meaning that it commutes with the total Hamiltonian up to non-perturbative terms in $\lambda$. As such, an initial state prepared in the adiabatic subspace remains in it during the dynamics, up to non-perturbative effects. The defining equations of this projector are then

$$[\hat{H}_{\mathrm{tot}}, \hat{\Pi}_\nu] = \mathcal{O}(\lambda^\infty), \tag{2.66a}$$

$$(\hat{\Pi}_\nu)^2 = \hat{\Pi}_\nu. \tag{2.66b}$$

Written in terms of the Weyl symbol $\Pi_\nu(\mathbf{x}, \mathbf{p})$, these defining equations read

$$(H_{\mathrm{tot}} \star \Pi_\nu)(\mathbf{x}, \mathbf{p}) = (\Pi_\nu \star H_{\mathrm{tot}})(\mathbf{x}, \mathbf{p}), \tag{2.67a}$$

$$(\Pi_\nu \star \Pi_\nu)(\mathbf{x}, \mathbf{p}) = \Pi_\nu(\mathbf{x}, \mathbf{p}). \tag{2.67b}$$

The Weyl symbol $\Pi_\nu(\mathbf{x}, \mathbf{p})$ of the adiabatic projector is constructed order by order inserting the decomposition (2.47) of the adiabatic projector and the expansion (2.116) of the $\star$-product into Eqs. (2.67).

The mathematical definition of the adiabatic projector is discussed in the book of S. Teufel [71], which contains a review of the various contributions to its definition. The most important ones are the mathematical work of Emmrich and Weinstein [74] who gave the detailed algorithm of computation based on the previous physical work of Littlejohn and Flynn [126], and the article of Stiepan and Teufel [124] who showed the existence under certain conditions[9].

### Zeroth order

In the Born-Oppenheimer treatment of a molecule, we identify a subspace of variational ansatz by a diagonalization of the Hamiltonian of the electrons fixing the position $\mathbf{R}$ of the nuclei. This subspace $\mathcal{H}_{\nu,0}$ is characterized by the Born-Oppenheimer projector $\hat{\Pi}_{\nu,0}$ (2.10).

For an electron in a crystal, we consider a band subspace $\mathcal{H}_{\nu,0}$ characterized by a spectral projector (2.39). It is defined from the diagonalization of the Bloch Hamiltonian for which the Bloch momentum $\mathbf{k}$ is a parameter.

We show that the zeroth order of the adiabatic projector $\hat{\Pi}_{\nu,0}$ has a similar structure. It is obtained from the diagonalization of the fast Hamiltonian by "freezing" the slow variables. Here we "freeze" the slow variables by considering the Weyl symbol $H_{\mathrm{tot}}(\mathbf{x}, \mathbf{p})$ of the total Hamiltonian $\hat{H}_{\mathrm{tot}}$.

Indeed, at zeroth order, Eq. (2.67) read

$$H_{\mathrm{tot}}(\mathbf{x}, \mathbf{p})\Pi_{\nu,0}(\mathbf{x}, \mathbf{p}) = \Pi_{\nu,0}(\mathbf{x}, \mathbf{p})H_{\mathrm{tot}}(\mathbf{x}, \mathbf{p}), \tag{2.68}$$

$$\Pi_{\nu,0}(\mathbf{x}, \mathbf{p})^2 = \Pi_{\nu,0}(\mathbf{x}, \mathbf{p}), \tag{2.69}$$

which is satisfied for the projector on an eigenstate $|\psi_\nu(\mathbf{x}, \mathbf{p})\rangle$ of $H_{\mathrm{tot}}(\mathbf{x}, \mathbf{p})$

$$\Pi_{\nu,0}(\mathbf{x}, \mathbf{p}) = |\psi_\nu(\mathbf{x}, \mathbf{p})\rangle \langle\psi_\nu(\mathbf{x}, \mathbf{p})| . \tag{2.70}$$

[9] Stiepan and Teufel [124] showed mathematically that (under certain conditions) the adiabatic projector is a true projector, in the sense that (2.66b) does not require non perturbative $\mathcal{O}(\lambda^\infty)$ corrections. In the literature preceding their work, the adiabatic projector is constructed as an almost projector $(\hat{\Pi}_\nu)^2 = \hat{\Pi}_\nu + \mathcal{O}(\lambda^\infty)$. The fact that (2.66b) does not require $\mathcal{O}(\lambda^\infty)$ terms is physically meaningful. It means that $\hat{\Pi}_\nu$ defines effectively a subspace of states the total Hilbert space, the adiabatic states. But this subspace is stable under time evolution only up to non-perturbative (Landau-Zener) effects in $\lambda$.

### Notation of the energies

To clarify the following notations, we note that from the decomposition of the total Hamiltonian (2.49), its symbol splits into

$$H_{\rm tot}(\mathbf{x},\mathbf{p}) = H_{\rm slow}(\mathbf{x},\mathbf{p})\mathbf{1}_{\mathcal{H}_{\rm fast}} + H(\mathbf{x},\mathbf{p}) \tag{2.71}$$

where $H_{\rm slow}(\mathbf{x},\mathbf{p})$ is the scalar Weyl symbol of the slow Hamiltonian $\hat{H}_{\rm tot}$, which is nothing but the classical Hamiltonian of the slow system.

We diagonalize the symbol of the total Hamiltonian $H_{\rm tot}(\mathbf{x},\mathbf{p})$, or equivalently the one of the fast system $H(\mathbf{x},\mathbf{p})$, for each value of the phase space coordinates of the slow variables $(\mathbf{x},\mathbf{p})$. We note $\mathcal{E}_\nu(\mathbf{x},\mathbf{p})$ the corresponding energies associated to the eigenstate $|\psi_\nu(\mathbf{x},\mathbf{p})\rangle \in \mathcal{H}_{\rm fast}$:

$$H_{\rm tot}(\mathbf{x},\mathbf{p})\,|\psi_\nu(\mathbf{x},\mathbf{p})\rangle = \mathcal{E}_\nu(\mathbf{x},\mathbf{p})\,|\psi_\nu(\mathbf{x},\mathbf{p})\rangle\,, \tag{2.72}$$

with

$$\mathcal{E}_\nu(\mathbf{x},\mathbf{p}) = H_{\rm slow}(\mathbf{x},\mathbf{p}) + E_\nu(\mathbf{x},\mathbf{p}), \tag{2.73}$$

and with $E_\nu(\mathbf{x},\mathbf{p})$ the eigenenergy of the fast Hamiltonian $H(\mathbf{x},\mathbf{p})$. The slow timescales will be derived from $\mathcal{E}_\nu$, from both $H_{\rm slow}$ and $E_\nu$, whereas the fast timescales will be derived from the gaps $\mathcal{E}_\nu - \mathcal{E}_\mu = E_\nu - E_\mu$, only from the fast Hamiltonian[10]. This is expressed by Eqs. (2.102) and (2.101) in Sec. 2.4.4.

### Adiabatic subspace

The specificity of the Born-Oppenheimer setting is that the fast quantum system couples only to one of the two conjugated variables of the slow subsystem, either $\mathbf{x}$ or $\mathbf{p}$. In such a case, the operator $\hat{\Pi}_{\nu,0}$ associated to the symbol $\Pi_{\nu,0}(\mathbf{x},\mathbf{p})$ is itself a projector acting on the total system $\mathcal{H}_{\rm tot}$. It thus defines a subspace of the total Hilbert space $\mathcal{H}_{\nu,0}$ introduced in Eq. (2.9) and Eq. (2.38).

The Born-Oppenheimer approximation assumes that the eigenstates lies in $\mathcal{H}_{\nu,0}$, while the electronic wavepacket approach assumes that the state stays in $\mathcal{H}_{\nu,0}$ during the dynamics. This is an approximation, this subspace is not stable under the dynamics of the total Hamiltonian. Equivalently the eigenstates of the total Hamiltonian are dressed with components in the different subspaces. It terms of operators, this just means $[\hat{H}_{\rm tot}, \hat{\Pi}_{\nu,0}] \neq 0$. The conditions of validity of this approximation are not easily derived within the Born-Oppenheimer method, nor from the wavepacket approach of the dynamics of an electron in a crystal.

The adiabatic projector $\hat{\Pi}_\nu$ defines the adiabatic subspace $\mathcal{H}_\nu$ of the total Hilbert space which is stable by the dynamics up to non-perturbative effects. The adiabatic subspace consists in the projected states

$$\boxed{\mathcal{H}_\nu = \left\{\ |\Psi\rangle \in \mathcal{H}_{\rm tot}\ |\ \hat{\Pi}_\nu\,|\Psi\rangle = |\Psi\rangle\ \right\}.} \tag{2.74}$$

[10] As explained in Sec. 2.3.2, this choice of notation separating the energy of the slow and fast subsystems is useful to interpret physically the results and to adopt similar notations to the historical Born-Oppenheimer problem, but it is not necessary for the general theory. One can deal solely with the energies $\mathcal{E}_\nu(\mathbf{x},\mathbf{p})$ of the symbol of the total Hamiltonian. Then their gaps are associated to the fast timescales and their phase space derivatives are associated to the slow timescales, in a sense which will be precised in Sec. 2.4.4.

Besides, in the case where the fast system couples to both conjugated variables $\hat{\mathbf{x}}$ and $\hat{\mathbf{p}}$, the operator $\hat{\Pi}_{\nu,0}$ is not even a projector acting on $\mathcal{H}_{\rm tot}$ despite the fact that for each $(\mathbf{x},\mathbf{p})$ its Weyl symbol (2.70) is a projector on $\mathcal{H}_{\rm fast}$. As such, there is no relevant notion of zeroth order adiabatic subspace outside the Born-Oppenheimer situation.

We further describe the adiabatic subspace in Sec. 2.4.4. The core problem consists in deriving the dynamics within this subspace.

### 2.4.2 Projected dynamics

#### Role of the classical equations of motion in the literature

In the Born-Oppenheimer problem, classical equations of motions of the nuclei are sometimes considered using a correspondence principle from the Hamiltonian (2.6), leading to a Lorentz force originating from the Berry curvature [80], as discussed in Sec. 2.1.4. In the context of the construction of WKB eigenstates of coupled linear wave equations, a classical Hamiltonian system is used to construct the eigenstate. This classical system is then sometimes interpreted as providing equations of motion of the slow variables. Littlejohn *et al.* showed the role of the Berry curvature in these equations [126, 138]. Finally, in the wavepacket approach of the dynamics of an electron in a crystal of Niu *et al.* [13], equations of motions governing the center of the wavepacket prepared in the zeroth order subspace $\mathcal{H}_{\nu,0}$ are derived, involving the Berry curvature.

The relation between these classical equations of motion and the adiabatic dynamics is indeed rather general. We present here the result of Stiepan and Teufel [124], which clarify this relation between the effective classical Hamiltonian and the quantum dynamics within the adiabatic subspace $\mathcal{H}_\nu$. They show that the effective classical Hamiltonian system governs in first order in $\lambda$ the time evolution of the Wigner function of the slow system, and of the Weyl symbol of the slow observables.

#### Classical equations of motion

To each subspace $\mathcal{H}_\nu$ is associated a classical Hamiltonian of the slow system, *i.e.* a function $h_\nu(\mathbf{x},\mathbf{p})$ defined on the phase space of the slow system

$$h_\nu(\mathbf{x},\mathbf{p}) = \mathcal{E}_\nu(\mathbf{x},\mathbf{p}) + \lambda M_\nu(\mathbf{x},\mathbf{p}), \tag{2.75}$$

where the correction of the energy $M_\nu(\mathbf{x},\mathbf{p})$ is expressed as

$$M_\nu(\mathbf{x},\mathbf{p}) = \hbar \sum_{i=1}^{N} \mathrm{Im}\, \langle \partial_{x_i}\psi_\nu(\mathbf{x},\mathbf{p})| \left(H_{\rm tot}(\mathbf{x},\mathbf{p}) - \mathcal{E}_\nu(\mathbf{x},\mathbf{p})\right) |\partial_{p_i}\psi_\nu(\mathbf{x},\mathbf{p})\rangle\,. \tag{2.76}$$

It corresponds to the "no-name" term of Littlejohn and Flynn's multicomponent WKB approximation [126]. It also corresponds to the modified energy Eq. (2.45) including the effect of the electron orbital magnetization of the electron wavepacket approach.

The classical equations of interest contains the components of the Berry curvature

$$F_{\nu,\alpha\beta}(\mathbf{x},\mathbf{p}) = i\left(\langle\partial_\alpha\psi_\nu(\mathbf{x},\mathbf{p})|\partial_\beta\psi_\nu(\mathbf{x},\mathbf{p})\rangle - (\alpha\leftrightarrow\beta)\right). \tag{2.77}$$

These equations are

$$\dot{x}_i = \frac{\partial h_\nu}{\partial p_i} + \lambda\hbar \sum_{j=1}^{N} \left( F_{\nu,p_i p_j} \frac{\partial h_\nu}{\partial x_j} - F_{\nu,p_i x_j} \frac{\partial h_\nu}{\partial p_j} \right) \tag{2.78a}$$

$$\dot{p}_i = -\frac{\partial h_\nu}{\partial x_i} - \lambda\hbar \sum_{j=1}^{N} \left( F_{\nu,x_i p_j} \frac{\partial h_\nu}{\partial x_j} - F_{\nu,x_i x_j} \frac{\partial h_\nu}{\partial p_j} \right). \tag{2.78b}$$

Classical Hamilton equations require a Poisson bracket or equivalently a symplectic form characterizing the geometry of the classical phase space[11]. These equations correspond to a modified symplectic form involving the Berry curvature $\Omega_\nu(\mathbf{x},\mathbf{p}) = \sum_{i=1}^{N} \mathrm{d}p_i \wedge \mathrm{d}x_i + \lambda\hbar F_\nu(\mathbf{x},\mathbf{p})$.

The solutions of these equations of motion are summarized by the classical Hamiltonian flow $\phi_\nu^t(\mathbf{x},\mathbf{p})$, which corresponds to the evolution in phase space after a time $t$ under the equations (2.78) for an initial condition, namely

$$(\mathbf{x}(t),\mathbf{p}(t)) = \phi_\nu^t\left(\mathbf{x}(t=0),\mathbf{p}(t=0)\right), \tag{2.79}$$

where $(\mathbf{x}(t),\mathbf{p}(t))$ satisfy Eqs. (2.78).

### Time evolution of a slow observable

We are interested in a first result of Stiepan and Teufel [124] which states that the equations of motion (2.78) govern the time evolution of a slow observable in Heisenberg representation. We consider an observable $\hat{a}$ of the slow subsystem, *i.e.* a hermitian operator acting on $\mathcal{H}_{\mathrm{slow}}$ only. We consider its time evolution in Heisenberg representation $\hat{a}(t)$. Stiepan and Teufel showed that the classical equations govern at first order the evolution of the Weyl symbol of the observable. More precisely, the observable $\hat{a}$ is associated to a Weyl symbol $a(\mathbf{x},\mathbf{p})$, a scalar function on the slow phase space defined from Eq. (2.52). The classical equations of motion leads to a classical evolution in phase space $a\circ\phi_\nu^t(\mathbf{x},\mathbf{p})$. This scalar function on phase space can then be translated with the Weyl quantization Eq. (2.53) into an operator $\widehat{a\circ\phi_\nu^t}$ acting on $\mathcal{H}_{\mathrm{slow}}$. When projected by $\hat{\Pi}_\nu$, *i.e.* for initial states within $\mathcal{H}_\nu$, $\widehat{a\circ\phi_\nu^t}$ corresponds to the quantum mechanical evolution $\hat{a}(t)$ at first order in $\lambda$:

$$\left|\left|\hat{\Pi}_\nu \left(\hat{a}(t) - \widehat{a\circ\phi_\nu^t}\right)\hat{\Pi}_\nu\right|\right| = \mathcal{O}(\lambda^2). \tag{2.80}$$

### Time evolution of an average value of observable

The above result illustrates that the classical equations are mainly useful in the phase space representation, using the Wigner-Weyl transform. Indeed, the Weyl quantization of the classically evolved symbol $a\circ\phi_\nu^t(\mathbf{x},\mathbf{p})$ is hardly trackable in practice. It is much more convenient to compute the average value of an observable using directly the phase space representation. To do so, we consider an initial state of the total system $|\Psi(t=0)\rangle$ lying in the adiabatic subspace $\mathcal{H}_\nu$. We insist on the fact that the following relation is

[11] We refer to [139] for a presentation of classical Hamiltonian mechanics within the formalism of symplectic geometry.

valid only for initial states prepared within this subspace, *i.e.* the initial state has to be projected

$$\hat{\Pi}_\nu \left|\Psi(t=0)\right\rangle = \left|\Psi(t=0)\right\rangle . \tag{2.81}$$

This condition is often overlooked in the literature. We will study its consequences in details in Chap. 5. We note $w(\mathbf{x},\mathbf{p})$ the Wigner function of the initial state $|\Psi(t=0)\rangle$, given by Eq. (2.59). The relation Eq. (2.80) translates into the evolution of the average value of observable $\langle\Psi(t)|\,\hat{a}\,|\Psi(t)\rangle$ in the projected state

$$\boxed{\langle\Psi(t)|\,\hat{a}\,|\Psi(t)\rangle = \int \mathrm{d}\mathbf{x}\mathrm{d}\mathbf{p}\; w(\mathbf{x},\mathbf{p})\; a\left(\phi_\nu^t(\mathbf{x},\mathbf{p})\right) + \mathcal{O}(\lambda^2).} \tag{2.82}$$

This relation is the precise sense in which the classical equations (2.78) govern the dynamics of the slow subsystem within the adiabatic subspace $\mathcal{H}_\nu$.

**Remark on the phase space measure** It is tempting to introduce a notion of time-evolution of the Wigner function of the slow subsystem from Eq. (2.82), with a change of variable leading to $w(\phi_\nu^{-t}(\mathbf{x},\mathbf{p}))$ as the time evolution of the Wigner function. However, such a change of variable does not preserve the phase space measure $\mathrm{d}\mathbf{x}\mathrm{d}\mathbf{p}$. Indeed, $\phi_\nu^t(\mathbf{x},\mathbf{p})$ is the Hamilton flow associated to a Hamilton system of symplectic two-form $\Omega_\nu = \sum_{i=1}^N \mathrm{d}p_i \wedge \mathrm{d}x_i + \lambda\hbar F_\nu$. The Liouville measure associated to this Hamilton system is the phase space measure invariant under the Hamilton flow. This measure is

$$(-1)^{N(N-1)/2}\frac{1}{N!}\underbrace{\Omega_\nu \wedge \cdots \wedge \Omega_\nu}_{N \text{ times}} = \left(1 - \lambda\hbar\sum_{i=1}^N F_{\nu,x_ip_i}\right)\mathrm{d}\mathbf{x}\mathrm{d}\mathbf{p} + \mathcal{O}(\lambda^2). \tag{2.83}$$

Accordingly, to be relevant, the notion of time-evolution of the Wigner function should contain the prefactor $\left(1 - \lambda\hbar\sum_{i=1}^N F_{\nu,x_ip_i}\right)$ of Eq. (2.83), see [124]. This prefactor is discussed as a modified phase space density in [140], which is important when we consider thermodynamic equilibrium quantities [13, 124]. We show in the next section that it also enters the condition of validity of the adiabatic expansion.

### 2.4.3 Adiabatic projector at first order

In this section, we derive an explicit expression of the first order term $\hat{\Pi}_{\nu,1}$ of the adiabatic projector $\hat{\Pi}_\nu$. Doing so, we obtain explicit conditions of validity of the adiabatic approximation. In particular, we precise in which sense the slow subsystem has to be "slow", and derive an extra condition based on new gauge covariant tensors. We define the gauge covariance and provide expressions of these tensors in Appendix 2.B.1.

The adiabatic projector $\hat{\Pi}_\nu$ can be constructed recursively order by order, as explained in Sec. 2.4.1. The corresponding procedure is provided by Emmrich and Weinstein in [74]. They show the existence at all order of the projector under certain conditions, but do not provide explicit expressions. In this section, we derive such an explicit expression of the Weyl symbol at first order $\Pi_{\nu,1}(\mathbf{x},\mathbf{p})$ in terms of gauge covariant quantities.

### First order equations

In the following, we give the expression of the first order correction of the adiabatic projector $\Pi_{\nu,1}(\mathbf{x},\mathbf{p})$ in the basis of $\mathcal{H}_{\text{fast}}$ consisting of the eigenstates $|\psi_\mu(\mathbf{x},\mathbf{p})\rangle$ of $H_{\text{tot}}(\mathbf{x},\mathbf{p})$. These matrix elements will involve the components of the non-abelian Berry connection

$$A_{\mu\nu,\alpha}(\mathbf{x},\mathbf{p}) = i\,\langle\psi_\mu(\mathbf{x},\mathbf{p})|\partial_\alpha\psi_\nu(\mathbf{x},\mathbf{p})\rangle\,, \tag{2.84}$$

where we note $\boldsymbol{\xi} = \{\xi^\alpha\} = (\mathbf{x},\mathbf{p})$ the phase space coordinates, and $\partial_\alpha = \frac{\partial}{\partial\xi^\alpha}$. These coefficients are gauge covariant for $\mu \neq \nu$. We provide further details in Appendix 2.B on the derivation of the following results. In the following expressions, we do not always write explicitly the dependence on $(\mathbf{x},\mathbf{p})$ of the symbols to lighten the notations.

Using the development (2.47) of the adiabatic projector and the expansion (2.57) of the Moyal product, the defining equations (2.67) give at first order

$$H_{\text{tot}}\Pi_{\nu,1} - \Pi_{\nu,1}H_{\text{tot}} = \frac{i\hbar}{2}\{\Pi_{\nu,0}, H_{\text{tot}}\} - \frac{i\hbar}{2}\{H_{\text{tot}}, \Pi_{\nu,0}\} \tag{2.85a}$$

$$\Pi_{\nu,1} - \Pi_{\nu,1}\Pi_{\nu,0} - \Pi_{\nu,0}\Pi_{\nu,1} = \frac{i\hbar}{2}\{\Pi_{\nu,0}, \Pi_{\nu,0}\} \tag{2.85b}$$

where, for two symbols $A(\mathbf{x},\mathbf{p})$ and $B(\mathbf{x},\mathbf{p})$, we define the Poisson bracket $\{A,B\}(\mathbf{x},\mathbf{p})$ by $\{A,B\} = \sum_{i=1}^N \left(\frac{\partial A}{\partial x_i}\frac{\partial B}{\partial p_i} - \frac{\partial A}{\partial p_i}\frac{\partial B}{\partial x_i}\right)$, not to be confused with an anticommutator.

### Block-diagonal matrix elements – Curvatures

From Eq. (2.85b) we obtain the first matrix element in terms of the Berry curvature $F_\nu$

$$\langle\psi_\nu(\mathbf{x},\mathbf{p})|\,\Pi_{\nu,1}(\mathbf{x},\mathbf{p})\,|\psi_\nu(\mathbf{x},\mathbf{p})\rangle = -\frac{\hbar}{2}\sum_{i=1}^N F_{\nu,x_ip_i}(\mathbf{x},\mathbf{p}). \tag{2.86}$$

The other block-diagonal matrix elements, for $\mu_1,\mu_2 \neq \nu$ are written in terms of the non-abelian curvature $F_{\overline{\{\nu\}}}$. This curvature is associated to the family of eigenstates $\overline{\{\nu\}}$ made of all the eigenstates $\mu \neq \nu$. This is an operator-valued two-form, whose components $F_{\overline{\{\nu\}},x_ip_i}(\mathbf{x},\mathbf{p})$ are operators acting on the subspace generated by the $|\psi_{\mu\neq\nu}(\mathbf{x},\mathbf{p})\rangle$. A simple expression of its matrix elements in terms of the connection (2.84) is

$$F^{(\mu_1\mu_2)}_{\overline{\{\nu\}},\alpha\beta}(\mathbf{x},\mathbf{p}) = i\left(A_{\mu_1\nu,\alpha}(\mathbf{x},\mathbf{p})A_{\nu\mu_2,\beta}(\mathbf{x},\mathbf{p}) - (\alpha\leftrightarrow\beta)\right). \tag{2.87}$$

We give further expression of this object in Appendix 2.B.1.

From Eq. (2.85b), we get the block diagonal matrix element for $\mu_1,\mu_2 \neq \nu$:

$$\langle\psi_{\mu_1}(\mathbf{x},\mathbf{p})|\,\Pi_{\nu,1}(\mathbf{x},\mathbf{p})\,|\psi_{\mu_2}(\mathbf{x},\mathbf{p})\rangle = \frac{\hbar}{2}\sum_{i=1}^N F^{(\mu_1\mu_2)}_{\overline{\{\nu\}},x_ip_i}(\mathbf{x},\mathbf{p}). \tag{2.88}$$

### Two levels energy tensor

To express the other matrix elements, we introduce a new tensor. It is homogeneous to an energy and associated to a pair of energy levels $(\mu,\nu)$. To motivate the definition of

this quantity, we first identify in the modification of energy $M_\nu$ (2.76) a rank 2 tensor $G_\nu$ homogeneous to an energy. Its components are given by

$$G_{\nu,\alpha\beta}(\mathbf{x},\mathbf{p}) = \langle \partial_\alpha \psi_\nu(\mathbf{x},\mathbf{p})| \left(H_{\rm tot}(\mathbf{x},\mathbf{p}) - \mathcal{E}_\nu(\mathbf{x},\mathbf{p})\right) |\partial_\beta \psi_\nu(\mathbf{x},\mathbf{p})\rangle \,. \tag{2.89}$$

If $x_i$ and $p_i$ are two conjugated coordinates, their product has the dimension of an action, and the component $\hbar G_{\nu,x_ip_i}(\mathbf{x},\mathbf{p})$ has the dimension of an energy. The modification of the energy takes the form

$$M_\nu(\mathbf{x},\mathbf{p}) = \hbar \sum_{i=1}^{N} \mathrm{Im}\, G_{\nu,x_ip_i}(\mathbf{x},\mathbf{p}). \tag{2.90}$$

The tensor $G_\nu$ enters the expression of the orbital magnetization of a Bloch electron [13,63] and is discussed in [141] for many-body physics.

We introduce a new tensor associated to a pair of energy levels. To motivate its definition, we first analyze the definition (2.89) of the tensor $G_\nu$ associated to the energy level $\nu$. It corresponds to matrix elements of the Hamiltonian whose energies are expressed with respect to $\mathcal{E}_\nu(\mathbf{x},\mathbf{p})$. We note this operator $\Delta_\nu H(\mathbf{x},\mathbf{p})$

$$\Delta_\nu H = H - E_\nu \mathbf{1}_{\mathcal{H}_{\rm fast}} \tag{2.91}$$

$$= \sum_{\sigma\neq\nu} \left(E_\sigma - E_\nu\right) |\psi_\sigma\rangle \langle\psi_\sigma| \,, \tag{2.92}$$

such that[12]

$$G_{\nu,\alpha\beta} = \langle \partial_\alpha \psi_\nu| \, \Delta_\nu H \, |\partial_\beta \psi_\nu\rangle \,. \tag{2.93}$$

We now introduce a new tensor $G_{\mu,\nu}$ homogeneous to an energy, which we call the two levels energy tensor. It is defined for a pair of energy levels $(\mu,\nu)$ as

$$G_{\mu,\nu,\alpha\beta} = \langle \partial_\alpha \psi_\mu| \, \Delta_{\mu,\nu} H \, |\partial_\beta \psi_\nu\rangle \,, \tag{2.94}$$

where

$$\Delta_{\mu,\nu} H = H - E_\mu \mathbf{1}_{\mathcal{H}_{\rm fast}} - \left(E_\nu - E_\mu\right) |\psi_\nu\rangle \langle\psi_\nu| \tag{2.95}$$

$$= \sum_{\sigma\notin\{\mu,\nu\}} \left(E_\sigma - E_\mu\right) |\psi_\sigma\rangle \langle\psi_\sigma| \,. \tag{2.96}$$

Note that $\mu$ and $\nu$ do not play symmetric roles.

Again, if $x_i$ and $p_i$ are two conjugated coordinates, their product has the dimension of an action and the component $\hbar G_{\mu,\nu,x_ip_i}(\mathbf{x},\mathbf{p})$ has the dimension of an energy. We give further expressions of the tensor $G_{\mu,\nu}$ in Appendix 2.B.1.

[12]Note that since we consider energy differences, from Eq. (2.73) the energy of the slow system $H_{\rm slow}(\mathbf{x},\mathbf{p})$ in the expression (2.71) of the total Hamiltonian $H_{\rm tot}(\mathbf{x},\mathbf{p})$ does not play a role in the expression. Only the fast Hamiltonian $H(\mathbf{x},\mathbf{p})$ with its eigenergies $E_\mu(\mathbf{x},\mathbf{p})$ are involved.

### Off-diagonal matrix elements

The relation (2.67a) gives the expression of the off-diagonal matrix elements of $\Pi_{\nu,1}$. We obtain for $\mu \neq \nu$ (omitting the implicit $(\mathbf{x}, \mathbf{p})$ dependence of all quantities)

$$\langle \psi_\mu | \, \Pi_{\nu,1} \, | \psi_\nu \rangle = \sum_{i=1}^{N} \left[ \frac{\partial}{\partial x_i} \left( \frac{\mathcal{E}_\nu + \mathcal{E}_\mu}{2} \right) \frac{\hbar A_{\mu\nu,p_i}}{E_\nu - E_\mu} - \frac{\partial}{\partial p_i} \left( \frac{\mathcal{E}_\nu + \mathcal{E}_\mu}{2} \right) \frac{\hbar A_{\mu\nu,x_i}}{E_\nu - E_\mu} + \frac{\hbar \operatorname{Im} G_{\mu,\nu,x_i p_i}}{E_\nu - E_\mu} \right] \tag{2.97}$$

$$= \left( \langle \psi_\nu | \, \Pi_{\nu,1} \, | \psi_\mu \rangle \right)^* .$$

## 2.4.4 Conditions of adiabaticity

As explained in Sec. 2.3.1, the condition of validity of the expansion of the adiabatic projector is obtained by constraining the first order correction $\hat{\Pi}_{\nu,1}$ to be small compared to the zeroth order $\hat{\Pi}_{\nu,0}$. We require the symbol $\Pi_{\nu,1}(\mathbf{x}, \mathbf{p})$ to be small compared to the symbol $\Pi_{\nu,0}(\mathbf{x}, \mathbf{p})$. Given the expression Eq. (2.70) of $\Pi_{\nu,0}(\mathbf{x}, \mathbf{p})$, we require all the matrix elements of $\Pi_{\nu,1}(\mathbf{x}, \mathbf{p})$ to be small compared to 1

$$\left| \langle \psi_{\sigma_1}(\mathbf{x}, \mathbf{p}) | \, \Pi_{\nu,1}(\mathbf{x}, \mathbf{p}) \, | \psi_{\sigma_2}(\mathbf{x}, \mathbf{p}) \rangle \right| \ll 1. \tag{2.98}$$

This gives a family of dimensionless quantities which have to be small. Let us discuss them.

The off-diagonal matrix element Eq. (2.97) is a sum of different terms. We require all of them to be small. We rewrite the first two terms to obtain similar conditions as the Eq. (1.40) we derived in the first chapter in the definition of the adiabatic states of a time dependent quantum system. We recognize in Eq. (2.97) derivatives of energies with respect to a phase space variable. This can be interpreted as the time derivative of its conjugated variable in a classical Hamiltonian formalism, for a classical Hamiltonian $(\mathcal{E}_\nu + \mathcal{E}_\mu)/2$. We note this classical Hamiltonian

$$\mathscr{H}_{\nu\mu}(\mathbf{x}, \mathbf{p}) = \frac{\mathcal{E}_\nu(\mathbf{x}, \mathbf{p}) + \mathcal{E}_\mu(\mathbf{x}, \mathbf{p})}{2} = H_{\text{slow}}(\mathbf{x}, \mathbf{p}) + \frac{E_\nu(\mathbf{x}, \mathbf{p}) + E_\mu(\mathbf{x}, \mathbf{p})}{2}, \tag{2.99}$$

which contains explicitly the Weyl symbol $H_{\text{slow}}(\mathbf{x}, \mathbf{p})$ of the slow Hamiltonian, *i.e.* its classical Hamiltonian in a classical description of the slow degrees of freedom. We interpret the partial derivatives of $\mathscr{H}_{\nu\mu}$ as phase space velocities of the slow degrees of freedom

$$\dot{x}_i^{\text{cl}}(\mathbf{x}, \mathbf{p}) = \frac{\partial \mathscr{H}_{\nu\mu}}{\partial p_i}(\mathbf{x}, \mathbf{p}) \tag{2.100a}$$

$$\dot{p}_i^{\text{cl}}(\mathbf{x}, \mathbf{p}) = -\frac{\partial \mathscr{H}_{\nu\mu}}{\partial x_i}(\mathbf{x}, \mathbf{p}). \tag{2.100b}$$

The first two terms of Eq. (2.97) give the conditions

$$\boxed{\begin{aligned} \left| \dot{p}_i^{\text{cl}}(\mathbf{x}, \mathbf{p}) A_{\mu\nu,p_i}(\mathbf{x}, \mathbf{p}) \right| &\ll \frac{|E_\nu(\mathbf{x}, \mathbf{p}) - E_\mu(\mathbf{x}, \mathbf{p})|}{\hbar} \quad \text{for } \mu \neq \nu \qquad (2.101) \\ \left| \dot{x}_i^{\text{cl}}(\mathbf{x}, \mathbf{p}) A_{\mu\nu,x_i}(\mathbf{x}, \mathbf{p}) \right| &\ll \frac{|E_\nu(\mathbf{x}, \mathbf{p}) - E_\mu(\mathbf{x}, \mathbf{p})|}{\hbar} \quad \text{for } \mu \neq \nu \qquad (2.102) \end{aligned}}$$

which are similar to Eq. (1.40). These equations express quantitatively how "slow" the slow subsystem has to be: the components of the multiband Berry connection $A_{\mu\nu,\alpha}$ translate the classical velocities $\dot{x}_i^{\mathrm{cl}}$ and $\dot{p}_i^{\mathrm{cl}}$ into frequency scales, which have to be small compared to the Bohr frequencies.

We obtain another condition from the third term of Eq. (2.97). It states that the components of the two-level tensor $\hbar G_{\mu,\nu}$ associated to conjugated variables have to be small compared to the gap in energy

$$\boxed{|\hbar \operatorname{Im} G_{\mu,\nu,x_ip_i}(\mathbf{x},\mathbf{p})| \ll |E_\nu(\mathbf{x},\mathbf{p}) - E_\mu(\mathbf{x},\mathbf{p})| \quad \text{for } \mu \neq \nu.} \tag{2.103}$$

From the block-diagonal matrix elements Eq. (2.86) and Eq. (2.88), we obtain conditions on the coefficients of the Berry curvature associated to conjugated phase space coordinates

$$|\hbar F_{\nu,x_ip_i}(\mathbf{x},\mathbf{p})| \ll 1 \qquad \text{and} \qquad \left|\hbar F^{(\mu_1\mu_2)}_{\overline{\{\nu\}},x_ip_i}(\mathbf{x},\mathbf{p})\right| \ll 1 \quad \text{for } \mu_1,\mu_2 \neq \nu. \tag{2.104}$$

We can interpret this condition from the effective classical dynamics Eq. (2.78) which involves a modified symplectic form $\Omega_\nu = \sum_{i=1}^N \mathrm{d}p_i \wedge \mathrm{d}x_i + \lambda\hbar F_\nu$. The condition $\hbar|F_{\nu,x_ip_i}| \ll 1$ compares the zeroth and first order in $\lambda$ of the component of $\Omega_\nu$ along $\mathrm{d}p_i \wedge \mathrm{d}x_i$. This can be interpreted in terms of phase space density comparing the trace of $\Pi_{\nu,0}(\mathbf{x},\mathbf{p})$ and $\Pi_{\nu,1}(\mathbf{x},\mathbf{p})$. From properties on the multilevel Berry curvature $F_{\overline{\{\nu\}}}$ given in Appendix 2.B.1, Eq. (2.86) and Eq. (2.88) gives

$$\mathrm{Tr}_{\mathcal{H}_{\mathrm{slow}}}[\Pi_{\nu,1}(\mathbf{x},\mathbf{p})] = -\hbar \sum_{i=1}^N F_{\nu,x_ip_i}(\mathbf{x},\mathbf{p}). \tag{2.105}$$

The trace of $\Pi_{\nu,0}(\mathbf{x},\mathbf{p})$ is 1. We then obtain the condition

$$\boxed{\left|\hbar \sum_{i=1}^N F_{\nu,x_ip_i}(\mathbf{x},\mathbf{p})\right| \ll 1} \tag{2.106}$$

where we recognize the correction of the phase space density discussed on Eq. (2.83).

Here we recover the same notion of phase space density by computing the total number of states within the adiabatic subspace $\mathcal{H}_\nu$. A state of the slow subsystem occupies a phase space volume $(2\pi\hbar\lambda)^N$. We have formally

$$\dim \mathcal{H}_{\mathrm{slow}} = \int \frac{\mathrm{d}\mathbf{x}\mathrm{d}\mathbf{p}}{(\lambda 2\pi\hbar)^N}. \tag{2.107}$$

The total number of states within the adiabatic subspace $\mathcal{H}_\nu$ is given by the trace of the adiabatic projector $\hat{\Pi}_\nu$. Using the expression of the trace of an operator from its Weyl symbol (2.54), we get

$$\dim \mathcal{H}_\nu = \dim \mathcal{H}_{\mathrm{slow}} - \lambda \sum_{i=1}^N \int \frac{\mathrm{d}\mathbf{x}\mathrm{d}\mathbf{p}}{(\lambda 2\pi\hbar)^N} \hbar F_{\nu,x_ip_i}(\mathbf{x},\mathbf{p}) + \mathcal{O}(\lambda^2). \tag{2.108}$$

The components of the Berry curvature with respect to conjugated variables gives the difference in number of states between the adiabatic subspace and the Hilbert space of the slow subsystem.

### Example: a two-level system as the fast subsystem

The interpretation of $\dot{x}_i^{\mathrm{cl}}$ and $\dot{p}_i^{\mathrm{cl}}$ as classical phase space velocities of the slow subsystem is even more natural if we consider the fast subsystem to be a two level system. In this case, the fast Hamiltonian $H(\mathbf{x},\mathbf{p})$ can be decomposed on Pauli matrices – without term proportional to $\mathbf{1}_{\mathcal{H}_{\mathrm{fast}}}$–, with two opposite eigenergies $E_\nu(\mathbf{x},\mathbf{p}) = -E_\mu(\mathbf{x},\mathbf{p})$. The Hamiltonian $\mathcal{H}_{\mu\nu}(\mathbf{x},\mathbf{p})$ then reduces to $H_{\mathrm{slow}}(\mathbf{x},\mathbf{p})$, such that $\dot{x}_i^{\mathrm{cl}}$ and $\dot{p}_i^{\mathrm{cl}}$ correspond precisely to the phase space velocities of the slow subsystem when we describe it classically.

Moreover, when the fast subsystem is a two-level system, the two-level energy tensor $G_{\mu,\nu}$ vanishes, as explicitly seen from Eq. (2.96). As such, $\hbar\,\mathrm{Im}\,G_{\mu,\nu,x_ip_i}(\mathbf{x},\mathbf{p})$ can be interpreted as a source of transition between two levels originating from the presence of additional levels.

We will study in details the situation where the fast subsystem is a two-level system in chapter 5.

### Domain of validity in phase space

We derived the conditions of validity of the adiabatic expansion Eqs. (2.101) to (2.103) and (2.106). They are conditions on different functions depending on the phase space coordinates $(\mathbf{x},\mathbf{p})$ of the slow subsystem. The most restrictive conditions are Eqs. (2.101) to (2.103) which require in particular that the eigenenergy $E_\nu(\mathbf{x},\mathbf{p})$ of the symbol of the fast Hamiltonian $H(\mathbf{x},\mathbf{p})$ is not degenerate.

For the operator $\hat{\Pi}_\nu$ to be defined, we require its Weyl symbol $\Pi_\nu(\mathbf{x},\mathbf{p})$ to be defined *a priori* on the whole phase space. This requires in particular $E_\nu(\mathbf{x},\mathbf{p})$ to be nowhere degenerate. This is the condition used to prove mathematically the existence of the adiabatic projector $\hat{\Pi}_\nu$ [74, 124].

This condition is satisfied when dealing with the dynamics of an electron in a band insulator. But it is quite strong and rarely satisfied in other physical contexts. As a consequence, in general, the adiabatic projector $\hat{\Pi}_\nu$ is not an operator well-defined on the whole Hilbert space $\mathcal{H}_{\mathrm{tot}}$. Mathematically, it is neither surprising nor annoying. After all, usually operators are not defined on an entire infinite dimensional Hilbert space but only on a restricted domain. Physically, it is not surprising either. It just states that some states of the total system lead to a dynamics containing a separation of timescales, and other states do not. The mathematically rigorous definition of this domain is certainly a difficult task. We provide a physically motivated definition, saying that it is made of the states whose phase space support is localized on the regions satisfying the required conditions.

We thus define the phase space domain on which the previous conditions hold

$$\mathcal{D}_\nu = \{\ (\mathbf{x},\mathbf{p}) \mid \text{Eqs. (2.101) to (2.103) and (2.106) holds }\}\,. \tag{2.109}$$

Then the domain of definition $\mathcal{D}_{\hat{\Pi}_\nu}$ of the adiabatic projector $\hat{\Pi}_\nu$ is defined to be made of the states $|\Psi\rangle \in \mathcal{H}_{\mathrm{tot}}$ of the total system whose Wigner function $w(\mathbf{x},\mathbf{p})$, defined by Eq. (2.59), has a support lying in $\mathcal{D}_\nu$. This makes sense because the product of two operators is local in phase space from the expression of the Moyal product. Hence, to compute the action of $\hat{\Pi}_\nu$ on $|\Psi\rangle$, only the values of the symbol $\Pi_\nu(\mathbf{x},\mathbf{p})$ for $(\mathbf{x},\mathbf{p})$ lying

in the support of $w(\mathbf{x},\mathbf{p})$ matters[13]. Physically, the subspace $\mathcal{D}_{\hat{\Pi}_\nu}$ of $\mathcal{H}_{\rm tot}$ corresponds to the states of the total system whose dynamics contains a separation of timescales. The adiabatic subspace $\mathcal{H}_\nu$ is then made of the projection of these states

$$\mathcal{H}_\nu = \left\{ \hat{\Pi}_\nu \left|\Psi\right\rangle \;\middle|\; \left|\Psi\right\rangle \in \mathcal{D}_{\hat{\Pi}_\nu} \right\}. \tag{2.110}$$

In a sense which will be precised in Chap. 5, they are those that evolve at the slow timescales.

Let us comment on the domain of validity of the adiabatic theory. The adiabatic theory applies for initial states localized within the phase space region $\mathcal{D}_\nu$. The theory describes the dynamics as long as the time-evolved state remains localized within this region. If we are interested in spectral properties of the total Hamiltonian or thermodynamic equilibrium quantities, we are often led to consider states which are delocalized in phase space, such as the electronic Bloch eigenstates of a crystal. The condition that the support of these eigenstates is localized within the region $\mathcal{D}_\nu$ is more restrictive. Hence, the use of the adiabatic projector would provide an incomplete description of eigenstates in general.

#### Presence of degeneracies

When the energy $E_\nu(\mathbf{x},\mathbf{p})$ of the fast Hamiltonian $H(\mathbf{x},\mathbf{p})$ is degenerate with a constant multiplicity in an extended region in phase space, an adiabatic projector can also be constructed. Technically, the symbol at lowest order $\Pi_{\nu,0}(\mathbf{x},\mathbf{p})$ in Eq. (2.70) is simply replaced by the spectral projector of $E_\nu(\mathbf{x},\mathbf{p})$ [74]. This is relevant when we consider an electron in a crystal within a degenerate or quasi-degenerate band, which can be the case when dealing with the electron spin. In this case, the semiclassical equations governing the center of an electron wavepacket involves a non-abelian Berry curvature [13].

The case where $E_\nu(\mathbf{x},\mathbf{p})$ is degenerate on localized regions in phase space leads to very different physical phenomena. These regions in phase space are called conical intersections in the Born-Oppenheimer treatment of a molecule [86]. They are called mode conversion points in the context of semiclassical analysis of wave equations [142]. Mode conversions are non-perturbative tunnelling processes between two adiabatic subspaces, reminiscent of Landau-Zener transitions discussed in the previous chapter. The semiclassical notions loose their relevance in this case. We come back to these aspects in Chap. 6.

## 2.5 Conclusion of chapter

We have considered closed, time independent, quantum systems which decompose into two types of degrees of freedom, the slow and the fast ones. The goal of this chapter was to present the adiabatic theory of such slow-fast quantum system. We considered in Sec. 2.1 the historical example of a molecule studied with the Born-Oppenheimer approximation. This example brings the notion of effective subspace of the total system, the Born-Oppenheimer subspace, within which the eigenstates are computed *via* the

[13]The Moyal product Eq. (2.56) is not rigorously local because it contains all the orders of phase space derivatives. If the Wigner function vanishes identically outside $\mathcal{D}_\nu$ we expect no problem to happen, up to maybe – once again – non-perturbative effects.

Born-Oppenheimer variational ansatz. We then considered another historical example in Sec. 2.2, which is the dynamics of an electron in a crystal perturbed by an electromagnetic field. In this example, the separation into slow and fast degrees of freedom is more subtle. A spectral band of the unperturbed crystal plays the role of the Born-Oppenheimer subspace. The theory based on localized electronic wavepacket projected in a band highlights the role of the Berry curvature in the effective dynamics. The equations of motion governing the center of a localized electronic wavepacket contain the Berry curvature, defining an anomalous velocity.

We then defined a theory of adiabatic dynamics of general slow-fast quantum systems. In Sec. 2.3, we introduced the framework on which this theory relies, which corresponds mainly to the use of the Wigner-Weyl representation to define a notion of order of perturbative expansion. The theory is presented in Sec. 2.4. The main idea is to construct perturbatively a subspace of the total system, the adiabatic subspace, which is stable under the dynamics (up to non-perturbative effects). The adiabatic dynamics is the dynamics of states within this subspace. This adiabatic subspace is defined from a projector, the adiabatic projector, which is constructed perturbatively from the Born-Oppenheimer projector. While the perturbative construction of the adiabatic projector was introduced by the mathematical physics community, we provide an original interpretation of the perturbative expansion. We then present results of the literature concerning the role of the Berry curvature in the effective dynamics within the adiabatic subspace, at first order in the perturbative expansion.

Our interpretation of the adiabatic expansion enabled us to derive in Sec. 2.4.4 quantitative conditions of validity of the adiabatic approximation, from a quantitative expression of the first order adiabatic projector detailed in Sec. 2.4.3. Doing so, we define the domain of the adiabatic projector, which, physically, are the states of the total system for which a separation of timescales exists. The projection of these states are the states of the total system for which the adiabatic dynamics is valid, *i.e.* the states within the adiabatic subspace.

These adiabatic states are tricky to characterize. This point is usually overlooked in the literature. We will study it in detail in Chap. 5. In particular, the slow and fast subsystems are usually physically distinct degrees of freedom. As such, it is natural to consider the entanglement between the subsystems. We quantify it in Chap. 5, and address the question of the experimental preparation of the projected states. In this Chap. 5, we establish the relation between the adiabatic states of a slowly driven quantum system, and the states of the total system lying in the adiabatic subspace $\mathcal{H}_\nu$, for a class of models. We also characterize the dynamics within this subspace beyond the center of wavepacket and beyond the average of observables, quantifying the time evolution of quantum fluctuations of the slow observables.

In the introduction of this thesis, we presented topological pumps as it was historically considered, namely a topological response of a slowly driven quantum system. As such, it mainly relies on the time-dependent adiabatic theory, in the sense that it focuses on the quantum dynamics of a slowly driven quantum system. We argued that to consider it as a pumping phenomenon, it is much more natural to embed it in a description of slow-fast system, where the topological property manifest itself in the dynamics of the slow subsystem. We develop such description in Chap. 3. We introduce a hybrid classical-quantum model enabling to identify the physical observables whose dynamics is affected

by the topological property, by defining a topological coupling between slow and fast systems.

# 2.A Wigner-Weyl phase space representation

We give further relations concerning the Wigner-Weyl representation in complement of the Sec. 2.3.3.

The trace of the product of two operators is given by

$$\mathrm{Tr}_{\mathcal{H}}\left(\hat{A}\hat{B}\right) = \frac{1}{(\lambda 2\pi\hbar)^N}\int \mathrm{d}\mathbf{x}\mathrm{d}\mathbf{p}\, A(\mathbf{x},\mathbf{p})B(\mathbf{x},\mathbf{p}). \tag{2.111}$$

The expression for more than two operators do not only involve the product of symbols, but also the Moyal $\star$-product.

### Expressions of the Moyal product

In the following, we do not write explicitly the phase space coordinates dependence of the Weyl symbols $A(\mathbf{x},\mathbf{p})$, $B(\mathbf{x},\mathbf{p})$ of the operators $\hat{A}$, $\hat{B}$ to lighten the notations.

The expansion of the Moyal $\star$-product in powers of $\lambda$ is simple for one degree of freedom, $N=1$,

$$A\star B = A\exp\left[\lambda\frac{i\hbar}{2}\left(\frac{\overleftarrow{\partial}}{\partial x}\frac{\overrightarrow{\partial}}{\partial p} - \frac{\overleftarrow{\partial}}{\partial p}\frac{\overrightarrow{\partial}}{\partial x}\right)\right]B \tag{2.112}$$

$$= \sum_{n=0}^{\infty}\lambda^n\frac{1}{n!}\left(\frac{i\hbar}{2}\right)^n\sum_{k=0}^{n}(-1)^k\binom{n}{k}\frac{\partial^n A}{\partial p^k\partial x^{n-k}}\frac{\partial^n B}{\partial x^k\partial p^{n-k}} \tag{2.113}$$

$$= AB + \lambda\frac{i\hbar}{2}\{A,B\} + \mathcal{O}(\lambda^2). \tag{2.114}$$

It generalizes for $N$ degrees of freedom $\mathbf{x}=(x_1,\ldots,x_N)$, $\mathbf{p}=(p_1,\ldots,p_N)$

$$A\star B = A\exp\left[\lambda\frac{i\hbar}{2}\sum_{i=1}^{N}\left(\frac{\overleftarrow{\partial}}{\partial x_i}\frac{\overrightarrow{\partial}}{\partial p_i} - \frac{\overleftarrow{\partial}}{\partial p_i}\frac{\overrightarrow{\partial}}{\partial x_i}\right)\right]B \tag{2.115}$$

$$= \sum_{n=0}^{\infty}\lambda^n\, C_n \tag{2.116}$$

where the symbol of order $\lambda^n$ is given by

$$C_n = \frac{1}{n!}\left(\frac{i\hbar}{2}\right)^n\sum_{k=0}^{n}(-1)^k\binom{n}{k}\sum_{i_1,\ldots,i_n=1}^{N}\frac{\partial^n A}{\partial p_{i_1}\ldots\partial p_{i_k}\partial x_{i_{k+1}}\ldots\partial x_{i_n}}\frac{\partial^n B}{\partial x_{i_1}\ldots\partial x_{i_k}\partial p_{i_{k+1}}\ldots\partial p_{i_n}}. \tag{2.117}$$

These expressions show that the order in $\lambda$ in the $\star$-product also corresponds to the order of phase space derivatives of the symbols.

In particular, if one of the two operators is polynomial in $\mathbf{x}$ and $\mathbf{p}$, the series contains a finite number of terms such that an exact expression of the $\star$-product is easily obtained.

# 2.B Derivation of the adiabatic projector at first order

## 2.B.1 Gauge covariant tensors

We provide relations concerning the gauge covariant tensors entering the matrix elements of $\Pi_{\nu,1}(\mathbf{x},\mathbf{p})$.

We note $\boldsymbol{\xi} = \{\xi^\alpha\} = (\mathbf{x},\mathbf{p})$ the phase space coordinates, and $\partial_\alpha = \frac{\partial}{\partial \xi^\alpha}$. We note $|\psi_\mu(\boldsymbol{\xi})\rangle$ the (continuous) normalized eigenstates of $H(\boldsymbol{\xi})$ of eigenenergy $E_\mu(\boldsymbol{\xi})$.

We introduce below different quantities depending on energy levels indices, written from a gauge choice $|\psi_\mu(\boldsymbol{\xi})\rangle$. A quantity $X_{\mu\nu}(\boldsymbol{\xi})$ is gauge covariant if under a gauge transformation,

$$\left|\tilde{\psi}_\mu(\boldsymbol{\xi})\right\rangle = e^{i\theta_\mu(\boldsymbol{\xi})}\,|\psi_\mu(\boldsymbol{\xi})\rangle\,, \tag{2.118}$$

it transforms as

$$\tilde{X}_{\mu\nu}(\boldsymbol{\xi}) = e^{-i\theta_\mu(\boldsymbol{\xi})} X_{\mu\nu}(\boldsymbol{\xi}) e^{i\theta_\nu(\boldsymbol{\xi})}, \tag{2.119}$$

such that it corresponds to the matrix elements of an operator.

In the following, the non-abelian Berry connection $A_{\mu\nu,\alpha}(\boldsymbol{\xi})$ is gauge covariant for $\mu \neq \nu$, the Berry curvature of a family $\mathscr{E}$ of levels $F^{(\mu\nu)}_{\mathscr{E},\alpha\beta}(\boldsymbol{\xi})$ is gauge covariant for $\mu,\nu \in \mathscr{E}$, and the two levels energy tensor $G_{\mu,\nu,\alpha\beta}(\boldsymbol{\xi})$ is gauge covariant.

To lighten the notations in the following, we omit the $\boldsymbol{\xi}$ dependence of the tensors.

### Berry connection

The components of the non-abelian Berry connection satisfy

$$A_{\mu\nu,\alpha} = i\,\langle\psi_\mu|\partial_\alpha\psi_\nu\rangle = -i\,\langle\partial_\alpha\psi_\mu|\psi_\nu\rangle\,. \tag{2.120}$$

They are gauge covariant for $\mu \neq \nu$. In the derivation, it is always useful to write the result in terms of the components of the non-abelian Berry connection.

We note the Berry connection of level $\nu$ as

$$A_{\nu,\alpha} = A_{\nu\nu,\alpha} = i\,\langle\psi_\nu|\partial_\alpha\psi_\nu\rangle\,. \tag{2.121}$$

It is gauge dependent. In the derivations, the components of the Berry connection for a single level $\nu$ have to be combined to the other components of the Berry connection to form the following gauge covariant tensors.

### Berry curvature of level $\nu$

$$F_{\nu,\alpha\beta} = i\left(\langle\partial_\alpha\psi_\nu|\partial_\beta\psi_\nu\rangle - (\alpha \leftrightarrow \beta)\right) \tag{2.122}$$

$$= i\sum_{\mu\neq\nu}\left(A_{\nu\mu,\alpha}A_{\mu\nu,\beta} - (\alpha \leftrightarrow \beta)\right) \tag{2.123}$$

### Berry curvature of the complement family of levels $\overline{\{\nu\}}$

We note $\overline{\{\nu\}} = \{1, 2, \dots\} \setminus \{\nu\}$ the ensemble of all the levels $\mu \neq \nu$.

The non-abelian curvature $F_{\overline{\{\nu\}}}$ is an operator-valued two-form, whose components $F_{\overline{\{\nu\}},x_i p_i}$ are operators acting on the subspace generated by the $|\psi_{\mu\neq\nu}\rangle$. Its matrix elements in terms of the connection (2.84) satisfies, for $\mu_1, \mu_2 \neq \nu$

$$F^{(\mu_1\mu_2)}_{\overline{\{\nu\}},\alpha\beta} = i\left(\langle\partial_\alpha\psi_{\mu_1}|\partial_\beta\psi_{\mu_2}\rangle - \sum_{\mu\neq\nu} A_{\mu_1\mu,\alpha}A_{\mu\mu_2,\beta} - (\alpha\leftrightarrow\beta)\right) \tag{2.124}$$

$$= i\left(A_{\mu_1\nu,\alpha}A_{\nu\mu_2,\beta} - (\alpha\leftrightarrow\beta)\right). \tag{2.125}$$

We have the following relation between $F_\nu$ and the trace of $F_{\overline{\{\nu\}}}$

$$\sum_{\mu\neq\nu} F^{(\mu\mu)}_{\overline{\{\nu\}},\alpha\beta} = -F_{\nu,\alpha\beta}. \tag{2.126}$$

### Berry curvature of an ensemble of levels

The two previous definitions generalize for an ensemble $\mathscr{E} = \{\nu_1, \nu_2, \dots\}$ of levels. The components of the Berry curvature of the ensemble $\mathscr{E}$ are, for $\nu_1, \nu_2 \in \mathscr{E}$

$$F^{(\nu_1\nu_2)}_{\mathscr{E},\alpha\beta} = i\left(\langle\partial_\alpha\psi_{\nu_1}|\partial_\beta\psi_{\nu_2}\rangle - \sum_{\nu\in\mathscr{E}} A_{\nu_1\nu,\alpha}A_{\nu\nu_2,\beta} - (\alpha\leftrightarrow\beta)\right) \tag{2.127}$$

$$= i\sum_{\mu\notin\mathscr{E}}\left(A_{\nu_1\mu,\alpha}A_{\mu\nu_2,\beta} - (\alpha\leftrightarrow\beta)\right). \tag{2.128}$$

The Berry curvature associated to two levels $\mathscr{E} = \{\mu, \nu\}$ will be involved in the following relations.

### Energy tensor of level $\nu$

From the spectral decomposition

$$H = \sum_\mu E_\mu |\psi_\mu\rangle\langle\psi_\mu| \tag{2.129}$$

and from the above relations, we derive the following expressions of the imaginary part of the energy tensor of band $\nu$ in terms of the eigenenergies and the Berry curvatures

$$\operatorname{Im} G_{\nu,\alpha\beta} = \operatorname{Im}\langle\partial_\alpha\psi_\nu|\left(H - E_\nu\right)|\partial_\beta\psi_\nu\rangle \tag{2.130}$$

$$= \operatorname{Im}\langle\partial_\alpha\psi_\nu|\left(\sum_{\mu\neq\nu}(E_\mu - E_\nu)|\psi_\mu\rangle\langle\psi_\mu|\right)|\partial_\beta\psi_\nu\rangle \tag{2.131}$$

$$= \frac{1}{2}E_\nu F_{\nu,\alpha\beta} - \frac{1}{2}\sum_{\mu\neq\nu} E_\mu F^{(\nu\nu)}_{\overline{\{\mu\}},\alpha\beta}. \tag{2.132}$$

**Two levels energy tensor of levels** $(\mu\nu)$

Similarly, we obtain the following expression of the imaginary part of the two-levels energy tensor of bands $\mu$ and $\nu$ in terms of the eigenenergies and the Berry curvatures

$$\operatorname{Im} G_{\mu,\nu,\alpha\beta} = \operatorname{Im} \langle \partial_\alpha \psi_\mu | \left( \sum_{\sigma \notin \{\mu,\nu\}} (E_\sigma - E_\mu) |\psi_\sigma\rangle \langle \psi_\sigma| \right) |\partial_\beta \psi_\nu\rangle \tag{2.133}$$

$$= \frac{1}{2} E_\mu F^{(\mu\nu)}_{\{\mu,\nu\},\alpha\beta} - \frac{1}{2} \sum_{\sigma \notin \{\mu,\nu\}} E_\sigma F^{(\mu\nu)}_{\overline{\{\sigma\}},\alpha\beta}. \tag{2.134}$$

## 2.B.2 Matrix elements of the first order projector

From Eq. (2.85b), we obtain

$$\langle \psi_\nu | \Pi_{\nu,1} | \psi_\nu \rangle = -\frac{i\hbar}{2} \langle \psi_\nu | \{\Pi_{\nu,0}, \Pi_{\nu,0}\} | \psi_\nu \rangle \tag{2.135}$$

$$= -\frac{i\hbar}{2} \sum_{i=1}^{N} \left( \langle \psi_\nu | \frac{\partial \Pi_{\nu,0}}{\partial x_i} \frac{\partial \Pi_{\nu,0}}{\partial p_i} |\psi_\nu\rangle - (x_i \leftrightarrow p_i) \right). \tag{2.136}$$

Inserting the identity $\sum_\mu |\psi_\mu\rangle \langle \psi_\mu|$ between the derivatives of $\Pi_{\nu,0} = |\psi_\nu\rangle \langle \psi_\nu|$, we obtain after development of the derivative of $|\psi_\nu\rangle \langle \psi_\nu|$

$$\langle \psi_\nu | \Pi_{\nu,1} | \psi_\nu \rangle = -\frac{i\hbar}{2} \sum_{i=1}^{N} \sum_{\mu \neq \nu} A_{\nu\mu,x_i} A_{\mu\nu,p_i} - (x_i \leftrightarrow p_i) \tag{2.137}$$

$$= -\frac{\hbar}{2} \sum_{i=1}^{N} F_{\nu,x_i p_i}, \tag{2.138}$$

where we use the expression of the Berry curvature in terms of the non-Abelian connection (2.123).

From Eq. (2.85b), we obtain for $\mu_1, \mu_2 \neq \nu$

$$\langle \psi_{\mu_1} | \Pi_{\nu,1} | \psi_{\mu_2} \rangle = \frac{i\hbar}{2} \langle \psi_{\mu_1} | \{\Pi_{\nu,0}, \Pi_{\nu,0}\} | \psi_{\mu_2} \rangle \tag{2.139}$$

$$= \frac{i\hbar}{2} \sum_{i=1}^{N} \left( \langle \psi_{\mu_1} | \frac{\partial \Pi_{\nu,0}}{\partial x_i} \frac{\partial \Pi_{\nu,0}}{\partial p_i} |\psi_{\mu_2}\rangle - (x_i \leftrightarrow p_i) \right) \tag{2.140}$$

$$= \frac{i\hbar}{2} \sum_{i=1}^{N} \left( A_{\mu_1\nu,x_i} A_{\nu\mu_2,p_i} - (x_i \leftrightarrow p_i) \right) \tag{2.141}$$

$$= \frac{\hbar}{2} \sum_{i=1}^{N} F^{(\mu_1\mu_2)}_{\overline{\{\nu\}},x_i p_i}. \tag{2.142}$$

From Eq. (2.85a), we obtain for $\mu \neq \nu$

$$\langle \psi_\mu | \Pi_{\nu,1} | \psi_\nu \rangle = \frac{i\hbar}{2} \frac{1}{\mathcal{E}_\nu - \mathcal{E}_\mu} \langle \psi_\mu | \left( \{H_{\text{tot}}, \Pi_{\nu,0}\} - \{\Pi_{\nu,0}, H_{\text{tot}}\} \right) |\psi_\nu\rangle . \tag{2.143}$$

$$= \frac{i\hbar}{2} \frac{1}{E_\nu - E_\mu} \sum_{i=1}^{N} \langle \psi_\mu | \left( \frac{\partial H_{\text{tot}}}{\partial x_i} \frac{\partial \Pi_{\nu,0}}{\partial p_i} - \frac{\partial \Pi_{\nu,0}}{\partial x_i} \frac{\partial H_{\text{tot}}}{\partial p_i} - (x_i \leftrightarrow p_i) \right) |\psi_\nu\rangle . \tag{2.144}$$

We then use the spectral decomposition

$$H_{\rm tot} = \sum_\sigma \mathcal{E}_\sigma \left|\psi_\sigma\right\rangle \left\langle\psi_\sigma\right| , \tag{2.145}$$

insert the identity $\sum_{\sigma'} \left|\psi_{\sigma'}\right\rangle \left\langle\psi_{\sigma'}\right|$ between the derivatives of the operators, and expand the derivatives. We first write the expression in terms of the non-abelian Berry connection (2.120), and then in terms of the Berry curvatures for ensemble of levels Eq. (2.128). It leads to

$$\begin{aligned}\left\langle\psi_\mu\right| \Pi_{\nu,1} \left|\psi_\nu\right\rangle = \frac{\hbar}{E_\nu - E_\mu} \sum_{i=1}^N \left( \frac{\partial}{\partial x_i} \left( \frac{\mathcal{E}_\nu + \mathcal{E}_\mu}{2} \right) A_{\mu\nu,p_i} - (x_i \leftrightarrow p_i) \right) \\ + \frac{1}{2} \frac{\hbar}{E_\nu - E_\mu} \sum_{i=1}^N \left( E_\mu F^{(\mu\nu)}_{\{\mu,\nu\},x_i p_i} - \sum_{\sigma \notin \{\mu,\nu\}} E_\sigma F^{(\mu\nu)}_{\overline{\{\sigma\}},x_i p_i} \right) . \end{aligned} \tag{2.146}$$

We recognize in the last term the expression of the two-level energy tensor provided in Eq. (2.134), leading to the final result Eq. (2.97).

Chapter 3

# Hybrid classical-quantum formulation of topological pumps

In the introduction of this thesis, we presented historical descriptions of topological pumping as the response of a driven quantum system. We discussed examples for quantum systems of different physical dimension $D$. These previous descriptions focused on the dynamics of the driven quantum system, imposed by an external classical drive. This description of pumping calls for a key generalization that includes explicitly the coupled degrees of freedom of the environment if one wants to model the observable topological transfer.

We develop such a global framework in this chapter. We discuss topological pumps as a particular type of couplings between a fast quantum system and slow degrees of freedom. We consider the driving fields as a dynamical system, and topological pumping manifests itself in the dynamics of these fields. This enables us to identify the physical observables affected by the topological property, and provides a unified framework for the description of different physical realizations of topological pumps. In particular, we show that to define a topological Chern coupling, what is important is not the physical dimension $D$ of the fast quantum system, but the number of slow degrees of freedom coupled to it. This allows us to define a notion of topological coupling between two slow degrees of freedom and a fast quantum system.

In this chapter, we restrict our attention to a classical treatment of the slow degrees of freedom of the environment. In particular, this is sufficient to identify the physical observable carrying the topological transfer. This hybrid classical-quantum framework is technically simpler than the general theory of slow-fast quantum systems introduced in Chap. 2. We pay attention on the case of classical modes, or action-angle variables, which describe the periodic drives of a quantum system. These drives were discussed as classical parameters in previous descriptions of topological pumps. Here we consider them as slow classical degrees of freedom. The interaction between them and the gapped quantum system, when treated within the adiabatic approximation, effectively reduces on average to a topological coupling leading to a quantized pumping between the classical subsystems composing the environment.

This chapter is based on the first three sections of the publication [56].

**Comment on the notations**

In this chapter, we adopt the notations of Chap. 2 regarding eigenstates and eigenenergies, which slightly differ from the Chap. 1. We are led to consider a Hamiltonian $H(\mathbf{q})$ of the fast subsystem depending on classical variables $\mathbf{q} = \{q_i\}$. Its eigenstates are noted $|\psi_\nu(\mathbf{q})\rangle$ and its eigenenergies $E_\nu(\mathbf{q})$.

## 3.1 Slow classical degrees of freedom coupled to a fast quantum system

We provide a general model of coupled fast and slow degrees of freedom by resorting to a mixed classical - quantum description, see Fig. 3.1. Hybrid classical-quantum dynamical systems have been considered in different contexts in the literature, not necessarily to describe slow-fast systems. For example, semiclassical theories of gravity have been discussed in this way [143, 144], introducing a notion of mixed brackets [145, 146]. Similar mixed classical-quantum descriptions for slow-fast systems were used by M.V. Berry and J. Robbins [73] to discuss a geometric force on the slow subsystem, without deriving an effective classical dynamics of the slow subsystem. Q. Zhang *et al.* [147] used a similar formalism to discuss the geometric forces in a restricted class of Hamiltonian, relying technically on canonical transformations. Such frameworks based on canonical transformations were also used in [148] to discuss the role of Berry phase and Hannay angle in the effective dynamics. Our general framework of coupled classical-quantum system enables us to derive the classical dynamics of the slow subsystem relying only on the adiabatic approximation described in chapters 1 and 2.

### 3.1.1 Hamilton equations of motion

The slow degrees of freedom are described by classical pairs of conjugated variables $q_i, p_i$, $i = 1, ...N$ satisfying the Poisson bracket relations $\{q_i, p_j\} = \delta_{ij}$ [149]. The dynamics of each pair of classical variables, prior to the coupling to the quantum system, is assumed to be slow and described by classical dynamics deduced from a classical Hamiltonian $\mathcal{H}_i(q_i, p_i)$ following

$$\dot{q}_i^{(0)} = \frac{\partial \mathcal{H}_i}{\partial p_i} \qquad \text{and} \qquad \dot{p}_i^{(0)} = -\frac{\partial \mathcal{H}_i}{\partial q_i}. \tag{3.1}$$

We consider the common case where the quantum system couples to only one of the variable of each pair of conjugate variables, which includes in particular the case of a driven quantum system. We note them collectively $\mathbf{q} = \{q_i\}$.

The quantum system is then described by a Hamiltonian $H(\mathbf{q})$ that depends on the states of the classical variables $q_i$. We focus on quantum systems that remain gapped during the evolution of the classical modes. This allows to approximate at shorter times the dynamics of the quantum system by an adiabatic evolution, driven by the slow dynamics of the classical modes. More precisely, we consider a quantum system prepared at time $t = 0$ into one of the eigenstates denoted $|\psi_\nu(\mathbf{q}(t = 0))\rangle$ of the $t = 0$ Hamiltonian $H(\mathbf{q}(t = 0))$. This amounts to assume an initial correlation between the state $\{q_i(t = 0)\}$ of the classical environment and the quantum system. Through the coupling to $q_i(t)$, the

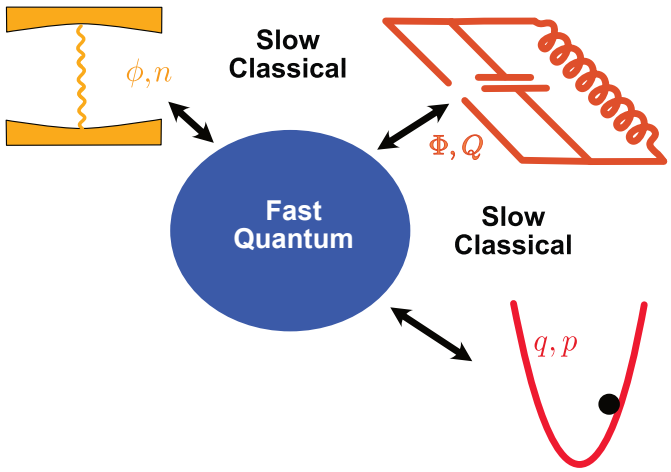


Figure 3.1: We consider a general gapped and fast system (in blue) coupled to slow variables of the environment (in red). The energy separation of the fast quantum system is assumed to be much larger than that of the slow degrees of freedom, allowing a description of the latter by classical pairs of conjugate variables. While of different nature, we denote generically these variables by $q_i, p_i$. The dynamics of each pair follows from a classical Hamiltonian $\mathcal{H}_i$. The quantum system couples instantaneously to a single variable $q_i$ of each degree of freedom of the classical environment.

quantum system will slowly evolve in time on a timescale dictated by the slow classical environment. We denote its instantaneous state $|\Psi(t)\rangle$ and assume that it remains approximately within the same eigensubspace of the Hamiltonian, which is the essence of the *adiabatic approximation* discussed in Chap. 1. In return, the coupling of the classical degrees of freedom to the quantum system also perturbs their dynamics and results in an effective coupling between different pairs of slow degrees of freedom.

The modified Hamilton equations of motion for the slow variables are

$$\dot{q}_i = \dot{q}_i^{(0)}, \tag{3.2}$$

$$\dot{p}_i = \dot{p}_i^{(0)} - \langle\Psi(t)| \frac{\partial H}{\partial q_i} |\Psi(t)\rangle . \tag{3.3}$$

Let us stress that the above description ensures the conservation of the total energy of both quantum and classical degrees of freedom. Indeed, the Schrödinger equation in finite dimension corresponds to classical Hamiltonian equations associated to a Hamiltonian function $E(\Psi) = \langle\Psi| H |\Psi\rangle$ and to a natural Poisson bracket structure on the Hilbert space [150,151]. Therefore, the total phase space also inherits a Poisson bracket structure and the above equations of motion derive from the Hamiltonian function $\mathcal{H}_{\rm tot}(\{q_i\},\{p_i\},\Psi) = \sum_i \mathcal{H}_i(q_i,p_i) + \langle\Psi| H(\{q_i\}) |\Psi\rangle$, thus abiding by the conservation of the total energy.

### Backaction of the quantum system

The second term in Eq. (3.3) represents the backaction of the quantum system onto the classical system. To evaluate it, we now describe the adiabatic evolution of the quantum state $|\Psi(t)\rangle$. Due to the slow evolution of the Hamiltonian $H(\mathbf{q}(t))$, the state $|\Psi(t)\rangle$ of the quantum system does not identify with the instantaneous eigenstate $|\psi_\nu(\mathbf{q}(t))\rangle$ defined by

$H(\mathbf{q}(t))\,|\psi_\nu(\mathbf{q}(t))\rangle = E_\nu(\mathbf{q}(t))\,|\psi_\nu(\mathbf{q}(t))\rangle$. Its expression is given by Eq. (1.8) of the first chapter. The corresponding correction to the dynamics of the slow classical variables $p_i$ in Eq. (3.3) is now expressed as

$$\dot{p}_i = \dot{p}_i^{(0)} - \frac{\partial E_\nu}{\partial q_i} + \hbar \sum_{j\neq i} \dot{q}_j^{(0)} F_{\nu,q_i q_j}, \tag{3.4}$$

see Appendix 3.A for the detailed derivation. The first correction relates to the energy variation of the quantum state and follows from the standard classical - quantum coupling. The last correction is more exotic: it manifests an effective coupling between the different slow variables $q_i, p_i$. The strength of this transverse coupling depends on the geometry of the eigenstates $|\psi_\nu(\mathbf{q})\rangle$ of the quantum system through the components $F_{\nu,q_i q_j}$ of the two-form Berry curvature which are defined as

$$F_{\nu,q_i q_j} = i \sum_{\mu\neq\nu} \frac{\langle\psi_\nu|\,\partial_{q_i} H\,|\psi_\mu\rangle\,\langle\psi_\mu|\,\partial_{q_j} H\,|\psi_\nu\rangle}{(E_\nu - E_\mu)^2} - (i \leftrightarrow j). \tag{3.5}$$

The equation (3.4) enables the identification of the physical observables affected by the geometrical and topological properties of the coupling between the slow and fast subsystems. They enter the dynamics of the variables $p_i$ conjugated to the variables $q_i$ coupled to the quantum system. We use this consideration of conjugated variables in the next chapter in an experimental proposal of topological coupling between a superconducting qubit and microwave modes, in order to identify the physical observables carrying the geometrical and topological properties.

#### Adiabatic states and slow manifold

As detailed in Appendix 3.A, to recover Eq. (3.4) at first order in the adiabatic approximation, the quantum system has to be initialized not in its instantaneous eigenstate $|\psi_\nu(\mathbf{q}(t=0))\rangle$ but in an adiabatic state, provided by Eq. (3.25). If the quantum system is initialized in its instantaneous eigenstates, then we have extra terms oscillating at the Bohr frequencies. In such a case, the classical variables do not evolve only on the slow timescales associated to the classical Hamiltonian, but also on the fast timescales of the quantum system.

We thus recover that the adiabatic states are the initial state on a slow manifold, leading to a slow evolution of the physical observables, as discussed in Sec. 1.2.1 of the first chapter. Eq. (3.4) is the equation of motion within this slow manifold.

#### Condition of adiabaticity

The condition of validity of the time dependent adiabatic approximation is discussed in details in Sec. 1.2.3 of the first chapter. In particular, the velocity $\dot{q}_i^{(0)}$ of the slow variable, given by Eq. (3.1), has to satisfy the condition (1.40), and the time of validity of the adiabatic approximation is given by Eq. (1.56).

### 3.1.2 Geometrical power transfer

The geometrical coupling in (3.4) between the different subsets of slow variables $q_i(t), p_i(t)$ is associated with an energy transfer between them. The change of energy of each classical

degree of freedom is:

$$\begin{aligned}\frac{\mathrm{d}\mathcal{E}_i}{\mathrm{d}t} &= \dot{q}_i \frac{\partial \mathcal{H}_i}{\partial q_i} + \dot{p}_i \frac{\partial \mathcal{H}_i}{\partial p_i} \\ &= -\dot{q}_i^{(0)} \frac{\partial E_\nu}{\partial q_i} + \hbar \sum_{j \neq i} \dot{q}_i^{(0)} \dot{q}_j^{(0)} F_{\nu, q_i q_j}. \end{aligned} \tag{3.6}$$

The antisymmetry of the Berry curvature ensures the conservation of the total energy.

### 3.1.3 Nature of classical degrees of freedom

Let us discuss briefly the implications of the previous modification of Hamilton equations for different types of classical slow degrees of freedom coupled to a quantum system.

#### Massive classical particles

The initial context of the Born-Oppenheimer approximation, at the origin of the adiabatic approximation, was the description of light particles, the electrons, coupled to heavy particles, the nuclei. In this situation, the slow degrees of freedom described classically are those of the massive particles: their position $q_i$ and conjugated momentum $p_i$. The corresponding Hamiltonian is $\mathcal{H}_i = p_i^2/(2M) + V(q_i)$, parametrized by the mass $M$ and potential $V(q)$. The equations of motion in this case take the form

$$\dot{q}_i = \frac{p_i}{M}, \tag{3.7}$$

$$\dot{p}_i = -V'(q_i) - \partial_{q_i} E_\nu + \hbar \sum_{j \neq i} \frac{p_j}{M} F_{\nu, q_i q_j}. \tag{3.8}$$

Equation (3.8) describes the associated anomalous geometrical force [73, 80].

#### Classical modes

While the previous adiabatic formalism was initially designed with classical massive degree of freedom in mind, it also applies to the case of slow action-angle $\phi_i, n_i$ variables, which we will call a *classical mode*. In more details, we consider a variable $p_i = \hbar n_i$ where $n_i$ takes only integer values and its canonical phase $q_i = \phi_i$, a $2\pi$ periodic phase. Of particular interest is the situation of a monochromatic mode, corresponding to the Hamiltonian $\mathcal{H}_i = \hbar \omega_i n_i = \omega_i p_i$ whose linearity in $n_i$ is the distinctive feature compared with the massive case. In this situation, the modified Hamilton equations of motion read

$$\dot{\phi}_i = \dot{q}_i = \omega_i, \tag{3.9}$$

$$\hbar \dot{n}_i = \dot{p}_i = -\frac{\partial E_\nu}{\partial \phi_i} + \hbar \sum_{j \neq i} \omega_j F_{\nu, \phi_i \phi_j}. \tag{3.10}$$

In the case of classical modes, the Eq. (3.10) describes the filling rate of mode $i$. The energy transferred between the different modes corresponds to

$$\frac{\mathrm{d}\mathcal{E}_i}{\mathrm{d}t} = -\omega_i \frac{\partial E_\nu}{\partial \phi_i} + \hbar \sum_{j \neq i} \omega_i \omega_j F_{\nu, \phi_i \phi_j}. \tag{3.11}$$

## 3.2 Topological pumps as coupling between a classical environment and a quantum system

In the following, we develop a slow-fast description of topological pumps by showing how they can naturally be described with the formalism of Sec. 3.1 of adiabatic topological coupling between classical slow variables of different nature.

### 3.2.1 Topological versus geometrical couplings

In the above section, we have shown how a geometrical quantity, the Berry curvature, encodes the strength of the effective coupling mediated by a quantum system between classical variables. Of particular interest is the case of two classical variables, *e.g.* $q_1$ and $q_2$ with a compact configuration space denoted $[0, 2\pi]^2$. In this situation, the Chern number $\mathcal{C}_{\nu,12}$, defined as

$$\int_{[0,2\pi]^2} \mathrm{d}q_1 \mathrm{d}q_2 \; F_{\nu,q_1 q_2} = 2\pi \; \mathcal{C}_{\nu,12}, \tag{3.12}$$

is an integer topological quantity, *i.e.* it is insensitive to perturbations of the quantum Hamiltonian $H$ provided the gap between $E_\nu$ and other states does not close.

Noting that (3.12) is nothing but the averaged Berry curvature over the configuration space, the case of a Hamiltonian $H$ characterized by a topological Chern number corresponds to a quantized averaged coupling in Eq. (3.4). We define the topological coupling as that between two slow degrees of freedom and the fast quantum system when the Chern number is non-zero.

When the Berry curvature fluctuates in the configuration space around its topological average, a quantized coupling between the classical variables is only recovered when averaging over initial position in configuration space, which is hardly practical. Alternatively, we can resort to a time average: if the evolution of classical phase variables is ergodic on the compact configuration space $[0, 2\pi]^2$, an average over the configuration space can be replaced by an average over a sufficiently long time.

### 3.2.2 $D = 2$ Quantum Hall pump

In an enlightening argument, B. Laughlin related the quantization of the transverse conductivity of the quantum Hall state to a transfer of charge between edges in a Corbino geometry as the flux threading the disk is increased by one quantum [6]. Later on, Niu, Thouless and Wu introduced the notion of generalized boundary conditions for quantum Hall states [27]. The quantum Hall topological properties are expressed as the Chern number of the ensemble of many-body groundstates over the closed manifold of phase boundary conditions. These boundary conditions parameters were later related to electromotive forces through loops connecting opposite edges of the sample [3, 29] effectively generalizing the topology of Laughlin's gedanken experiment to that of a torus and allowing for a dynamical description of the quantum Hall effect over a classical parameter space [54].

Here we consider the classical phases entering the generalized boundary conditions as dynamical variables. This effectively amounts to realize a quantum Hall topological pump between two $LC$ harmonic circuits. Let us consider a quantum Hall sample coupled to

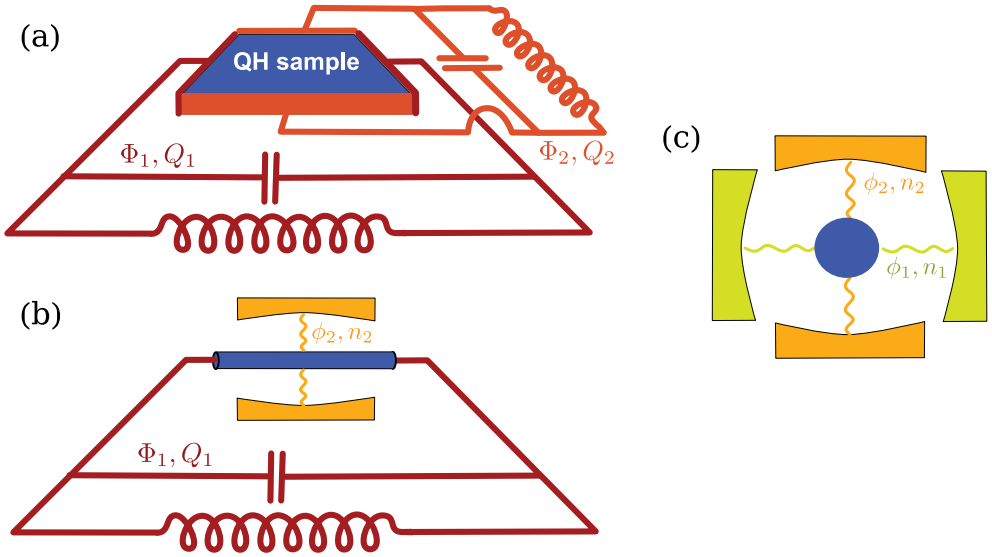


Figure 3.2: (a) Schematic quantum Hall circuit where two LC branches, described by classical conjugate variables $\Phi$ and $Q$, are connected through a quantum Hall sample. (b) Schematic Thouless pump driven by a phase $\phi_2 = \omega_2 t$ conjugate to a variable $n_2$, and coupled to an LC branch. Topological pumping gives rise to a current in the $LC$ circuit. (c) Topological mode coupler, or frequency converter, in which two classical modes described by $\phi_1, n_1$ and $\phi_2, n_2$ variables are coupled topologically through a quantum system.

two independent electrical circuits in the $x$ and $y$ direction, see Fig. 3.2(a). The coupling between each circuit and the quantum Hall sample follows from the boundary conditions of Niu *et al.* [27] on the many-body ground state wave function $\Psi(x_k, y_k)$:

$$\Psi(x_k + L_x, y_k) = e^{i\Phi_1}\ \Psi(x_k, y_k), \tag{3.13a}$$
$$\Psi(x_k, y_k + L_y) = e^{i\Phi_2}\ \Psi(x_k, y_k). \tag{3.13b}$$

The two phases $\Phi_1, \Phi_2$ are related to the voltage drop $V_i$ in each directions as $\Phi_i(t) = (e/\hbar)\int^t V_i(t')dt'$. If we model each electric branch associated to this voltage drop as an LC circuit [152], these phases are dynamical classical variables, whose canonically conjugate momenta are the (rescaled) accumulated charge in each circuit $Q_i = (\hbar/e)\int^t I_i(t')dt'$, $I_i$ being the current in each circuits. The classical Hamiltonian describing each LC circuit is

$$\mathcal{H}_i = \frac{e^2}{2\hbar^2 C_i} Q_i^2 + \frac{\hbar^2}{2e^2 L_i}\Phi_i^2\ , \tag{3.14}$$

where $L_i$ is the inductance and $C_i$ the capacitance of the corresponding circuit [152]. Hence, the dynamics of an LC circuit identifies to that of a massive particle of position $q_i = \Phi_i$ and momentum $p_i = Q_i$, in a harmonic potential.

The Hamilton's equations (3.7 and 3.8) include a correction to the usual relations between flux and current

$$\dot{Q}_1 = \frac{\hbar}{e} I_1 = -\left(\frac{\hbar}{e}\right)^2 \frac{\Phi_1}{L_1} + \hbar F_{\Phi_1\Phi_2}\frac{e}{\hbar}V_2 \tag{3.15}$$

*via* the Berry curvature $F_{\Phi_1\Phi_2}$ of the quantum Hall effect ground states derived by Niu *et al.* [27]. This Berry curvature being independent of the external fluxes and thus constant over the parameter space, it is related to the quantum Hall Chern number $\mathcal{C}_{12}$ via $F_{\Phi_1\Phi_2} = \mathcal{C}_{12}/(2\pi)$. Thus, the corrected classical equation of motion of the $LC$ circuits reads

$$I_1 = -\frac{\hbar}{e}\frac{\Phi_1}{L_1} + \frac{e^2}{h}\mathcal{C}_{12}V_2. \tag{3.16}$$

We recover the quantization of Hall conductivity in the limit $L_1 \to \infty$.

Note that the energy transferred from one LC circuit to the other, following (3.6), is

$$\frac{\mathrm{d}E_1}{\mathrm{d}t} = \hbar F_{\Phi_1\Phi_2}\dot{\Phi}_1\dot{\Phi}_2 = \mathcal{C}_{12}\left(\frac{e^2}{h}\right)V_1V_2 = \delta I_1 V_1. \tag{3.17}$$

In the limit of an ideal Hall measurement, where the $L_1C_1$ circuit corresponds to an ammeter, we get $V_1 = 0$, and no energy is transferred between the two circuits.

### 3.2.3 $D = 1$ Thouless pump

Let us now turn to the canonical example of a topological pump, proposed by D. Thouless [11], which consists in a $D = 1$ crystal suitably periodically driven in time, such as the Rice-Mele model [12]. The single electron dynamics is thus described by a time-dependent Bloch Hamiltonian $H(k, \phi(t))$ periodic both in momentum over the Brillouin zone, and in a $2\pi$ periodic phase $\phi(t) = \omega t$. This Hamiltonian is assumed to be gapped at all time, and with energy band eigenstates $|\psi_\nu(k,\phi)\rangle$ possessing a finite Chern number $\mathcal{C}_{\nu,k\phi}$ over the 2-torus constituted of the $D = 1$ Brillouin zone and periodic phase configuration space of phase $\phi$. In such a system, topological pumping is usually described as the appearance of a steady current in the bulk of a closed ring, corresponding to an anomalous geometric velocity for semi-classical states in band $\nu$ $\langle\dot{x}\rangle = \langle F_{\nu,k\phi}\rangle\partial_t\phi = 2\pi\,\mathcal{C}_{\nu,k\phi}\,\omega$ [13,101]. We refer to the review [26] on Thouless pumping, which in particular discusses its generalizations and experimental realizations.

The difference between topological and geometrical coupling discussed in Sec. 3.2.1 is reminiscent of the difference between topological and geometrical charge pumping in the context of Thouless pumps [153], while the use of a time-average on the slow variables is reminiscent of the use of Bloch oscillations to recover a topologically quantized Thouless pumping [154, 155].

We propose an alternative description of such a Thouless pump, by considering an open $D = 1$ crystal of size $L$ connected on both ends to an electrical $LC$ circuit, analogous to the quantum Hall pump, see Fig. 3.2(b). The coupling between the charged particles in the crystal and the $LC$ circuit follows from the boundary conditions (3.13) on the many-body groundstate wavefunction $\Psi(x = 0, \phi(t)) = e^{i\Phi_1}\Psi(x = L, \phi(t))$. This amounts to couple the crystal to a pair of classical conjugated variables $Q_1, \Phi_1$ identical to those in the quantum Hall pump, with a classical Hamiltonian (3.14) describing their dynamics. The periodic driving of the Hamiltonian is now interpreted as the coupling between the charges of the crystal and a dynamical classical variable $\phi_2 = \omega t$, conjugated to a variable $n_2$. The dynamics $\dot{\phi}_2 = \omega, \dot{n}_2 = 0$, correspond to that of a classical mode introduced in Sec. 3.1.3.

In this representation, the topological coupling between the $LC$ circuit and the classical mode leads to a modified equation of motion in the $LC$ circuit, manifesting the appearance

of a charged current. The modified Hamilton equation (3.7) reads

$$\dot{Q}_1 = \frac{\hbar}{e} I_1 = -\left(\frac{\hbar}{e}\right)^2 \frac{\Phi_1}{L} + \hbar F_{\Phi_1\phi_2}\omega, \tag{3.18}$$

which leads to a steady charge current $I_1 = e2\pi F_{\Phi_1\phi_2}/T$ through the driven crystal, corresponding to an average number $\mathcal{C}_{\nu,\Phi_1\phi_2} = \mathcal{C}_{\nu,k\phi}$ of charge transferred across the chain per period $T$ of the drive. This result identifies with the standard steady anomalous velocity in the bulk of the Thouless pump.

### 3.2.4 $D = 0$ Power pump

In the previous section, we interpreted a time-periodic quantum Hamiltonian as a coupling between a fast quantum system and a slow classical mode. A natural extension consists in considering a single quantum system coupled to the phases $\phi_i$ of an arbitrary number $N$ of classical modes, see Fig. 3.2(c). The quantum dynamics of such a system can be described within Floquet theory [44]. The topological Chern numbers of such a quantum system are defined in Floquet space, and, when non-zero, leads to a topological frequency conversion mechanism.

The description of such a *quantum mode coupler* is natural in terms of an effective classical dynamics of the modes. We assume that the quantum system couples only to the phases of the modes, corresponding to a Hamiltonian $H(\phi_1(t), \ldots, \phi_N(t))$. In such a case, the equations of motions are given by (3.9, 3.10) with a power leaving each mode given by Eq. (3.11). In the particular case of two modes of frequency $\omega_1, \omega_2$, we recover the result of Martin *et al.* for the averaged power transfer between two modes given by $\mathrm{d}\mathcal{E}_1/\mathrm{d}t = \hbar\omega_1\omega_2\, \mathcal{C}_{\nu,\phi_1\phi_2}/(2\pi)$ [44].

## 3.3 Conclusion of chapter

We presented a formalism of slow-fast quantum system, where the slow subsystem is described classically. The formalism focuses on the effective slow dynamics of the classical system. It is motivated by the modelization the observable topological transfer occurring in topological pumps. These topological pumps were discussed historically through the dynamics of a driven quantum system. Considering this driving as originating from the coupling to external dynamical variables, we show that the geometrical properties of the coupling impact the dynamics of the conjugated observables of these variables. To define a topological Chern coupling, what is essential is not the physical dimension $D$ of the fast quantum system, but the number of slow degrees of freedom coupled to it. We defined a topological coupling between two slow degrees of freedom and a fast quantum system. We described the $D = 2$ quantum Hall effect, the $D = 1$ Thouless pump, and the $D = 0$ topological frequency conversion within this formalism of topological coupling between classical slow variables of different nature.

In the next chapter, building on this general description of topological pumping, we propose a realization of such a quantum topological coupler between microwaves modes using an artificial 3 level atom, a qutrit. We identify the physical observables carrying the topological property. The experimental proposal is designed for their measure to be of experimental reach.

This hybrid classical-quantum formulation of topological coupling between slow and fast systems misses fundamental quantum aspects, such the entanglement between the two subsystems, the quantum fluctuations of the slow degrees of freedoms, or the dynamics of non-classical states. We describe these aspects in Chap. 5. Besides, we emphasize the importance of the preparation of the initial state in this chapter.

# 3.A Derivation of the backaction at first order

In this appendix, we derive the expression of the backaction of the quantum system onto the dynamics of the variable $p_i$.

We consider the time-evolution $|\Psi(t)\rangle$ of the quantum system evolving according to the Hamiltonian $H(\mathbf{q}(t))$ which is time-dependent due to the coupling to the time dependent variables $\mathbf{q}(t)$. According to Sec. 1.1 in the first chapter, when prepared in an instantaneous eigenstate $|\Psi(t=0)\rangle = |\psi_\nu(\mathbf{q}(t=0))\rangle$, the time evolution of the quantum state at first order in adiabatic perturbation theory is given by

$$|\Psi(t)\rangle = e^{i\gamma^d_{\nu,0}(t)+i\gamma^g_{\nu,0}(t)}\left(|\psi_\nu(\mathbf{q}(t))\rangle - \hbar\sum_{\mu\neq\nu}\sum_j \dot{q}_j(t)\frac{A_{\mu\nu,q_j}(\mathbf{q}(t))}{E_\nu(\mathbf{q}(t))-E_\mu(\mathbf{q}(t))}\,|\psi_\mu(\mathbf{q}(t))\rangle\right) + \hbar\sum_{\mu\neq\nu}\sum_j e^{i\gamma^d_{\mu,0}(t)+i\gamma^g_{\mu,0}(t)}\left[\dot{q}_j(t)\frac{A_{\mu\nu,q_j}(\mathbf{q}(t))}{E_\nu(\mathbf{q}(t))-E_\mu(\mathbf{q}(t))}\right]_{t=0}|\psi_\mu(\mathbf{q}(t))\rangle\,, \quad (3.19)$$

with the components of the non-abelian Berry connection satisfying for $\mu\neq\nu$

$$A_{\mu\nu,q_i}(\mathbf{q}) = i\,\langle\psi_\mu(\mathbf{q})|\partial_{q_i}\psi_\nu(\mathbf{q})\rangle = i\frac{\langle\psi_\mu(\mathbf{q})|\,\frac{\partial H}{\partial q_i}(\mathbf{q})\,|\psi_\nu(\mathbf{q})\rangle}{E_\nu(\mathbf{q})-E_\mu(\mathbf{q})}, \quad (3.20)$$

and where the zeroth order dynamical phase reads

$$\gamma^d_{\nu,0}(t) = -\frac{1}{\hbar}\int_0^t E_\nu(\mathbf{q}(t'))\mathrm{d}t', \quad (3.21)$$

and the zeroth order geometric phase reads

$$\gamma^g_{\nu,0}(t) = \int_0^t \langle\psi_\nu(\mathbf{q}(t'))|\,i\frac{\mathrm{d}}{\mathrm{d}t'}\,|\psi_\nu(\mathbf{q}(t'))\rangle\,\mathrm{d}t'. \quad (3.22)$$

We recall that, in this chapter, we use the notations $|\psi_\nu(\mathbf{q})\rangle$ for the eigenstates and $E_\nu(\mathbf{q})$ for the eigenenergies of the Hamiltonian of the fast system, in contrast to the first chapter.

The correction to the equation of motion of the variable $p_i$ at first order is then

$$\begin{aligned}-\langle\Psi(t)|\frac{\partial H}{\partial q_i}|\Psi(t)\rangle &= -\langle\psi_\nu|\frac{\partial H}{\partial q_i}|\psi_\nu\rangle \\ &\quad + \hbar\sum_{\mu\neq\nu}\sum_j \dot{q}_j(t)\left(i\frac{\langle\psi_\nu|\frac{\partial H}{\partial q_i}|\psi_\mu\rangle\langle\psi_\mu|\frac{\partial H}{\partial q_j}|\psi_\nu\rangle}{(E_\nu-E_\mu)^2}+\text{c.c.}\right) \\ -\hbar\sum_{\mu\neq\nu}\sum_j &\left(e^{i\gamma^{\text{Bohr}}_{\mu\nu,0}(t)}e^{i\gamma^g_{\mu,0}(t)-i\gamma^g_{\nu,0}(t)}\frac{\dot{q}_j(0)A_{\mu\nu,q_j}(\mathbf{q}(0))}{E_\nu(\mathbf{q}(0))-E_\mu(\mathbf{q}(0))}\langle\psi_\nu(\mathbf{q}(t))|\frac{\partial H}{\partial q_i}(\mathbf{q}(t))\,|\psi_\mu(\mathbf{q}(t))\rangle+\text{c.c.}\right)\end{aligned} \quad (3.23)$$

where in the first two lines, the derivatives of the Hamiltonian, the eigenstates, and the eigenenergies are evaluated at $\mathbf{q}(t)$. The last term of (3.23) corresponds to terms rapidly oscillating at the bare instantaneous Bohr frequencies

$$\gamma^{\text{Bohr}}_{\mu\nu,0}(t) = \gamma^d_{\mu,0}(t) - \gamma^d_{\nu,0}(t) = -\frac{1}{\hbar}\int_0^t \mathrm{d}t'(E_\nu(\mathbf{q}(t'))-E_\mu(\mathbf{q}(t'))). \quad (3.24)$$

They come from the fact that the effective adiabatic dynamics is actually valid for the quantum states prepared in an adiabatic state rather than in an eigenstate. Indeed, these terms are canceled at first order if the initial state is prepared in an adiabatic state at this order, namely

$$|\Psi(t=0)\rangle = |\psi_\nu(\mathbf{q}(t=0))\rangle - i\hbar \sum_{\mu\neq\nu} \sum_j \frac{\dot{q}_j(t=0) A_{\mu\nu,q_j}(\mathbf{q}(t=0))}{E_\nu(\mathbf{q}(t=0)) - E_\mu(\mathbf{q}(t=0))} |\psi_\mu(\mathbf{q}(t=0))\rangle \,. \tag{3.25}$$

We recover that the adiabatic states are the initial states on a slow manifold, leading to slow evolution of the physical observables as discussed in Chap. 1.

Returning to Eq. (3.23), the dynamics of the classical variables $q_j$ is not modified by the coupling to the quantum system, $\dot{q}_j = \dot{q}_j^{(0)} = \frac{\partial \mathcal{H}_j}{\partial p_j}$. Thus, using the relation $\langle\psi_\nu| \frac{\partial H}{\partial q_i} |\psi_\nu\rangle = \frac{\partial E_\nu}{\partial q_i}$ and the expression of the components of the Berry curvature two form given in (3.5), we obtain for the correction of $\dot{p}_i$

$$-\langle\Psi| \frac{\partial H}{\partial q_i} |\Psi\rangle = -\frac{\partial E_\nu}{\partial q_i} + \hbar \sum_{j\neq i} \dot{q}_j^{(0)} F_{q_i q_j}. \tag{3.26}$$

Chapter 4

# Topological pump in quantum circuits: the topological qutrit

In the previous chapter, we developed a formalism of topological pumps as topological coupling between a quantum system and slow degrees of freedom of its environment. The topological nature of the coupling leads to a quantized energy transfer between the classical subsystems composing the environment. To illustrate the virtues of this formalism, we propose a realization of a Chern mode coupler enabling to measure a topologically protected power transferred between electromagnetic modes. The proposed setup consists in using a three level quantum system, a qutrit, realized from the first three levels of a highly anharmonic superconducting circuit, a fluxonium, driven at multiple microwave frequencies. The driven fluxonium realizes a time-dependent version of a Haldane model on a Lieb lattice. The corresponding phase diagram can directly be revealed by measuring the power transfer between the microwave modes. The topological pumping leads to a topological redistribution of energy between the three microwave modes. This experimental proposal is guided by the goal to measure directly the physical observables carrying the quantized energy flow. For pedagogical introductions of the field of circuit quantum electrodynamics, we refer to [156, 157], and to [158] for a review on recent progress of the field.

This chapter is based of the section IV of the publication [56].

## 4.1 Case of a qubit

It is possible to apply the concept of geometrical and topological response of gapped states to the simplest quantum system, the quantum bit or qubit. The first experimental measure of a Berry phase using a superconducting qubit was done in 2007 [159]. The measure of a Berry curvature from the inner dynamics of a superconducting qubit, in order to deduce its associated topological Chern number, was done in 2014 [160, 161]. The role of geometrical response in dephasing of a superconducting qubit was also demonstrated [162]. A quantum metric was measured with a superconducting qubit in [163] to infer the value of a Chern number.

The seminal work of Martin, Refael, and Halperin [44] proposed to use a spin-1/2 under two frequency drives to observe the quantized pumping of energy from one drive to

the other. Measuring such a power transfer presents a substantial experimental challenge. Recently, Malz and Smith [164] used the IBM Quantum Experience to observe the inner dynamics of a superconducting qubit state that would correspond to a topological quantum transition. However, their control scheme was mixing the flows of power between the drives – hindering a direct measurement of the power transfer. As such, this protocol is similar to the previous experiments [160, 161]. Similarly, other experiments on NV centers demonstrate a topological transition in the qubit dynamics but could not explore the quantized pumping of power [165].

Essentially, the model proposed in Ref. [44] consists in engineering the Hamiltonian

$$H(\phi_1, \phi_2) \propto \sin(\phi_1)\sigma_X + \sin(\phi_2)\sigma_Y + (M - \cos(\phi_1) - \cos(\phi_2))\,\sigma_Z, \tag{4.1}$$

where $\sigma_i$ are the Pauli operators of the qubit, $M$ is a parameter that drives the topological transition and the phases $\phi_1 = \omega_1 t$ and $\phi_2 = \omega_2 t$ are driven at two incommensurate frequencies. We envision three ways to realize this Hamiltonian.

- As in Ref. [164], it is possible to drive a single superconducting qubit, i.e. a transmon, with a complex amplitude $[X(t) + iY(t)]\, e^{-2i\pi f_q t - 2i\int_0^t Z(\tau)\mathrm{d}\tau}$, where $f_q$ is the qubit frequency in order to implement any driving term of the sort $H(t) = X(t)\sigma_X + Y(t)\sigma_Y + Z(t)\sigma_Z$. However, while it is possible to infer what is the transferred power between frequency components at $\omega_1$ and $\omega_2$ from the measured qubit dynamics, this power flow lacks physical embodiment and cannot be measured using any known apparatus.

- Alternatively, the $\sigma_Z$ term in the Hamiltonian (4.1) can be achieved by controlling the frequency of the qubit directly, hence physically separating the source of power from the three terms corresponding to each Pauli operator in Eq. (4.1). The frequency of flux tunable qubits can be tuned rapidly using an on-chip flux control. However, measuring the power of the drive used for such a flux-tunable bias has never been achieved to our knowledge and requires some important technical development.

- Lastly, the frequency of the qubit can be controlled by exploiting the AC-Stark shift created by a drive far detuned from the qubit transition frequency. The AC-Stark shift is a commonly used method to engineer the spectrum of artificial atoms but the relatively low anharmonicity of transmons imposes a finite bandwidth on the control parameter $Z(t)$.

All these solutions present serious practical limitations either on the achievable Z-control or – more importantly – on the ability to measure the quantized power transfer. To circumvent this difficulty, we propose to extend the size of the Hilbert space. In this extended pumping scheme, we use a qutrit to engineer gapped states.

## 4.2 Implementation with a superconducting qutrit

### 4.2.1 Principle of the experiment

The experiment we propose consists in driving a superconducting qutrit at several frequencies in order to establish a topologically given power flow between microwave modes

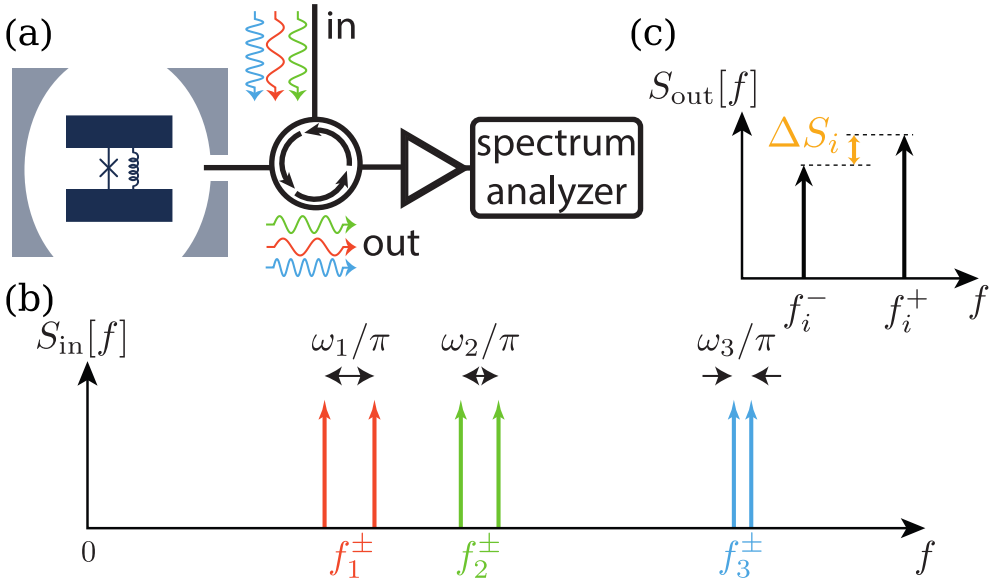


Figure 4.1: (a) Schematic of the experimental setup. A fluxonium circuit is embedded in a host cavity. The transitions between the first three levels of the fluxonium are driven with a detuning $\delta_i$, an amplitude $\Omega_i$, and a modulation frequency $\omega_i$ (blue, red and green). The power of the outgoing signals are recorded with a power spectrum analyzer that provides the instantaneous photon flux of each frequency mode. (b) Spectrum of the driving tones. Each fluxonium transition is driven with two side-bands used to implement a topologically protected power transfer. (c) For decoherence rates smaller than the modulation frequencies $\omega_i$, the power of each sideband can be resolved. The quantized power transferred is expressed as a function of the difference of the spectral power $\Delta S_i$ in the sidebands of each reflected driving tone according to Eq. (4.8).

at various frequencies. We propose to use a superconducting circuit behaving as a qutrit where every transition can be addressed individually with a well-defined phase. In the following, we denote the transitions $|0\rangle - |1\rangle$ as 1, $|1\rangle - |2\rangle$ as 2, and $|0\rangle - |2\rangle$ as 3 for the sake of simplicity. By modulating the drive amplitude $\Omega_i$ of each transition $i$ at a frequency $\dot{\phi}_i = \omega_i$, it is possible to engineer an effective Hamiltonian in a configuration space defined by the phases $\phi_1, \phi_2, \phi_3$. By enforcing $\phi_3 = \phi_1 - \phi_2$, the dimension is reduced while still enabling the observation of a topological transition in the power transferred between the various driving tones. The difference between any two transition frequencies of the qutrit shall be much greater than any drive amplitude $\Omega_i$ and modulation frequency $\omega_i$ in order to enable the direct measurement of the power transfer between any driving modes. Finally, all the above-mentioned timescales should be much smaller than the coherence time of the qutrit transitions.

An example of a superconducting circuit satisfying these requirements is the fluxonium artificial atom. The fluxonium is a highly anharmonic superconducting circuit whose first three energy levels can be used as a three level atom, a qutrit. The circuit is a loop composed of a Josephson junction shunted by a large inductance, see Fig. 4.1(a). When the loop is threaded by an external magnetic flux corresponding to almost (but not exactly) half a flux quantum, no selection rule prevents the direct driving of all three transitions while the circuit transitions have been shown to display record long coherence times [166–168].

The circuit is embedded in a cavity with a single port connected to a transmission line. The cavity is used as an off-resonant readout mode dispersively coupled to the circuit transitions [169]. The cavity also acts as a filter that protects the circuit from direct energy dissipation into the electromagnetic environment of the transmission line, while preserving fast microwave control through the direct coupling of the input port to the circuit antenna.

Incoming microwave modes carry the modulated drives [see Fig. 4.1(b)] to the qutrit and outgoing modes carry the reflected signal before being measured by a power spectrum analyzer. At the input, each drive at frequency $f_i$ is modulated in amplitude at a frequency $\omega_i$, resulting in the pairs of sidebands in Fig. 4.1(b). The geometrical and topological signatures can be observed in the power transfer between these various frequency modes. We model the propagating mode in the transmission lines at frequency $f$ as a classical mode of energy $hfn_f$ such that the net photon flux is given by the difference between the outgoing and incoming signals at this frequency $(S_{\text{out}}[f] - S_{\text{in}}[f])/hf$. Precisely, one first needs to probe the difference $\Delta S_i$ in power spectral density between two sidebands [see Fig. 4.1(c)] and convert it in photon flux $\dot{n}_i = \Delta S_i / hf_i$ (see Appendix 4.B for a refined expression).

### 4.2.2 Hamiltonian in the rotating frame

The fluxonium Hamiltonian reads [170]

$$H_{\text{fluxonium}} = 4E_C\hat{N}^2 + \frac{E_L}{2}\hat{\varphi}^2 - E_J\cos(\hat{\varphi} - \varphi_{\text{ext}}), \tag{4.2}$$

where $\hat{N}$ is the charge on the capacitor of the circuit, $\hat{\varphi}$ is the phase twist across the inductance, $\varphi_{\text{ext}}$ is the external magnetic flux threading the loop, and $E_C$, $E_L$, $E_J$ are

respectively the charging energy, inductive energy and Josephson energy of the circuit. The fluxonium is addressed by a microwave drive applied on a capacitance, so that each pump induces a term proportional to $\cos(\phi_i)\cos(\theta_i)\hat{N}$ in the Hamiltonian, where $\theta_i(t) = 2\pi f_i t + \theta_i^0$ is the phase of each tone and $\phi_i(t) = \omega_i t$ is the phase of their amplitude modulation. We denote as $|0\rangle, |1\rangle, |2\rangle$ the first three energy levels of the fluxonium (4.2). The frequencies of the three drives $f_1$, $f_2$ and $f_3$ are constrained to satisfy $f_3 = f_1 + f_2$ such that each tone drives a single transition of the fluxonium. This constraint can be enforced in the microwave domain by using mixers to generate a tone at $f_3$ using tones at $f_1$ and $f_2$ or by direct numerical synthesis.

We use a rotating frame description by applying the unitary diagonal transformation $U(t) = \mathrm{diag}(1, \exp(-2i\pi f_1 t), \exp(-2i\pi f_3 t))$. One can choose the initial phases $\theta_i^0$ of the tones such that, in the rotating frame and using the rotating wave approximation, the dynamics of the qutrit is governed by the Hamiltonian

$$\tilde{H}(\phi_1, \phi_2, \phi_3) = \hbar \begin{pmatrix} 0 & \Omega_1 \cos(\phi_1) & -i\Omega_3 \cos(\phi_3) \\ \Omega_1 \cos(\phi_1) & \delta_1 & \Omega_2 \cos(\phi_2) \\ i\Omega_3 \cos(\phi_3) & \Omega_2 \cos(\phi_2) & \delta_3 \end{pmatrix}, \tag{4.3}$$

which depends on the phases $\phi_i(t) = \omega_i t$ of the drive amplitude modulations, the two $\delta_1 = 2\pi f_{01} - 2\pi f_1$ and $\delta_3 = 2\pi f_{02} - 2\pi f_3$ being the frequency detuning between the fluxonium transition frequencies and the drive frequencies (see Appendix 4.A for details). Note that the above constraint on drive frequencies sets $\delta_2 = \delta_3 - \delta_1$. Besides, in order to simplify the dynamics, we impose an additional constraint on the modulation frequencies, namely $\phi_3 = \phi_1 - \phi_2$. Therefore, the effective Hamiltonian can be described by a Hamiltonian evolution controlled by two phases only $H(\phi_1, \phi_2) \equiv \tilde{H}(\phi_1, \phi_2, \phi_1 - \phi_2)$. The rotating wave approximation is valid if the detunings $\delta_i$ and the drive amplitudes $\Omega_i$ are much lower than the fluxonium transitions frequencies $f_{ij}$ and the difference between any two transition frequencies, which is one of the requirements detailed above.

### 4.2.3 Chern insulator on the Lieb lattice

In this section, we show that the fluxonium qutrit emulates in time the physics in momentum space of a Chern insulator on a Lieb lattice, which is illustrated in Fig. 4.2(a). This proposal thus provides a missing implementation of a new three level topological model, which in particular supersedes a recent proposal based on molecular enantiomers [53]. In this quantum simulation correspondence, the drive detunings $\delta_1$ and $\delta_3$ correspond to onsite potential energies on the Lieb lattice, while the drive amplitudes $\Omega_1$ and $\Omega_2$ mimic nearest-neighbor tight-binding amplitudes, and $\Omega_3$ simulates a next-nearest-neighbor coupling along one diagonal direction. The relative $\pi$ phase between the $\Omega_1, \Omega_2$ and $\Omega_3$ terms in Eq. (4.3) originates from a periodic pattern of staggered magnetic fluxes, as shown in Fig. 4.2(a). These fluxes break the time-reversal symmetry of the tight-binding model, while preserving the translation invariance of the Bravais lattice.

We thus end up with a generalization of the celebrated Haldane's model [171] but on the Lieb instead of the honeycomb lattice. In the sublattice basis $(0, 1, 2)$ [see Fig. 4.2(a)],

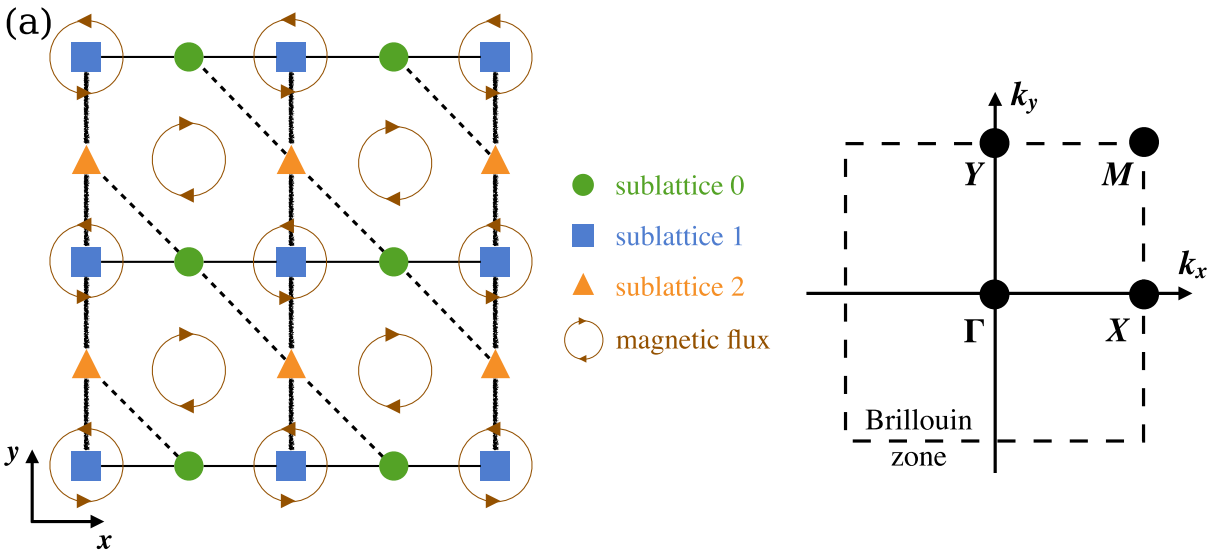


(b)

Trivial atomic limit

| $\nu$ | 0 | 1 | 2 |
|---|---|---|---|
| $p_\nu(\boldsymbol{\Gamma})$ | + | + | + |
| $p_\nu(\boldsymbol{X})$ | − | + | + |
| $p_\nu(\boldsymbol{Y})$ | + | + | − |
| $p_\nu(\boldsymbol{M})$ | − | + | − |
| $\pi_\nu$ | + | + | + |

Topological insulator

| $\nu$ | 0 | 1 | 2 |
|---|---|---|---|
| $p_\nu(\boldsymbol{\Gamma})$ | + | + | + |
| $p_\nu(\boldsymbol{X})$ | + | − | + |
| $p_\nu(\boldsymbol{Y})$ | + | − | + |
| $p_\nu(\boldsymbol{M})$ | − | + | − |
| $\pi_\nu$ | − | + | − |

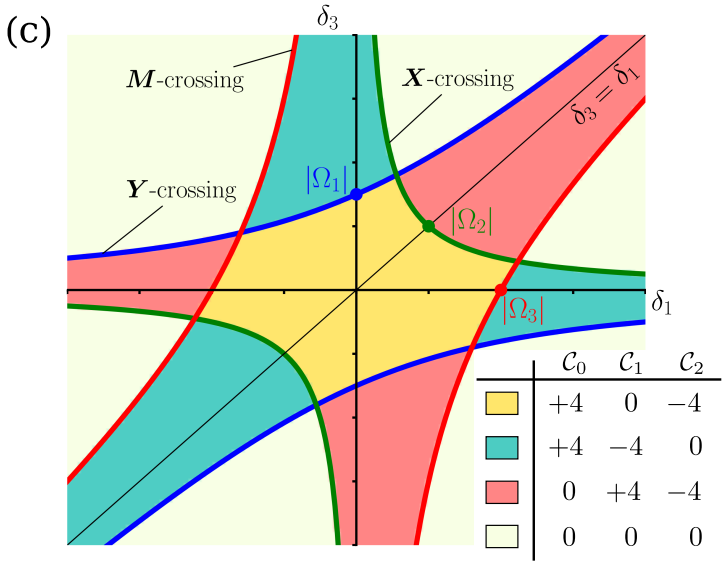


Figure 4.2: (a) Schematic representations of a Haldane model on the Lieb lattice and its square Brillouin zone with the four inversion-invariant momenta. The sublattices 0, 1, and 2 respectively have on-site potential energies 0, $\delta_1$, and $\delta_3$. The regular and bold black lines represent the nearest-neighbor tight-binding amplitudes $\Omega_1$ and $\Omega_2$. The dashed black lines depict the next-nearest-neighbor coupling $\Omega_3$. (b) Two allowed configurations of the band parities $p_\nu$ at the inversion-invariant momenta. A trivial insulator can be adiabatically connected to an atomic limit, which is necessarily characterized here by positive parity products $\pi_\nu = +1$. A band insulator exhibiting negative parity products $\pi_\nu = -1$ is therefore topological. Identifying all the configurations of the parity eigenvalues of the different phases of the model allows to identify their topological nature and leads to the topological phase diagram in panel (c) (see Appendix 4.C). (c) Phase diagram of the qutrit model. Each colored region corresponds to a set of band Chern numbers. On the boundaries one of the two gaps closes for at least one combination of phases $\phi_1$ and $\phi_2$.

the corresponding Bloch Hamiltonian is

$$H(\boldsymbol{k}) = \hbar \begin{pmatrix} 0 & \Omega_1 \cos\left(\frac{k_x}{2}\right) & -i\Omega_3 \cos\left(\frac{k_x - k_y}{2}\right) \\ \Omega_1 \cos\left(\frac{k_x}{2}\right) & \delta_1 & \Omega_2 \cos\left(\frac{k_y}{2}\right) \\ i\Omega_3 \cos\left(\frac{k_x - k_y}{2}\right) & \Omega_2 \cos\left(\frac{k_y}{2}\right) & \delta_3 \end{pmatrix}. \tag{4.4}$$

The pseudo-momentum $\boldsymbol{k}$ is dimensionless, corresponding to a lattice constant chosen as a length unit. The qutrit Hamiltonian (4.3) is then recovered through the substitutions $k_x \to 2\phi_1$ and $k_y \to 2\phi_2$. Note that our model also captures the dynamics of other quantum systems such as spin chains [172].

First, we determine the phase diagram of the model (4.4). This is achieved by determining the conditions for a crossing between two of the bands. The parity symmetry constrains these crossing to occur at the high symmetry points $\boldsymbol{\Gamma}, \boldsymbol{X}, \boldsymbol{Y}, \boldsymbol{M}$ of the Brillouin zone, which simplifies greatly the analysis, see App. 4.C. The resulting phase diagram is shown in Fig. 4.2(c). In more details, we aim at determining the nature of the various phases in this diagram, *i.e.* the range of drive parameters $\Omega_i, \delta_i$ that lead to topologically nontrivial band structures for the model of Eq. (4.4). By definition, a topological band structure cannot be smoothly deformed to that of an atomic limit [173]. In contrast, a trivial band structure admits some band representations of the crystal space group on a basis of symmetric localized orbitals [174–177]. An efficient strategy to detect topological band structures then consists in enumerating all possible band representations of a space group and identifying band structures that do not support such representations. This strategy lies at the heart of the recent paradigm of Topological Quantum Chemistry and led to the predictions of exhaustive catalogues of topological materials [178–182]. We can use this methodology to efficiently determine the phase diagram of model (4.4).

We first determine the band representations of the Lieb lattice in Fig. 4.2(a) for the atomic limit $\Omega_{1,2,3} = 0$. For non-degenerate onsite energies $\delta_{1,3} \neq 0$ and $\delta_1 \neq \delta_3$, and in the presence of staggered magnetic fluxes, the lattice only has inversion symmetry and belongs to the wallpaper space group $p2$. The three orbitals occupy the maximal Wyckoff positions $q_0 = (1/2, 0)$, $q_1 = (0, 0)$, and $q_2 = (0, 1/2)$ in the primitive unit cell. Their elementary band representations are determined from the band parities $p_\nu = \pm 1$ — i.e. eigenvalues of the parity operator — at the inversion-invariant momenta in the Brillouin zone depicted in Fig. 4.2(a) [183]. It leads to the band representations summarized in the top panel in Fig. 4.2(b). The parity product

$$\pi_\nu = p_\nu(\boldsymbol{\Gamma}) p_\nu(\boldsymbol{X}) p_\nu(\boldsymbol{Y}) p_\nu(\boldsymbol{M}) \tag{4.5}$$

of each band $\nu$ is always positive in the atomic limit. Therefore, band structures with negative parity products $\pi_\nu$ fall outside these band representations and are topological.

Away from the atomic limit, *i.e.* for $\Omega_{1,2,3} \neq 0$, we identify all the parity configurations of the band structure $H(\boldsymbol{k})$ at the inversion-invariant momenta (see Appendix 4.C and Fig. 4.6). Each configuration leads to a colored region in the $\delta_1\delta_3$-plane in Fig. 4.2(c). The ivory colored regions correspond to the parity configurations of the atomic limit in Fig. 4.2(b). Thus, they describe trivial band insulators. In contrast, we find that the red, green, and yellow regions exhibit negative parity products, thus characterizing topological insulators. As an illustration, the bottom panel in Fig. 4.2(b) specifies the parity configuration of the yellow region, where $\pi_\nu = -1$ for $\nu = 0$ and $\nu = 2$. It shows

that the change of parity products between the trivial atomic limit and the topological insulator requires the bands $\nu = 1$ and $\nu = 0$ ($\nu = 2$) to switch parities at point $\boldsymbol{X}$ ($\boldsymbol{Y}$) of the Brillouin zone. More generally, a parity switch cannot occur continuously and requires the band gap to close at one of the inversion-invariant momentum (see Appendix 4.C).

We recover the announced very efficient determination of the phase diagram of Fig. 4.2(c) by considering the gap closing at these inversion-invariant momenta as a function of the $\Omega_i$ and $\delta_i$. Such band crossings mark the borders between topologically distinct regions in the phase diagram represented in Fig. 4.2(c), where from now on we use the shorthand notation for the Chern number $\mathcal{C}_\nu = \int_{[0,2\pi]^2} \mathrm{d}\phi_1 \mathrm{d}\phi_2 \; F_{\nu,\phi_1\phi_2}/(2\pi)$. One can further show that this Chern number is non-zero when the parity product is negative [184, 185]. Since the qutrit Hamiltonian in Eq. (4.3) is recovered via the substitutions $k_{x,y} \to 2\phi_{1,2}$, the Chern number for the fluxonium qutrit is four times larger than for the Lieb insulator, hence the values summarized in the table in Fig. 4.2(c).

### 4.2.4 Topological power transfer between three modes

We now discuss how the topological nature of the qutrit pump manifests itself in filling rates of the three modes. The dynamical system consists of three classical modes described by the classical phases $\phi_i$ conjugated to $n_i$ coupled to the qutrit through the Hamiltonian (4.3) in the rotating frame. The equations of motion have the same form in the rotating frame $\dot{n}_i = -\frac{1}{\hbar} \langle \Psi | \, \partial_{\phi_i} \tilde{H} \, | \Psi \rangle \, , i = 1, 2, 3$ where the dynamics of the qutrit state $|\Psi(t)\rangle$ in the rotating frame is governed by the Hamiltonian (4.3), see Appendix 4.D for details.

As said above, the frequencies of amplitude modulation satisfies $\omega_3 = \omega_1 - \omega_2$ such that $\phi_{III} = \phi_1 - \phi_2 - \phi_3$ is a constant of motion. Hence, we can keep $\phi_1 - \phi_2 - \phi_3 = 0$ at all time. As such, the qutrit is effectively coupled to two dynamical phases $\phi_1$ and $\phi_2$. According to the model described in Chap. 3, the backaction of the qutrit affects the dynamics of their conjugated numbers of quanta $n_I$ and $n_{II}$. They are defined such that they satisfy the canonical commutation relations with $\phi_1$ and $\phi_2$, while commuting with the constraint $\phi_1 - \phi_2 - \phi_3$. We identify them by the following canonical transformation $n_I = n_1 + n_3$, $n_{II} = n_2 - n_3$, $\phi_I = \phi_1$, $\phi_{II} = \phi_2$. If the qutrit is prepared in its $\nu$-th eigenstate, the dynamics of $n_I$ and $n_{II}$ is then given by

$$\dot{n}_I = \dot{n}_1 + \dot{n}_3 = -\frac{1}{\hbar}\frac{\partial E_\nu}{\partial \phi_1} + F_{\nu,\phi_1\phi_2}\omega_2 \tag{4.6a}$$

$$\dot{n}_{II} = \dot{n}_2 - \dot{n}_3 = -\frac{1}{\hbar}\frac{\partial E_\nu}{\partial \phi_2} - F_{\nu,\phi_1\phi_2}\omega_1 \tag{4.6b}$$

with $E_\nu$ the energy and $F_\nu$ the Berry curvature of the band $\nu$ of the Hamiltonian $H(\phi_1, \phi_2) \equiv \tilde{H}(\phi_1, \phi_2, \phi_1 - \phi_2)$ in which the qutrit is initially prepared (see Appendix 4.D for details). Then, the topological power transfer between the modes $1, 2, 3$ is

$$\hbar\omega_1 \langle \dot{n}_1 + \dot{n}_3 \rangle_t = \hbar \frac{\mathcal{C}_\nu}{2\pi} \omega_1 \omega_2 = -\hbar\omega_2 \langle \dot{n}_2 - \dot{n}_3 \rangle_t, \tag{4.7}$$

with $\mathcal{C}_\nu$ the Chern number of the band $\nu$ of the Hamiltonian.

Let us recall that, as explained in Sec. 3.1 of Chap. 3, to recover Eq. (4.6), the qutrit has to be initialized in an adiabatic state, which slightly differs from the eigenstate at

first order. A superconducting qutrit is fully controllable, and any quantum state can be prepared [186–188]. For this experimental proposal, a preparation in an eigenstate is sufficient. It would induce subdominants corrections to the pumping rate. We discuss in details the role of the initial state in Chap 5.

From a more experimental point of view, the power transfer to demonstrate is

$$\frac{\Delta S_1}{hf_1} + \frac{\Delta S_3}{hf_3} = \frac{\mathcal{C}_\nu}{2\pi}\omega_2 \quad \text{and} \quad \frac{\Delta S_2}{hf_2} - \frac{\Delta S_3}{hf_3} = -\frac{\mathcal{C}_\nu}{2\pi}\omega_1. \tag{4.8}$$

In order to get a sense of how feasible this measurement is, let us set some possible figures for the experiment that fulfill the criterion discussed earlier. The fluxonium frequencies could be set to $f_{01} = 4$ GHz, $f_{12} = 6$ GHz and $f_{02} = 10$ GHz. It is then possible to drive the transitions with $\Omega_{1,2,3}/2\pi = 100$ MHz and a similar range of variation for the detunings. The modulation frequencies could then be $\omega_1/2\pi = 5$ MHz, $\omega_2/2\pi \simeq 3$ MHz. From the simulations below, we see that the topological power transfer can be resolved in about 30 periods $2\pi/\omega_i$, which is a few $\mu$s. This is well below the typical decoherence times of fluxonium qubits, which will not limit the dynamics of the system during the measurement. Thus, verifying Eq. (4.8) requires measuring instantaneous powers in the range of $hf_i\omega_i$. This corresponds to a power of several dozens of aW, which is a level of precision that is now routinely reached experimentally [189–191].

## 4.3 Numerical analysis of topological pumping

### 4.3.1 Topological power transfer

In order to perform numerical simulations of the proposed experiment, we solve the time-dependent Schrödinger equation of the qutrit under the rotating wave approximation (4.3). We first determine the optimal parameters for the pump: the stability of the adiabaticity evolution requires the largest gap. This is reached at the resonant drive $\delta_1 = \delta_3 = 0$, point A in the phase diagram in Fig. 4.4(a), and with equal driving amplitudes $\Omega_{1,2,3} = \Omega$, resulting in a gap $0.87\ \hbar\Omega$. In these conditions, from the analysis of Fig. 4.2(c) both bands 0 and 2 have non-zero Chern number $\mathcal{C} = \pm 4$, whereas the band 1 is topologically trivial with $\mathcal{C} = 0$. Therefore, the two lowest energy states do not constitute an effective topological qubit, given than only one of these bands is topological: this will lead to a different dynamics than for a conventional 2 level pump as we will see below. To ensure an ergodic exploration of the classical configuration space of the pump, we choose an irrational ratio between phases frequencies $\omega_1/\omega_2 = (1+\sqrt{5})/2$.

Keeping parameters of the pump to point A in the phase diagram in Fig. 4.4(a), we initialize the qutrit at $t = 0$ in its ground state. The evolution of the filling $n_i$ of each individual modes is represented in Fig. 4.3(a), and varies linearly in time. However, the filling rate $\dot{n}_i$ are not set by the topological nature of the pump, and depend on the precise values of the pump parameters: changing slightly these from point A to point B in the same topological region of Fig. 4.4(a) leads to different filling rates, as seen in Fig. 4.3(a). On the other hand, the linear combination corresponding to the topological power transfer defined in Eq. (4.7) is insensitive to the precise values of the pump parameters, as shown in Fig. 4.3(b).

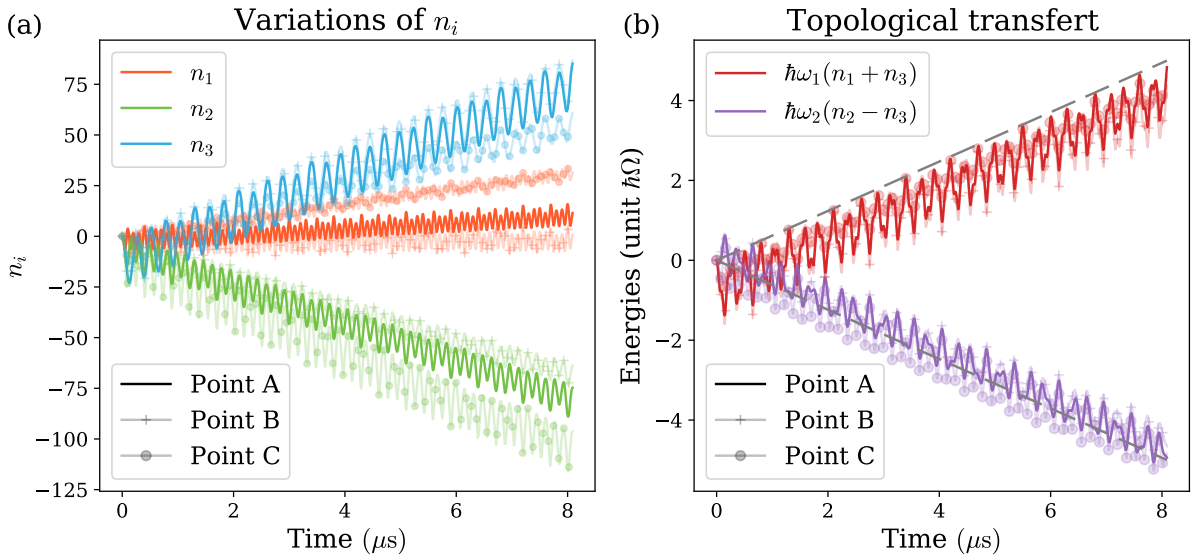


Figure 4.3: Pumping by a qutrit initialized in its ground state. (a) Filling of the different modes $n_i$ as a function of time, for three different sets of pump parameters corresponding to points A, B and C in Fig. 4.4(a). The driving amplitudes are chosen all equals $\Omega_{1,2,3} = \Omega$. The filling rates are found to depend on the parameters of the pump. (b) The two different combinations of fillings display the topological power $\hbar\omega_1\omega_2\mathcal{C}_0/2\pi$ (grey dashed lines), invariant on the region of stability of the phase diagram, where $\mathcal{C}_0 = 4$ is the Chern number of the ground state for all parameter sets A,B,C.

Besides the linear topological evolution in time, this power transfer displays temporal fluctuations which have two different origins as deduced from Eq. (4.6): a dominant spectral term, corresponding to variation of the energy $E_0$ of the qutrit, and a geometrical contribution originating from fluctuations of the Berry curvature around its topologically quantized average value (see Appendix 4.E). Thus, the order of magnitude of the correlation timescale of these fluctuations corresponds to the period of the drive. A reasonable requirement to detect the topological power transfer is to average it over 30 such independent fluctuations, leading to a measurement time of 8 $\mu$s, as announced in the previous section.

### 4.3.2 Numerical detection of topological transitions

Having established that the average topological power transfer gives access to the Chern number of the band in which the qutrit was initialized, we now address the detection of the topological phase transitions of Fig. 4.2(c) when the detuning parameters $\delta_1, \delta_2$ are varied. The richness of the adiabatic dynamics of the qutrit pumps requires different experimental protocols adjusted to each phase transition. For example, sets A and C of parameters in Fig. 4.4(a) lead to exactly the same topological power rate for a qutrit initialized in the ground state, as shown in Fig. 4.3(b), but corresponds to a different topological qutrit phase. Indeed, the corresponding qutrit phases differ by the topological nature of the excited bands 1 and 2, while the nature of the ground state is unchanged. Thus detecting this particular transition requires an initialization of the qutrit in the first

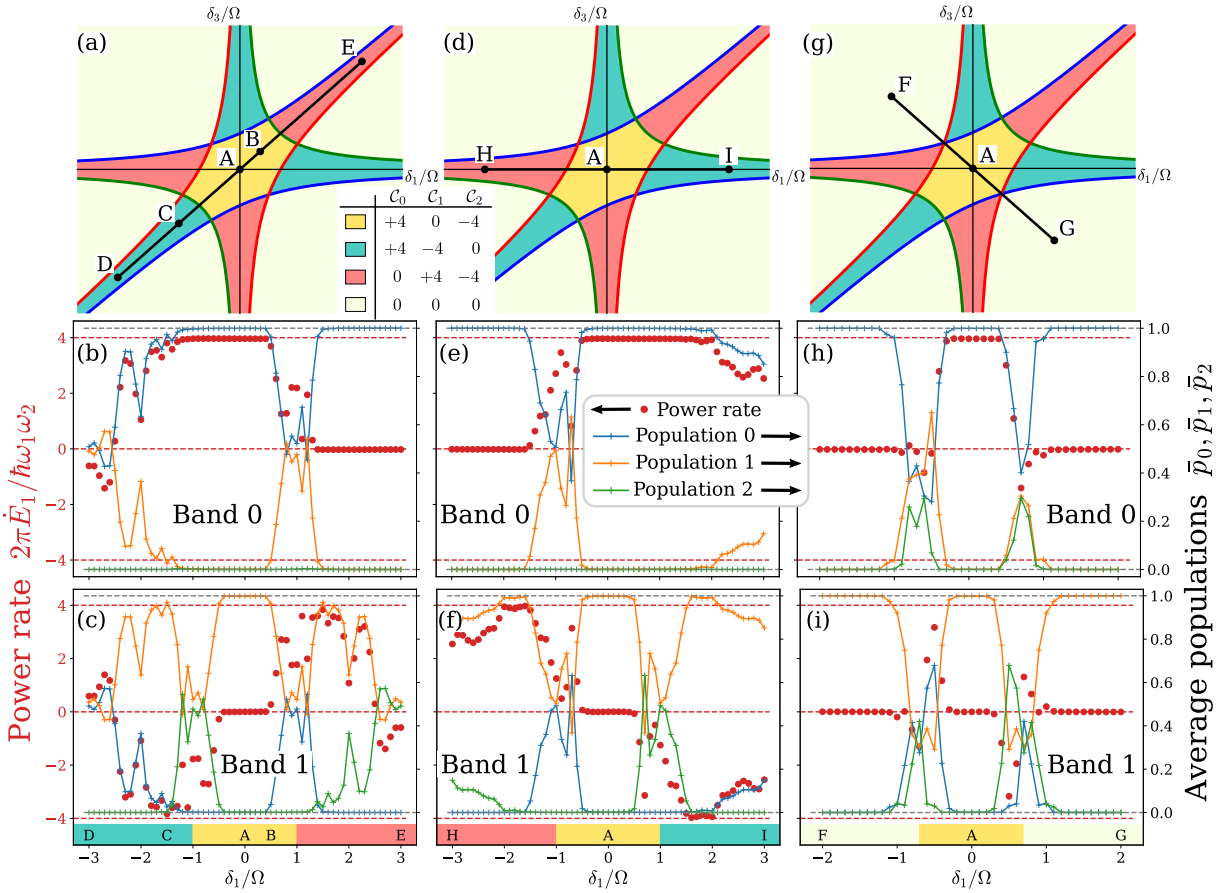


Figure 4.4: Topological transitions for bands 0 and 1 in the case of drive amplitudes $\Omega_{1,2,3} = \Omega$. For each working point of the phase diagram, we fit the time evolution of the energy $E_1 = \hbar\omega_1(n_1 + n_3)$ linearly over a time $\Delta t = 8\mu$s to construct the reduced power rate $2\pi\dot{E}_1/\hbar\omega_1\omega_2$ (red dots) when the qutrit is initialized in band 0, panels [(b),(e),(h)], or in band 1, panels [(c),(f),(i)]. The average populations of the qutrit $\bar{p}_\mu = \frac{1}{\Delta t}\int_0^{\Delta t} |\langle\psi_\mu(t)|\Psi(t)\rangle|^2 \mathrm{d}t$ are displayed to evaluate adiabaticity. [(a)-(c)] Transition line DE, with a transition between bands 1 and 2 at $\delta_1/\Omega = -1$, and between bands 0 and 1 at $\delta_1/\Omega = 1$. [(d)-(f)] Transition line HI, with a transition between bands 0 and 1 at $\delta_1/\Omega = -1$, and between bands 1 and 2 at $\delta_1/\Omega = 1$. [(g)-(i)] Transition line FG, with a transition between the three bands at $\delta_1/\Omega = \pm\sqrt{2}/2$.

excited state 1.

To detect all transitions, we monitor the evolution of the pumps with both initialization in the 0 and 1 states. Figure 4.4 displays the resulting power rate, determined by a linear fit using Eq. (4.7), as well as the average populations $\bar{p}_\mu = \frac{1}{\Delta t}\int_0^{\Delta t} |\langle\psi_\mu(t)|\Psi(t)\rangle|^2 \mathrm{d}t$ of the qutrit state $|\Psi(t)\rangle$ on the three instantaneous eigenstates $|\psi_\mu(t)\rangle$. Figures 4.4(b,e,h) correspond to a pump with qutrit initialized in band 0, while Fig. 4.4(c,f,i) correspond to an initial preparation in band 1.

Along the lines DE and HI in Fig. 4.4(a,d), the topological transitions occur between two bands only, whereas along the line FG in Fig. 4.4(g) the gaps between all three bands close at the transitions. Along any line, the transition is detected by the evolution of the populations. Moreover, a quantized power transfer in a given state appears as a direct test of the adiabatic nature of the evolution, related to the distance to the transitions. In that respect, optimal choice of parameters for the pump correspond to point A in the yellow topological phase of the phase diagram, in which the bands 0 and 2 are non-trivial and spectrally separated by a trivial band 1 and thus generically separated from a trivial phase by two transitions. Far from any transition near point A, the instantaneous energy separation with different eigenstates is large, resulting in an adiabatic evolution: the average population of the qutrit in the initial band remains close to 1 and the power rate is quantized and set by the Chern number of the band.

In the other topological states of the qutrit, the effects of non-adiabaticity are manifest, resulting from shorter distances to phase transitions and thus small gaps. For example along line DE for a qutrit prepared in band 1, while the Chern number $\mathcal{C}_1$ takes values $-4$ and $+4$ for respectively $\delta_1/\Omega < -1$ and $\delta_1/\Omega > 1$, the qutrit does not evolve adiabatically and the dynamics of the classical variables (4.6) must be corrected, leading to an unquantized power transfer shown in Fig. 4.4(c). Similarly, in Fig. 4.4(b) the Chern number $+4$ of band 0 for $\delta_1/\Omega < 1$ manifests itself as a pleateau of power rate for a reduced set of parameters for $-1.5 < \delta_1/\Omega < 0.5$ (between points C and B).

### 4.3.3 Non-adiabatic pumping

The importance of the non-adiabatic effects can be anticipated from the estimation of the time of validity of the adiabatic approximation $\tau_{\mathrm{adiab}}$ introduced in Eq. (1.56) of the first chapter. In this expression, we consider the maximum of the adiabatic parameter $\varepsilon_{\mu\nu}$ – given by Eq. (1.38) – evaluated on all the values of phases $\phi_1$ and $\phi_2$. The mean free time $\tau_{\mathrm{mft}}$ is the time between two successive Landau-Zener transition whose order of magnitude is the phases' periodicity, we take $\tau_{\mathrm{mft}} = 2\pi/\omega_2 \sim 0.3$ $\mu$s. For the point A, B and C of the phase diagram, the Landau-Zener collision time $\tau_{01}^{\mathrm{col}}$ associated to the transition between states 0 and 1 is one order of magnitude below this mean free time, which is consistent with the assumptions made in the derivation of the adiabatic time $\tau_{\mathrm{adiab}}$ discussed in Sec. 1.2.5.

For the point A of maximal stability with a preparation in band 0, we get $\tau_{\mathrm{adiab}}^{\mathrm{A}} \sim$ 150 ms such that the non-adiabatic effects will not be a limiting factor for experiments with these parameters values. This is illustrated in Fig. 4.5(a), where the evolution for 100 $\mu$s of the energy $\hbar\omega_1(n_1 + n_3)$ and the populations $p_\mu(t) = |\langle\psi_\mu(t)|\Psi(t)\rangle|^2$ of the qutrit state $|\Psi(t)\rangle$ on the three instantaneous eigenstates $|\psi_\mu(t)\rangle$ are displayed. The qutrit stays in the ground state with $p_0(t) > 0.997$, and the energy is transferred at the

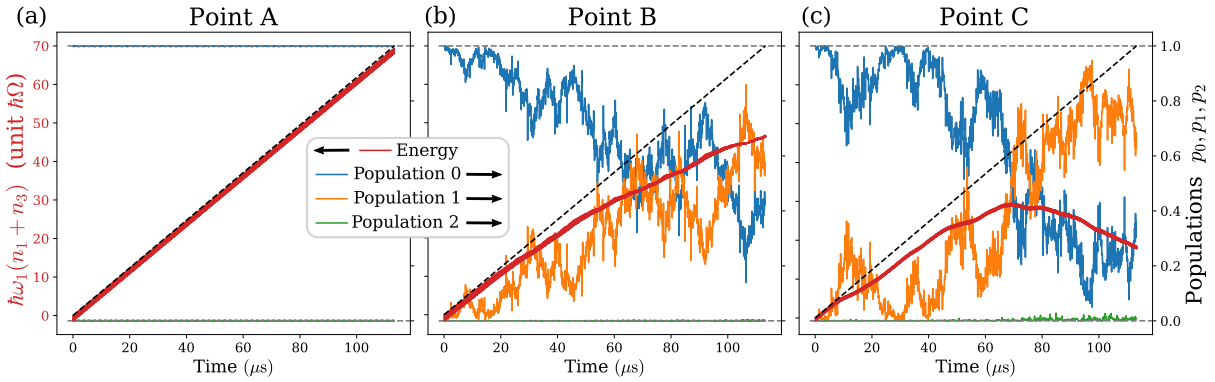


Figure 4.5: Non-adiabatic effects at longer time. The time evolution for the qutrit prepared in band 0 of the topological energy combination $\hbar\omega_1(n_1 + n_3)$ and qutrit populations $p_\mu(t)$ in the instantaneous eigenstates are displayed for three working points A, B and C in the phase diagram of Fig. 4.4(a). (a) Point A, case of resonance $\delta_1 = \delta_3 = 0$ where the evolution of the qutrit remains adiabatic during 200 periods, so the pumping rate is stable. (b) Point B, limit case beyond which pumping is no longer quantized on Fig. 4.4(b), where the evolution of the qutrit is no longer adiabatic after approximately 8 $\mu$s, so the pumping rate is no longer quantized. (c) Point C, other limit case beyond which pumping is no longer quantized on Fig. 4.4(b), where in this phase the Chern number of band 1 is opposite to band 0, so we see pumping in the other direction when band 1 is mainly populated. Downsampling of data has been applied for clarity of presentation.

topologically quantized rate.

Figure 4.5(b) corresponds to point B closer to the topological transition line towards the phase where $\mathcal{C}_0 = 0$. The estimated time of adiabaticity for band 0 is $\tau^{\mathrm{B}}_{\mathrm{adiab}} \sim 6$ $\mu$s. After this typical time, the population on state 1 exceeds 0.1, in agreement with the definition of $\tau_{\mathrm{adiab}}$, and the pumping rate deviates from its topologically quantized value. Figure 4.5(c) corresponds to point C, where we crossed a different topological transition line, where the ground state remains topological but the first excited state switches from trivial to non-trivial with Chern number $\mathcal{C}_1 = -4$. We compute here $\tau^{\mathrm{C}}_{\mathrm{adiab}} \sim 8$ $\mu$s in agreement with the observed deviations from the adiabatic evolution. At longer times, about 70 $\mu$s, the first excited state is mostly populated and the energy pumping is reversed, manifesting the associated change of Chern number.

## 4.4 Conclusion of chapter

We have proposed an experiment that is able to observe a topologically protected power exchange. The topological properties appear in the measured incoming and outgoing energy flows that drive a quantum system. Considering a qutrit instead of a qubit is key for two aspects. First, it offers a path to circumvent the tremendous challenge to probe the power flows that drive a two level topological pump. Second, owing to its richer dynamics, which simulates the topological band properties of a 3-band Chern model, it gives access to various protocols of pumping which can be freely chosen by setting the initial state of the qutrit.

Besides the fascinating perspective to actually measure this topological power transfer,

such a system also opens the paths to the study of the interplay between decoherence and the topological adiabatic evolution of the quantum system. Our framework raises two natural questions. Topological pumping requires an initial correlation between the qutrit and the classical modes. How long does this correlation and thus the pumping survive in presence of qutrit decoherence? Besides, could we revert the perspective and use the developed framework and measurable pumping rate as a tool to characterize the correlations between the quantum system and the classical modes. We consider this aspect in the next chapter.

Let us stress that while we have proposed an experiment demonstrating the topologically protected transfer of microwave power using a superconducting circuit, our general framework can be applied to any quantum system and its driving environment such as cold atoms, mechanical oscillators or polaritons. Besides, symmetries are essential to classify topological matter and in particular topological pumps [192]. The enforcement of these symmetries to protected topological pumping in these different systems is another stimulating perspective.

# 4.A Details on the derivation of the Hamiltonian

We detail here the derivation of the Hamiltonian of the qutrit in the rotating frame explained in Sec. 4.2.2. The circuit is driven by three drives whose amplitudes are modulated in time according to the drive Hamiltonian

$$H_{\text{drive}} = \hbar \sum_{i=1}^{3} g_i \cos(\phi_i) \cos(\theta_i) \hat{N}, \tag{4.9}$$

with $\theta_i(t) = 2\pi f_i t + \theta_i^0$ the phase of the electromagnetic field of frequency $f_i$, $\phi_i(t) = \omega_i t$ the phase of the time modulation of the amplitude, and $g_i$ the coupling rates. In the basis $(|0\rangle, |1\rangle, |2\rangle)$ of the three eigenstates of $H_{\text{flux}}$ (4.2) of lowest energy, the Hamiltonian in the laboratory frame $H_{\text{labo}} = H_{\text{flux}} + H_{\text{drive}}$ has the form:

$$H_{\text{labo}} = 2\pi\hbar f_{01} |1\rangle\langle 1| + 2\pi\hbar f_{02} |2\rangle\langle 2| + \hbar \sum_{a,b=0}^{2} \sum_{i=1}^{3} \Omega_{i,ab} \cos(\phi_i) \cos(\theta_i) \ |a\rangle\langle b| \tag{4.10}$$

where $f_{01}$ and $f_{02}$ are the transition frequencies of $H_{\text{flux}}$, and $\Omega_{i,ab} = g_i \langle a| \hat{N} |b\rangle$. We change of reference frame with the unitary transformation $U(t) = \text{diag}(1, \exp(-i2\pi f_1 t), \exp(-i2\pi f_3 t))$. The frequencies of the three pumps satisfy the constraint $f_3 = f_1 + f_2$, so the Hamiltonian in the rotating frame is

$$\begin{aligned} H_{\text{rot}} &= U^\dagger H_{\text{labo}} U - i\hbar U^\dagger \frac{\mathrm{d}U}{\mathrm{d}t} \qquad (4.11) \\ &= \hbar\delta_1 |1\rangle\langle 1| + \hbar\delta_3 |2\rangle\langle 2| + \hbar \sum_{a=0}^{2} \sum_{i=1}^{3} \Omega_{i,aa} \cos(\phi_i) \cos(\theta_i) \ |a\rangle\langle a| \\ &\quad + \left( e^{-i2\pi f_1 t} \sum_{i=1}^{3} \Omega_{i,01} \cos(\phi_i) \cos(\theta_i) \ |0\rangle\langle 1| + \text{h.c.} \right) \\ &\quad + \left( e^{-i2\pi f_2 t} \sum_{i=1}^{3} \Omega_{i,12} \cos(\phi_i) \cos(\theta_i) \ |1\rangle\langle 2| + \text{h.c.} \right) \\ &\quad + \left( e^{-i2\pi f_3 t} \sum_{i=1}^{3} \Omega_{i,02} \cos(\phi_i) \cos(\theta_i) \ |0\rangle\langle 2| + \text{h.c.} \right), \qquad (4.12) \end{aligned}$$

with the detuning $\delta_i$ given by

$$\delta_1 = 2\pi f_{01} - 2\pi f_1 \tag{4.13}$$
$$\delta_2 = 2\pi f_{12} - 2\pi f_2 \tag{4.14}$$
$$\delta_3 = 2\pi f_{02} - 2\pi f_3 = \delta_1 + \delta_2. \tag{4.15}$$

The phases of the drives are given by $\theta_i(t) = 2\pi f_i t + \theta_i^0$. In the rotating wave approximation, we ignore the terms of the Hamiltonian in the rotating frame which oscillate at the frequency of the drives, so we approximate the Hamiltonian by

$$H_{\text{rot}}(t) \simeq H(\phi_1, \phi_2, \phi_3) = \hbar \begin{pmatrix} 0 & \frac{1}{2}\Omega_{1,01} \cos(\phi_1) e^{i\theta_1^0} & \frac{1}{2}\Omega_{3,02} \cos(\phi_3) e^{i\theta_3^0} \\ c.c. & \delta_1 & \frac{1}{2}\Omega_{2,12} \cos(\phi_2) e^{i\theta_2^0} \\ c.c. & c.c. & \delta_3 \end{pmatrix} \tag{4.16}$$

where the other terms oscillate at the frequency $f_i \pm f_j$. We recover the Hamiltonian (4.3) by noting the drive amplitudes $\Omega_1 = \frac{1}{2}|\Omega_{1,01}| = \frac{1}{2}g_1|\langle 0|\hat{N}|1\rangle|$, $\Omega_2 = \frac{1}{2}|\Omega_{2,12}| = \frac{1}{2}g_2|\langle 1|\hat{N}|2\rangle|$ and $\Omega_3 = \frac{1}{2}|\Omega_{3,02}| = \frac{1}{2}g_3|\langle 0|\hat{N}|2\rangle|$, and by choosing the initial pump phases $\theta_i^0$ to set the complex phase of the couplings at the desired value. The rotating wave approximation is valid if the drive amplitudes and detunings are much lower than the frequencies $f_i \pm f_j$ of the oscillating terms, which means that they must be much lower than the difference between any two transition frequencies of the fluxonium as said in the Sec. 4.2.1.

## 4.B Classical variables coupled to the qutrit

In terms of slow-fast system, the total system is actually made of three subsystems. The slowest subsystem is made of the three degrees of freedom associated to the phases of amplitude modulation $\phi_1$, $\phi_2$, and $\phi_3$ of the microwave modes introduced in Appendix 4.A. The fastest subsystem is made of the bare fluxonium and of the three degrees of freedom associated to the phases of the carrier waves $\theta_1$, $\theta_2$ and $\theta_3$. The intermediate system emerges after the rotating wave approximation discussed in Appendix 4.A. It is made of the fluxonium highly dressed by the carrier waves, which reduces to a qutrit whose dynamics is governed by Eq. (4.16). So the rotating wave approximation is a first adiabatic elimination, reducing the total dynamics to the dressed fluxonium coupled to the slow degrees of freedom $\phi_i$. The second adiabatic elimination reduces the dynamics to $\phi_1$, $\phi_2$, $\phi_3$, and their conjugated number of quanta $n_i$. We identify these observables $n_i$ in the following.

The fluxonium is coupled to three drives whose amplitudes are modulated in time. The coupling Hamiltonian in the laboratory frame is

$$H_{\text{drive}} = \hbar \left( \sum_{i=1}^{3} g_i \cos(\phi_i) \cos(\theta_i) \right) \hat{N} \tag{4.17}$$

where $\theta_i(t) = 2\pi f_i t$ is the phase of the drive and $\phi_i(t) = \omega_i t$ is the phase of time-modulation of the amplitude of the drive. The term in parentheses is proportional to the amplitude of the propagating wave on the line

$$\mathcal{A}(t) = \sum_{i=1}^{3} 2\mathcal{A}_i \cos(\phi_i(t)) \cos(\theta_i(t)) \tag{4.18}$$

$$= \sum_{i=1}^{3} \mathcal{A}_i \left( \cos\left(\theta_i^+(t)\right) + \cos\left(\theta_i^-(t)\right) \right) \tag{4.19}$$

with $\theta_i^\pm = \theta_i \pm \phi_i$. Thus, the transmission line contains six modes at frequencies $f_i^\pm = f_i \pm \omega_i/2\pi$, for $i = 1, 2, 3$ (see Fig. 4.1). As explained in Sec. 4.2.1, we model the propagating mode at frequency $f_i^\pm$ as a classical mode of energy $hfn_i^\pm$, where the phase $\theta_i^\pm$ of each mode is conjugated to $\hbar n_i^\pm$, such that the net photon flux is given by the difference between the outgoing and incoming signals at this frequency $hf_i^\pm \dot{n}_i^\pm = S_{\text{out}}[f_i^\pm] - S_{\text{in}}[f_i^\pm]$.

The topological pumping describes the dynamics of the observables conjugated to $\phi_i$.

Let us identify these observables. The change of variables

$$\theta_i = \frac{1}{2}\left(\theta_i^+ + \theta_i^-\right) \tag{4.20}$$

$$\phi_i = \frac{1}{2}\left(\theta_i^+ - \theta_i^-\right) \tag{4.21}$$

$$m_i = n_i^+ + n_i^- \tag{4.22}$$

$$n_i = n_i^+ - n_i^- \tag{4.23}$$

is a canonical change of variables, which means that it preserves the Poisson brackets, so the variable $\hbar n_i = \hbar(n_i^+ - n_i^-)$ is conjugated to the phase $\phi_i$. The topological pumping relates the rates $\dot{n}_i$, so we want to measure

$$\dot{n}_i = \frac{S_{\text{out}}[f_i^+] - S_{\text{in}}[f_i^+]}{hf_i^+} - \frac{S_{\text{out}}[f_i^-] - S_{\text{in}}[f_i^-]}{hf_i^-} \tag{4.24}$$

$$\simeq \frac{\Delta S_i}{hf_i} \tag{4.25}$$

with $\Delta S_i = S_{\text{out}}[f_i^+] - S_{\text{out}}[f_i^-]$ if we consider $f_i^\pm \simeq f_i$ and $S_{\text{in}}[f_i^+] = S_{\text{in}}[f_i^-]$.

## 4.C Chern insulator on the Lieb lattice

The three-band insulator on the Lieb lattice satisfies inversion symmetry. We write the inversion operator as $P(\boldsymbol{k})$=diag($e^{ik_x}$,1,$e^{ik_y}$). It leads to four inversion-invariant momenta in the 2D Brillouin zone: $\boldsymbol{\Gamma} = (0,0)$, $\boldsymbol{X} = (\pi,0)$, $\boldsymbol{Y} = (0,\pi)$, and $\boldsymbol{M} = (\pi,\pi)$. At these high-symmetry points, the Bloch Hamiltonian commutes with the inversion operator. Thus, the parities $p_\nu$ – eigenvalues of the inversion operator – are good quantum numbers to label each energy band $\nu$ at the inversion-invariant momenta. We sort the energy bands as $E_0 < E_1 < E_2$ and introduce the triplet $\boldsymbol{\pi} = (\pi_0, \pi_1, \pi_2)$, where $\pi_\nu$ is the band parity product

$$\pi_\nu = p_\nu(\boldsymbol{\Gamma}) p_\nu(\boldsymbol{X}) p_\nu(\boldsymbol{Y}) p_\nu(\boldsymbol{M}) = \pm 1 \ . \tag{4.26}$$

We now determine the different configurations of parity products allowed for the three bands emulated by the fluxonium.

At momentum $\boldsymbol{\Gamma}$, the parity operator reduces to the identity matrix. All energy bands have the same parity, regardless of the Hamiltonian parameters. This leads to the parity triplet $\boldsymbol{p}(\boldsymbol{\Gamma}) = (p_0(\boldsymbol{\Gamma}), p_1(\boldsymbol{\Gamma}), p_2(\boldsymbol{\Gamma})) = (+,+,+)$.

At momentum $\boldsymbol{X}$, the parity operator and the Bloch Hamiltonian read $P(\boldsymbol{X}) = \text{diag}(-1,1,1)$ and

$$H(\boldsymbol{X}) = \begin{pmatrix} 0 & 0 & 0 \\ 0 & \delta_1 & \Omega_2 \\ 0 & \Omega_2 & \delta_3 \end{pmatrix}. \tag{4.27}$$

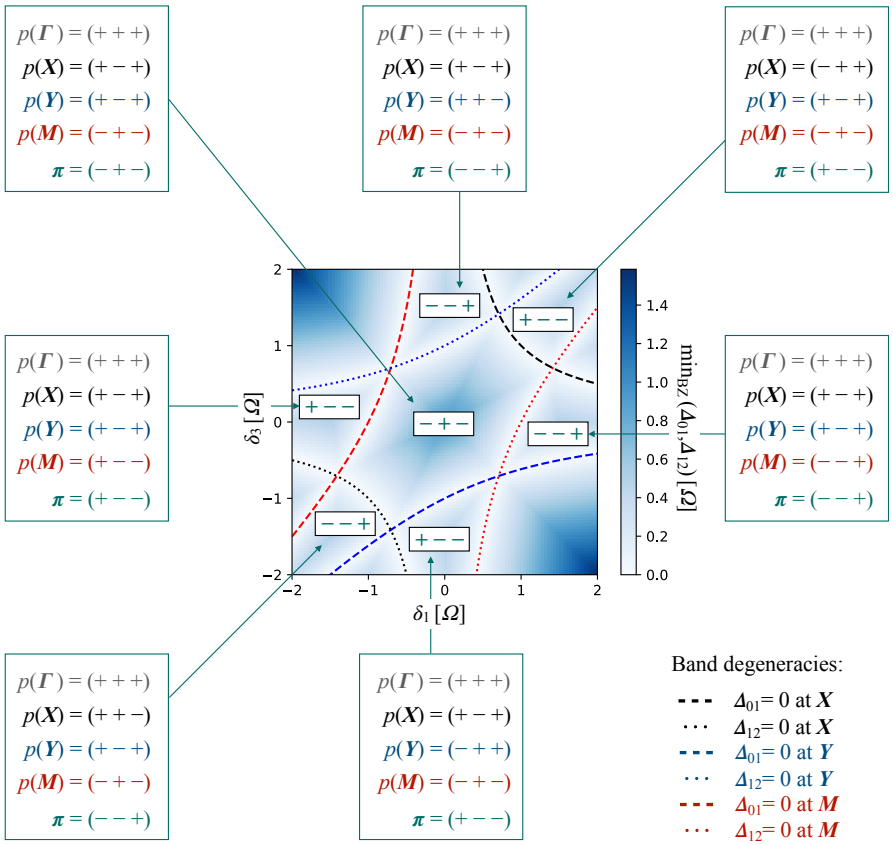


Figure 4.6: **Parity product of the bands**: The central map represents the minimum value of the lower gap ($\Delta_{01}$) or upper gap ($\Delta_{12}$) over the Brillouin zone, as a function of the detunings $\delta_1$ and $\delta_3$. It is obtained from numerical diagonalization of the Bloch Hamiltonian (4.4). Energy is in units of $\Omega_1 = \Omega_2 = \Omega_3 = \Omega$. The white areas correspond to values of the detuning for which a band gap closes. They are well described by the dashed (dotted) lines obtained analytically from the closing conditions of gap $\Delta_{01}$ ($\Delta_{12}$) at the inversion-invariant momenta $\boldsymbol{\Gamma}$, $\boldsymbol{X}$, $\boldsymbol{Y}$, and $\boldsymbol{M}$ in the Brillouin zone. These degeneracy lines mark the transitions between topologically nonequivalent band insulators, where the parity product $\pi_\nu$ of certain bands changes signs. The inversion eigenvalues labeling the bands at $\boldsymbol{\Gamma}$, $\boldsymbol{X}$, $\boldsymbol{Y}$, and $\boldsymbol{M}$ are shown in the green boxed insets, as a parity triplet $\boldsymbol{p} = (p_0, p_1, p_2)$ associated with the band energies $E_0 < E_1 < E_2$. It is only shown for insulating regions that exhibit negative band parity products. In such regions, the band structures do not support any band representation and cannot be adiabatically connected to an atomic limit. The fluxonium qutrit then simulates nontrivial Chern insulators.

The eigenspace of parity $-1$ is associated with the energy level $E_*(\boldsymbol{X}) = 0$. This is fixed regardless of the Hamiltonian parameters. In contrast, the eigenspace of parity $+1$ refers to the energy levels

$$E_\pm(\boldsymbol{X}) = \frac{\delta_1 + \delta_3}{2} \pm \frac{1}{2}\sqrt{4\Omega_2^2 + (\delta_1 - \delta_3)^2} \,, \tag{4.28}$$

which depends on the fluxonium drives. This allows three different configurations of parities:

- $E_*(\boldsymbol{X}) < E_-(\boldsymbol{X}) < E_+(\boldsymbol{X})$ with parities $\boldsymbol{p}(\boldsymbol{X}) = (-,+,+)$. It occurs when $\delta_1 > 0$, $\delta_3 > 0$, and $\delta_3 > \Omega_2^2/\delta_1$.
- $E_-(\boldsymbol{X}) < E_+(\boldsymbol{X}) < E_*(\boldsymbol{X})$ with parities $\boldsymbol{p}(\boldsymbol{X}) = (+,+,-)$. It occurs when $\delta_1 < 0$, $\delta_3 < 0$, and $\delta_3 < \Omega_2^2/\delta_1$.
- $E_-(\boldsymbol{X}) < E_*(\boldsymbol{X}) < E_+(\boldsymbol{X})$ with parities $\boldsymbol{p}(\boldsymbol{X}) = (+,-,+)$ otherwise.

At momentum $\boldsymbol{Y}$, the parity operator and the Bloch Hamiltonian read $P(\boldsymbol{Y}) = \mathrm{diag}(1,1,-1)$ and

$$H(\boldsymbol{Y}) = \begin{pmatrix} 0 & \Omega_1 & 0 \\ \Omega_1 & \delta_1 & 0 \\ 0 & 0 & \delta_3 \end{pmatrix}. \tag{4.29}$$

The eigenspace of parity $-1$ is associated with the energy level $E_*(\boldsymbol{Y}) = \delta_3$. The eigenspace of parity $+1$ refers to the energy levels

$$E_\pm(\boldsymbol{Y}) = \frac{\delta_1}{2} \pm \frac{1}{2}\sqrt{4\Omega_1^2 + \delta_1^2} \,. \tag{4.30}$$

This allows three different configurations of parities:

- $E_*(\boldsymbol{Y}) < E_-(\boldsymbol{Y}) < E_+(\boldsymbol{Y})$ with parities $\boldsymbol{p}(\boldsymbol{Y}) = (-,+,+)$. It occurs when $2\delta_3 < \delta_1 - \sqrt{4\Omega_1^2 + \delta_1^2}$.
- $E_-(\boldsymbol{Y}) < E_+(\boldsymbol{Y}) < E_*(\boldsymbol{Y})$ with parities $\boldsymbol{p}(\boldsymbol{Y}) = (+,+,-)$. It occurs when $2\delta_3 > \delta_1 + \sqrt{4\Omega_1^2 + \delta_1^2}$.
- $E_-(\boldsymbol{Y}) < E_*(\boldsymbol{Y}) < E_+(\boldsymbol{Y})$ with parities $\boldsymbol{p}(\boldsymbol{Y}) = (+,-,+)$ otherwise.

At momentum $\boldsymbol{M}$, the parity operator and the Hamiltonian read $P(\boldsymbol{M}) = \mathrm{diag}(-1,1,-1)$ and

$$H(\boldsymbol{M}) = \begin{pmatrix} 0 & 0 & -i\Omega_3 \\ 0 & \delta_1 & 0 \\ i\Omega_3 & 0 & \delta_3 \end{pmatrix}. \tag{4.31}$$

The eigenspace of parity $+1$ is associated with the energy level $E_*(\boldsymbol{M}) = \delta_1$. The eigenspace of parity $-1$ refers to the energy levels

$$E_\pm(\boldsymbol{M}) = \frac{\delta_3}{2} \pm \frac{1}{2}\sqrt{4\Omega_3^2 + \delta_3^2} \,. \tag{4.32}$$

This allows three different energy configurations:

- $E_*(\boldsymbol{M}) < E_-(\boldsymbol{M}) < E_+(\boldsymbol{M})$ with parities $\boldsymbol{p}(\boldsymbol{M}) = (+,-,-)$. It occurs when $\delta_1 < 0$ and $\delta_3 > \delta_1 - \Omega_3^2/\delta_1$.
- $E_-(\boldsymbol{M}) < E_+(\boldsymbol{M}) < E_*(\boldsymbol{M})$ with parities $\boldsymbol{p}(\boldsymbol{M}) = (-,-,+)$. It occurs when $\delta_1 > 0$ and $\delta_3 < \delta_1 - \Omega_3^2/\delta_1$.
- $E_-(\boldsymbol{M}) < E_*(\boldsymbol{M}) < E_+(\boldsymbol{M})$ with parities $\boldsymbol{p}(\boldsymbol{M}) = (-,+,-)$ otherwise.

This shows that any change of band parity requires the band gap to close at the inversion-invariant momenta. All the band-parity configurations determined above, as well as their parity products, are summarized in the insets of Fig. 4.6 as a function of $\delta_1$ and $\delta_3$.

## 4.D Dynamics in the rotating frame

The equations of motion of the classical variables $n_i$ conjugated to the phases $\phi_i$ are first written in the laboratory frame

$$\dot{n}_i = -\frac{1}{\hbar} \langle \Psi_{\text{labo}}(t)| \frac{\partial H_{\text{labo}}}{\partial \phi_i} |\Psi_{\text{labo}}(t)\rangle \,, \tag{4.33}$$

where the dynamics of state $|\Psi_{\text{labo}}(t)\rangle$ of the qutrit in the laboratory frame is governed by the Hamiltonian $H_{\text{labo}}(\{\phi_j, \theta_j\})$, introduced before (4.10). In the rotating frame, the dynamics of $|\Psi_{\text{rot}}(t)\rangle = U^\dagger(t)\,|\Psi_{\text{labo}}(t)\rangle$ is governed by $H_{\text{rot}} = U^\dagger H_{\text{labo}} U - i\hbar U^\dagger \frac{\mathrm{d}U}{\mathrm{d}t}$ which satisfies $\frac{\partial H_{\text{rot}}}{\partial \phi_i} = U^\dagger \frac{\partial H_{\text{labo}}}{\partial \phi_i} U$ since the unitary transformation $U(t)$ does not depend on the phase $\phi_i$. Thus, the equation of the dynamics of $n_i$ has the same form in the rotating frame

$$\dot{n}_i = -\frac{1}{\hbar} \langle \Psi_{\text{rot}}(t)| \frac{\partial H_{\text{rot}}}{\partial \phi_i} |\Psi_{\text{rot}}(t)\rangle \tag{4.34}$$

where in the rotating wave approximation, we consider $H_{\text{rot}}(\{\phi_j, \theta_j\}, t) \simeq \tilde{H}(\phi_1, \phi_2, \phi_3)$, with the 3 phases Hamiltonian given by (4.3). This is, as explained in Appendix 4.B, a first adiabatic elimination of the fastest degrees of freedom $\{\theta_j\}$.

As derived in Chap. 3, under the approximation, the equations of motions of the variables $n_i$ are given by Eq. (3.10). This provides the equations of motion of the three degrees of freedom $(\phi_i, n_i)$, $i = 1, 2, 3$. We further impose a condition on the frequencies $\omega_i$, leading to $\phi_1 - \phi_2 - \phi_3$ being a conserved quantity. Thus, the dynamics finally simplifies to two effective slow degrees of freedom. We note them $(\phi_I, n_I)$ and $(\phi_{II}, n_{II})$. We identify them by the following canonical change of variable

$$n_I = n_1 + n_3 \quad ; \quad \phi_I = \phi_1 \tag{4.35a}$$
$$n_{II} = n_2 - n_3 \quad ; \quad \phi_{II} = \phi_2 \tag{4.35b}$$
$$n_{III} = -n_3 \quad ; \quad \phi_{III} = \phi_1 - \phi_2 - \phi_3 \tag{4.35c}$$

satisfying $\{\phi_A, n_B\} = 1/\hbar$, $A, B = I, II, III$. Since these new variables are conjugated, the equations of motion are

$$\dot{n}_A = -\frac{1}{\hbar}\frac{\partial E_\nu}{\partial \phi_A} + \sum_{B \neq A} \dot{\phi}_B F_{\nu, \phi_A \phi_B} \tag{4.36}$$

with $E_\nu$ the energy and $F_\nu$ the Berry curvature of the band $\nu$ of $H(\phi_I, \phi_{II}, \phi_{III}) = \tilde{H}(\phi_I, \phi_{II}, \phi_I - \phi_{II} - \phi_{III})$. The frequencies of the phases $\phi_1, \phi_2, \phi_3$ are chosen such that $\omega_3 = \omega_1 - \omega_2$, thus $\dot{\phi}_{III} = 0$ and we keep $\phi_{III} = 0$ at all time with the initial condition. Thus, the equations of motion reduce to (4.6).

## 4.E Temporal fluctuations

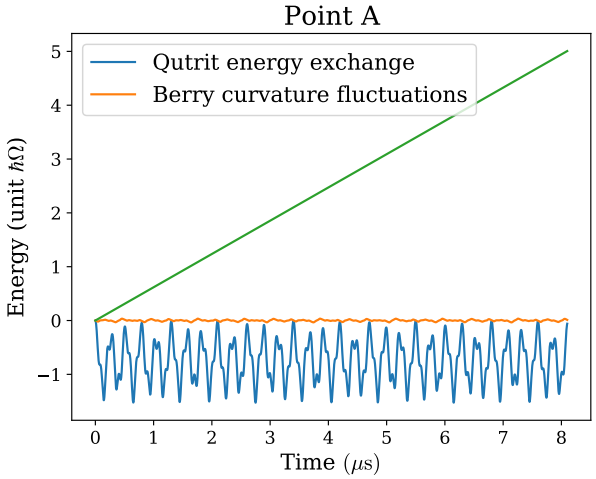


Figure 4.7: Different terms in the variation of the energy $\hbar\omega_1(n_1 + n_3)$, in the case of resonance $\delta_1 = \delta_3 = 0$, point A in Fig. 4.4(a). In blue: Time-integration of the term of variation of the energy of the qutrit $-\omega_1 \frac{\partial E_\nu}{\partial \phi_1}$. In orange: Time-integration of the term of fluctuation of the geometrical coupling $\hbar\omega_1\omega_2(F_{\nu,\phi_1\phi_2} - \frac{\mathcal{C}_\nu}{2\pi})$. In green: Topological energy transfer at constant rate $\hbar\frac{\omega_1\omega_2}{2\pi}\mathcal{C}_\nu$. The fluctuation of the energy of the qutrit is the predominant source of temporal fluctuation of the energy.

During the adiabatic evolution, the time derivative of the energy of a mode can be decomposed into a sum of three terms

$$\hbar\omega_1(\dot{n}_1 + \dot{n}_3) = -\omega_1 \frac{\partial E_\nu}{\partial \phi_1} + \hbar\omega_1\omega_2(F_{\nu,\phi_1\phi_2} - \frac{\mathcal{C}_\nu}{2\pi}) + \hbar\frac{\omega_1\omega_2}{2\pi}\mathcal{C}_\nu. \tag{4.37}$$

The first term is the variation of the energy $E_\nu$ of the band $\nu$ of the qutrit, corresponding to an energy exchange between the qutrit and the mode. The second term corresponds to the fluctuation of the Berry curvature $F_{\nu,\phi_1\phi_2}$ around its topologically quantized average value $\frac{\mathcal{C}_\nu}{2\pi}$, with $\mathcal{C}_\nu$ the Chern number. This corresponds to the fluctuation of the geometrical transfer of energy between the two modes. The last term is the topological power rate, the only non-zero term in time-average. The two first terms are responsible for the time fluctuation of the energy of the mode.

In Fig. 4.7 is represented the time-integration of each term in the case of resonance $\delta_1 = \delta_3 = 0$, point A in Fig. 4.4(a). We see that the temporal fluctuation of the energy is mainly due to the energy exchange between the qutrit and the mode, and the fluctuation of the Berry curvature is much lower. This is the case for every value of parameters in the region of interest of the phase diagram.

These temporal fluctuations are further discussed in the following chapter.

Chapter 5

# Adiabatic cat states

In Chap. 3, we described topological pumps as a topological coupling between a fast quantum system and slow classical degrees of freedom of its environment. In particular, we described the mechanism of topological frequency conversion as a topological coupling between two slow classical modes driving a quantum system, focusing on the dynamics of the slow classical modes. We showed that the topological nature of the coupling induces a transfer of energy from one mode to the other. In this chapter, we consider on equal footing the drives and the quantum system, describing all of them quantum mechanically. We model the drives as quantum modes, characterized by a pair of conjugated operators accounting for their phase and number of quanta. This extends previous mixed quantum-classical descriptions of the drives [56, 193–195]. We will focus on the simplest case where the fast quantum system is a two-level system, a qubit.

We thus consider such a topological pump as a particular example of a slow-fast quantum system in the sense discussed in Chap. 2, where we introduced the general adiabatic theory of such system, which amounts to define effective dynamics of peculiar initial states, the adiabatic states lying in the adiabatic subspace. At first order in the perturbative theory, this effective dynamics involves a Berry curvature which carries the topological property discussed in Chap. 3. While most of the works on slow-fast quantum systems focus on the derivation of the effective dynamics, here we pay attention on the nature of the states of the total system for which it applies. We show that these adiabatic states entangle the slow and the fast subsystems. As such, they are not naturally prepared experimentally, but they form a basis on which any initial state decomposes. The adiabatic dynamics acts on all three components of the pump. In the case of topological couplings, it separates in phase space the components of the two modes, leading to a creation of a cat state. We denote cat state a superposition of two states distinguishable through measures of the modes' energy, but not necessarily an equal weight superposition. In this sense, we show that the creation of cat states is generic and not accidental.

This chapter also makes the bridge between Chap. 1 and Chap. 2 concerning the nature of adiabatic states. In Chap. 1, we introduced a notion of adiabatic state of a slowly driven quantum system, here corresponding to the qubit. We introduce a model of quantum modes coupled to a fast quantum system which enables the generalization of these states into adiabatic states of the fast quantum system – the qubit – parametrized by the phases of the slow quantum modes. This enables us to define a notion of dressed Berry curvature, which generalizes the Berry curvature beyond the order 0 of the adiabatic

expansion. The dynamics of the slow quantum modes involve this dressed Berry curvature instead of the bare Berry curvature. We show that both carry the same topology. We further show that the entanglement between the slow and fast subsystems – between the quantum modes and the qubit – depends on the geometric properties of these adiabatic states. We unveil the role of their quantum metric tensor in this entanglement, as well as in the weight of the cat states.

Interestingly, similar qubit-modes quantum systems were recently proposed [196] and experimentally realized in quantum optical devices [197] to simulate topological lattice models. In this context, the Hamiltonians of a qubit coupled to cavities was expressed in terms of Fock-state lattices, and shown, with two cavities, to realize a chiral topological phase [198, 199], and, with three cavities, the quantum or valley Hall effect [196, 200]. Indeed, the focus of these realizations was on synthetic topological models and their associated zero-energy states. Our approach bridges the gap between the study of topological pumping of driven systems and these studies of quantum optical devices.

This chapter is organized as follows. In Sec. 5.1 we introduce the model of a qubit driven by two quantum modes (Sec. 5.1.1) and discuss qualitatively the typical dynamics of adiabatic cat states (Sec. 5.1.2). In Sec. 5.2 we characterize the two components of the cat states as adiabatic states and identify their effective dynamics which splits them apart in energy. We characterize the weight of each cat component for a separable initial state. In Sec. 5.3 we study each cat component, relating the entanglement between the qubit and the modes to the quantum geometry of the adiabatic states (Sec. 5.3.1), and discussing the evolution of the number of quanta of each mode in relation with Bloch oscillations and Bloch breathing (Sec. 5.3.2).

This chapter is based on the submitted article [57].

### Comment on the notations

In this chapter, we are lead to consider the Hamiltonian $H(\mathbf{\Phi})$ of the fast quantum system – the qubit – parametrized by the phases $\mathbf{\Phi}$ of the slow modes. We adopt similar notations than in Chap. 1. We note $|\psi_{\nu,0}(\mathbf{\Phi})\rangle$ the eigenstates of $H(\mathbf{\Phi})$, $E_{\nu,0}(\mathbf{\Phi})$ their eigenenergy, and $F_{\nu,\phi_i\phi_j,0}(\mathbf{\Phi}) = i\left(\left\langle \partial_{\phi_i}\psi_{\nu,0}(\mathbf{\Phi})\middle|\partial_{\phi_j}\psi_{\nu,0}(\mathbf{\Phi})\right\rangle - (i \leftrightarrow j)\right)$ the Berry curvature. We will define the adiabatic states of the qubit noted $|\psi_\nu(\mathbf{\Phi})\rangle$, their energy $E_\nu(\mathbf{\Phi})$, and their dressed Berry curvature $F_\nu(\mathbf{\Phi}) = i\left(\langle\partial_{\phi_1}\psi_\nu(\mathbf{\Phi})|\partial_{\phi_2}\psi_\nu(\mathbf{\Phi})\rangle - (1 \leftrightarrow 2)\right)$.

In this chapter, we use the convention for the conjugated quantum phase and number of quanta $[\hat{n}, \hat{\phi}] = i$, rather than the convention $\{\phi, \hbar n\} = 1$ of conjugated classical phase and number of quantum used in Chap. 3. With the classical convention $\{\hbar n, \phi\} = 1$ corresponding to the quantum convention adopted in this chapter, the classical equations of motion (3.9), (3.10) read

$$\hbar\dot{n}_i = \frac{\partial E_{\nu,0}}{\partial \phi_i} + \hbar\sum_{j\neq i}\omega_j F_{\nu,\phi_i\phi_j,0}, \tag{5.1a}$$

$$\dot{\phi}_i = -\omega_i. \tag{5.1b}$$

We will recover similar equations with this convention of signs in this chapter.

## 5.1 A qubit driven by two quantum modes

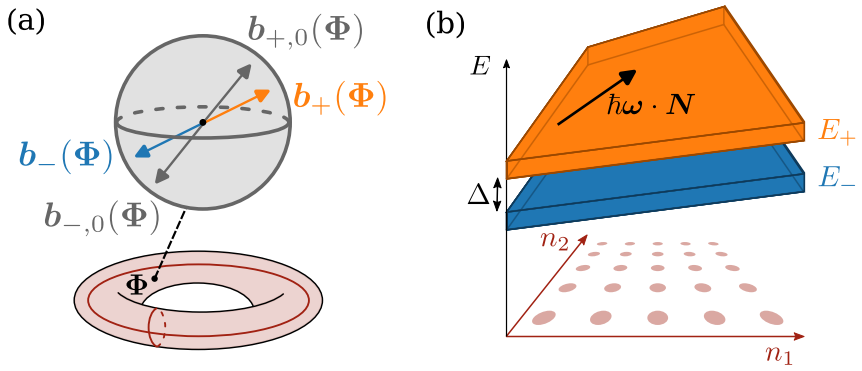


Figure 5.1: *Phase and number representations of a quantum qubit – 2 modes model.* (a) Phase representation, convenient to represent the dynamics of the qubit. At each value of the phases $\boldsymbol{\Phi}$ are associated qubit eigenstates $|\psi_{\pm,0}(\boldsymbol{\Phi})\rangle$ represented by a vector $\boldsymbol{b}_{\pm,0}(\boldsymbol{\Phi}) = \pm\boldsymbol{h}(\boldsymbol{\Phi})/|\boldsymbol{h}(\boldsymbol{\Phi})|$ on the Bloch sphere (in grey). The adiabatic states $|\psi_{\pm}(\boldsymbol{\Phi})\rangle$, represented by a vector $\boldsymbol{b}_{\pm}(\boldsymbol{\Phi})$, are a perturbative deformation of the eigenstates. (b) Number representation, convenient to represent the dynamics of the modes. In this viewpoint the model can be interpreted as an unusual model of spin-half particle on a discrete lattice where $\boldsymbol{N} = (n_1, n_2) \in \mathbb{Z}^2$ represents its position on the lattice and $\boldsymbol{\Phi} \in [0, 2\pi]^2$ the Bloch momenta. This particle is submitted to an electric field $\hbar\boldsymbol{\omega} \cdot \hat{\boldsymbol{N}}$ and a strong spin-orbit coupling $\boldsymbol{h}(\hat{\boldsymbol{\Phi}}) \cdot \boldsymbol{\sigma}$. As a consequence, the adiabatic states are associated to energy bands $E_\pm$ tilted in the direction $\boldsymbol{\omega}$ of the electric field and separated by the gap $\Delta$ due to the spin-orbit coupling.

### 5.1.1 Model of quantum rotors

We consider the dynamics of two quantum modes coupled to a fast quantum degree of freedom, chosen for clarity as a two level system, a qubit. Each slow mode is described by a phase operator $\hat{\phi}_i$ of continuum spectrum $[0, 2\pi]$, conjugated to a number operator $\hat{n}_i$ of discrete spectrum $\mathbb{Z}$, such that $[\hat{n}_i, \hat{\phi}_j] = \mathrm{i}\delta_{ij}$ [90]. We assume that the fast degree of freedom couples only to the phases of the modes, through a Hamiltonian $H(\hat{\boldsymbol{\Phi}})$ with $\hat{\boldsymbol{\Phi}} = (\hat{\phi}_1, \hat{\phi}_2)$. Noting $\boldsymbol{\omega} = (\omega_1, \omega_2)$ the frequencies of the modes, and $\hat{\boldsymbol{N}} = (\hat{n}_1, \hat{n}_2)$ their respective number operators, the dynamics of the full quantum system is governed by the Hamiltonian

$$\hat{H}_{\mathrm{tot}} = \hbar\boldsymbol{\omega} \cdot \hat{\boldsymbol{N}} \otimes \mathbf{1} + H(\hat{\boldsymbol{\Phi}}), \quad H(\hat{\boldsymbol{\Phi}}) = \sum_{\alpha=1}^{3} h_\alpha(\hat{\boldsymbol{\Phi}}) \otimes \sigma_\alpha . \tag{5.2}$$

Such a model appears as the natural quantization of a 2-tone Floquet systems, where the time-dependent parameters $\phi_i(t) = \omega_i t$ of the qubit Hamiltonian $\boldsymbol{h}(\phi_1(t), \phi_2(t)) \cdot \boldsymbol{\sigma}$ are here considered as true quantum degrees of freedom. Note that we will focus on the adiabatic dynamics of such a Floquet model, valid for slow frequencies $\hbar\omega_i$ compared with the qubit's spectral gap $2|\boldsymbol{h}|$.

Physically, the two modes of model (5.2) often result from the coupling to harmonic oscillators [193, 195, 196, 198]. Describing this oscillator by a pair of conjugated operators

$\hat{n}_i, \hat{\phi}_i$ is valid for states with a number of quanta $\bar{n}$ large compared to any dynamical variation of and spreading of $n$, $\Delta n \ll \bar{n}$ [193]. We will come back to these aspects in Chap. 6, showing in addition that such rotor model captures very well the dynamics of quantum harmonic oscillators coupled to a two level system on a first part of the dynamics, at short times.

The modes' intrinsic energies depend on the number of quanta $\boldsymbol{N}$ while the qubit's energy depends on their phases: hence we will use two dual representations of the dynamics of the system through this paper. When focusing on the qubit's evolution, the phase representation is natural, represented in Fig. 5.1(a): at each value of the phases $\boldsymbol{\Phi}$ are associated qubit's eigenstates $|\psi_{\pm,0}(\boldsymbol{\Phi})\rangle$. The modes' dynamics translate into an evolution with time of the phase, and thus an evolution of the associated qubit's states $|\psi_{\pm}(\boldsymbol{\Phi})\rangle$ which slightly differ from the eigenstates and will be discussed in section 5.2.1.

Focusing on the quantum modes, their dynamics is conveniently represented in number representation, Fig. 5.1(b). In this viewpoint, we can interpret the model as that of a particle on a 2D lattice of sites $\boldsymbol{N} = (n_1, n_2)$, $\boldsymbol{\Phi} = (\phi_1, \phi_2)$ being the associated Bloch momenta in the first Brillouin zone. The Hamiltonian (5.2) describes its motion, submitted to both a spin-orbit coupling $H(\hat{\boldsymbol{\Phi}})$ and an electric field $\hbar\boldsymbol{\omega}$. We will use this analogy to relate the geometrical and topological properties of gapped phases on a lattice to those of the above quantum model. Note that in this case, there is no embedding of this lattice in $\mathbb{R}^2$ as opposed to the Bloch theory of crystals discussed in Sec. 2.2.1 of Chap. 2. The position operator identifies with coordinate operator on the lattice. As a consequence, there is no ambiguity in a choice of Bloch convention and definition of the Berry curvature [62, 93].

### Topological coupling

In the following, we consider a topological coupling between the qubit and the two quantum modes. This corresponds to the situation where the qubit remains gapped irrespective of the phase $\boldsymbol{\Phi}$ of the quantum modes, *i.e.* $|\boldsymbol{h}(\boldsymbol{\Phi})| \geq \Delta > 0$ for all values of $\boldsymbol{\Phi}$. Besides, the topological nature of the drive originates from the condition that the map $\boldsymbol{\Phi} \in [0, 2\pi]^2 \to \boldsymbol{h}(\boldsymbol{\Phi})$ wraps around the origin in $\mathbb{R}^3$. This is a condition of strong coupling between the qubit and the drive. Indeed, if we represent the qubit's eigenstates by a vector $\boldsymbol{b}_{\pm,0}(\boldsymbol{\Phi}) = \pm\boldsymbol{h}(\boldsymbol{\Phi})/|\boldsymbol{h}(\boldsymbol{\Phi})|$ on the Bloch sphere, then any point of the sphere corresponds to a ground state of the qubit for a particular phase state of the drive. This is in contrast with the familiar weak coupling limit where states around the south pole, $|\downarrow\rangle$, are associated to the ground states and those close to the north pole, $|\uparrow\rangle$, to excited states. In the present case, knowledge of the state of the qubit is not sufficient to determine whether it is in the excited or ground state: information on the state of the driving modes is necessary.

Throughout this paper, the numerical results are obtained by considering an example of such a topological coupling provided by the quantum version of the Bloch Hamiltonian

of the half Bernevig-Hughes-Zhang (BHZ) model [201]:

$$h_x(\hat{\mathbf{\Phi}}) = \frac{\Delta}{2}\sin\left(\hat{\phi}_1\right), \tag{5.3a}$$

$$h_y(\hat{\mathbf{\Phi}}) = -\frac{\Delta}{2}\sin\left(\hat{\phi}_2\right), \tag{5.3b}$$

$$h_z(\hat{\mathbf{\Phi}}) = \frac{\Delta}{2}\left(1-\cos\left(\hat{\phi}_1\right)-\cos\left(\hat{\phi}_2\right)\right), \tag{5.3c}$$

where the parameter $\Delta > 0$ is the gap of the qubit. See appendix 5.F for details on the numerical method.

### 5.1.2 Topological dynamics of adiabatic cat states

In this section, we illustrate the topological dynamics of the system starting from a typical state. This dynamics is analyzed quantitatively in the remaining of this paper. We focus on separable initial state, easier to prepare experimentally:

$$|\Psi(t=0)\rangle = |\chi_1\rangle \otimes |\chi_2\rangle \otimes |\psi_q\rangle\,. \tag{5.4}$$

Each quantum mode is prepared in a Gaussian state $|\chi_i\rangle$, characterized by an average number of quanta $n_i^0$ and a phase $\phi_i^0 = 0$, with widths $\Delta n_i, \Delta\phi_i$ satisfying $\Delta\phi_i\Delta n_i = \frac{1}{2}$. The qubit is prepared in a superposition $|\psi_q\rangle = (|\uparrow_z\rangle + |\downarrow_z\rangle)/\sqrt{2}$.

We consider modes with frequency of the same order of magnitude, $\hbar\omega_1 = 0.075\Delta$ and $\omega_2/\omega_1 = (1+\sqrt{5})/2 \simeq 1.618$, such that in the following, time is arbitrarily expressed in unit of period of the first mode $T_1 = 2\pi/\omega_1$. In Fig. 5.2, we represent the dynamics of this state $|\Psi(t)\rangle$ by displaying the associated number distribution of the modes $P_{n_1n_2}(t) = \langle n_1, n_2|\,\hat{\rho}_{12}(t)\,|n_1, n_2\rangle$, with $\hat{\rho}_{12}(t)$ the corresponding reduced density matrix of the modes. Three initial states with respective initial number width $\Delta n = \Delta n_1 = \Delta n_2 = 5$, $\Delta n = 0.7$ and $\Delta n = 1/(2\pi)$ (quasi-Fock state delocalized in phase $\Delta\phi = \pi$) are shown respectively in Fig. 5.2 (a1), (b1) and (c1). The time evolved states at respectively $t = 0, 8/3, 16/3, 8$ and $t = 32/3$ are represented respectively on columns 1 to 5 of Fig. 5.2. We observe a splitting of the initial state into a superposition of two states

$$|\Psi(t)\rangle = |\Psi_-(t)\rangle + |\Psi_+(t)\rangle\,. \tag{5.5}$$

The photon number distributions of $|\Psi_-(t)\rangle$ and $|\Psi_+(t)\rangle$ drift in opposite directions, corresponding to energy transfers between modes 1 and 2 in opposite directions. This drift is a manifestation of the topological pumping discussed in classical-quantum models of Chap. 3. This pumping is conveniently represented by introducing rotated number coordinates

$$n_E = \frac{1}{|\boldsymbol{\omega}|}(\omega_1 n_1 + \omega_2 n_2), \tag{5.6}$$

$$n_\perp = \frac{1}{|\boldsymbol{\omega}|}(-\omega_2 n_1 + \omega_1 n_2), \tag{5.7}$$

with $|\boldsymbol{\omega}| = \sqrt{\omega_1^2+\omega_2^2}$. $\hbar|\boldsymbol{\omega}|n_E$ corresponds to the total energy of the modes and is constant up to the instantaneous energy exchange with the qubit. $n_\perp$ is the coordinate in the

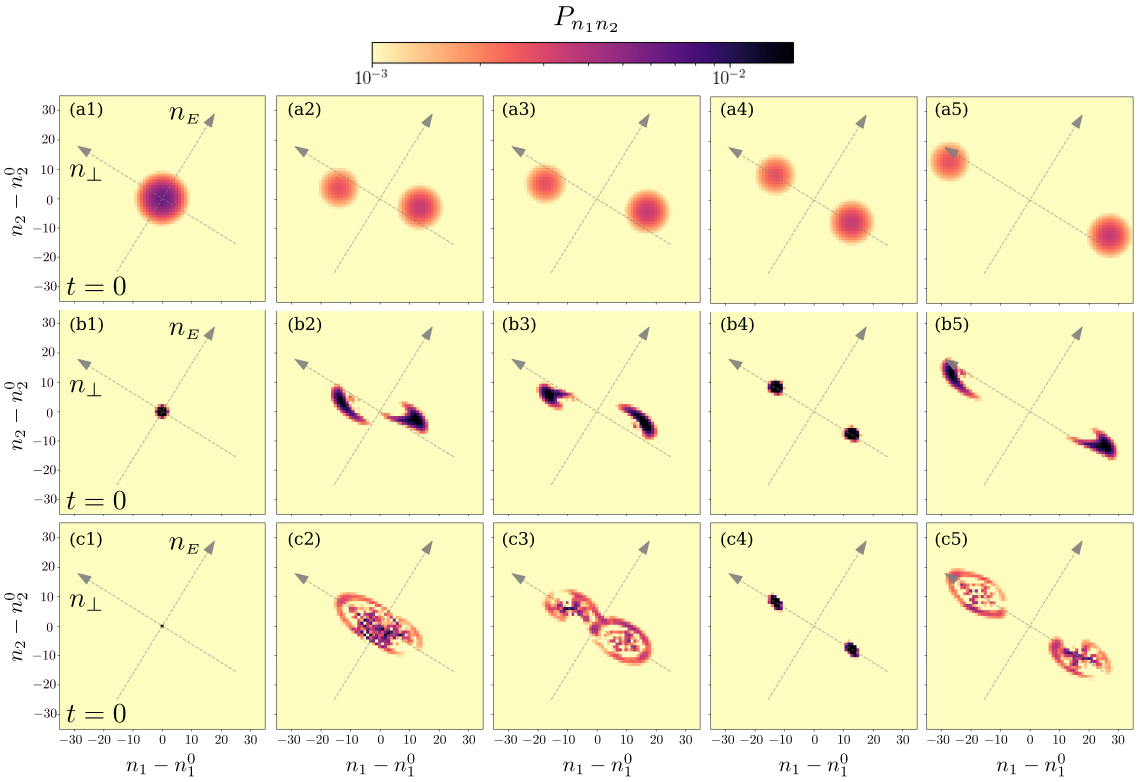


Figure 5.2: Typical dynamics of adiabatic cat states. Distribution of number of quanta of the two modes $P_{n_1 n_2} = \langle n_1, n_2 | \hat{\rho}_{12} | n_1, n_2 \rangle$ at different times for three initial states. The modes are prepared in a Gaussian state with an average value of phase $\phi_1^0 = \phi_2^0 = 0$ and an equal width in number of quanta $\Delta n_1 = \Delta n_2 = \Delta n$, corresponding to a width $\Delta\phi = 1/(2\Delta n)$ in phase. The qubit is prepared in $(|\uparrow\rangle + |\downarrow\rangle)/\sqrt{2}$. The evolution of states with different initial width $\Delta n$ is represented: line (a), $\Delta n = 5$, $\Delta\phi \simeq 0.03\pi$; line (b), $\Delta n = 0.7$, $\Delta\phi \simeq 0.23\pi$, and line (c), Quasi-Fock state $\Delta n = 1/(2\pi)$, delocalized in phase $\Delta\phi = \pi$. The columns (2) to (5) represent the time evolved state at respectively $t = 8/3$, $16/3$, $8$ and $t = 32/3$ in units of the period of the first mode $T_1 = 2\pi/\omega_1$. The dynamics splits the initial state in a cat state in the sense of a superposition of two states with distinguishable energy content.

direction perpendicular to $\boldsymbol{\omega}$. A transfer of energy between mode 1 and mode 2 naturally translates into a drift in the $n_\perp$ direction, at fixed average $n_{_E}$. We also observe that for small initial $\Delta n$, corresponding to lines (b) and (c), each component $|\Psi_-(t)\rangle$ and $|\Psi_+(t)\rangle$ undergoes a complex breathing dynamics around the drift. This oscillatory behavior is reminiscent of Bloch oscillations of the associated particle submitted to an electric field, superposed with a topological drift originating from the anomalous transverse velocity. After an initial time of separation, the number distributions for $|\Psi_-(t)\rangle$ and $|\Psi_+(t)\rangle$ no longer overlap (Fig. 5.2 columns 4 and 5). The system is then in a cat state: a superposition of two states with well distinguishable energy content.

We will now study quantitatively these cat states and their dynamics. In section 5.2, we identify the two components $|\Psi_\pm(t)\rangle$ as adiabatic states (Sec. 5.2.1). We study their topological dynamical separation into a cat state (Sec. 5.2.2). We characterize the weight of each component of the cat (Sec. 5.2.3) and identify a family of cat states with equal weight on each component. In section 5.3.1 we analyze the entanglement between the qubit and the modes for each cat component, and relate it to the quantum geometry of the adiabatic states. Finally, we discuss the dynamics of each cat component around the average drift, in relation with Bloch oscillations and Bloch breathing on the associated lattice (Sec. 5.3.2).

## 5.2 Adiabatic decomposition

### 5.2.1 Adiabatic projector

When the driving frequencies remain small compared to the qubit's gap, $\hbar\omega_i \ll \Delta$, we naturally describe the effective dynamics of the coupled qubit and drives in terms of fast and slow quantum degrees of freedom. This is traditionally the realm of the Born-Oppenheimer approximation, discussed in Sec. 2.1 of Chap. 2. Historically both degrees of freedom were those of massive particles, the slow modes being associated with the heavy nucleus of a molecule and the fast ones with the light electrons [68,79,86]. In this context, the Born-Oppenheimer approximation assumes that the time evolved state decomposes onto the instantaneous eigenstates of the fast degrees of freedom – more precisely remains projected on the Born-Oppenheimer subspace introduced in Sec. 2.1.2 –, and describes the resulting effective dynamics of the slow degree of freedom.

The distinctive characteristic of the present quantum modes - qubit model from the usual Born-Oppenheimer setting is the linearity of the Hamiltonian (5.2) in the variable $\hat{\boldsymbol{N}}$. This allows to express in a simple form the corrections to the Born-Oppenheimer approximation for the adiabatic states. This rotor model enables to express the states of the adiabatic subspace of a slow-fast quantum system introduced in Sec. 2.4 of Chap. 2 in terms of the adiabatic states of a slowly driven quantum system introduced in Sec. 1.2 of Chap. 1. Let us explain the procedure to construct such states, while referring to appendix 5.B for technical details.

We note $|\boldsymbol{\Phi}\rangle$ the eigenstates of the phase operator of the modes $\hat{\boldsymbol{\Phi}}$. Due to the linearity in $\hat{\boldsymbol{N}}$ of the Hamiltonian (5.2), the time evolution of a phase eigenstate $|\boldsymbol{\Phi}\rangle \otimes |\psi\rangle$, where $|\psi\rangle$ is a state of the qubit, is $|\boldsymbol{\Phi} - \boldsymbol{\omega}t\rangle \otimes U(t;\boldsymbol{\Phi})\,|\psi\rangle$. The time evolution operator $U$ is

deduced from that for the time-dependent model parametrized by classical phases $\boldsymbol{\omega}t$:

$$U(t;\boldsymbol{\Phi}) = \mathcal{T}\exp\left[-\frac{\mathrm{i}}{\hbar}\int_0^t \mathrm{d}\tau\ H(\boldsymbol{\Phi}-\boldsymbol{\omega}\tau)\right]\ , \tag{5.8}$$

where $\mathcal{T}$ denotes time ordering. See Appendix 5.A for details. This property is the reason why the adiabatic projector (as defined in Chap. 2) of the quantum rotors model is going to be written in terms of adiabatic states of the fast subsystem as defined for a slow driven quantum system in Chap. 1.

### Adiabatic projector of the qubit

We denote by $|\psi_{\nu,0}(\boldsymbol{\Phi})\rangle$, $\nu = \pm$, the normalized eigenstates of the two-level Hamiltonian $H(\boldsymbol{\Phi})\,|\psi_{\nu,0}(\boldsymbol{\Phi})\rangle = \nu|\boldsymbol{h}(\boldsymbol{\Phi})|\,|\psi_{\nu,0}(\boldsymbol{\Phi})\rangle$ for each $\boldsymbol{\Phi}$ in $[0,2\pi]^2$. For small frequencies $\omega_i$, given the time evolution of phase eigenstates, we can reasonably expect that the coupled qubit-modes system prepared in an eigenstate $|\boldsymbol{\Phi}\rangle \otimes |\psi_{\nu,0}(\boldsymbol{\Phi})\rangle$ will remain in a translated eigenstate. However, this simple picture is only qualitatively valid: eigenstates get hybridized by adiabatic dynamics, even at arbitrarily small driving frequencies. As a consequence, we identify the family of *adiabatic states* $|\psi_\nu(\boldsymbol{\Phi})\rangle$ such that the dynamics occurs within each family of states $|\boldsymbol{\Phi}\rangle \otimes |\psi_\nu(\boldsymbol{\Phi})\rangle$. Adiabatic evolution is then represented as a transport from $|\boldsymbol{\Phi}\rangle\otimes|\psi_\nu(\boldsymbol{\Phi})\rangle$ to $|\boldsymbol{\Phi}'\rangle\otimes|\psi_\nu(\boldsymbol{\Phi}')\rangle$ within this family, indexed by translations of $\boldsymbol{\Phi} \to \boldsymbol{\Phi}' = \boldsymbol{\Phi} - \boldsymbol{\omega}t$.

In practice, the adiabatic states of the fast subsystem $|\psi_\nu(\boldsymbol{\Phi})\rangle$ are conveniently determined from their adiabatic projector $\pi_\nu(\boldsymbol{\Phi}) = |\psi_\nu(\boldsymbol{\Phi})\rangle\langle\psi_\nu(\boldsymbol{\Phi})|$, similarly to the adiabatic state of a slowly driven system defined from their density matrix in Chap. 1. As in Chap. 1 and 2, we define them perturbatively from the limit of infinitely slow subsystem. In this model of rotors, this limit is simply reached by rescaling the frequencies $\boldsymbol{\omega}$ by a dimensionless factor $\lambda$, such that the limit $\lambda \to 0$ corresponds to the limit of infinitely slow quantum modes, and the limit $\lambda \to 1$ to our problem of interest. $\pi_\nu(\boldsymbol{\Phi})$ is defined as a series in $\lambda$: $\pi_\nu(\boldsymbol{\Phi}) = \sum_k \lambda^k \pi_{\nu,k}(\boldsymbol{\Phi})$. Stability of each family of adiabatic states under the dynamics amounts to impose the condition

$$U(t;\boldsymbol{\Phi};\lambda)\pi_\nu(\boldsymbol{\Phi})U(t;\boldsymbol{\Phi};\lambda)^\dagger = \pi_\nu(\boldsymbol{\Phi}-\lambda\boldsymbol{\omega}t)\,, \tag{5.9}$$

where the evolution operator $U(t;\boldsymbol{\Phi};\lambda)$ is defined in (5.8) replacing $\boldsymbol{\omega}$ by $\lambda\boldsymbol{\omega}$. Solving order by order in $\lambda$ for this equation, together with the constituting property of a projector $\pi_\nu^2(\boldsymbol{\Phi}) = \pi_\nu(\boldsymbol{\Phi})$, leads to the solution at order 0: $\pi_{\nu,0}(\boldsymbol{\Phi}) = |\psi_{\nu,0}(\boldsymbol{\Phi})\rangle\langle\psi_{\nu,0}(\boldsymbol{\Phi})|$ and to first order

$$\pi_{\nu,1}(\boldsymbol{\Phi}) = \sum_{\mu\neq\nu} |\psi_{\mu,0}(\boldsymbol{\Phi})\rangle \frac{\sum_i \hbar\omega_i A_{\mu\nu,i,0}(\boldsymbol{\Phi})}{E_{\mu,0}(\boldsymbol{\Phi}) - E_{\nu,0}(\boldsymbol{\Phi})} \langle\psi_{\nu,0}(\boldsymbol{\Phi})| + \text{h.c.} \tag{5.10}$$

with $A_{\mu\nu,i,0}(\boldsymbol{\Phi}) = i\,\langle\psi_{\mu,0}(\boldsymbol{\Phi})|\partial_{\phi_i}\psi_{\nu,0}(\boldsymbol{\Phi})\rangle$ the components of the non-abelian Berry connection of the eigenstates, and $E_{\pm,0}(\boldsymbol{\Phi}) = \pm|\boldsymbol{h}(\boldsymbol{\Phi})|$ the eigenenergies, similarly to the derivation of Chap. 1.

### Adiabatic grading of the Hilbert space

The above adiabatic decomposition of the qubit states allows for a natural decomposition of all states of the qubit-modes system. We proceed by extending the adiabatic projector

of the qubit $\pi_\nu(\mathbf{\Phi})$ to the adiabatic projector acting on the Hilbert space of the whole system

$$\hat{\Pi}_\nu = \int \mathrm{d}\mathbf{\Phi} \;\; |\mathbf{\Phi}\rangle\langle\mathbf{\Phi}| \otimes \pi_\nu(\mathbf{\Phi}) \;\; , \;\; \nu = \pm \; . \tag{5.11}$$

This projector provides a decomposition of any qubit-mode state $|\Psi\rangle$ into two adiabatic states

$$|\Psi\rangle = |\Psi_-\rangle + |\Psi_+\rangle \;\; , \;\; |\Psi_\nu\rangle = \hat{P}_\nu |\Psi\rangle \;\; , \;\; \nu = \pm \; . \tag{5.12}$$

For a separable initial state (5.4), each adiabatic component $|\Psi_\nu\rangle$ is characterized by a wave amplitude $\chi_\nu(\mathbf{\Phi})$ according to

$$|\Psi_\nu\rangle = \int \mathrm{d}^2\mathbf{\Phi} \;\; \chi_\nu(\mathbf{\Phi}) \, |\mathbf{\Phi}\rangle \otimes |\psi_\nu(\mathbf{\Phi})\rangle \;\; , \tag{5.13}$$

$$\chi_\nu(\mathbf{\Phi}) = \chi(\mathbf{\Phi}) \, \langle\psi_\nu(\mathbf{\Phi})|\psi_q\rangle \;\; . \tag{5.14}$$

with $\chi(\mathbf{\Phi}) = \langle\phi_1|\chi_1\rangle \, \langle\phi_2|\chi_2\rangle$ the wavefunction of the modes in the initial state (5.4). This splits the total Hilbert space $\mathcal{H}_{\rm tot}$ in two adiabatic subspaces $\mathcal{H}_{\rm tot} = \mathcal{H}_- \oplus \mathcal{H}_+$, where $\mathcal{H}_-$ and $\mathcal{H}_+$ are respectively the images of the projectors $\hat{\Pi}_-$ and $\hat{\Pi}_+$.

### Topology of the family of adiabatic states

The ensemble of adiabatic states $|\psi_\nu(\mathbf{\Phi})\rangle$ parametrized by the classical configuration space $\mathbf{\Phi} \in [0, 2\pi]^2$ defines a vector bundle, the adiabatic bundle. This vector bundle is a smooth deformation parametrized of the eigenstates bundle $|\psi_{\nu,0}(\mathbf{\Phi})\rangle$ associated to a spectral projector (Fig. 5.1(a)).

As a consequence, the local curvature associated with the adiabatic bundle

$$F_\nu(\mathbf{\Phi}) = i \, \langle\partial_{\phi_1}\psi_\nu(\mathbf{\Phi})|\partial_{\phi_2}\psi_\nu(\mathbf{\Phi})\rangle - (1 \leftrightarrow 2), \tag{5.15}$$

differs from the canonical Berry curvature associated with the eigenstates bundle [64]. The curvature (5.15) generalizes the Berry curvature to all orders in the adiabatic parameter $\lambda$, in a similar way that the Aharonov-Anandan phase [202] generalizes the Berry phase.

On the other hand, the Chern number $\mathcal{C}_\nu$ of both bundles are identical. Indeed, the switching on of finite but small frequencies $\omega_1$ and $\omega_2$ is a smooth transformation of the fiber bundle of the eigenstates $|\psi_{\nu,0}(\mathbf{\Phi})\rangle$ to that of the adiabatic states $|\psi_\nu(\mathbf{\Phi})\rangle$. Such a smooth transformation does not change the bundle topology. This fails for larger frequencies comparable with the spectral gap. In other words, the perturbative variable $\lambda \in [0, 1]$ defines a smooth transformation between the eigenstate bundle and the adiabatic bundle. As such, they are topologically equivalent and share the same Chern number.

The decomposition of the total Hilbert space is not a spectral decomposition of the total Hamiltonian. It cannot be deduced from a measure on the two-level system alone, since for a topologically non-trivial decomposition of states $|\psi_\pm(\mathbf{\Phi})\rangle$, any qubit state corresponds either to a state $|\psi_-(\mathbf{\Phi})\rangle$ of the ground bundle or to a state $|\psi_+(\mathbf{\Phi}')\rangle$ in its complementary bundle depending on the states $\mathbf{\Phi}$ and $\mathbf{\Phi}'$ of the modes.

### Non-adiabatic Landau-Zener transitions

The adiabatic splitting of the Hilbert space is defined perturbatively in the perturbative variable $\lambda$ by the stability condition (5.9). As discussed in the first two chapters, this

stability is valid up to non-perturbative effects with typical exponential dependence of the form $\exp(-\alpha/\lambda)$. The adiabatic dynamics is the effective dynamics on each subspace, and the non-perturbative transitions between the two subspaces are Landau-Zener transitions. The amplitude of the Landau-Zener transitions can be estimated to obtain the time of validity of the adiabatic approximation as presented in Sec. 1.2.5, $\tau_{\text{adiab}} \approx 0.1 \exp(\pi/(4\varepsilon_{\text{adiab}}))T_1$, with $\varepsilon_{\text{adiab}} = \max_{\boldsymbol{\Phi}} \hbar |\langle\psi_{+,0}| \frac{\mathrm{d}H}{\mathrm{d}t} |\psi_{-,0}\rangle| / (E_{+,0} - E_{-,0})^2$. In this work, we choose the coupling and the frequencies of the modes such that $\tau_{\text{adiab}} \approx 3100 T_1$, allowing to neglect such Landau-Zener transitions. Within this approximation the weight on each adiabatic subspace

$$W_\nu(\Psi) = ||\hat{\Pi}_\nu |\Psi\rangle||^2 = \langle\Psi_\nu|\Psi_\nu\rangle \tag{5.16}$$

is a conserved quantity.

#### Comment on the linearity in number of quanta

In terms of slow-fast quantum system, the specificity of the rotor model is the linearity of the total Hamiltonian in $\hat{\boldsymbol{N}}$, and the coupling of the fast subsystem – the qubit – only to its conjugated variable $\hat{\boldsymbol{\Phi}}$. This property is at the origin of the decomposition (5.11) of the adiabatic projector in phase representation: $\hat{\Pi}_\nu$ is written only in terms of the phase operators of the modes $\hat{\Pi}_\nu = \Pi_\nu(\hat{\boldsymbol{\Phi}})$. This enables us to define adiabatic states of the fast subsystem $|\psi_\nu(\boldsymbol{\Phi})\rangle$ depending only on the value of the phases $\boldsymbol{\Phi}$ of the slow subsystem.

For other models which are not linear in $\boldsymbol{N}$, for example if quadratic terms proportional to $\hat{n}_i^2$ are added to the total Hamiltonian, we can show that the adiabatic projector at all orders $\hat{\Pi}_\nu$ is written also in terms of $\hat{\boldsymbol{N}}$. Projected states then have the form $\int \mathrm{d}^2\boldsymbol{\Phi}\ f(\boldsymbol{\Phi}) |\boldsymbol{\Phi}\rangle \otimes |\psi_{\nu,f}(\boldsymbol{\Phi})\rangle$ with states of the qubit $|\psi_{\nu,f}(\boldsymbol{\Phi})\rangle$ depending both on the value of the phase $\boldsymbol{\Phi}$ and on the derivatives of the envelope function $f(\boldsymbol{\Phi})$ (which is related to the value of $\boldsymbol{N}$). This is natural: the adiabatic states of the fast subsystem depend on both conjugated variables of the slow subsystem. The use of a phase-space representation, such as the Wigner-Weyl representation, may be more suited to study this particular situation.

However, for initial states such that the matrix elements of the linear term of the Hamiltonian $\hbar\boldsymbol{\omega} \cdot \hat{\boldsymbol{N}}$ are dominant over the non-linear terms, we expect Eq. (5.11) to be a very good estimate of the adiabatic projector defined in Sec. 2.4 of Chap. 2. The rotor model is a model from which we can characterize quantitatively many aspects of the dynamics which are expected to remain present in realistic situations. Such terms quadratic in the slow variables are natural in the Born-Oppenheimer context, corresponding to the kinetic energy of the nuclei. If $\boldsymbol{\Phi}$ and $\boldsymbol{N}$ correspond respectively to superconducting phases and number of Cooper pairs of superconducting leads, capacitive elements are also associated to quadratic Hamiltonian in $n_i$. The characterization of the adiabatic states in situations where they are significant goes beyond the scope of this thesis.

### 5.2.2 Topological splitting of adiabatic components

In this section, we show that the topological dynamics splits in energy the two adiabatic components, thereby creating an adiabatic cat state.

### Equation of motion

The energy function $E_\nu(\mathbf{\Phi}) = \langle\psi_\nu(\mathbf{\Phi})|\, H(\mathbf{\Phi})\, |\psi_\nu(\mathbf{\Phi})\rangle$ as well as the curvature (5.15) govern the adiabatic dynamics of the slow modes. Using the Ehrenfest theorem, for each adiabatic component of the initial state, we get

$$\frac{\mathrm{d}}{\mathrm{d}t}\langle\hat{n}_1\rangle_{\Psi_\nu(t)} = \int \mathrm{d}^2\mathbf{\Phi}\ \frac{|\chi_\nu(\mathbf{\Phi})|^2}{W_\nu(\Psi)}\, \langle\psi_\nu(\mathbf{\Phi}-\boldsymbol{\omega}t)|\, \frac{1}{\hbar}\frac{\partial H}{\partial\phi_1}\, |\psi_\nu(\mathbf{\Phi}-\boldsymbol{\omega}t)\rangle \tag{5.17}$$

$$= \int \mathrm{d}^2\mathbf{\Phi}\ \frac{|\chi_\nu(\mathbf{\Phi})|^2}{W_\nu(\Psi)} \left(\frac{1}{\hbar}\frac{\partial E_\nu}{\partial\phi_1}(\mathbf{\Phi}-\boldsymbol{\omega}t) + \omega_2 F_\nu(\mathbf{\Phi}-\boldsymbol{\omega}t)\right). \tag{5.18}$$

A similar relation obtained by the exchange $1 \leftrightarrow 2$ holds for the second mode. See appendix 5.D for details. This expression differs by two aspects from the first order average power transfer obtained within a classical-quantum description [44, 56] described in Chap. 3.

First, the instantaneous rate in parentheses is averaged by the normalized phase wavepacket density $|\chi_\nu(\mathbf{\Phi})|^2/W_\nu(\Psi)$ of the adiabatic component. The phase density plays the role of density probability of the initial phase, due to its quantum fluctuations. The linearity in $\hat{\boldsymbol{N}}$ of the rotor model induces a non-dispersive evolution of the phase, such that, during time evolution, the phase density is just translated on the torus $[0, 2\pi]^2$. Second, at all orders in adiabatic theory, the equation of motion takes a similar form as the first order theory of Chap. 3 and Chap. 2, obtained by replacing respectively the eigenenergy and Berry curvature by the adiabatic energy and dressed Berry curvature. The geometric details of the dynamics changes, but the topological drift is the same, as discussed below.

### Topological splitting

As in the case of a hybrid classical-quantum description of a topological pump [44, 56] of Chap. 3 and Chap. 4, we assume an incommensurate ratio between the frequencies $\omega_1$ and $\omega_2$ such that a time average of the rate of change (5.18) reduces by ergodicity to an average over the phases $\mathbf{\Phi} \in [0, 2\pi]^2$. The average of the derivative of the energy in Eq. (5.18) vanishes by periodicity, while the average of the adiabatic curvature $F_\nu(\mathbf{\Phi})$ is quantized by the first Chern number $\mathcal{C}_\nu$ of the vector bundle of adiabatic states $|\psi_\nu(\mathbf{\Phi})\rangle$. The topological coupling between the modes and the qubit corresponds to two non-vanishing Chern numbers $\mathcal{C}_+ = -\mathcal{C}_-$. In this situation, we recover a topological pumping or topological frequency conversion between the two modes. In terms of the rotated coordinates of Eq. (5.6,5.7), the topological pumping corresponds to opposite evolutions of $n_\perp$ for the two adiabatic components $|\Psi_\pm\rangle$:

$$\langle\hat{n}_\perp\rangle_{\Psi_\pm(t)} = \langle\hat{n}_\perp\rangle_{\Psi_\pm(0)} \mp \frac{|\boldsymbol{\omega}|t}{2\pi}\mathcal{C}_- + \delta n_\perp(t), \tag{5.19}$$

where $\delta n_\perp(t)$ denotes bounded oscillations, the temporal fluctuations of pumping, discussed in Sec. 5.3.2.

As a result, the topological dynamics splits in energy the two adiabatic components of the initial state from each other. A cat state is created when the two adiabatic components no longer overlap. We note $\Delta n_\perp^{\max}$ the maximal spread in $n_\perp$ developed during

the dynamics, which is discussed in section 5.3.2. The time of separation of the two cat components reads

$$t_{\rm sep} \approx \frac{2\pi}{|\boldsymbol{\omega}|\mathcal{C}} \Delta n_\perp^{\max} \tag{5.20}$$

with $\mathcal{C} = |\mathcal{C}_\pm|$. After $t_{\rm sep}$, the weight of the state on the region $n_\perp < n_\perp^0$ identifies with the adiabatic weight $W_-(\Psi)$.

### 5.2.3 Weight of the adiabatic cat state

In this section, we focus on the weight $W_\nu(\Psi)$ (5.16) of each component of the cat state. This will allow us to show that the dynamical splitting into a cat state is generic, and to identify the conditions on the initial states to realize ideal adiabatic cat states with equal weights $W_+(\Psi) = W_-(\Psi)$.

We can represent the states $|\psi_\nu(\boldsymbol{\Phi})\rangle$ and $|\psi_q\rangle$ by vectors on the Bloch sphere, respectively $\boldsymbol{b}_\nu(\boldsymbol{\Phi})$ and $\boldsymbol{Q}$, see Fig. 5.3(a). The qubit's state representation $\boldsymbol{Q}$ is parametrized by the angle $\theta_q$ with the $z$-axis and its azimuthal angle $\varphi_q$. In this section, we focus without loss of generality on $\varphi_q = 0$, *i.e.* on $\boldsymbol{Q}$ lying in the $xz$ plane, and on the mode prepared in a Gaussian state centered on $\phi_1^0 = \phi_2^0 = 0$. The adiabatic states are obtained in a perturbative expansion around the eigenstates $|\psi_{\nu,0}(\boldsymbol{\Phi})\rangle$. Hence, they are represented by $\boldsymbol{b}_\nu(\boldsymbol{\Phi})$ which is perturbatively close to $\boldsymbol{b}_{\nu,0}(\boldsymbol{\Phi})$.

#### General expression of the weights

The phase states in the decomposition (5.13) being orthogonal, the weight $W_\nu(\Psi)$, $\nu = \pm$ is the weight of the wave amplitude $\chi_\nu(\boldsymbol{\Phi}) = \chi(\boldsymbol{\Phi})\,\langle\psi_\nu(\boldsymbol{\Phi})|\psi_q\rangle$:

$$W_\nu(\Psi) = \int \mathrm{d}^2\boldsymbol{\Phi}\ |\chi_\nu(\boldsymbol{\Phi})|^2. \tag{5.21}$$

The overlap between $|\psi_\nu(\boldsymbol{\Phi})\rangle$ and $|\psi_q\rangle$ is $|\,\langle\psi_\nu(\boldsymbol{\Phi})|\psi_q\rangle\,|^2 = (1+\boldsymbol{b}_\nu(\boldsymbol{\Phi})\cdot\boldsymbol{Q})/2$ such that the weight (5.21) now reads

$$W_\nu(\Psi) = \frac{1}{2}\left(1 + \bar{\boldsymbol{b}}_\nu \cdot \boldsymbol{Q}\right)\ ,\ \nu = \pm, \tag{5.22}$$

with

$$\bar{\boldsymbol{b}}_\nu = \int \mathrm{d}^2\boldsymbol{\Phi}\ |\chi(\boldsymbol{\Phi})|^2\ \boldsymbol{b}_\nu(\boldsymbol{\Phi}) \tag{5.23}$$

the statistical average of the adiabatic states with respect to the initial phase distribution $|\chi(\boldsymbol{\Phi})|^2$. The phase density $|\chi(\boldsymbol{\Phi})|^2$ on the torus translates via the map $\boldsymbol{\Phi} \mapsto \boldsymbol{b}_\nu(\boldsymbol{\Phi})$ to a density of adiabatic states on the Bloch sphere. $\bar{\boldsymbol{b}}_\nu$ is the average of this density. We represent the density associated to the ground state $\boldsymbol{b}_{-,0}(\boldsymbol{\Phi})$ in colored density plot on Fig. 5.3(b) as well as the average ground state $\bar{\boldsymbol{b}}_{-,0}$ for four widths $\Delta\phi = \Delta\phi_1 = \Delta\phi_2$. $\bar{\boldsymbol{b}}_-$ is perturbatively close to $\bar{\boldsymbol{b}}_{-,0}$.

For small $\Delta\phi$, the phase density is localized around $\boldsymbol{\Phi}^0$ and $\bar{\boldsymbol{b}}_\nu \approx \boldsymbol{b}_\nu(\boldsymbol{\Phi}^0)$ close to the surface of the Bloch sphere. When increasing the width $\Delta\phi$, we average vectors over an increasing support on the Bloch sphere, reducing the norm $|\bar{\boldsymbol{b}}_\pm|$ which controls the minimum weight of the cat (Fig. 5.3(d)). For the chosen value $\phi_1^0 = \phi_2^0 = 0$, $\bar{\boldsymbol{b}}_{-,0}$ lies on the $z$-axis as inferred from (5.3). In the extreme case of $\Delta\phi = \pi$ (Fock state), the

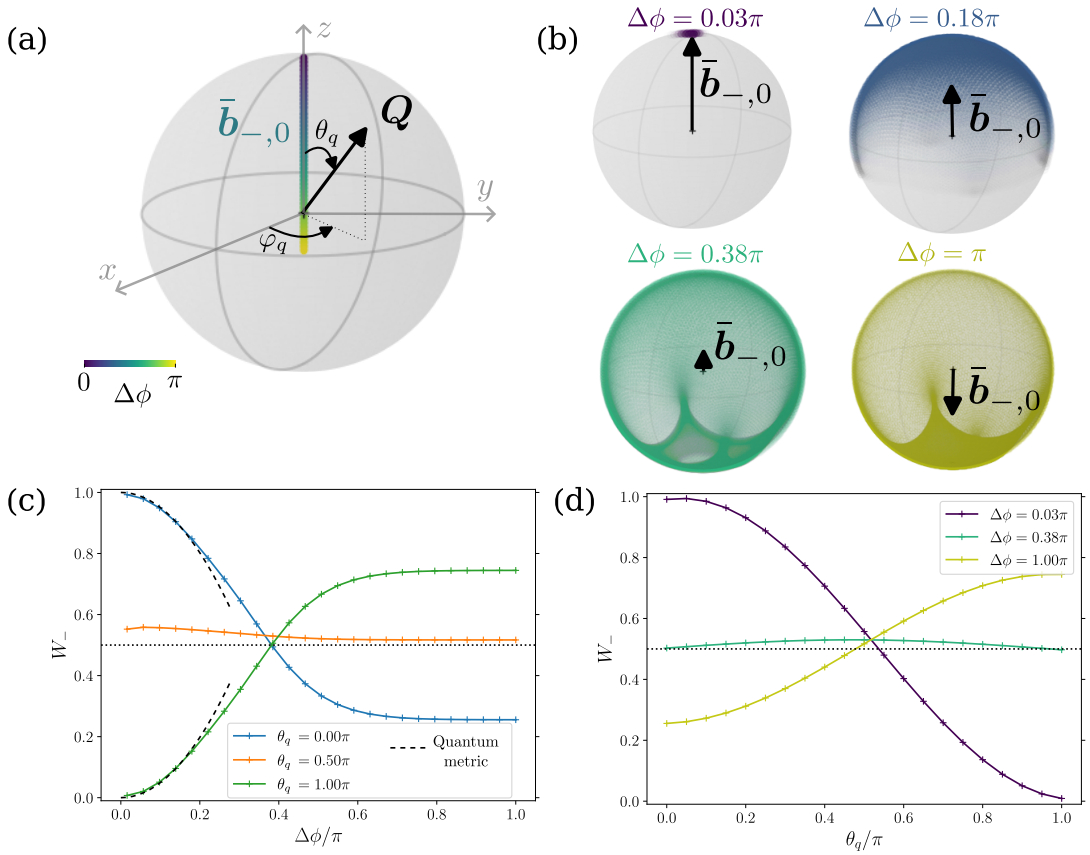


Figure 5.3: Weight $W_-$ of the adiabatic states superposition. The modes are in a Gaussian state centered on $\phi_1^0 = \phi_2^0 = 0$. We vary the width $\Delta\phi$ of the Gaussian state and the qubit initial state $|\psi_q\rangle$ represented by its polarization $\boldsymbol{Q}$ on the Bloch sphere. (a) Averaged ground state $\bar{\boldsymbol{b}}_{-,0}$, lying on the $z$-axis. The average adiabatic state $\bar{\boldsymbol{b}}_-$ is perturbatively close to $\bar{\boldsymbol{b}}_{-,0}$. (b) The phase density $|\chi(\boldsymbol{\Phi})|^2$ on the torus translates via the map $\boldsymbol{\Phi} \mapsto \boldsymbol{b}_-(\boldsymbol{\Phi})$ to a density of adiabatic states on the Bloch sphere represented in color for different $\Delta\phi$. $\bar{\boldsymbol{b}}_-$ is the average of this density. (c) Weight of the cat depending on the width in phase $\Delta\phi$. The average Bloch vector remains approximately on the z-axis, such that a cat with $W_- = \frac{1}{2}$ is obtained for the qubit on the equator $\theta_q = \pi/2$. The deviation from $W_- = 1/2$ at $\theta_q = \pi/2$ is due to the difference between the eigenstates and the adiabatic states. In the limit of small $\Delta\phi$ for $|\psi_q\rangle = |\psi_-(\boldsymbol{\Phi}^0)\rangle$ ($\theta_q = 0$) and $|\psi_q\rangle = |\psi_+(\boldsymbol{\Phi}^0)\rangle$ ($\theta_q = \pi$) the weight of adiabaticity is controlled by the quantum metric $g_{-,ij}(\boldsymbol{\Phi}^0)$ of the adiabatic states. (d) Weight of the cat depending on the initial state of the qubit, varying $\theta_q$ at $\varphi_q = 0$. The norm of the average adiabatic state defines the bounds $(1 \pm |\bar{\boldsymbol{b}}_-|)/2$ of the weight. For $\Delta\phi = 0.38\pi$, $|\bar{\boldsymbol{b}}_\pm| \simeq 0$ such that a cat with almost equal weight is created independently of the initial state of the qubit.

density is homogeneous on the torus. However, while $\boldsymbol{b}_\pm(\boldsymbol{\Phi})$ covers the whole sphere, the associated density is not homogeneous due to the anisotropy of the couplings (5.3). This leads to a non-vanishing $\bar{\boldsymbol{b}}_-$.

### Symmetric cat states

Following the analysis above, we can identify two types of initial states that give rise to symmetric cat states with $W_+ = W_- = \frac{1}{2}$. The first class is obtained by preparing the qubit orthogonally to this average adiabatic state $\bar{\boldsymbol{b}}_\pm$. For our initial phase $\boldsymbol{\Phi}^0$, this average adiabatic state is perturbatively closed to the $z$-axis as discussed above. Hence, a qubit prepared on the equator of the Bloch sphere corresponds to two almost equal weights for all $\Delta\phi$. This corresponds to the choice made for Fig. 5.2. This case is represented by the orange curve on Fig. 5.3(c). The adiabatic weight is computed numerically from the topological splitting of the adiabatic components discussed in the previous section. The deviation to $W_- = 1/2$ originates from the difference between the eigenstates and the adiabatic states, see appendix 5.G for details. The second class of symmetric cat states is obtained for well-chosen gaussian states of the modes: the weight (5.22) of the cat is bounded by $(1 + |\bar{\boldsymbol{b}}_\pm|)/2$. For $\Delta\phi = 0.38\pi$, $\bar{\boldsymbol{b}}_\pm \simeq 0$ such that the cat has (almost equal) weights $W_+ = W_-$ independently of the initial state of the qubit $\theta_q$ (Fig. 5.3(d) green curve).

### Quasi phase states

The only separable states lying in an adiabatic subspace, corresponding to $W_+ = 1$ or $W_- = 1$, are pure phase states $|\boldsymbol{\Phi}^0\rangle \otimes |\psi_\pm(\boldsymbol{\Phi}^0)\rangle$ for which $|\bar{\boldsymbol{b}}_\pm| = 1$, shown as the blue and green curves of Fig. 5.3(c) in the $\Delta\phi = 0$ limit. Given that these states are fully delocalized in quanta number $\boldsymbol{N}$, and thus in energy according to (5.2), we expect them to be hard to realize. Any other separable state lies at a finite distance from each adiabatic subspace and will be split into a cat state under time evolution. Let us comment on this adiabatic decomposition for almost pure phase states with small $\Delta\phi$. In this case, the correction to adiabaticity is controlled by the quantum metric $g_{\pm,ij}$ of the adiabatic states [80, 203]:

$$g_{\pm,ij} = \mathrm{Re}\,\langle \partial_{\phi_i}\psi_\pm|\,(1 - |\psi_\pm\rangle\langle\psi_\pm|)\,\big|\partial_{\phi_j}\psi_\pm\big\rangle\,. \tag{5.24}$$

Indeed, the weight (5.21) is dominated by the local variations of the adiabatic states $|\psi_\pm(\boldsymbol{\Phi})\rangle$ over the narrow phase support $|\chi(\boldsymbol{\Phi})|^2$. These variations are encoded by the quantum metric: $|\langle\psi_\pm(\boldsymbol{\Phi}^0 + \delta\boldsymbol{\Phi})|\psi_\pm(\boldsymbol{\Phi}^0)\rangle|^2 = 1 - \sum_{i,j} g_{\pm,ij}(\boldsymbol{\Phi}^0)\delta\phi_i\delta\phi_j + \mathcal{O}(\delta\phi^3)$. In the limit of a small width $(\Delta\phi_1, \Delta\phi_2)$ the weight (5.21) for $|\psi_q\rangle = |\psi_\pm(\boldsymbol{\Phi}^0)\rangle$ reduces to

$$W_\pm(\Psi) = 1 - (\Delta\phi_1)^2 g_{\pm,11}(\boldsymbol{\Phi}^0) - (\Delta\phi_2)^2 g_{\pm,22}(\boldsymbol{\Phi}^0) + \mathcal{O}(\Delta\phi^4). \tag{5.25}$$

Hence for a state close to a phase state, the first correction to $W_\nu$ is quadratic in $\Delta\phi = 1/(2\Delta n)$ with a factor set by the quantum metric of the adiabatic states, as shown in black dashed line on Fig. 5.3(c).

## 5.3 Characterization of cat components

Having characterized the balance between the two components of an adiabatic cat state, we now study the dynamics of each component. We will focus first on the entanglement

between the qubit and the two modes, before focusing on their Bloch oscillatory dynamics in the number of quanta representation.

### 5.3.1 Entanglement

Adiabatic states naturally entangle the fast qubit with the slow driving modes, a phenomenon out-of-reach of previous Floquet or classical descriptions of the drives [44, 45, 47, 48, 51–53, 56]. We focus on cat states with almost equal weight $W_\nu \simeq 1/2$, obtained with $\mathbf{\Phi}^0 = 0$ and $\theta_q = \pi/2$ following the analysis of section 5.2.3. In the following, we study the entanglement of the qubit with the modes for the different types of cat states, varying the initial spread $\Delta\phi$ of the modes and the initial azimuthal angle $\varphi_q$ of the qubit.

The entanglement between the qubit and the two modes in an adiabatic component $|\Psi_\nu(t)\rangle$, $\nu = \pm$, is captured by the purity $\gamma_\nu(t) = \mathrm{Tr}\big(\rho_{q,\nu}^2(t)\big) = (1 + |\boldsymbol{Q}_\nu(t)|^2)/2$ of the qubit, where $\rho_{q,\nu}(t)$ is the reduced density matrix of the qubit and $\boldsymbol{Q}_\nu(t)$ its polarization. From the adiabatic time evolution (5.9), we deduce the reduced density matrix $\rho_{q,\nu}(t)$ of the qubit in the adiabatic state $|\Psi_\nu(t)\rangle$ as

$$\rho_{q,\nu}(t) = \int \mathrm{d}^2\mathbf{\Phi}\ \frac{|\chi_\nu(\mathbf{\Phi} + \boldsymbol{\omega}t)|^2}{W_\nu} |\psi_\nu(\mathbf{\Phi})\rangle \langle\psi_\nu(\mathbf{\Phi})| \tag{5.26}$$

$$= \frac{1}{2}(\mathbf{1} + \boldsymbol{Q}_\nu(t) \cdot \boldsymbol{\sigma}), \tag{5.27}$$

where the polarization of the qubit $\boldsymbol{Q}_\nu(t)$ reads

$$\boldsymbol{Q}_\nu(t) = \int \mathrm{d}^2\mathbf{\Phi}\ \frac{|\chi_\nu(\mathbf{\Phi} + \boldsymbol{\omega}t)|^2}{W_\nu} \boldsymbol{b}_\nu(\mathbf{\Phi}). \tag{5.28}$$

The qubit is in the statistical mixture of the adiabatic states $|\psi_\nu(\mathbf{\Phi})\rangle$ weighted by the translated normalized phase density $|\chi_\nu(\mathbf{\Phi} + \boldsymbol{\omega}t)|^2/W_\nu$.

#### Entanglement of quasi-phase states.

Let us first focus on the adiabatic component of a cat obtained from a quasi-phase state of small $\Delta\phi$. We show below that entanglement between the qubit and the quantum modes of such a state is set by the quantum metric of the adiabatic states.

The translated phase density $|\chi(\mathbf{\Phi} + \boldsymbol{\omega}t)|^2$ of the modes is a normalized $2\pi$-periodic Gaussian centered on $\mathbf{\Phi}^0 - \boldsymbol{\omega}t$ and of width $(\Delta\phi_1, \Delta\phi_2)$. Plugging expansions of Eqs. (5.14) and (5.21), and $\boldsymbol{b}_\nu(\mathbf{\Phi})$ around $\mathbf{\Phi}^0 - \boldsymbol{\omega}t$ in the limit of small $\Delta\phi_1, \Delta\phi_2$ into Eq. (5.28) we get

$$\boldsymbol{Q}_\nu(t) = \boldsymbol{b}_\nu(\mathbf{\Phi}^0 - \boldsymbol{\omega}t) + \frac{1}{2}\sum_i (\Delta\phi_i)^2 \frac{\partial^2 \boldsymbol{b}_\nu}{\partial\phi_i^2}(\mathbf{\Phi}^0 - \boldsymbol{\omega}t) + \mathcal{O}(\Delta\phi^4). \tag{5.29}$$

Note that in the limit $\Delta\phi_1 = \Delta\phi_2 = 0$ of the classical description of the phase, we recover that the qubit follows the instantaneous adiabatic state $\boldsymbol{b}_\nu(\mathbf{\Phi}^0 - \boldsymbol{\omega}t)$. From the normalization of the adiabatic states $|\boldsymbol{b}_\nu|^2 = 1$, we deduce the relation $\boldsymbol{b}_\nu \cdot \partial_{\phi_i}^2 \boldsymbol{b}_\nu = -\partial_{\phi_i}\boldsymbol{b}_\nu \cdot \partial_{\phi_i}\boldsymbol{b}_\nu = -4g_{\nu,ii}$ where the last equation is an expression of the quantum metric of a two-level system in terms of the Bloch vectors [204, 205]. From this, we unveil the role

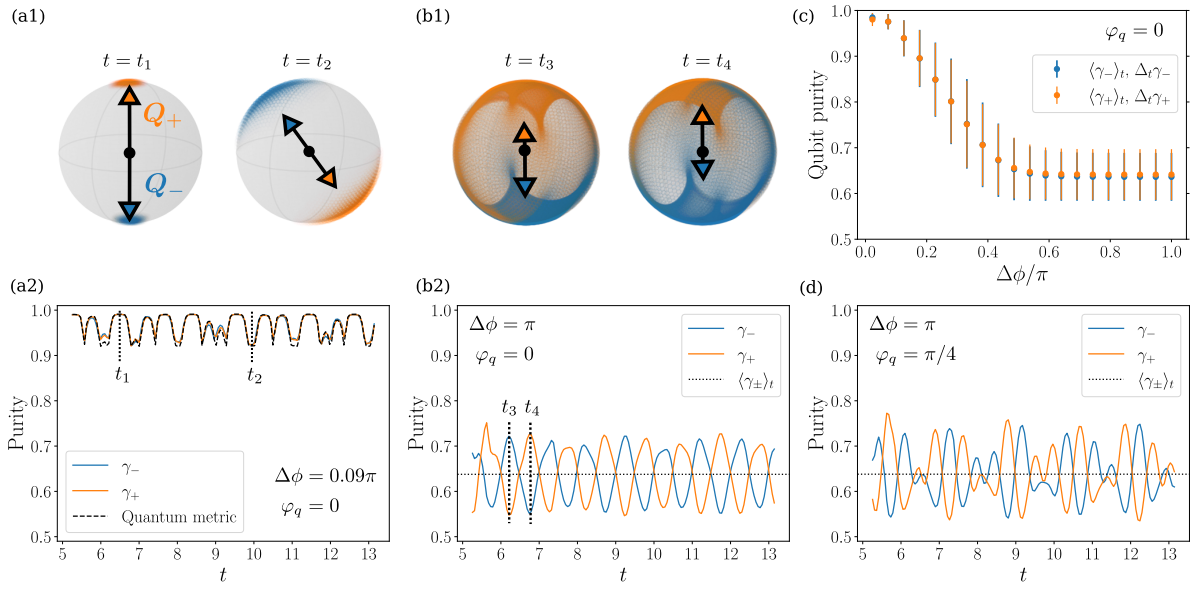


Figure 5.4: Purity of the qubit $\gamma_+(t)$ and $\gamma_-(t)$ in each cat components $|\Psi_+(t)\rangle$ and $|\Psi_-(t)\rangle$. The qubit is prepared on the equator $\theta_q = \pi/2$ to create a cat of equal weight $W_\pm = 1/2$ for all values of $\Delta\phi$ and $\varphi_q$. (a1), (b1) The phase densities $|\chi_-(\boldsymbol{\Phi} + \boldsymbol{\omega}t)|^2$ and $|\chi_+(\boldsymbol{\Phi} + \boldsymbol{\omega}t)|^2$ of each cat components translate to densities of adiabatic states on the Bloch sphere (respectively in blue and orange). The qubit state is the statistical mixture weighted according to these densities with resulting polarizations $\boldsymbol{Q}_\pm$. (a2) For small $\Delta\phi$, the phase densities are localized around $\boldsymbol{\Phi}^0 - \boldsymbol{\omega}t$. The adiabatic states have small variations around $\boldsymbol{\Phi}^0 - \boldsymbol{\omega}t_1$ and larger variation around $\boldsymbol{\Phi}^0 - \boldsymbol{\omega}t_2$, inducing $\gamma_-(t_1) > \gamma_-(t_2)$. These local variations are quantified by the quantum metric of the adiabatic states. (b2) (d) For large $\Delta\phi$, the adiabatic states cover a large part of the Bloch sphere, corresponding to a high entanglement. The phase densities of the two components have complementary support on the torus, leading to different densities on the Bloch sphere. The purity of each component oscillates in opposite phase around their temporal average (black dotted line). The details of the oscillations depend on the shape of the phase densities which changes with the qubit initial state $\varphi_q$. (c) Time average of the purity and temporal fluctuations (errorbars) depending on $\Delta\phi$. A large support $\Delta\phi$ on the torus translates to a large support on the Bloch sphere due to the topological nature of the coupling, and thus a large entanglement.

of the quantum metric in the entanglement between the qubit and the quantum modes. We obtain the expansion at order $\Delta\phi^2$ of the purity

$$\gamma_\nu(t) = 1 - 2(\Delta\phi_1)^2 g_{\nu,11}(\mathbf{\Phi}^0 - \boldsymbol{\omega} t) - 2(\Delta\phi_2)^2 g_{\nu,22}(\mathbf{\Phi}^0 - \boldsymbol{\omega} t) + \mathcal{O}(\Delta\phi^4). \tag{5.30}$$

For a two level system, the quantum metric of the two levels identifies $g_{+,ij} = g_{-,ij}$ such that the qubit is equally entangled with the modes in each adiabatic component $|\Psi_\pm\rangle$. The topological coupling corresponds to a non-vanishing average Berry curvature $F_\nu$. From the inequality $g_{\nu,11} + g_{\nu,22} \geq |F_\nu|$ originating from the positive semidefiniteness of the quantum geometric tensor [206] we obtain a lower bound on the entanglement between the qubit and the modes:

$$\langle \gamma_\nu \rangle_t \leq 1 - \frac{|\mathcal{C}_-|}{\pi} (\Delta\phi)^2 + \mathcal{O}(\Delta\phi^4). \tag{5.31}$$

This demonstrates that a topological pump necessarily entangles the qubit with the modes, a property only captured by the quantum description provided in this paper.

The statistical average of the adiabatic states is represented on Fig. 5.4(a1) for an initial width of the Gaussian state $\Delta\phi = \Delta\phi_1 = \Delta\phi_2 \simeq 0.09\pi$, corresponding to $\Delta n_1 = \Delta n_2 \simeq 2.6$, with the qubit initialized in $\varphi_q = 0$. At a given time $t$, the densities on the torus of each component $|\chi_\pm(\mathbf{\Phi} + \boldsymbol{\omega} t)|^2 / W_\nu$ is centered on $\mathbf{\Phi}^0 - \boldsymbol{\omega} t$ with the initial width $\Delta\phi$. This translates into complementary densities of adiabatic states on the Bloch sphere (in blue and orange) encoding the statistical mixture of the qubit in $|\Psi_\pm\rangle$. In Fig. 5.4(a2), the purity of the qubit after the time of separation $t_{\rm sep}$ is represented respectively in blue and orange for each component $|\Psi_\pm(t)\rangle$. The temporal fluctuations of this purity follow those of the quantum metric at $\mathbf{\Phi}^0 - \boldsymbol{\omega} t$ represented by a black dashed line, as predicted by Eq. (5.30). As an illustration, we notice that the quantum metric is smaller at time $t_1$ than at $t_2$, manifesting that the evolution of adiabatic states with the phase $\mathbf{\Phi}$ is weaker at $\mathbf{\Phi} = \mathbf{\Phi}^0 - \boldsymbol{\omega} t_1$ than at $\mathbf{\Phi} = \mathbf{\Phi}^0 - \boldsymbol{\omega} t_2$. This translates into a larger purity of the qubit at $t = t_1$ than at $t = t_2$.

### Entanglement of quasi-Fock state

We now consider states with an increasing initial width in phase $\Delta\phi$. The dependence on $\Delta\phi$ of the time averaged qubit purity $\langle \gamma_\pm \rangle_t$ is represented on Fig. 5.4(c) for each adiabatic component. The amplitude of its temporal fluctuations are represented as errorbars. This average purity decreases with $\Delta\phi$, corresponding to an increase of entanglement: the larger the phase support on the torus, the larger the support on the Bloch sphere, and thus the smaller the polarization (5.28). The large support on the Bloch sphere originates from the topological nature of the coupling, which imposes that the adiabatic states $\boldsymbol{b}_\pm(\mathbf{\Phi})$ reaches all points of the Bloch sphere as $\mathbf{\Phi}$ varies. A topologically trivial coupling would lead to a localized distribution of adiabatic states on the Bloch sphere corresponding to an almost pure state of the qubit. This is another manifestation that topological pumping and entanglement between the qubit and the modes are strongly intertwined.

The time average of the purity is the same for the two adiabatic components $\langle \gamma_+ \rangle_t = \langle \gamma_- \rangle_t$ for every $\Delta\phi$. A qualitative explanation is the following. Given (5.28) the purity $\langle \gamma_\pm \rangle_t$ corresponds to an average of adiabatic states with respect to translated phase

distributions. The time average depends only on the extension of the phase density $|\chi_\pm(\mathbf{\Phi})|^2$, which, from (5.14), satisfies

$$|\chi_+(\mathbf{\Phi}+\boldsymbol{\omega}t)|^2+|\chi_-(\mathbf{\Phi}+\boldsymbol{\omega}t)|^2=|\chi(\mathbf{\Phi}+\boldsymbol{\omega}t)|^2. \tag{5.32}$$

Hence, they split the phase density of the total system $|\chi(\mathbf{\Phi}+\boldsymbol{\omega}t)|^2$ in two complementary supports, as illustrated in appendix 5.H. For cat states with equal weight $W_+ = W_-$, according to (5.21) these two supports have equal weight, leading to the same average purity over time.

As discussed above, for quasi phase states the purity of both components fluctuates temporally in phase Fig. 5.4(a2). In the opposite limit of an initial Fock state fully delocalized in phase with $\Delta\phi = \pi$, these two purities fluctuates in phase opposition. This is represented Fig. 5.4(b2) and (d), where the qubit is initialized respectively on $\varphi_q = 0$ and $\varphi_q = \pi/4$. The phase density of the modes is uniform $|\chi(\mathbf{\Phi})|^2 = 1/(2\pi)^2$, such that according to (5.32) the phase density of the two cat components have complementary supports on all the torus $[0, 2\pi]^2$. We represent on Fig 5.4(b1) in blue the density of adiabatic states $\boldsymbol{b}_-(\mathbf{\Phi})$ associated to the support $|\chi_-(\mathbf{\Phi}-\boldsymbol{\omega}t)|^2$ and in orange the density of adiabatic states $\boldsymbol{b}_+(\mathbf{\Phi})$ associated to the support $|\chi_+(\mathbf{\Phi}-\boldsymbol{\omega}t)|^2$. At $t = t_3$, the density $|\chi_+(\mathbf{\Phi}-\boldsymbol{\omega}t_3)|^2$ covers a larger portion of the sphere than the density $|\chi_-(\mathbf{\Phi}-\boldsymbol{\omega}t_3)|^2$, corresponding to $|\boldsymbol{Q}_+(t_3)|^2 < |\boldsymbol{Q}_-(t_3)|^2$ and $\gamma_+(t_3) < \gamma_-(t_3)$ on Fig. 5.4(b2), while the situation is opposite at $t = t_4$. The details of the temporal variations of the purity depend on the details of the shape of the densities $|\chi_\pm(\mathbf{\Phi})|^2$, which depends on the initial state $\varphi_q$ of the qubit. Temporal oscillations for $\varphi_q = \pi/4$ are represented on Fig 5.4(d): the temporal average remains of the same order of magnitude and the temporal fluctuations of the purity of each component remain in phase opposition.

### 5.3.2 Breathing dynamics and Bloch oscillations

We now discuss in more details the oscillations of both the center of mass and of the width in number of each adiabatic component of cat states that manifest themselves on the examples of Fig. 5.2. This dynamics is reminiscent of Bloch oscillations and Bloch breathing [195, 207–209]. As discussed in Sec. 2.2.2 of Chap. 2, Bloch oscillations correspond to temporal oscillations of the center of a wavepacket on a lattice when submitted to an electric field. Bloch breathing corresponds to temporal oscillations of the width of this wavepacket. The nature of these oscillations and breathing depends on the width of the wavepacket's momentum distribution. In our context, the lattice corresponds to the numbers of quanta $\boldsymbol{N} = (n_1, n_2)$. The first term of the Hamiltonian (5.2) is linear in $\boldsymbol{N}$ and plays the role of the coupling to an electric field $\boldsymbol{\omega}$, while the second term corresponds to a spin-orbit coupling as discussed in section 5.1.1. Hence, the dynamics in $\boldsymbol{N}$ representation of the adiabatic components identifies with the Bloch oscillations and breathing in the presence of both a longitudinal electric field and an anomalous transverse topological velocity.

#### Qualitative evolution of an adiabatic component

Two trajectories of the average value of number of quanta $\langle\hat{\boldsymbol{N}}\rangle_{\Psi_\pm(t)}$ are represented on Fig. 5.5(a) and (b) for two widths $\Delta\phi$. The two adiabatic subspaces $\nu = \pm$ are associated

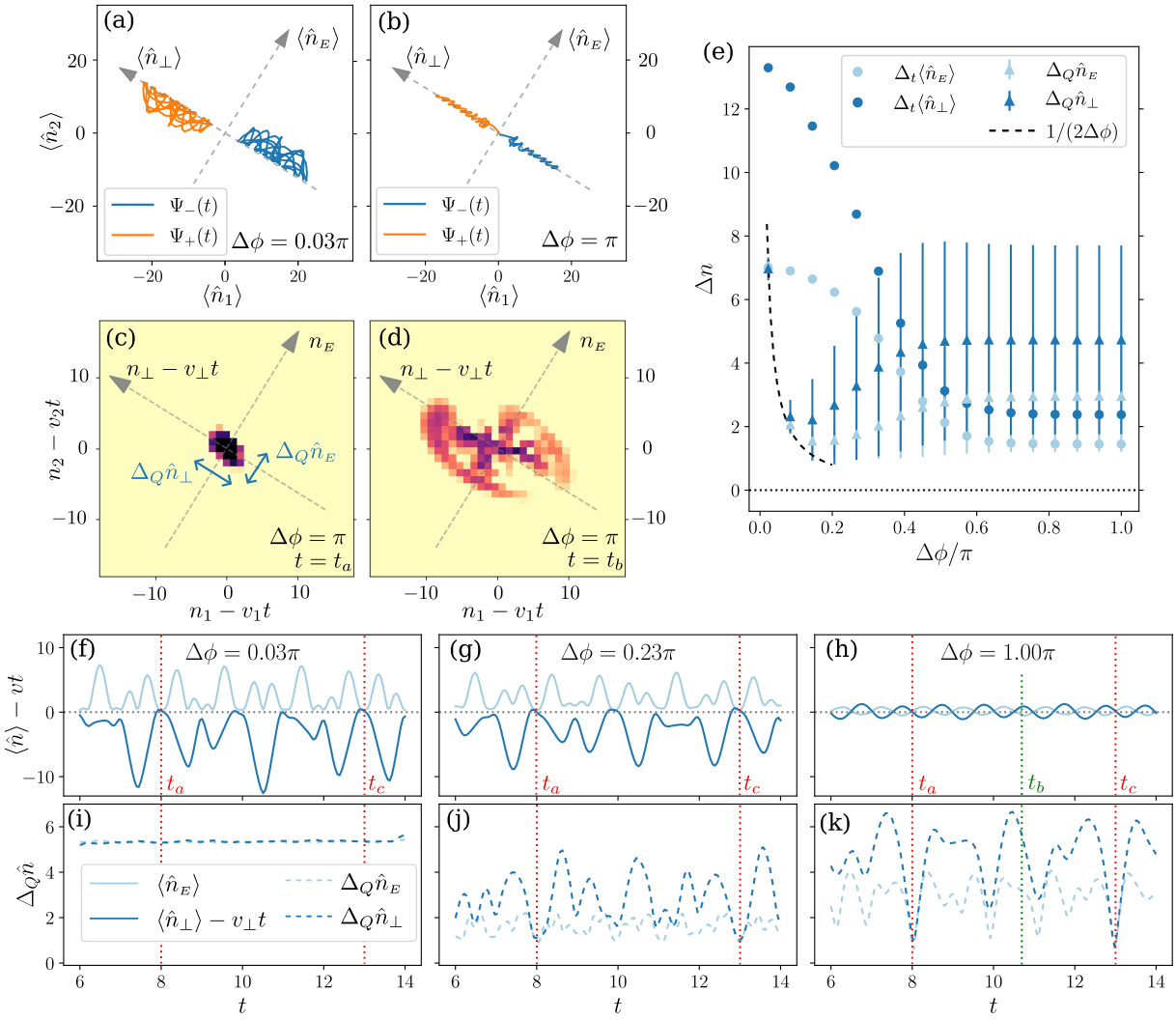


Figure 5.5: From Bloch oscillations to Bloch breathing. (a) Trajectories of the average values of numbers of quanta of each cat component $|\Psi_\pm(t)\rangle$ for the example of Fig. 5.2(a) localized in phase. The two components split along $n_\perp$ at an average velocity $\pm\boldsymbol{v} = \mp(-\omega_2, \omega_1)\mathcal{C}/(2\pi)$. Bloch oscillations are the temporal fluctuations of the average number of quanta around this drift. (b) Trajectories for the initial Fock state of Fig. 5.2(c). The temporal fluctuations are reduced. (c) Photon number distribution of Fig. 5.2(c4) zoomed on the component $|\Psi_-(t)\rangle$ for $t = t_a$ a quasi-period. (d) Photon number distribution of Fig. 5.2(c5) zoomed on the component $|\Psi_-(t)\rangle$ for $t = t_b$ a time of expansion. (e) Circles: amplitude $\Delta_t\langle\hat{n}_E\rangle$ and $\Delta_t\langle\hat{n}_\perp\rangle$ of the Bloch oscillations depending on the width in phase $\Delta\phi$. Triangles: temporal average of the spreading $\Delta_Q\hat{n}_E$ and $\Delta_Q\hat{n}_\perp$, with the amplitude of their temporal fluctuations in errorbar. In small $\Delta\phi$ limit, the spreading is constant, the state remains gaussian with $\Delta_Q\hat{n}_i = 1/(2\Delta\phi)$. When $\Delta\phi$ increases, the amplitude of the Bloch oscillations $\Delta_t\langle\hat{n}_i\rangle$ decreases and the temporal fluctuations of the spreading increase, corresponding to a breathing. (f,g,h) Bloch oscillations. Temporal fluctuations of the average value of number of quanta $\langle\hat{\boldsymbol{N}}\rangle$ in the component $|\Psi_-(t)\rangle$ around the quantized drift $\boldsymbol{v}t$. At quasi-periods $t = t_a$ and $t = t_b$, the evolution is almost given by the quantized drift $\langle\hat{\boldsymbol{N}}\rangle = vt$. The increase of $\Delta\phi$ corresponds to a decrease of the temporal fluctuations. (i) Time evolution of the spreading $\Delta_Q\hat{n}_i$ in the component $|\Psi_-(t)\rangle$ for an initial state localized in phase. The state remains Gaussian with constant spreading $\Delta_Q\hat{n}_i = 1/(2\Delta\phi)$. (j,k) Bloch breathing of the spreading for small $\Delta\phi$. The wavepacket localizes at quasi-periods $t = t_a$ and $t = t_c$, and expands in between ($t = t_b$).

to opposite anomalous velocities $\mp\boldsymbol{v}$ with $\boldsymbol{v} = (\omega_2, -\omega_1)\mathcal{C}_-/(2\pi)$. This induces a drift of the two wavepackets in opposite directions along $n_\perp$, shown on the figure. We highlight the dynamics of the component $|\Psi_-(t)\rangle$ around this drift on Fig. 5.5(c) and (d), the results for $|\Psi_+(t)\rangle$ being similar. In this figure, we note $\langle\hat{n}_i\rangle(t)$ the average values of $\hat{n}_i$ in $|\Psi_-(t)\rangle$ in the rotated coordinates (5.6), $\hat{n}_i$ referring to $\hat{n}_{E}$ or $\hat{n}_\perp$. We denote as $\Delta_Q\hat{n}_i(t) = [\langle\hat{n}_i^2\rangle(t) - \langle\hat{n}_i\rangle(t)^2]^{\frac{1}{2}}$ the quantum fluctuations, or spreading of $\hat{n}_i$ in $|\Psi_-(t)\rangle$ Fig. 5.5(c-d).

The numbers of quanta $\langle\hat{\boldsymbol{N}}\rangle(t)$ have temporal fluctuations around the quantized drift $\boldsymbol{v}t$ represented on Fig. 5.5(f-h) for the three adiabatic cats of Fig. 5.2. When we increase the width $\Delta\phi$ of the initial state, the amplitude $\Delta_t\langle\hat{n}_i\rangle$ of these temporal fluctuations is reduced, while the spreading of the wavepacket $\Delta_Q\hat{n}_i$ increases. For small $\Delta\phi$, $\Delta_Q\hat{n}_i$ is almost constant (Fig. 5.5(i)), the state remains Gaussian with its initial width $\Delta_Q\hat{n}_i = 1/(2\Delta\phi)$ as illustrated on Fig. 5.2(a1-a4). When $\Delta\phi$ increases, $\Delta_Q\hat{n}_i$ oscillates in time 5.5(j-k). This corresponds to breathing: oscillations, such as at $t = t_b$ on Fig. 5.5(d), between relocalization occurring *e.g.* at $t = t_a$ and $t_c$ on Fig. 5.5(c). The corresponding time evolution of the width $\Delta_Q\hat{n}_i$ is represented on Fig. 5.5(i-k).

### Quasi-periods

In Fig. 5.5(j-k), we observe, for a large initial $\Delta\phi$, a relocalization of the wavepacket at specific times such as $t_a$ and $t_c$. These fluctuations in time of the adiabatic wavepacket correspond to two-dimensional Bloch oscillations [207–209]. We first introduce the quasi-periods associated to two-dimensional Bloch oscillations before discussing wavepacket relocalization below.

Historically, Bloch oscillations were first considered in one dimension [102]. The electric field induces a constant increase of the Bloch momenta of a semiclassical wavepacket, which crosses periodically the one dimensional Brillouin zone. As a consequence the average position of the wavepacket oscillates periodically. In two dimensions, Bloch oscillations are richer. The Bloch momenta evolves on the two-dimensional Brillouin zone along the direction of the electric field: $\boldsymbol{\Phi}(t) = \boldsymbol{\Phi}^0 - \boldsymbol{\omega}t$. Such an evolution is periodic for a commensurate ratio between $\omega_1$ and $\omega_2$, corresponding to an electric field in a crystalline direction. Noting $\omega_1/\omega_2 = p_1/p_2$ with $p_1$ and $p_2$ coprime integers, the trajectory of the Bloch momenta on the two-dimensional Brillouin zone is periodic with period $T = p_1 2\pi/\omega_1 = p_2 2\pi/\omega_2$. In practice any real number $\omega_1/\omega_2$ can be approximated by a set of rational numbers [195, 208]. Each rational approximation leads to a quasi period $T$ for which $\boldsymbol{\Phi}^0 - \boldsymbol{\omega}T \simeq \boldsymbol{\Phi}^0$. The times $t_a$ and $t_c$ on Fig. 5.5 are two examples of these quasi-periods for our choice of $\omega_1, \omega_2$.

The periodicity of a trajectory on the Brillouin zone translates into a periodic motion in the direction of the electric field $n_{E}$ but not in the transverse direction $n_\perp$, even in the absence of an anomalous velocity [209, 210]. For an initial phase $\boldsymbol{\Phi}^0$, the classical equations of motion in adiabatic space $\nu$ of the center of the wavepacket, recovered from Eq. (5.18), can be written as

$$n_{E}(t) = \int_0^t \frac{1}{\hbar}\frac{\partial E_\nu}{\partial \phi_{E}}(\boldsymbol{\Phi}(t'))\mathrm{d}t' \ , \tag{5.33}$$

$$n_\perp(t) = \int_0^t \left(\frac{1}{\hbar}\frac{\partial E_\nu}{\partial \phi_\perp}(\boldsymbol{\Phi}(t')) - |\boldsymbol{\omega}|F_\nu(\boldsymbol{\Phi}(t'))\right)\mathrm{d}t', \tag{5.34}$$

where the evolution of the phase reads in the rotated phase coordinates: $\phi_{\scriptscriptstyle E}(t) = \phi^0_{\scriptscriptstyle E} - |\boldsymbol{\omega}|t$ and $\phi_\perp(t) = \phi^0_\perp$. We choose the origin of the number of quanta set by their initial values, such that $n_{\scriptscriptstyle E}(0, \boldsymbol{\Phi}^0) = n_\perp(0, \boldsymbol{\Phi}^0) = 0$. The time integral can be rewritten as a line integral over $\phi_{\scriptscriptstyle E}$, leading to the conservation equation $\hbar|\boldsymbol{\omega}|n_{\scriptscriptstyle E}(t, \boldsymbol{\Phi}^0) = E_\nu(\boldsymbol{\Phi}^0) - E_\nu(\boldsymbol{\Phi}(t))$, which is vanishingly small at a quasi-period $T$ such that $\boldsymbol{\Phi}(T) \simeq \boldsymbol{\Phi}^0$. A quasi-period defines an almost closed trajectory on the torus. The line integral of (5.34) does not vanish on this closed trajectory, and reads $n_\perp(T, \boldsymbol{\Phi}^0) \simeq vT$. The approximation gets better for longer quasi-periods $T$, *i.e.* large $p_1$ and $p_2$.

### Bloch oscillations of the average number of quanta

In the hybrid classical-quantum description of a topological pump [44,56], the topological quantization of the pumping rate is recovered under a time-average of the instantaneous flux of quanta $\dot{n}_i(t)$. This time average of the Berry curvature entering the pumping rate is set by the Chern number of the adiabatic states over the torus $[0, 2\pi]^2$. The quantum nature of the mode induces another source of averaging. The time evolution of the average number of quanta (5.18) corresponds to an average of the classical evolution (5.34) with respect to the phase density $|\chi_\nu(\boldsymbol{\Phi})|^2$ of the adiabatic component. Thus, an increase of the support $|\chi_\nu(\boldsymbol{\Phi})|^2$ reduces the temporal fluctuations of the average number of quanta around its average drift. The quantization of topological pumping is indeed better between quantum than classical modes. This is represented on Fig. 5.5(e). We note $\Delta_t\langle\hat{n}_i\rangle$ the amplitude of the fluctuations with time of the average value of $\langle\hat{n}_i\rangle$. These temporal fluctuations are reduced when $\Delta\phi$ increases (circles on Fig. 5.5(e)).

The reduction of the temporal fluctuations of pumping is set by the width of the phase density $|\chi_\nu(\boldsymbol{\Phi})|^2$. One would expect that a complete delocalization in phase, $|\chi_\nu(\boldsymbol{\Phi})|^2 = 1/(2\pi)^2$, averages instantaneously the classical pumping rate over the whole phase space such that $\langle\hat{\boldsymbol{N}}\rangle(t) \simeq \boldsymbol{v}t$ without any temporal fluctuations. Such a projected state with uniform delocalization in $\boldsymbol{\Phi}$ corresponds to a Wannier state for a particle on a lattice which is topologically obstructed [211–213]. First, let us note that the spreading $\Delta_Q\hat{n}_i$ is infinite in such obstructed Wannier state, making them hard to realize experimentally. Moreover, due to the adiabatic decomposition (5.12) of the initial (separable) state, such adiabatic states are never realized: the phase density $|\chi_\nu(\boldsymbol{\Phi})|^2$, defined in (5.14) contains the density of projection of the qubit initial state $|\langle\psi_\nu(\boldsymbol{\Phi})|\psi_q\rangle|^2$ which necessarily vanishes on the configuration space for a topological pump, irrespective of $|\psi_q\rangle$. A Wannier state cannot be obtained by the adiabatic decomposition of a separable state, and the temporal fluctuations of the pumping remain finite.

### Bloch breathing of the spreading

When the phase density $|\chi_\nu(\boldsymbol{\Phi})|^2$ is localized around $\boldsymbol{\Phi}^0$, the center of mass performs Bloch oscillations following the classical trajectory $\boldsymbol{N}(t, \boldsymbol{\Phi}^0)$ (5.33), (5.34). Intuitively, when the adiabatic state has a large support in phase $|\chi_\nu(\boldsymbol{\Phi})|^2$, the different trajectories $\boldsymbol{N}(t, \boldsymbol{\Phi})$ on this support superpose, inducing a spreading of the wavepacket. The spreading of the wavepacket is then captured by the variance $\mathrm{Var}_{|\chi_\nu|^2}[n_i(t, \boldsymbol{\Phi})]$ of the classical trajectories with respect to the (normalized) initial phase distribution $|\chi_\nu(\boldsymbol{\Phi})|^2/W_\nu$:

$$\mathrm{Var}_{|\chi_\nu|^2}[n_i(t, \boldsymbol{\Phi})] = \int \mathrm{d}^2\boldsymbol{\Phi}\ \frac{|\chi_\nu(\boldsymbol{\Phi})|^2}{W_\nu} n_i(t, \boldsymbol{\Phi})^2 - \left(\int \mathrm{d}^2\boldsymbol{\Phi}\ \frac{|\chi_\nu(\boldsymbol{\Phi})|^2}{W_\nu} n_i(t, \boldsymbol{\Phi})\right)^2 . \tag{5.35}$$

We show in appendix 5.I that the time evolution of the spreading $\Delta_Q \hat{n}_i$ in the adiabatic state $|\Psi_\nu(t)\rangle$ is indeed related to this variance, and is the sum of three different terms.

For a quasi-phase state with a narrow distribution $|\chi_\nu(\mathbf{\Phi})|^2$, the classical trajectories for an initial phase on this support are all similar, such that the variance term (5.35) vanishes. The quantum fluctuations weakly evolve in time $\Delta_Q \hat{n}_i(t) \simeq \Delta_Q \hat{n}_i(0) \simeq 1/(2\Delta\phi)$, as shown in Fig. 5.5(i). In the case of large $\Delta\phi$, the classical evolution $n_i(t, \mathbf{\Phi})$ follows different trajectories for the different values of $\mathbf{\Phi}$ on $|\chi_\nu(\mathbf{\Phi})|^2$, leading to a large $\mathrm{Var}_{|\chi_\nu|^2}[n_i(t, \mathbf{\Phi})]$ and an expansion of the wavepacket, seen for example at $t = t_b$ on Fig. 5.5(d)(k). At a quasi-period $T$ discussed in Sec. 5.3.2, the classical trajectories lead almost to the same quantized drift $\boldsymbol{N}(T, \mathbf{\Phi}) \simeq \boldsymbol{\nu} T$ for all initial phases $\mathbf{\Phi}$, such that $\mathrm{Var}_{|\chi_\nu|^2}[n_i(T, \mathbf{\Phi})] \simeq 0$. The wavepacket refocuses at these quasi-periods, seen at $t = t_a$ and $t = t_c$ on Fig. 5.5(k).

The default of refocusing is usually discussed in the literature in relation with the default of rephasing $\mathrm{Var}_{|\chi_\nu|^2}[n_i(T, \mathbf{\Phi})] \neq 0$ [195, 207], such that $(\Delta_Q \hat{n}_i)(T) \gtrsim (\Delta_Q \hat{n}_i)(t = 0)$. We note an important point about these rephasing events: even if the refocusing is perfect $(\Delta_Q \hat{n}_i)(T) = (\Delta_Q \hat{n}_i)(t = 0)$ the spread at these refocusing times corresponds to the initial spread of the adiabatic component $|\Psi_-(t = 0)\rangle$ and not to the initial state $|\Psi(t = 0)\rangle$. This is the reason why on Fig. 5.5(c) the state does not refocus into a Fock state. Indeed, as discussed above the phase distribution $|\chi_-(\mathbf{\Phi})|^2$ is not fully delocalized on the torus, such that by Heisenberg inequality the distribution of number of quanta in $|\Psi_-(t = 0)\rangle$ is not fully localized. For the cat state with equal weight, we discussed in section 5.3.1 that $|\chi_-(\mathbf{\Phi})|^2$ covers approximately half the torus, corresponding to a spread of order $\pi/4$, such that $\Delta_Q \hat{n}_i(t = 0) \geq 2/\pi \simeq 0.63$. This is approximately the values of the spreading at the refocusing times on Fig. 5.5(k).

## 5.4 Conclusion of chapter

In this chapter, we have shown that the dynamics of a qubit topologically coupled to two slow quantum modes generically creates a cat state, a superposition of two adiabatic states with mesoscopically distinct energy content. For each adiabatic component of the cat, the topological nature of the coupling induces an intrinsic entanglement between the qubit and the modes, characterized by the geometry of adiabatic states of the qubit, their quantum metric.

Let us stress that we have focused on the adiabatic limit of a quantum description of a Floquet system. We characterized the entanglement between the drives and the driven quantum system in terms of the quantum geometry of adiabatic states. Extending this relation between entanglement and geometry beyond the adiabatic limit [214, 215] is a natural and stimulating perspective.

The realization of such topological adiabatic cat states opens interesting perspectives, in particular to elaborate protocols to disentangle the qubit from the quantum modes, creating an entangled cat state between the modes. One can build on existing protocols for a superconducting qubit dispersively coupled to quantum cavities, with cats composed of coherent states non-entangled with the qubit, of typical form $(|\alpha_1, \alpha_2, \uparrow\rangle + |\beta_1, \beta_2, \downarrow\rangle)/\sqrt{2}$ [216]. From our analysis of Sec. 5.3.1, similar states are obtained from an adiabatic cat state in the quasi-phase limit at a time $t$ where a small value of the quantum metric $g_{ij}(\mathbf{\Phi}^0 - \boldsymbol{\omega} t)$ is reached. Besides, it is worth pointing out that the topological splitting of the two adiabatic components allows for the experimental preparation of adiabatic

states, by using a projection on the number of quanta $(n_1, n_2)$ such that $n_1 - n_2 > n_1^0 - n_2^0$ after the time of separation. In the perspective of a superconducting qubit coupled to quantum cavities, such a measurement protocol can be adapted from the methods of photon number resolution [217] using an additional qubit dispersively coupled to the two cavities.

Our model of quantum rotors coupled to a qubit shows that the adiabatic curvature, which generalizes the Berry curvature while carrying the same topology, governs the dynamics of adiabatic states. The models of quantum rotors describes accurately the dynamics of quantum harmonic oscillators topologically coupled to a fast quantum system. In the next chapter, we consider the dynamics of such system on longer timescales, unveiling a rich dynamics combining adiabatic pumping and Landau-Zener scattering, which leads to a non-standard notion of chaos.

## 5.A Time evolution of phase states

We consider a model of quantum rotors whose Hamiltonian is $\hat{H}_{\text{tot}} = \hbar\boldsymbol{\omega}\cdot\hat{\boldsymbol{N}} + H(\hat{\boldsymbol{\Phi}})$ where $\boldsymbol{\omega} = (\omega_1, \cdots, \omega_N)$, $\hat{\boldsymbol{N}} = (\hat{n}_1, \cdots, \hat{n}_N)$, $\hat{\boldsymbol{\Phi}} = (\hat{\phi}_1, \cdots, \hat{\phi}_N)$, where the operators $\hat{n}_i$ and $\hat{\phi}_i$ are conjugated $[\hat{n}_i, \hat{\phi}_j] = \mathrm{i}\delta_{ij}\mathbf{1}$, and $\boldsymbol{\omega}\cdot\hat{\boldsymbol{N}} = \sum_i \omega_i\hat{n}_i$. We determine the time evolution of a phase eigenstate $|\Psi(t=0)\rangle = |\boldsymbol{\Phi}\rangle \otimes |\psi\rangle$ with $|\psi\rangle$ an arbitrary state of the two-level system. In the interaction representation with respect to the Hamiltonian of the modes, the time evolved state is:

$$|\Psi_I(t)\rangle = \exp\left[\mathrm{i}t\boldsymbol{\omega}\cdot\hat{\boldsymbol{N}}\right]|\Psi(t)\rangle\,. \tag{5.36}$$

The dynamics of $|\Psi_I(t)\rangle$ is governed by the Hamiltonian in the interaction representation:

$$\begin{aligned}\hat{H}_I(t) &= \exp\left[\mathrm{i}t\boldsymbol{\omega}\cdot\hat{\boldsymbol{N}}\right] H(\hat{\boldsymbol{\Phi}}) \exp\left[-\mathrm{i}t\boldsymbol{\omega}\cdot\hat{\boldsymbol{N}}\right] &(5.37)\\ &= H(\hat{\boldsymbol{\Phi}} - \boldsymbol{\omega}t) &(5.38)\end{aligned}$$

since the operators $\hat{n}_i$ are generators of phase translations. As a consequence,

$$\hat{H}_I(t)\left(|\boldsymbol{\Phi}\rangle \otimes |\psi\rangle\right) = |\boldsymbol{\Phi}\rangle \otimes H(\boldsymbol{\Phi} - \boldsymbol{\omega}t)\,|\psi\rangle \tag{5.39}$$

such that the time-evolution of the initial state $|\boldsymbol{\Phi}\rangle \otimes |\psi\rangle$ in the interaction representation is

$$\begin{aligned}|\Psi_I(t)\rangle &= \mathcal{T}\exp\left[-\frac{\mathrm{i}}{\hbar}\int_0^t \mathrm{d}\tau\ \hat{H}_I(\tau)\right]|\boldsymbol{\Phi}\rangle \otimes |\psi\rangle\\ &= |\boldsymbol{\Phi}\rangle \otimes U(t;\boldsymbol{\Phi})\,|\psi\rangle &(5.40)\end{aligned}$$

where $\mathcal{T}$ denotes time-ordering and $U(t;\boldsymbol{\Phi}) = \mathcal{T}\exp\left[-\frac{\mathrm{i}}{\hbar}\int_0^t \mathrm{d}\tau\ H(\boldsymbol{\Phi} - \boldsymbol{\omega}\tau)\right]$ is the time evolution operator associated to the time-dependent Hamiltonian $H(\boldsymbol{\Phi} - \boldsymbol{\omega}t)$ for classical modes. We then obtain the time-evolved state in the Schrödinger representation

$$\begin{aligned}|\Psi(t)\rangle &= \exp\left[-\mathrm{i}t\boldsymbol{\omega}\cdot\hat{\boldsymbol{N}}\right]|\Psi_I(t)\rangle &(5.41)\\ &= |\boldsymbol{\Phi} - \boldsymbol{\omega}t\rangle \otimes U(t;\boldsymbol{\Phi})\,|\psi\rangle\,. &(5.42)\end{aligned}$$

## 5.B Definition of the adiabatic subspaces

For the sake of completeness, we detail the definition of the adiabatic states of the qubit, which is similar to the construction of adiabatic states in Chap. 1.

We construct the states of the two-level system $|\psi_\nu(\boldsymbol{\Phi})\rangle$ such that the family of states $|\boldsymbol{\Phi}\rangle \otimes |\psi_\nu(\boldsymbol{\Phi})\rangle$ with $\boldsymbol{\Phi} \in [0, 2\pi]^2$ is stable under the dynamics governed by the total Hamiltonian $\hat{H}_{\text{tot}} = \sum_i \hbar\omega_i\hat{n}_i + H(\hat{\boldsymbol{\Phi}})$. This family of states corresponds to the image of the associated adiabatic projector

$$\begin{aligned}\hat{\Pi}_\nu &= \int \mathrm{d}\boldsymbol{\Phi}\ \ |\boldsymbol{\Phi}\rangle\langle\boldsymbol{\Phi}| \otimes |\psi_\nu(\boldsymbol{\Phi})\rangle\langle\psi_\nu(\boldsymbol{\Phi})| &(5.43)\\ &= \int \mathrm{d}\boldsymbol{\Phi}\ \ |\boldsymbol{\Phi}\rangle\langle\boldsymbol{\Phi}| \otimes \pi_\nu(\boldsymbol{\Phi}). &(5.44)\end{aligned}$$

We first construct the family of projectors of the two-level system $\pi_\nu(\mathbf{\Phi}) = |\psi_\nu(\mathbf{\Phi})\rangle \langle\psi_\nu(\mathbf{\Phi})|$. As detailed in appendix 5.A, for an arbitrary state $|\psi\rangle$ of the fast quantum degree of freedom, the phase eigenstates evolve according to

$$\exp\Big(-i\hat{H}_{\rm tot}t/\hbar\Big)\left(|\mathbf{\Phi}\rangle \otimes |\psi\rangle\right) = |\mathbf{\Phi} - \boldsymbol{\omega}t\rangle \otimes U(t;\mathbf{\Phi})\,|\psi\rangle \tag{5.45}$$

with $U(t;\mathbf{\Phi})$ the time evolution operator associated to the Floquet Hamiltonian $H(\mathbf{\Phi} - \boldsymbol{\omega}t)$. Thus, the previous family of states is stable if the projectors $\pi_\nu(\mathbf{\Phi})$ satisfy

$$U(t;\mathbf{\Phi})\pi_\nu(\mathbf{\Phi})U(t;\mathbf{\Phi})^\dagger = \pi_\nu(\mathbf{\Phi} - \boldsymbol{\omega}t)\,, \tag{5.46}$$

or equivalently $-i\hbar\boldsymbol{\omega}\cdot\nabla_{\mathbf{\Phi}}\pi_\nu(\mathbf{\Phi}) = [H(\mathbf{\Phi}), \pi_\nu(\mathbf{\Phi})]$. This equation can be solved perturbatively from the limit of infinitely slow subsystem. We introduce the dimensionless parameter $\lambda$ connecting this limit to our problem by rescaling the frequencies: $\boldsymbol{\omega} \to \lambda\boldsymbol{\omega}$. We search a projector $\pi_\nu(\mathbf{\Phi})$ expressed a formal series of $\lambda$

$$\pi_\nu(\mathbf{\Phi}) = \sum_k \lambda^k \pi_{\nu,k}(\mathbf{\Phi}) = \pi_{\nu,0}(\mathbf{\Phi}) + \lambda\pi_{\nu,1}(\mathbf{\Phi}) + \dots \tag{5.47}$$

solution of (5.46), which translates into

$$-\lambda i\hbar\boldsymbol{\omega}\cdot\nabla_{\mathbf{\Phi}}\pi_\nu(\mathbf{\Phi}) = [H(\mathbf{\Phi}), \pi_\nu(\mathbf{\Phi})] \tag{5.48}$$

$$\pi_\nu(\mathbf{\Phi})^2 = \pi_\nu(\mathbf{\Phi})\,. \tag{5.49}$$

The algorithm of construction of $\pi_\nu(\mathbf{\Phi})$ from these equations is identical to the algorithm detailed in Sec. 1.2.2 of Chap. 1, leading to the expression provided in Sec. 5.2.1.

## 5.C Time evolution of the adiabatic states

For the sake of completeness, we derive the time evolution of the adiabatic states of the fast subsystem, which is similar to the one derived in Chap. 1 for a driven system, replacing time dependence by dependence on $\mathbf{\Phi} - \boldsymbol{\omega}t$. The only difference is that here we keep track of the initial phase $\mathbf{\Phi}$, such that the dynamical and geometrical phases, summarized into $\theta_\nu(t;\mathbf{\Phi})$ below, depend on this initial phase. This aspect is relevant when considering the time evolution of quantum fluctuations in appendix 5.I.

In appendix 5.B we constructed the projectors $\pi_\nu(\mathbf{\Phi}) = |\psi_\nu(\mathbf{\Phi})\rangle \langle\psi_\nu(\mathbf{\Phi})|$ on the states of the two-level system such that the image of the adiabatic projector $\hat{\Pi}_\nu$ is stable under the dynamics. As discussed in the main text, such states $|\psi_\nu(\mathbf{\Phi})\rangle$ have to satisfy

$$U(t;\mathbf{\Phi})\,|\psi_\nu(\mathbf{\Phi})\rangle = e^{i\theta_\nu(t;\mathbf{\Phi})}\,|\psi_\nu(\mathbf{\Phi} - \boldsymbol{\omega}t)\rangle \tag{5.50}$$

with $U(t;\mathbf{\Phi})$ the time evolution operator associated to the time-dependent Hamiltonian $H(\mathbf{\Phi} - \boldsymbol{\omega}t)$ and with $\theta_\nu(t;\mathbf{\Phi})$ a phase factor to be determined. By definition, the time evolution operator $U(t;\mathbf{\Phi})$ satisfies

$$i\hbar\frac{\mathrm{d}}{\mathrm{d}t}U(t;\mathbf{\Phi}) = H(\mathbf{\Phi} - \boldsymbol{\omega}t)U(t;\mathbf{\Phi}), \tag{5.51}$$

such that (5.50) leads to

$$\frac{1}{i\hbar}H(\mathbf{\Phi}-\boldsymbol{\omega}t)\left|\psi_\nu(\mathbf{\Phi}-\boldsymbol{\omega}t)\right\rangle = i\frac{\partial\theta_\nu}{\partial t}(t;\mathbf{\Phi})\left|\psi_\nu(\mathbf{\Phi}-\boldsymbol{\omega}t)\right\rangle - \sum_i \omega_i \left|\partial_{\phi_i}\psi_\nu(\mathbf{\Phi}-\boldsymbol{\omega}t)\right\rangle . \quad (5.52)$$

The phase factor $\theta_\nu(t;\mathbf{\Phi})$ is then given by

$$\theta_\nu(t;\mathbf{\Phi}) = \int_0^t \mathrm{d}t' \left(-\frac{1}{\hbar}E_\nu(\mathbf{\Phi}-\boldsymbol{\omega}t') - \sum_i \omega_i A_{\nu,i}(\mathbf{\Phi}-\boldsymbol{\omega}t')\right) \quad (5.53)$$

with the energy function

$$E_\nu(\mathbf{\Phi}) = \left\langle\psi_\nu(\mathbf{\Phi})\right| H(\mathbf{\Phi})\left|\psi_\nu(\mathbf{\Phi})\right\rangle \quad (5.54)$$

and the connection

$$A_{\nu,i}(\mathbf{\Phi}) = i\left\langle\psi_\nu(\mathbf{\Phi})|\partial_{\phi_i}\psi_\nu(\mathbf{\Phi})\right\rangle \quad (5.55)$$

of the adiabatic states $|\psi_\nu(\mathbf{\Phi})\rangle$.

## 5.D Pumping rate in an adiabatic state

We derive the time-evolution (5.18) of the pumping rate $\langle\hat{n}_1\rangle$ for an initial state (5.12) projected in the adiabatic subspace $\nu$

$$|\Psi_\nu(t=0)\rangle = \int \mathrm{d}^2\mathbf{\Phi}\ \chi_\nu(\mathbf{\Phi})\left|\mathbf{\Phi}\right\rangle \otimes \left|\psi_\nu(\mathbf{\Phi})\right\rangle . \quad (5.56)$$

From appendix 5.C, the time evolution of this projected state is

$$|\Psi_\nu(t)\rangle = \int \mathrm{d}^2\mathbf{\Phi}\ \chi_\nu(\mathbf{\Phi})e^{i\theta_\nu(t;\mathbf{\Phi})}\left|\mathbf{\Phi}-\boldsymbol{\omega}t\right\rangle \otimes \left|\psi_\nu(\mathbf{\Phi}-\boldsymbol{\omega}t)\right\rangle , \quad (5.57)$$

with the phase factor $\theta_\nu(t;\mathbf{\Phi})$ given by (5.53). The Ehrenfest theorem reads

$$\frac{\mathrm{d}}{\mathrm{d}t}\langle\hat{n}_1\rangle_{\Psi_\nu(t)} = \frac{1}{i\hbar}\langle[\hat{n}_1,\hat{H}_{\mathrm{tot}}]\rangle_{\Psi_\nu(t)} \quad (5.58)$$

where from the Hamiltonian (5.2) we have $[\hat{n}_1,\hat{H}_{\mathrm{tot}}] = i\frac{\partial H}{\partial\phi_1}(\hat{\mathbf{\Phi}})$ such that

$$\frac{\mathrm{d}}{\mathrm{d}t}\langle\hat{n}_1\rangle_{\Psi_\nu(t)} = \int \mathrm{d}^2\mathbf{\Phi}\ \frac{|\chi_\nu(\mathbf{\Phi})|^2}{W_\nu}\frac{1}{\hbar}\left\langle\psi_\nu(\mathbf{\Phi}-\boldsymbol{\omega}t)\right| \frac{\partial H}{\partial\phi_1}(\mathbf{\Phi}-\boldsymbol{\omega}t)\left|\psi_\nu(\mathbf{\Phi}-\boldsymbol{\omega}t)\right\rangle \quad (5.59)$$

with $W_\nu = \langle\Psi_\nu(t)|\Psi_\nu(t)\rangle$ given by (5.23). The average value of the derivative of the Hamiltonian can be written

$$\left\langle\psi_\nu\right| \frac{\partial H}{\partial\phi_1}\left|\psi_\nu\right\rangle = \frac{\partial}{\partial\phi_1}\left(\left\langle\psi_\nu\right| H\left|\psi_\nu\right\rangle\right) - \left\langle\partial_{\phi_1}\psi_\nu\right| H\left|\psi_\nu\right\rangle - \left\langle\psi_\nu\right| H\left|\partial_{\phi_1}\psi_\nu\right\rangle \quad (5.60)$$

where the dependence on $\mathbf{\Phi}-\boldsymbol{\omega}t$ is implicit. The first term of this equation gives the term of variation of energy in (5.18). We recall that $|\psi_\nu\rangle$ are not the eigenstates of the Hamiltonian, but the adiabatic states, such that $H\left|\psi_\nu\right\rangle$ is given by (5.52). Using this relation as well as the normalization condition $\langle\partial_{\phi_1}\psi_\nu|\psi_\nu\rangle = -\langle\psi_\nu|\partial_{\phi_1}\psi_\nu\rangle$, we write the last two terms of (5.60) in terms of the curvature $F_\nu$ (5.15) such that we obtain the expression (5.18) of the pumping rate

$$\frac{\mathrm{d}}{\mathrm{d}t}\langle\hat{n}_1\rangle_{\Psi_\nu(t)} = \int \mathrm{d}^2\mathbf{\Phi}\ \frac{|\chi_\nu(\mathbf{\Phi})|^2}{W_\nu}\left(\frac{1}{\hbar}\frac{\partial E_\nu}{\partial\phi_1}(\mathbf{\Phi}-\boldsymbol{\omega}t) + \omega_2 F_\nu(\mathbf{\Phi}-\boldsymbol{\omega}t)\right) \quad (5.61)$$

with the energy function $E_\nu(\mathbf{\Phi}) = \left\langle\psi_\nu(\mathbf{\Phi})\right| H(\mathbf{\Phi})\left|\psi_\nu(\mathbf{\Phi})\right\rangle$ and the curvature $F_\nu(\mathbf{\Phi})$ (5.15).

## 5.E Gaussian phase states

The modes are prepared in a Gaussian state $\langle n_i|\chi_i\rangle \propto \exp(-(n_i-n_i^0)^2/(2\Delta n_i)^2 + i\phi_i^0 n_i)$ centered on $(n_i^0, \phi_i^0)$, and of width $\Delta n_i$. In the case of a quantum harmonic oscillator for which $\hat{n}_i = \hat{a}^\dagger\hat{a}$, a coherent state $|\alpha\rangle$ with $\alpha = \sqrt{n_i^0}e^{i\phi_i^0}$ with an average number of quanta $n_i^0 \gg 1$ reduces to a Gaussian state with $\Delta n_i = \sqrt{n_i^0}$. By Fourier transform, the phase distribution $|\langle\phi_i|\chi_i\rangle|^2$ of the modes is a periodic normalized Gaussian centered on $\phi_i^0$ and of width $\Delta\phi_i = 1/(2\Delta n_i)$ in each direction

$$|\langle\phi_i|\chi_i\rangle|^2 = f(\phi_i - \phi_i^0, \Delta\phi)\exp\left(-\frac{(\phi_i-\phi_i^0)^2}{2(\Delta\phi_i)^2}\right) \tag{5.62}$$

where $f(\phi_i - \phi_i^0, \Delta\phi)$ is a function ensuring normalization and periodicity. Explicitly

$$f(\phi_i-\phi_i^0,\Delta\phi) = 2(\Delta n_i)^2\frac{\left|\vartheta_3\left(-2\mathrm{i}\pi(\Delta n_i)^2(\phi_i-\phi_i^0),\ e^{-4\pi^2(\Delta n_i)^2}\right)\right|^2}{\vartheta_3\left(0,\ e^{-\frac{1}{2(\Delta n_i)^2}}\right)}, \tag{5.63}$$

with $\vartheta_3$ the third Jacobi theta function. Such phase distribution is almost uniform for $\Delta\phi \gtrsim \pi$.

## 5.F Numerical construction of the adiabatic projector

For the numerical simulation, we diagonalize the Hamiltonian in $(n_1, n_2)$ representation, where $e^{i\hat{\phi}_i}|n_i\rangle = |n_i - 1\rangle$, with the truncation $-59 \le n_1 \le 59$ and $-52 \le n_2 \le 52$. We keep only the positions $(n_1, n_2)$ in a rectangle oriented along the directions $n_\perp$ and $n_E$ (5.6), corresponding to

$$|n_E| = \frac{1}{\sqrt{\omega_1^2+\omega_2^2}}|\omega_1 n_1 + \omega_2 n_2| \le 30 \tag{5.64}$$

$$|n_\perp| = \frac{1}{\sqrt{\omega_1^2+\omega_2^2}}|-\omega_2 n_1 + \omega_1 n_2| \le 50 \tag{5.65}$$

with $\omega_2/\omega_1 = (1+\sqrt{5})/2$. We use open boundary conditions.

We construct numerically the adiabatic projector up to order 1 in the perturbative variable $\lambda$. The adiabatic projector $\hat{\Pi}_\nu$ is defined by an asymptotic series in the formal dimensionless variable $\lambda$

$$\hat{\Pi}_\nu = \sum_{k=0}^{\infty}\lambda^k\hat{\Pi}_{\nu,k} = \hat{\Pi}_{\nu,0} + \lambda\hat{\Pi}_{\nu,1} + \dots \tag{5.66}$$

such that

$$[\hat{H}_{\mathrm{tot}}, \hat{\Pi}_\nu] = 0 \tag{5.67}$$

$$\hat{\Pi}_\nu\hat{\Pi}_\nu = \hat{\Pi}_\nu \tag{5.68}$$

with

$$\hat{H}_{\text{tot}} = H(\hat{\phi}_1, \hat{\phi}_2) + \lambda(\omega_1 \hat{n}_1 + \omega_2 \hat{n}_2). \tag{5.69}$$

We use the half-BHZ model for the qubit (5.3) with the gap parameter $\Delta = 2$. The maximum on $(\phi_1, \phi_2)$ of the ground state energy of $H(\phi_1, \phi_2)$ for these values of parameters is $E^{\max}_{-,0} = -1$, and the minimum of excited state energy is $E^{\min}_{+,0} = 1$.

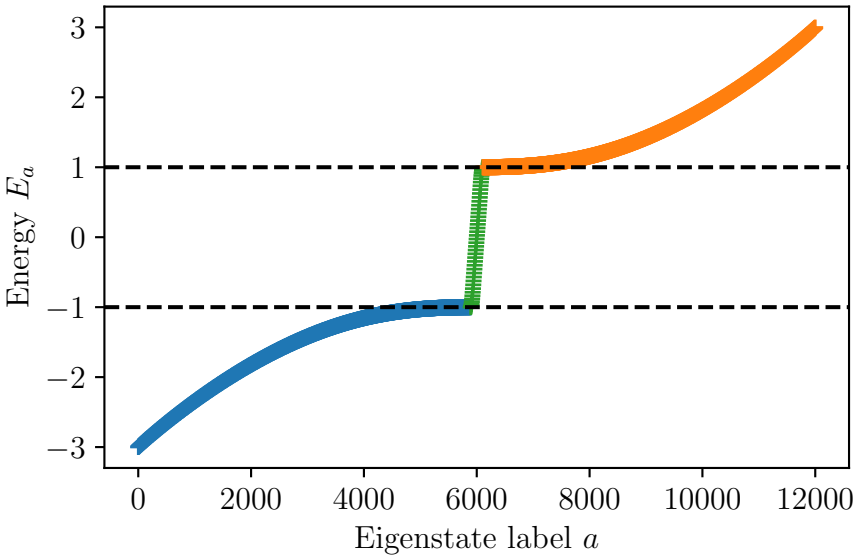


Figure 5.6: Numerical spectrum of the truncated Hamiltonian $H(\hat{\phi}_1, \hat{\phi}_2)$. In green, edge states whose energy lies in the gap of the untruncated Hamiltonian $H(\hat{\phi}_1, \hat{\phi}_2)$. We do not take them into account in the definition of the adiabatic projector. The zeroth order adiabatic projector $\hat{\Pi}_{-,0}$ is the spectral projector on the ground band of $H(\hat{\phi}_1, \hat{\phi}_2)$ (states in blue). The first order correction $\hat{\Pi}_{-,1}$ of the adiabatic projector has matrix elements between the ground and excited band (states in orange) of $H(\hat{\phi}_1, \hat{\phi}_2)$, given by Eq. (5.74).

At order 0, $\hat{\Pi}_\nu$ is a spectral projector of the Hamiltonian $H(\hat{\phi}_1, \hat{\phi}_2)$. We diagonalize numerically the Hamiltonian at zero frequency $H(\hat{\phi}_1, \hat{\phi}_2)$ in the truncated Hilbert space, providing the energies $E_a$ and states $|\Psi_a\rangle$ such that

$$H(\hat{\phi}_1, \hat{\phi}_2) \, |\Psi_a\rangle = E_a \, |\Psi_a\rangle \, . \tag{5.70}$$

The projector at order 0 is the projector on the states of the ground band, i.e. on the states such that $E_a < E^{\max}_{-,0}$

$$\hat{\Pi}_{-,0} = \sum_{\substack{a \\ E_a < E^{\max}_{-,0}}} |\Psi_a\rangle \langle\Psi_a| \tag{5.71}$$

Note that we do not take into account the edge states whose energy lie in the gap for the construction of the projectors, as illustrated on Fig. 5.6.

The conditions (5.67) and (5.68) translate into recursive conditions for the different

orders $\hat{\Pi}_{\nu,k}$ of the projector

$$\hat{\Pi}_{\nu,k} = \sum_{l=0}^{k} \hat{\Pi}_{\nu,l}\hat{\Pi}_{\nu,k-l} \tag{5.72}$$

$$[H(\hat{\boldsymbol{\Phi}}), \hat{\Pi}_{\nu,k}] = [\hat{\Pi}_{\nu,k-1}, \hbar\boldsymbol{\omega}\cdot\hat{\boldsymbol{N}}] \tag{5.73}$$

from which we can deduce order by order the expression of $\hat{\Pi}_{\nu,k}$ in the basis of $|\Psi_a\rangle$. At order 1 we obtain

$$\hat{\Pi}_{-,1} = \sum_{\substack{a,b \\ E_a<E^{\max}_{-,0} \\ E_b>E^{\min}_{+,0}}} |\Psi_a\rangle \frac{\langle\Psi_a|\,\hbar\boldsymbol{\omega}\cdot\hat{\boldsymbol{N}}\,|\Psi_b\rangle}{E_a - E_b} \langle\Psi_b| + \text{h.c.} \tag{5.74}$$

which can be evaluated numerically.

## 5.G Difference between eigenstates and adiabatic states.

**Fidelity**

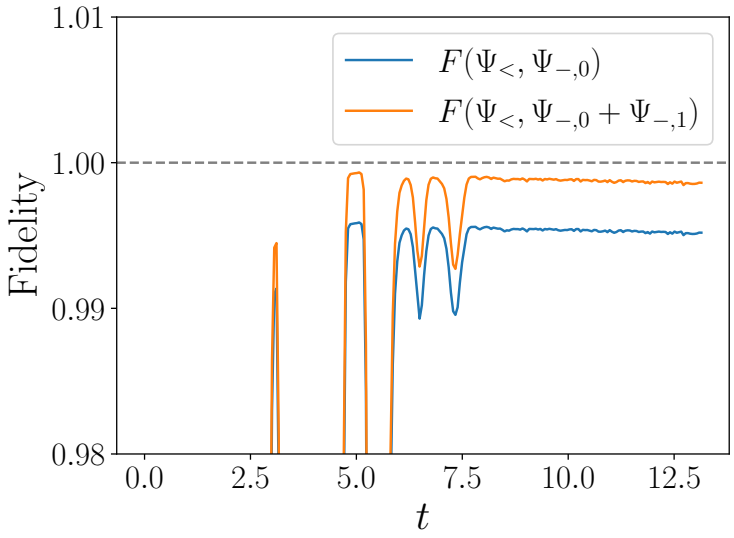


Figure 5.7: Fidelity $F(\Psi_<, \Psi_{-,0})$ and $F(\Psi_<, \Psi_{-,0} + \Psi_{-,1})$ between the cat component $|\Psi_<(t)\rangle$ and the adiabatic projections at order 0 $|\Psi_{-,0}(t)\rangle$ and at order 1 $|\Psi_{-,0}(t)\rangle + |\Psi_{-,1}(t)\rangle$. After the time of separation $t_{\text{sep}} \simeq 8$, the cat component $|\Psi_<(t)\rangle$ is very close to the lowest order adiabatic approximation $|\Psi_{-,0}(t)\rangle$ with a fidelity of 99.5%. The fidelity further increases with the adiabatic projection of order 1, such that $|\Psi_<(t)\rangle$ identifies with $|\Psi_-(t)\rangle$.

We show that after the time of separation $t_{\text{sep}}$, the cat component which splits in the direction $n_\perp < n_\perp^0$ identifies with the adiabatic component $\hat{\Pi}_-\,|\Psi(t)\rangle$ of the total state.

We note $\hat{\Pi}_<$ the projector on the states $|n_1\rangle\otimes|n_2\rangle\otimes|s\rangle$ with $n_\perp = (-\omega_2 n_1+\omega_1 n_2)/|\boldsymbol{\omega}| < n_\perp^0$, $s =\uparrow_z,\downarrow_z$, and $|\Psi_<(t)\rangle = \hat{\Pi}_< |\Psi(t)\rangle$ the component of the system on this region $n_\perp < n_\perp^0$. We aim at comparing $\hat{\Pi}_< |\Psi(t)\rangle$ and $\hat{\Pi}_- |\Psi(t)\rangle$.

The adiabatic projector $\hat{\Pi}_-$ is constructed perturbatively by Eq. (5.66) detailed in App. 5.F. The adiabatic projection of the total states then decomposes into

$$\hat{\Pi}_- |\Psi(t)\rangle = \sum_k |\Psi_{-,k}(t)\rangle \tag{5.75}$$

with the $k$-th order projection $|\Psi_{-,k}(t)\rangle = \hat{\Pi}_{-,k} |\Psi(t)\rangle$. Note that we let $\lambda = 1$ since we consider the adiabatic projector of our problem of interest.

We note $F(\Psi_1, \Psi_2) = \langle\Psi_1|\Psi_2\rangle / (\langle\Psi_1|\Psi_1\rangle \langle\Psi_2|\Psi_2\rangle)$ the fidelity between two states $|\Psi_1\rangle$ and $|\Psi_2\rangle$. The figure 5.7 represents the fidelity between the $n_\perp < n_\perp^0$ cat components and the adiabatic states computed numerically respectively at zeroth and first order, namely respectively $F(\Psi_<, \Psi_{-,0})$ and $F(\Psi_<, \Psi_{-,0} + \Psi_{-,1})$. After the time of separation $t_{\text{sep}} \simeq 8$, the cat component has a fidelity of approximately 99.5% with the zeroth order $|\Psi_{-,0}(t)\rangle$ and 99.9% with the first order $|\Psi_{-,0}(t)\rangle + |\Psi_{-,1}(t)\rangle$. As such, the adiabatic projection at order 0 gives a very good approximation of the cat component, corrected at higher orders to give the full adiabatic component $|\Psi_-(t)\rangle$. The slight decrease with time of the fidelity after the time of separation is due to the successive Landau-Zener transitions.

**Weight**

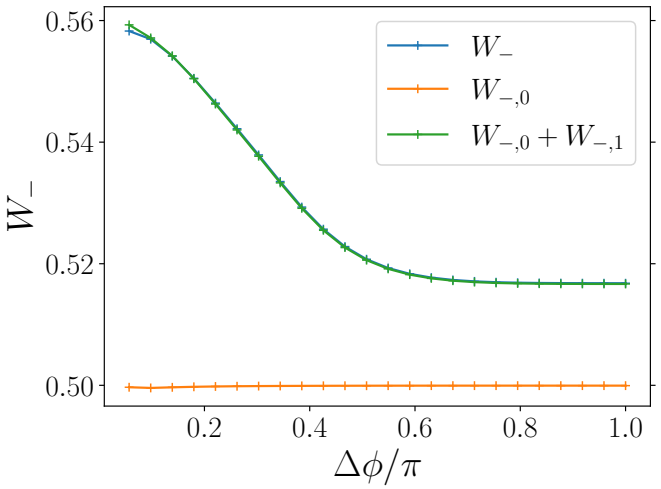


Figure 5.8: Effect of the difference between eigenstates and adiabatic states on the weight of the cat. Initial state of the Fig. 5.3(c) with $\theta_q = \pi/2$. In blue, weight $W_-$ of the cat computed dynamically from the splitting (same as Fig. 5.3(c)). In orange, weight $W_{-,0} = \langle\Psi(t=0)| \hat{\Pi}_{-,0} |\Psi(t=0)\rangle$ computed from the zeroth order adiabatic projector $\hat{\Pi}_-, 0$. In green, weight $W_{-,0} + W_{-,1} = \langle\Psi(t=0)| (\hat{\Pi}_{-,0} + \hat{\Pi}_{-,1}) |\Psi(t=0)\rangle$ from the projector at order 1, which almost identifies with the weight obtained dynamically.

The difference between the adiabatic projector $\hat{\Pi}_-$ and the spectral projector $\hat{\Pi}_{-,0}$ is visible in the weight of the cat state. We represent on Fig. 5.8 the weight of the

adiabatic projection computed dynamically from the splitting $W_- = \langle\Psi_<(t_{\rm sep})|\Psi_<(t_{\rm sep})\rangle = \langle\Psi(t_{\rm sep})|\,\hat{\Pi}_<\,|\Psi(t_{\rm sep})\rangle$. We also represent the weight in the adiabatic subspace computed from the numerical construction of the adiabatic projector

$$W_- = \langle\Psi(t=0)|\,\hat{\Pi}_-\,|\Psi(t=0)\rangle = \sum_k W_{-,k} \tag{5.76}$$

with the weight of order $k$ given by $W_{-,k} = \langle\Psi(t=0)|\,\hat{\Pi}_{-,k}\,|\Psi(t=0)\rangle$.

The initial state is a Gaussian state centered on $\mathbf{\Phi}^0 = (0,0)$ and the qubit in $\varphi_q = 0$, $\theta_q = \pi/2$. As discussed in Sec. 5.2.3, the corresponding average ground state $\bar{\boldsymbol{b}}_{-,0}$ lies on the $z$-axis for all $\Delta\phi$ such that $W_{-,0} = \frac{1}{2}$. As seen in Fig. 5.8, this zeroth order provides a good approximation with the weight of the cat, while the weight computed at first order $W_{-,0} + W_{-,1}$ almost identifies with the weight obtained dynamically $W_-$.

## 5.H Purity from initial Fock state

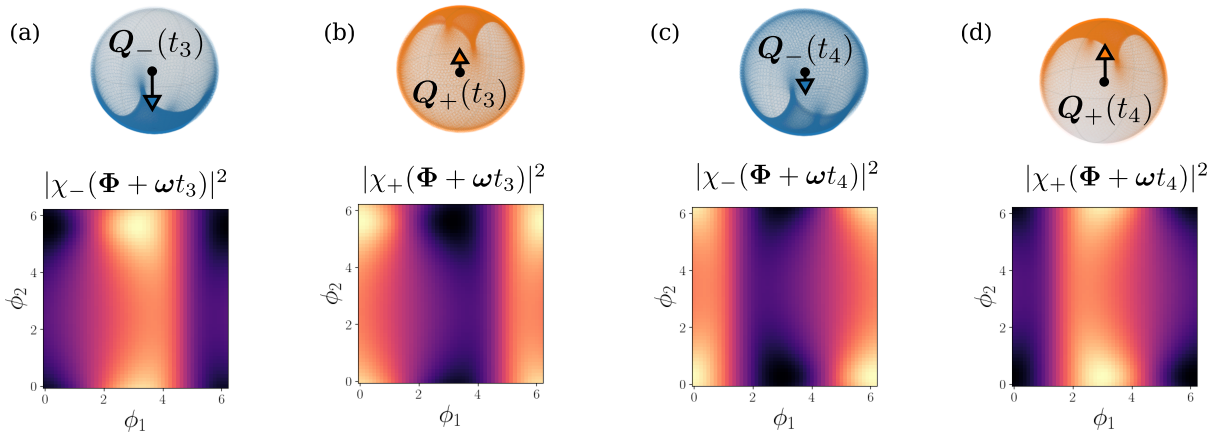


Figure 5.9: Phase densities $|\chi_\pm(\mathbf{\Phi}-\boldsymbol{\omega}t)|^2$ of the cat components $|\Psi_\pm(t)\rangle$ translated to densities of adiabatic states on the Bloch sphere via the map $\mathbf{\Phi} \mapsto \boldsymbol{b}_\pm(\mathbf{\Phi})$. The polarization of the qubit $\boldsymbol{Q}_\pm(t)$ is the average of adiabatic states with respect to these densities.

We illustrate the role of the phase densities in the entanglement between the qubit and the modes in the cat components $|\Psi_\pm(t)\rangle$ for a quasi-Fock initial state $\Delta\phi = \pi$, and the qubit initialized in $\theta_q = \pi/2$, $\varphi_q = 0$. As discussed in Sec. 5.3.1, for an initial quasi-Fock state the phase densities $|\chi_\pm(\mathbf{\Phi}+\boldsymbol{\omega}t)|^2$ of the two components of the cat split the torus in two complementary supports of equal weight. We represent these densities on Fig. 5.9 at the time $t = t_3$ and $t = t_4$ indicated on Fig. 5.4(b2). The densities on the torus translate into densities of adiabatic states on the Bloch sphere via the map $\mathbf{\Phi} \mapsto \boldsymbol{b}_\pm(\mathbf{\Phi})$.

At $t = t_3$, $|\chi_-(\mathbf{\Phi}+\boldsymbol{\omega}t_3)|^2$ covers a smaller part of the Bloch sphere than $|\chi_+(\mathbf{\Phi}+\boldsymbol{\omega}t_3)|^2$, such that the qubit is more entangled with the modes in $|\Psi_+(t_3)\rangle$ than in $|\Psi_-(t_3)\rangle$: $|\boldsymbol{Q}_+(t_3)| < |\boldsymbol{Q}_-(t_3)|$. During the dynamics, the phase densities are translated on the torus with no dispersion, changing the densities on the Bloch sphere and the purity of the qubit. At $t = t_4$, the domains have been almost exchanged $|\chi_-(\mathbf{\Phi}-\boldsymbol{\omega}t_4)|^2 \simeq |\chi_+(\mathbf{\Phi}-\boldsymbol{\omega}t_3)|^2$, such that $\boldsymbol{Q}_-(t_4) \simeq -\boldsymbol{Q}_+(t_3)$ and $\boldsymbol{Q}_+(t_4) \simeq -\boldsymbol{Q}_-(t_3)$.

For the figures, the densities are computed from the eigenstates $|\psi_{-,0}(\mathbf{\Phi})\rangle$.

## 5.I Time evolution of the quantum fluctuations

We derive the time evolution of the quantum fluctuation, or spreading, of the modes' number of quanta in an adiabatic component $|\Psi_\nu(t)\rangle$ (5.13)

$$[\Delta_Q \hat{n}_i(t)]^2 = \langle \hat{n}_i^2 \rangle_{\Psi_\nu(t)} - \langle \hat{n}_i \rangle^2_{\Psi_\nu(t)} \tag{5.77}$$

with $\langle \hat{\mathcal{O}} \rangle_{\Psi_\nu(t)} = \langle \Psi_\nu(t)| \hat{\mathcal{O}} |\Psi_\nu(t)\rangle / \langle \Psi_\nu(t)|\Psi_\nu(t)\rangle$, and $i = 1, 2$. We show that due to the linearity in $\hat{\boldsymbol{N}}$ of the Hamiltonian we can relate these quantum fluctuations to the variance of the classical trajectories $n_i(t; \boldsymbol{\Phi})$ [44, 56] which are obtained in a hybrid classical-quantum description of the qubit-mode coupling

$$n_i(t, \boldsymbol{\Phi}) = \int_0^t \mathrm{d}t' \left( \frac{1}{\hbar} \frac{\partial E_\nu}{\partial \phi_i}(\boldsymbol{\Phi} - \boldsymbol{\omega} t') + \sum_j \omega_j F_{\nu,ij}(\boldsymbol{\Phi} - \boldsymbol{\omega} t') \right). \tag{5.78}$$

According to (5.57) the time evolution of the adiabatic component is given by

$$|\Psi_\nu(t)\rangle = \int \mathrm{d}^2\boldsymbol{\Phi}\ \xi_\nu(t, \boldsymbol{\Phi})\, |\boldsymbol{\Phi} - \boldsymbol{\omega} t\rangle \otimes |\psi_\nu(\boldsymbol{\Phi} - \boldsymbol{\omega} t)\rangle \tag{5.79}$$

with

$$\xi_\nu(t, \boldsymbol{\Phi}) = \tilde{\chi}_\nu(\boldsymbol{\Phi}) e^{i\theta_\nu(t;\boldsymbol{\Phi})}, \tag{5.80}$$

$\tilde{\chi}_\nu(\boldsymbol{\Phi}) = \chi_\nu(\boldsymbol{\Phi})/W_\nu$ the normalized wave-function of the decomposition (5.12) of the initial state and $\theta_\nu(t; \boldsymbol{\Phi})$ the phase factor (5.53). This form of the time evolution is due to the linearity in $\boldsymbol{N}$ of the Hamiltonian: the phase density is translated without dispersion and the acquired phase $\theta_\nu(t; \boldsymbol{\Phi})$ is given by the energy function $E_\nu(\boldsymbol{\Phi})$ (5.54) and the connection $A_{\nu,i}(\boldsymbol{\Phi})$ (5.55).

As derived in appendix 5.D, the time evolution of the average number of quanta reduces to a statistical average of the classical trajectories with respect to the initial phase density $|\tilde{\chi}_\nu(\boldsymbol{\Phi})|^2$

$$\langle \hat{n}_i \rangle_{\Psi_\nu(t)} = \langle \hat{n}_i \rangle_{\Psi_\nu(t=0)} + \int \mathrm{d}^2\boldsymbol{\Phi}\ |\tilde{\chi}_\nu(\boldsymbol{\Phi})|^2 n_i(t, \boldsymbol{\Phi}). \tag{5.81}$$

Using $\langle \phi_i'| \hat{n}_i |\phi_i\rangle = -i\partial_{\phi_i} \delta(\phi_i' - \phi_i)$, we get after a few lines

$$\langle \hat{n}_i^2 \rangle_{\Psi_\nu(t)} = \int \mathrm{d}\boldsymbol{\Phi}\ \xi_\nu(t, \boldsymbol{\Phi})^* \left( i\frac{\partial}{\partial \phi_i} + A_{\nu,i}(\boldsymbol{\Phi} - \boldsymbol{\omega} t) \right)^2 \xi_\nu(t, \boldsymbol{\Phi}) + \int \mathrm{d}^2\boldsymbol{\Phi}\ |\xi_\nu(t, \boldsymbol{\Phi})|^2 g_{\nu,ii}(\boldsymbol{\Phi} - \boldsymbol{\omega} t) \tag{5.82}$$

with $g_{\nu,ii}$ the quantum metric of the adiabatic states (5.24). Let us comment this equation. In a single band approximation of Bloch oscillations, we ignore the rotation of the states $|\psi_\nu(\boldsymbol{\Phi})\rangle$ such that we assume that $\xi_\nu(t, \boldsymbol{\Phi})$ is the wavefunction of the modes ignoring the role of the projection $\hat{\Pi}_\nu$. The average value of $\hat{n}_i^2$ is then given by (5.82) without the connection $A_{\nu,i}$ and the metric $g_{\nu,ii}$. Here the first term corresponds to the average value of the projected observable $(\hat{\Pi}_\nu \hat{n}_i \hat{\Pi}_\nu)^2$, where $\hat{\Pi}_\nu \hat{n}_i \hat{\Pi}_\nu$ reduces to a covariant derivative with the connection $A_{\nu,i}$ in the representation $|\boldsymbol{\Phi}\rangle \otimes |\psi_\nu(\boldsymbol{\Phi})\rangle$. The second term

involving the quantum metric originates from the difference between the observables and the projected observables

$$\hat{\Pi}_\nu \hat{n}_i^2 \hat{\Pi}_\nu = (\hat{\Pi}_\nu \hat{n}_i \hat{\Pi}_\nu)^2 + \hat{\Pi}_\nu \hat{n}_i (1 - \hat{\Pi}_\nu) \hat{n}_i \hat{\Pi}_\nu, \tag{5.83}$$

such that we show $\langle \hat{\Pi}_\nu \hat{n}_i (1 - \hat{\Pi}_\nu) \hat{n}_i \hat{\Pi}_\nu \rangle = \int \mathrm{d}^2\mathbf{\Phi} |\xi_\nu(t, \mathbf{\Phi})|^2 g_{\nu,ii}(\mathbf{\Phi} - \boldsymbol{\omega} t)$.

We express the time evolution (5.82) it terms of the classical trajectories $n_i(t, \mathbf{\Phi})$ (5.78). Using $A_{\nu,i}(\mathbf{\Phi} - \boldsymbol{\omega} t) - A_{\nu,i}(\mathbf{\Phi}) = \int_0^t \mathrm{d}t' \sum_j \omega_j \partial_j A_{\nu,j}(\mathbf{\Phi} - \boldsymbol{\omega} t')$ and $F_{\nu,ij} = \partial_i A_{\nu,j} - \partial_j A_{\nu,i}$, these trajectories can be expressed in terms of the phase factor $\theta_\nu(t, \mathbf{\Phi})$ (5.53)

$$n_i(t, \mathbf{\Phi}) = -\frac{\partial \theta_\nu}{\partial \phi_i}(\mathbf{\Phi}; t) + A_{\nu,i}(\mathbf{\Phi} - \boldsymbol{\omega} t) - A_{\nu,i}(\mathbf{\Phi}), \tag{5.84}$$

such that after expanding the time evolution (5.80) of the wavefunction $\xi_\nu(t, \mathbf{\Phi})$ we obtain

$$\begin{aligned} \langle \hat{n}_i^2 \rangle_{\Psi_\nu(t)} = & \int \mathrm{d}^2\mathbf{\Phi}\ \tilde{\chi}_\nu(\mathbf{\Phi})^* \left( i \frac{\partial}{\partial \phi_i} + A_{\nu,i}(\mathbf{\Phi}) \right)^2 \tilde{\chi}_\nu(\mathbf{\Phi}) + \int \mathrm{d}^2\mathbf{\Phi}\ |\tilde{\chi}_\nu(\mathbf{\Phi})|^2 n_i(t, \mathbf{\Phi}) \\ & + 2 \int \mathrm{d}^2\mathbf{\Phi}\ J_{\nu,i}(\mathbf{\Phi}) n_i(t, \mathbf{\Phi}) + \int \mathrm{d}^2\mathbf{\Phi}\ |\tilde{\chi}_\nu(\mathbf{\Phi})|^2 g_{\nu,ii}(\mathbf{\Phi} - \boldsymbol{\omega} t) \qquad (5.85) \\ = & \langle \hat{n}_i^2 \rangle_{\Psi_\nu(t=0)} + \int \mathrm{d}^2\mathbf{\Phi}\ |\tilde{\chi}_\nu(\mathbf{\Phi})|^2 n_i(t, \mathbf{\Phi}) + 2 \int \mathrm{d}^2\mathbf{\Phi}\ J_{\nu,i}(\mathbf{\Phi}) n_i(t, \mathbf{\Phi}) \\ & + \int \mathrm{d}^2\mathbf{\Phi}\ |\tilde{\chi}_\nu(\mathbf{\Phi})|^2 (g_{\nu,ii}(\mathbf{\Phi} - \boldsymbol{\omega} t) - g_{\nu,ii}(\mathbf{\Phi})) \qquad (5.86) \end{aligned}$$

with the current density of the initial state

$$J_{\nu,i} = \frac{i}{2} \left( \tilde{\chi}_\nu^* \frac{\partial \tilde{\chi}_\nu}{\partial \phi_i} - \tilde{\chi}_\nu \frac{\partial \tilde{\chi}_\nu^*}{\partial \phi_i} \right) + |\tilde{\chi}_\nu|^2 A_{\nu,i} \tag{5.87}$$

satisfying $\langle \hat{n}_i \rangle_{\Psi_\nu(t=0)} = \int J_{\nu,i}(\mathbf{\Phi}) \mathrm{d}\mathbf{\Phi}$.

As a result, the time evolution of the spreading is given by the variance (5.35) of the classical trajectories and by two other terms

$$\begin{aligned} [(\Delta_Q \hat{n}_i)(t)]^2 = & [(\Delta_Q \hat{n}_i)(t=0)]^2 + \mathrm{Var}_{|\chi_\nu|^2}[n_i(t, \mathbf{\Phi})] \\ & + \int \mathrm{d}\mathbf{\Phi}\ |\tilde{\chi}_\nu(\mathbf{\Phi})|^2 \left( g_{\nu,ii}(\mathbf{\Phi} - \boldsymbol{\omega} t) - g_{\nu,ii}(\mathbf{\Phi}) \right) + \delta C_i(t), \end{aligned} \tag{5.88}$$

where $\delta C_i(t)$ is a bounded term taking the form of correlations between the classical trajectories $n_i(t, \mathbf{\Phi})$ and a current density of the initial state $J_{\nu,i}(\mathbf{\Phi})$

$$\delta C_i(t) = 2 \int \mathrm{d}^2\mathbf{\Phi}\ J_{\nu,i}(\mathbf{\Phi}) n_i(t, \mathbf{\Phi}) - 2 \langle \hat{n}_i \rangle_{\Psi_\nu(t=0)} \int \mathrm{d}^2\mathbf{\Phi}\ |\tilde{\chi}_\nu(\mathbf{\Phi})|^2 n_i(t, \mathbf{\Phi}) \tag{5.89}$$

As discussed above, the classical trajectories $n_i(t, \mathbf{\Phi})$ characterize the spreading of the projected observables $\hat{\Pi}_\nu \hat{n}_i \hat{\Pi}_\nu$, and the quantum metric relates the spreading of the projected and non-projected observables. Concerning Bloch oscillations and Bloch breathing, the important feature of this quantum metric contribution is that it is small compared to the initial value $[(\Delta_Q \hat{n}_i)(t=0)]^2$ in the case of small $\Delta\phi$, and it is vanishingly small at quasi-periods $T$ such that $\mathbf{\Phi} - \boldsymbol{\omega} T \simeq \mathbf{\Phi}$. The last term $\delta C_i(t)$ has the same features. It is vanishingly small at quasi-periods $T$ since $n_i(T, \mathbf{\Phi}) \simeq 0$. It is also small in the small $\Delta\phi$

limit since it can be written as classical correlations with respect to the density $|\tilde{\chi}_\nu(\mathbf{\Phi})|^2$ between the function $\partial_i\alpha(\mathbf{\Phi}) + A_{\nu,i}(\mathbf{\Phi})$ and $n_i(t, \mathbf{\Phi})$, with $\alpha(\mathbf{\Phi})$ the complex argument of $\tilde{\chi}_\nu(\mathbf{\Phi})$.

We thus recover the behaviors of Bloch oscillations and Bloch breathing discussed in Sec. 5.3.2: the spreading of the cat component remains almost constant $(\Delta_Q\hat{n}_i)(t) \simeq (\Delta_Q\hat{n}_i)(t = 0)$ in the case of localization in phase $\Delta\phi \ll 1$, and it refocuses at quasi-periods $T$, $(\Delta_Q\hat{n}_i)(T) \simeq (\Delta_Q\hat{n}_i)(t = 0)$ irrespective to the value of $\Delta\phi$.

Chapter 6

# Long-time topological dynamics and chaos

The model of rotors couped to a two-level system studied in Chap. 5 describes accurately the dynamics of quantum modes on short timescales for initial states localized in number of quanta. It is an approximation of more natural couplings between quantum harmonic oscillators and a qubit. In the rotor model, we consider a coupling of the qubit to the phase of the quantum modes only. When considering harmonic oscillators, natural coupling involve quadratures, such that the qubit couples also to the number of quanta. In this chapter, we study the consequences of topological coupling between two harmonic oscillators and a qubit on the dynamics on long time-scales and on the spectral properties of the model.

In Sec. 6.1, we define the topological coupling between two harmonic oscillators and a qubit. The main difference with Chap. 5 is that, due to the coupling of the qubit to the number of quanta, the topological nature of the coupling depends on the number of quanta, leading to topologically trivial and non-trivial domain in the space of number of quanta.

In Sec. 6.2, we study the long time dynamics of the system. Initial states prepared inside the topological domain leads to topological pumping dynamics on short timescales, non-adiabatic Landau-Zener scattering on intermediate timescales, and reaches a quasi-stationary state on long timescales with a notion of ergodicity within the topological domain. On the other hand, initial states prepared in the topologically trivial domain remains localized, without any notion of ergodicity.

In Sec. 6.3, we study the spectrum of the system from the perspective of quantum signatures of chaos. The two families of initial states translate into two families of eigenstates of the total system lying at the same energy. The trivial family of eigenstates has no signature of chaos, whereas the topological family displays such signatures. Estimating the Thouless energy of the topological family of eigenstates, we argue that they lie in the limit of validity of random matrix theory, in contrast with standard quantum chaotic systems.

This chapter is based on an article in preparation.

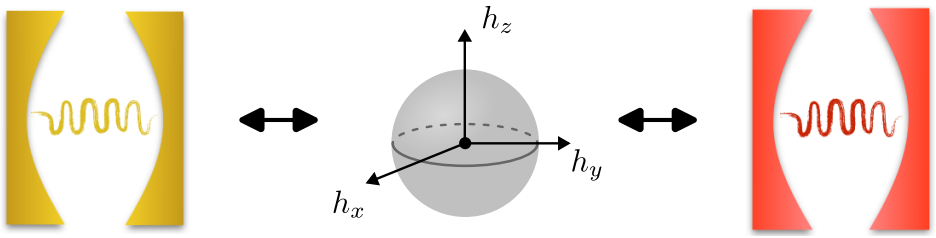


Figure 6.1: Two quantum harmonic oscillators, represented by cavities, coupled to a two level system, represented by the Bloch sphere. Generically every Pauli direction of the qubit can couple to the quadratures of the oscillators, leading to a total Hamiltonian of the form $\hat{H}_{\rm tot} = \hbar\omega_1 \hat{a}_1^\dagger \hat{a}_1 + \hbar\omega_2 \hat{a}_2^\dagger \hat{a}_2 + \sum_{\alpha=x,y,z} h_\alpha(\hat{a}_1, \hat{a}_1^\dagger, \hat{a}_2, \hat{a}_2^\dagger)\sigma_\alpha$.

## 6.1 Topological coupling between a qubit and two harmonic oscillators

In Chap. 5, we considered two quantum modes topologically coupled to a two-level system, a qubit. We described the modes by quantum rotors, with number of quanta and phase operators $\hat{n}$, $\hat{\phi}$. A rotor model is a natural approximation of a quantum harmonic oscillator, described by creation and annihilation operators $\hat{a}_i$, $\hat{a}_i^\dagger$, $i = 1, 2$, satisfying $[\hat{a}_i, \hat{a}_j^\dagger] = \delta_{ij}\mathbf{1}$. In terms of phase and number of quanta, $\hat{a}_i$ and $\hat{a}_i^\dagger$ correspond to $\sqrt{n_i}e^{\pm i\phi_i}$ in the classical limit. In this case, the natural couplings between a qubit and the modes involve linear combinations between the qubit observables and these operators. The rotor model ignores the $n_i$ dependence of these coupling. The analysis of Chap. 3 and Chap. 5 based on the phase dependence of the qubit Hamiltonian enables to define a notion of topological coupling between a qubit and quantum harmonic oscillators. Let us precise this definition.

### 6.1.1 Topological coupling

We consider two quantum harmonic oscillators coupled to a two level system, a qubit. We denote "mode" each harmonic oscillator in the following. The annihilation and creation operators of the modes are noted $\hat{a}_i$, $\hat{a}_i^\dagger$, $i = 1, 2$, satisfying $[\hat{a}_i, \hat{a}_j^\dagger] = \delta_{ij}\mathbf{1}$. Using similar notations as those of Chap. 2 and Chap. 5, the Hamiltonian of the total system reads

$$\hat{H}_{\rm tot} = \hbar\omega_1 \hat{a}_1^\dagger \hat{a}_1 + \hbar\omega_2 \hat{a}_2^\dagger \hat{a}_2 + \hat{H}, \tag{6.1}$$

where $\hat{H}$ contains the bare Hamiltonian of the qubit and the coupling to the modes. Generically, we decompose this Hamiltonian on the Pauli matrices of the qubit, considering that each of them can couple to the quadratures of the modes,

$$\hat{H} = \sum_{\alpha=x,y,z} h_\alpha(\hat{a}_1, \hat{a}_1^\dagger, \hat{a}_2, \hat{a}_2^\dagger)\sigma_\alpha. \tag{6.2}$$

This is represented schematically on Fig. 6.1. For example, for one mode only, the Hamiltonian of the frequently considered quantum Rabi model [218,219] contains the bare qubit Hamiltonian, corresponding to a $z$ component in the above decomposition, and a coupling to a quadrature in the perpendicular $x$ component, $\hat{H}/\hbar = \omega_q\sigma_z/2 - ig(\hat{a} - \hat{a}^\dagger)\sigma_x$, with $\omega_q$ the qubit bare frequency and $g$ a coupling strength.

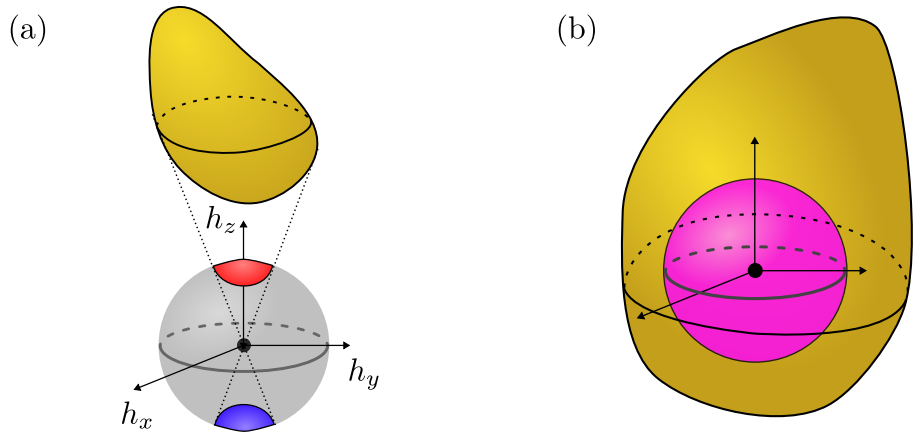


Figure 6.2: Topologically trivial and non-trivial coupling. Yellow surface: closed surface defined by the ensemble of vectors $\boldsymbol{h}(\phi_1, \phi_2, n_1, n_2)$ for all values of the phases $\phi_1, \phi_2 \in [0, 2\pi]$ at fixed $(n_1, n_2)$. (a) Trivial coupling: the surface does not enclose the origin. In blue and red: ensemble of respectively excited and ground state of the qubit for all values of phases. (b) Topological coupling: the surface encloses the origin. Any qubit state on the Bloch sphere corresponds either to a ground or excited state depending on the value of the phases.

As in Chap. 3, the definition of topological couplings relies on a classical description of the modes, because we need to assign definite values to both $n_i$ and $\phi_i$ variables. Of course, having said this, the model has to be solved fully quantum-mechanically. It amounts to replacing respectively the operators $\hat{a}_i$ and $\hat{a}_i^\dagger$ by the classical variables $\sqrt{n_i}e^{i\phi_i}$ and $\sqrt{n_i}e^{-i\phi_i}$, where the phase $\phi_i$ and number of quanta $n_i$ satisfy the classical Poisson bracket relation $\{\hbar n_i, \phi_j\} = \delta_{ij}$. This is precised by considering the Hamiltonian $\hat{H}$ in the Weyl representation introduced in Chap. 2, see appendix 6.A for details. We then consider the Hamiltonian of the qubit parametrized by the phase space variables of the modes

$$H(\phi_1, \phi_2, n_1, n_2) = \boldsymbol{h}(\phi_1, \phi_2, n_1, n_2) \cdot \boldsymbol{\sigma}, \tag{6.3}$$

with $\boldsymbol{h}(\phi_1, \phi_2, n_1, n_2)$ a vector of $\mathbb{R}^3$ parametrized by the phases and numbers of quanta of the modes. At fixed value of the number of quanta, we recover a quantum system coupled to two periodic phases for which we can define the regime of topological coupling as in section 3.2.1. We provide here a simple condition for a two-level system.

When we fix $n_1, n_2$ and vary the periodic phases $\phi_1, \phi_2$ in their compact configuration space $[0, 2\pi]$, the ensemble of vectors $\boldsymbol{h}(\phi_1, \phi_2, n_1, n_2)$ defines a closed surface in $\mathbb{R}^3$. Such a surface is represented schematically on Fig. 6.2. The bare qubit Hamiltonian $\hbar\omega_q\sigma_z/2$ leads to a component of these vectors along the $z$-axis, defining the center of the surface. The size of the surface is related to the amplitude of the couplings between the qubit and the phases.

In the usual case where the qubit bare transition frequency $\omega_q$ is very large compared to these couplings, the surface is high along the $z$ direction and does not enclose the origin. This is the situation of topologically trivial coupling, represented on Fig. 6.2(a). The eigenstates of the qubit for a given value of phases and numbers of quanta are given

by the Bloch vectors $\pm\boldsymbol{h}(\phi_1,\phi_2,n_1,n_2)/|\boldsymbol{h}(\phi_1,\phi_2,n_1,n_2)|$. The ensemble of excited states of the qubit at fixed $(n_1,n_2)$ is represented on the Bloch sphere by the projection of the surface, represented in red, whereas the ensemble of qubit ground states is the blue surface. Since the blue and red surfaces do not overlap, we can determine whether the qubit is in its ground or excited state without any knowledge on the state of the modes. This is the common situation of a weak coupling.

In contrast, the topological coupling corresponds to the case where the surface encloses the origin. Then any point on the Bloch sphere can correspond either to a ground or excited state, depending on the state of the modes. There is no relevant notion of qubit ground or excited state independently of the modes. The topological coupling is a regime of strong coupling, in the sense explained above: the coupling of the qubit to the phases have to be of same order of magnitude as the bare qubit frequency. We will consider linear couplings between the modes' quadratures and the qubit Pauli matrices, of the form $g(\hat{a}_i+\hat{a}_i^\dagger)\sigma_\alpha$, such that topological coupling requires $g\sqrt{n_i}$ of same order of magnitude as the bare qubit frequency. Moreover, this picture shows that the topological coupling requires to couple all three Pauli matrices of the qubit to the quadratures of the modes.

### 6.1.2 Model

Any model of quantum system topologically coupled to classical periodic phases $\phi_1$, $\phi_2$ provides a model of topological coupling between harmonic oscillators by replacing $\cos(\phi_i)$ and $\sin(\phi_i)$ by respectively $(\hat{a}_i+\hat{a}_i^\dagger)/2$ and $(\hat{a}_i-\hat{a}_i^\dagger)/(2i)$. In the following numerical results, we consider the simplest example of Hamiltonian displaying this regime of topological coupling, the quantum oscillators version of the half Bernevig-Hughes-Zhang model considered in Chap. 5:

$$\hat{H}/\hbar = -ig_1(\hat{a}_1-\hat{a}_1^\dagger)\sigma_x + ig_2(\hat{a}_2-\hat{a}_2^\dagger)\sigma_y + \left(\frac{\omega_q}{2} - g_1(\hat{a}_1+\hat{a}_1^\dagger) - g_2(\hat{a}_2+\hat{a}_2^\dagger)\right)\sigma_z, \quad (6.4)$$

with $\omega_2/\omega_q = 0.1$ ; $g_1/\omega_q = 0.0925$ ; $g_2/\omega_q = 0.0675$, and we use the same ratio between the frequencies as in Chap. 5, $\omega_1/\omega_2 = \frac{1+\sqrt{5}}{2} \simeq 1.618$. We thus consider the regime where the coupling rates are of the same order of magnitude as the frequency of the modes. This is a regime of deep strong coupling [220, 221]. In the following, we express the energies in units of the bare transition energy of the qubit $\hbar\omega_q$.

We use the same notations as in Chap. 5, $\boldsymbol{\Phi} = (\phi_1,\phi_2)$ and $\boldsymbol{N} = (n_1,n_2)$. The qubit Hamiltonian with classical description of the slow modes (*i.e.* its Weyl symbol) is given by Eq. (6.3) with

$$h_x(\boldsymbol{\Phi},\boldsymbol{N})/\hbar = 2g_1\sqrt{n_1}\sin(\phi_1), \quad (6.5a)$$
$$h_y(\boldsymbol{\Phi},\boldsymbol{N})/\hbar = -2g_2\sqrt{n_2}\sin(\phi_2), \quad (6.5b)$$
$$h_z(\boldsymbol{\Phi},\boldsymbol{N})/\hbar = \frac{\omega_q}{2} - 2g_1\sqrt{n_1}\cos(\phi_1) - 2g_2\sqrt{n_2}\cos(\phi_2), \quad (6.5c)$$

such that the symbol of the total Hamiltonian reads

$$H_{\mathrm{tot}}(\boldsymbol{\Phi},\boldsymbol{N}) = \hbar\omega_1 n_1 + \hbar\omega_2 n_2 + \boldsymbol{h}(\boldsymbol{\Phi},\boldsymbol{N})\cdot\boldsymbol{\sigma}. \quad (6.6)$$

The following numerical results are obtained from an exact diagonalization of the Hamiltonian in a truncated Hilbert space. We detail the numerical method in appendix 6.C.

The frequencies of the modes are chosen to be an order of magnitude smaller than the bare transition frequency of the qubit, leading to a slow-fast system with the slow modes and the fast qubit. We thus describe the dynamics of this system using the general adiabatic theory described in Chap. 2.

## 6.2 Dynamics

### 6.2.1 Adiabatic dynamics

#### Domain of adiabaticity in phase space

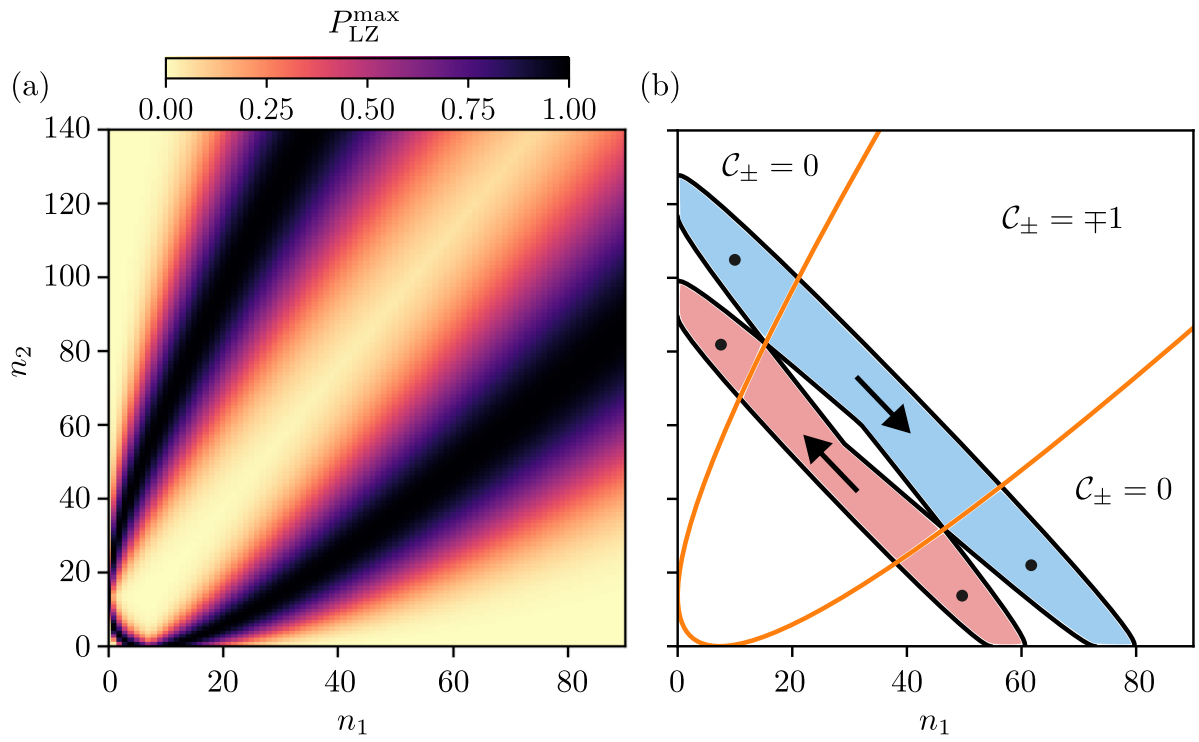


Figure 6.3: Adiabatic dynamics. (a) Domain of adiabaticity in phase space, estimated with a maximum of Landau-Zener transition probability. The adiabatic theory describes the evolution of states localized in the region of small $P_{\mathrm{LZ}}^{\max}$. When $P_{\mathrm{LZ}}^{\max} = 1$, the gap of the qubit closes for one value of phases, corresponding to the orange curve on (b). (b) Sketch of adiabatic classical trajectories of the two adiabatic subspaces. At a fixed energy $E$, they are confined in domains of constant energy $\tilde{\mathcal{E}}_\pm(\boldsymbol{\Phi}, \boldsymbol{N}) = E$, represented respectively in red and blue for the subspaces $+$ and $-$. The regions of non-zero Chern number are the domains of topological coupling and lead to topological drifts in opposite directions for the two subspaces, represented by opposite arrows. In the region of vanishing Chern number, the trajectories are confined without average drift, represented by a black dot.

The first step of the adiabatic theory is to identify its domain of validity in the phase space of the slow modes, as detailed in Sec. 2.4.4. To do so, we consider the dimensionless adiabatic ratio $\varepsilon_{\mathrm{adiab}}(\boldsymbol{\Phi}, \boldsymbol{N})$ which has to be small, defined by Eqs. (2.101) to (2.103)

and (2.106). Following the notations of Chap. 2, we note $\mathcal{E}_\pm(\boldsymbol{\Phi},\boldsymbol{N})$ and $|\psi_\pm(\boldsymbol{\Phi},\boldsymbol{N})\rangle$ the energy and eigenstates of the symbol of the total Hamiltonian (6.6). We have

$$\mathcal{E}_\pm(\boldsymbol{\Phi},\boldsymbol{N}) = \hbar\omega_1 n_1 + \hbar\omega_2 n_2 \pm |\boldsymbol{h}(\boldsymbol{\Phi},\boldsymbol{N})|. \tag{6.7}$$

The condition (2.103) is not involved for a two level fast system, since the two level energy tensor vanishes. As a first estimate of the adiabatic ratio, let us consider the sole conditions (2.102) and (2.101) which provide

$$\varepsilon_{\text{adiab}}(\boldsymbol{\Phi},\boldsymbol{N}) = \left|\sum_{i=1}^{2} \frac{\hbar\omega_i A_{+-,\phi_i}(\boldsymbol{\Phi},\boldsymbol{N})}{\mathcal{E}_+(\boldsymbol{\Phi},\boldsymbol{N}) - \mathcal{E}_-(\boldsymbol{\Phi},\boldsymbol{N})}\right| \tag{6.8}$$

with $A_{\mu\nu,\phi_i} = i\,\langle\psi_\mu|\partial_{\phi_i}\psi_\nu\rangle = i\,\langle\psi_\mu|\,\frac{\partial H}{\partial\phi_i}\,|\psi_\nu\rangle\,/(\mathcal{E}_\nu - \mathcal{E}_\mu)$.

We represent the domain of validity of adiabatic dynamics projected in the $(n_1, n_2)$ plane. To do so, at a given value of number of quanta, we use the adiabatic parameter (6.8) to express a maximum probability of Landau-Zener transition, following the analysis of Chap. 1:

$$P_{\text{LZ}}^{\max}(\boldsymbol{N}) = \max_{\boldsymbol{\Phi}\in[0,2\pi]^2} \exp\left(-\frac{\pi}{4\varepsilon_{\text{adiab}}(\boldsymbol{\Phi},\boldsymbol{N})}\right). \tag{6.9}$$

We come back to the Landau-Zener processes in the next section, explaining in more details the meaning of this maximum of Landau-Zener transition probability. In the regions of small $P_{\text{LZ}}^{\max}$, the dynamics is well described by the adiabatic theory. It is represented for the model on Fig. 6.3(a). The black domain corresponds to a transition probability close to one, meaning that the adiabatic parameter is high for some values of phases: adiabaticity breaks down when the phase density approaches this point.

### Classical equations of motion

Let us consider an initial state located in the phase space region for which $\varepsilon_{\text{adiab}}(\boldsymbol{\Phi},\boldsymbol{N})$ is small (see Fig. 6.3(a)). It decomposes into a sum of two adiabatic states, lying in the adiabatic subspaces $\mathcal{H}_\pm$ discussed in the previous chapter 5. The dynamics within each subspace at first order in adiabatic expansion is governed by the equations of motion[1] discussed in Sec. 2.4.2 of Chap. 2:

$$\dot{n}_i = \frac{1}{\hbar}\frac{\partial\tilde{\mathcal{E}}_\pm}{\partial\phi_i} + \frac{1}{\hbar}\sum_j \left(F_{\pm,\phi_i\phi_j}\frac{\partial\tilde{\mathcal{E}}_\pm}{\partial n_j} - F_{\pm,\phi_i n_j}\frac{\partial\tilde{\mathcal{E}}_\pm}{\partial\phi_j}\right), \tag{6.10a}$$

$$\dot{\phi}_i = -\frac{1}{\hbar}\frac{\partial\tilde{\mathcal{E}}_\pm}{\partial n_i} - \frac{1}{\hbar}\sum_j \left(F_{\pm,n_i\phi_j}\frac{\partial\tilde{\mathcal{E}}_\pm}{\partial n_j} - F_{\pm,n_i n_j}\frac{\partial\tilde{\mathcal{E}}_\pm}{\partial\phi_j}\right). \tag{6.10b}$$

The Hamiltonian containing the modified energy function

$$\tilde{\mathcal{E}}_\pm(\boldsymbol{\Phi},\boldsymbol{N}) = \hbar\omega_1 n_1 + \hbar\omega_2 n_2 \pm |\boldsymbol{h}(\boldsymbol{\Phi},\boldsymbol{N})| + M_\pm(\boldsymbol{\Phi},\boldsymbol{N}), \tag{6.11}$$

[1] We have factors $1/\hbar$ in the equations of motion because $n_i$ and $\phi_i$ are dimensionless, namely their Poisson bracket is $\{\hbar n_i, \phi_i\} = 1$. Writing Eqs (2.78) with $x_i = \hbar n_i$ and $p_i = \phi_i$ leads to (6.10). In other words, Eqs. (6.10) are the Hamilton equations of motion associated to the classical Hamiltonian $\tilde{\mathcal{E}}_\pm$ and the symplectic form $\Omega_\pm = \hbar\sum_i \mathrm{d}\phi_i \wedge \mathrm{d}n_i + \hbar F_\pm$, at first order in the Berry curvature $F_\pm$.

where the modification of energy $M_\pm(\boldsymbol{\Phi}, \boldsymbol{N})$ is given by[2] Eq. (2.76). The Berry curvature is defined by

$$F_{\pm,\alpha\beta}(\boldsymbol{\Phi}, \boldsymbol{N}) = i\left(\langle\partial_\alpha\psi_\pm(\boldsymbol{\Phi}, \boldsymbol{N})|\partial_\beta\psi_\pm(\boldsymbol{\Phi}, \boldsymbol{N})\rangle - (\alpha \leftrightarrow \beta)\right), \tag{6.12}$$

with the phase space coordinate notation $\boldsymbol{\xi} = \{\boldsymbol{\Phi}, \boldsymbol{N}\} = \{\xi^\alpha\}$ and $\partial_\alpha = \frac{\partial}{\partial\xi^\alpha}$.

Let us show that we recover the equations of motion of the rotor model in the limit of large $n_1$ and $n_2$. For a coupling between the qubit and the modes linear in the quadratures, such as the model we consider, we show in Appendix 6.B the following scaling of the energies and Berry curvature components in the limit $n_1, n_2 \gg 1$

$$|\boldsymbol{h}| = \mathcal{O}\left(\sqrt{n_i}\right) \quad ; \quad M_\pm = \mathcal{O}\left(\frac{1}{\sqrt{n_i}}\right) \tag{6.13}$$

$$F_{\pm,\phi_i\phi_j} = \mathcal{O}(1) \quad ; \quad F_{\pm,\phi_i n_j} = \mathcal{O}\left(\frac{1}{n_j}\right) \quad ; \quad F_{\pm,n_i n_j} = \mathcal{O}\left(\frac{1}{n_i n_j}\right) \tag{6.14}$$

such that, in the limit $n_1, n_2 \gg 1$, the classical equations of motions reads

$$\dot{n}_i = \pm\frac{1}{\hbar}\frac{\partial|\boldsymbol{h}|}{\partial\phi_i} + \sum_{j\neq i}\omega_j F_{\pm,\phi_i\phi_j} + \mathcal{O}\left(\frac{1}{\sqrt{n_i}}\right), \tag{6.15}$$

$$\dot{\phi}_i = -\omega_i + \mathcal{O}\left(\frac{1}{\sqrt{n_i}}\right). \tag{6.16}$$

We thus recover Eqs (5.1) and the topological pumping dynamics when the Berry curvature carries a non-vanishing Chern number, which depends on the value of $\boldsymbol{N}$

$$\mathcal{C}_\pm(\boldsymbol{N}) = \frac{1}{2\pi}\int_{[0,2\pi]^2} \mathrm{d}^2\boldsymbol{\Phi}\; F_{\pm,\phi_1\phi_2}(\boldsymbol{\Phi}, \boldsymbol{N}) \in \mathbb{Z}. \tag{6.17}$$

The regions of non-vanishing Chern number correspond to the topological coupling regime defined in Sec. 6.1. The Chern number is an integer associated to a gapped spectrum of qubit eigenstates. Discontinuous changes of Chern number occur when the gap closes for at least one value of phase $\boldsymbol{\Phi}$, which correspond to the curve $P_{\mathrm{LZ}}^{\max} = 1$ on Fig. 6.3(a) and to the orange curve on Fig. 6.3(b). It separates the $(n_1, n_2)$ plane into regions of different Chern number configurations.

### Classical trajectories

We sketch on Fig. 6.3(b) the structures of the classical trajectories (6.10) projected on the $(n_1, n_2)$ plane. At a given energy $E$, the classical trajectories lie in the region of phase space of constant Hamiltonian $\tilde{\mathcal{E}}_\pm(\boldsymbol{\Phi}, \boldsymbol{N}) = E$. The projection of these domains on the $(n_1, n_2)$ plane for the ground and excited adiabatic subspaces are represented respectively in blue and red on Fig. 6.3(b). Within the region of non-vanishing Chern number, the topological pumping dynamics corresponds to an average drift in $\boldsymbol{N}$ represented by the arrows, in opposite directions for the two subspaces, as described in Chap. 5. For the numerical illustration, we used $\mathcal{E}_\pm(\boldsymbol{\Phi}, \boldsymbol{N})$ as an approximation of $\tilde{\mathcal{E}}_\pm(\boldsymbol{\Phi}, \boldsymbol{N})$, ignoring the subdominant correction $M_\pm(\boldsymbol{\Phi}, \boldsymbol{N})$.

[2]The expression of the modified energy is obtained from Eq. (2.76) with $x_i = \hbar n_i$ and $p_i = \phi_i$.

In the region of zero Chern number, the trajectories correspond to confined Bloch oscillations described in Chap. 5, without any topological drift. As such, an initial state prepared outside the topological region – at a distance to the topological boundaries larger than the amplitude of Bloch oscillations – remains confined within the domain of adiabaticity, whereas a preparation in the topological region leads to a topological drift towards a domain of breakdown of adiabaticity, leading to a Landau-Zener scattering process discussed below. Topology manifests itself as an inherent breakdown of adiabaticity at an intermediate timescale, and leads to a new type of dynamics described below.

### 6.2.2 Landau-Zener scattering

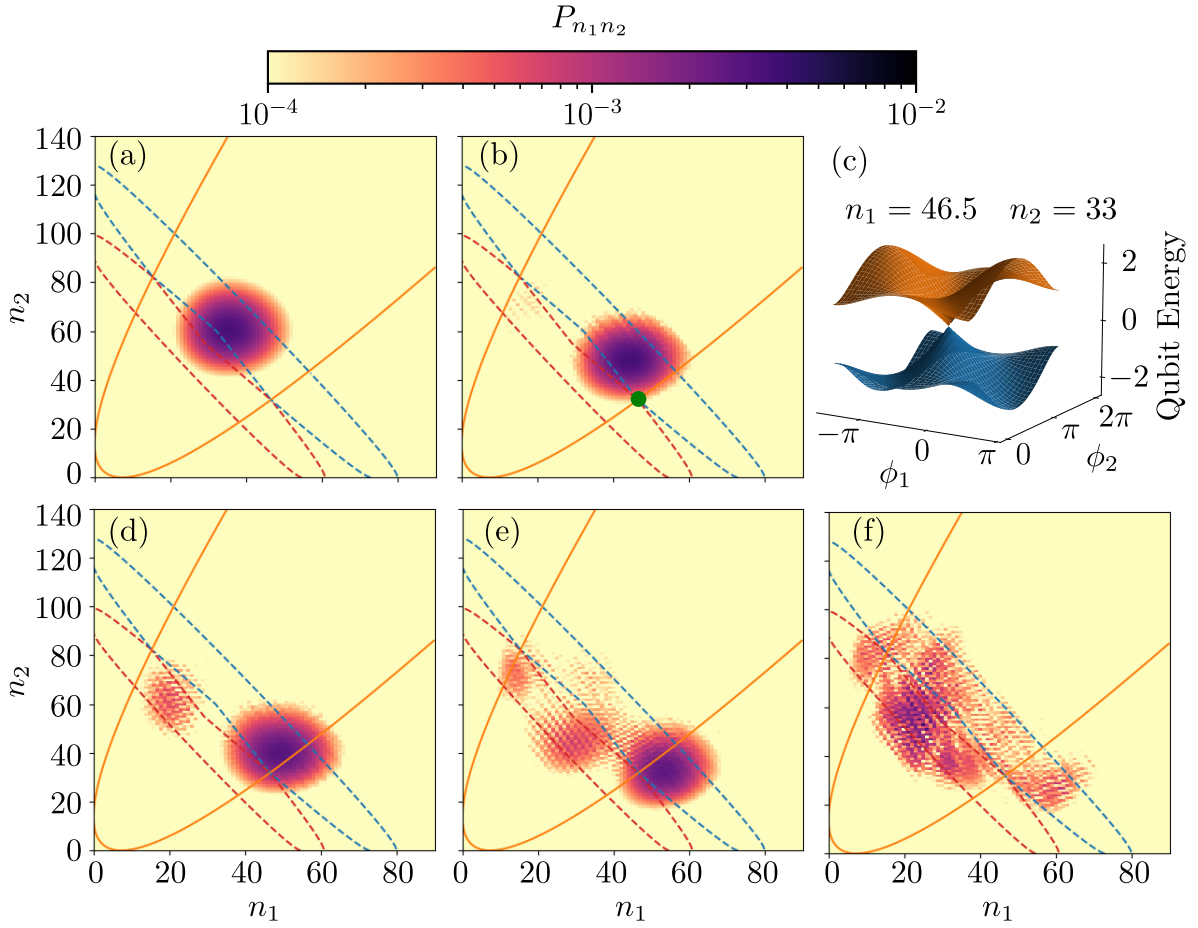


Figure 6.4: Landau-Zener scattering. (a) Photon number distribution $P_{n_1 n_2}$ of the initial state. (b) Adiabatic drift in (mostly) the ground-space, $t = 12.7\ T_1$. (c) Qubit ground and excited energy $\pm|\boldsymbol{h}(\boldsymbol{\Phi}, \boldsymbol{N})|$ respectively in blue and orange, for $\boldsymbol{N} = (46.5, 33)$ on the topological transition line (green point on (b)). The gap closes locally at $\boldsymbol{\Phi} = (0, \pi)$. (d) First Landau-Zener tunnelling at $t = 16.11\ T_1$ when the center of wavepacket reaches a small gap minimum in phase space. (e) Second Landau-Zener tunneling at $t = 27.92\ T_1$ (f) Succession of Landau-Zener tunnelling leading to a complex scattering process between the two adiabatic subspaces, $t = 48.32\ T_1$.

### Initial state decomposition

Let us start our discussion of the Landau-Zener scattering by an illustration on a numerical example. We first discuss briefly the initial state. We consider the quantum modes in coherent states $|\alpha_i\rangle$, with $\alpha_i = \sqrt{n_i^0}e^{i\phi_i^0}$, $n_i^0$ and $\phi_i^0$ the respective average number of quanta and phase of the coherent state, and the qubit in the groundstate associated to the center of the coherent state

$$|\Psi(t=0)\rangle = |\alpha_1\rangle \otimes |\alpha_2\rangle \otimes \left|\psi_-(\boldsymbol{\Phi}^0, \boldsymbol{N}^0)\right\rangle . \tag{6.18}$$

We consider an initial state in the topological region. The photon number distribution of this initial state is represented on Fig. 6.4(a), for $n_1^0 = 36$, $n_2^0 = 61$, $\phi_1^0 = 0$, $\phi_2^0 = \pi/2$. We represent in blue and red the lines delimitating the phase space regions of the classical dynamics corresponding to the energy of the initial state $E = \langle\Psi(t=0)|\, \hat{H}_{\text{tot}}\, |\Psi(t=0)\rangle$.

As shown in Chap. 5, such an initial state is close to but not exactly an adiabatic state: it splits in two components of unequal weights during the adiabatic dynamics. The time evolution at $t = 12.7\ T_1$, with $T_1 = 2\pi/\omega_1$ the period of the first mode, is represented on Fig. 6.4(b). The component in the excited band is small for large $n_i^0$, barely seen in the red excited region, whereas the dominant ground-space component drifts from mode 2 to mode 1, with its center localized in the blue ground region.

We estimate the weight $W_+$ in the excited subspace from the expression (5.25) which provides a contribution $(\Delta\phi_i)^2 g_{-,\phi_i\phi_i}(\boldsymbol{\Phi}^0, \boldsymbol{N}^0)$ to the weight due to the quantum fluctuation $\Delta\phi_i$ of each phase variable and due to the phase dependence of the qubit eigenstates, with $g_-$ the quantum metric of the qubit groundstates[3]. The formula does not take into account the dependence on $\boldsymbol{N}$ of the eigenstates. The spreads in photon number and phase of a coherent state are given respectively by $\Delta n_i = \sqrt{n_i^0}$, and $\Delta\phi_i = 1/(2\Delta n_i) = 1/(2\sqrt{n_i^0})$. We extend the relation (5.25) to take into account the dependence on the number of photons as

$$W_+ \approx \frac{1}{4n_1^0} g_{-,\phi_1\phi_1}(\boldsymbol{\Phi}^0, \boldsymbol{N}^0) + \frac{1}{4n_2^0} g_{-,\phi_2\phi_2}(\boldsymbol{\Phi}^0, \boldsymbol{N}^0) + n_1^0 g_{-,n_1n_1}(\boldsymbol{\Phi}^0, \boldsymbol{N}^0) + n_2^0 g_{-,n_2n_2}(\boldsymbol{\Phi}^0, \boldsymbol{N}^0) \tag{6.19}$$

where the quantum metric components satisfy the scaling relations $g_{-,\phi_i\phi_i} = \mathcal{O}(1)$ and $g_{-,n_in_i} = \mathcal{O}(1/(n_i^2))$ for $n_i \gg 1$.

Let us now illustrate the Landau-Zener scattering process, leading to a splitting of the wavepacket and a reverse direction of pumping. A similar process was discussed qualitatively in [193] in the restricted case where one of the two modes is not a dynamical quantum mode but a Floquet drive, which in particular does not allow for the following analysis based on energy domains.

### Landau-Zener tunnelling

Landau-Zener transitions split the wavepacket, and correspond to partial tunneling between the two adiabatic subspaces. Following the analysis of Chap. 1, we expect such a tunnelling to occur when the center of the wavepacket reaches a local gap minimum, located at a point $(\boldsymbol{\Phi}_{\text{col}}, \boldsymbol{N}_{\text{col}})$ of phase space. This is illustrated on Fig. 6.4(c) where we

[3] We consider here the qubit eigenstates rather than adiabatic states as a first estimate.

represent the qubit energies $\pm|\boldsymbol{h}|(\boldsymbol{\Phi}, \boldsymbol{N})$ for $\boldsymbol{N} = (46.5, 33)$ on the topological boundary (green point on Fig. 6.4(b)), the gap closing locally for $\boldsymbol{\Phi} = (0, \pi)$. A wavepacket component of relative weight proportional to $\exp(-\pi/(4\epsilon_{\text{adiab}}(\boldsymbol{\Phi}_{\text{col}}, \boldsymbol{N}_{\text{col}})))$ scatters between the two subspaces. In particular, the relative weight is given by the maximum Landau-Zener probability $P_{\text{LZ}}^{\max}(\boldsymbol{N}_{\text{col}})$ (6.9), when the phase distribution of the state is localized around $(0, \pi)$. Note that when the center of wavepacket approaches the topological transition line in $\boldsymbol{N}$-space, Landau-Zener tunnelling does not immediately occur. It requires the phase distribution of the state (which is almost translated in time on the torus according to (6.16)) to be localized near $(0, \pi)$ in $\boldsymbol{\Phi}$-space. We observe such a transition at $t = 16.11\ T_1$ (Fig. 6.4(d)), where part of the wavepacket tunneled from the blue to the red region. This component now follows the adiabatic dynamics of the excited space, pumping energy in the direction opposite to the initial component, such that it drifts away from the Landau-Zener region and does not tunnel back in the ground-space (in first approximation).

We have a succession of Landau-Zener splittings of the initial wavepacket, at all times where the phases reach a gap minimum, which are separated typically by timescales of order of magnitude of a few modes' period. Indeed, a second transition is visible at $t = 27.92\ T_1$ (Fig. 6.4(e)). The succession of Landau-Zener tunnelling leads to a complex scattering process between the two adiabatic subspaces, until most of the ground-space component has tunneled to the excited space (Fig. 6.4(f) at $t = 48.32\ T_1$). In Fig. 6.4(f), we also see weight in the ground-space region, due to split wavepackets that underwent already two Landau-Zener scattering.

We expect this process combining topological pumping and Landau-Zener scattering to occur in any model of topological coupling between two harmonic oscillators and a qubit. Indeed, such a model contains topologically distinct sectors in $\boldsymbol{N}$-space, associated to regimes of topologically trivial or non-trivial coupling. The topological pumping dynamics carries wavepackets towards transition curves between these domains, necessarily associated to a gap closure, *i.e.* a breakdown of adiabaticity and a Landau-Zener scattering process.

### 6.2.3 Long time quasi-stationary state

After the first Landau-Zener scattering on a topological boundary, the wavepacket has been split in several wavepackets in the excited band. Each of them evolves adiabatically, with a pumping in the opposite direction toward the other topological boundary. This leads to a series of Landau-Zener scattering events, separated by the time of pumping between the two topological boundaries.

After a few scattering processes, the wavepacket reaches a quasi-stationary state delocalized in $\boldsymbol{N}$ in the region delimited approximately by the topological transition lines and the region of energy conservation. We represent the photon number distribution of this long time quasi-stationary state at $t = 150\ T_1$ on Fig. 6.5(a).

We obtain a notion of ergodicity in phase space, in the sense that at long times the state is delocalized in the entire region allowed by energy conservation, and (approximately) by the topological constraint.

On the other hand, an initial state prepared outside the topological region remains localized in $\boldsymbol{N}$ space, on a scale given by the amplitude of Bloch oscillations, without any

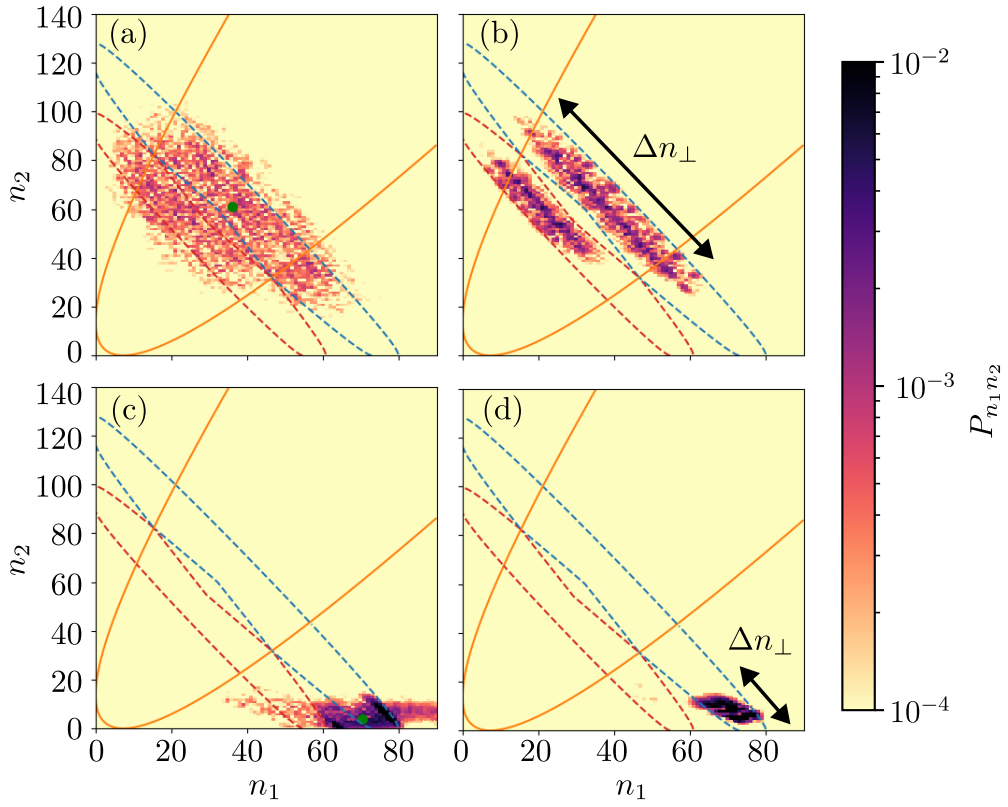


Figure 6.5: Long time quasi-stationary states vs eigenstates. (a) Quasi-stationary state at $t = 150\ T_1$ for an initial state prepared inside the topological region (center on green dot). After multiple Landau-Zener scattering processes between the topological regions, the state is delocalized in a domain delimited by the topological boundaries and energy conservation. (b) Eigenstate delocalized within the topological region, with components on both adiabatic domains. (c) Quasi-stationary state at $t = 150\ T_1$ for an initial state outside topological region (initial center on green dot). The state remains localized outside the topological domain. (d) Eigenstate localized outside the topological region, confined mainly on one adiabatic domain (the blue ground-space domain).

notion of ergodicity. We represent such a state at $t = 150\ T_1$ on Fig. 6.5(c), for an initial state prepared with $\boldsymbol{N}^0 = (70.4, 4)$ (green dot).

The two initial states corresponding to the long time quasi-stationary states of Fig. 6.5(a,c) have the same total energy $E = \langle\Psi|\,\hat{H}_{\rm tot}\,|\Psi\rangle \simeq 10.7$. We identified two families of initial states, whether they lie inside or outside the topological region, leading to very different long times quasi-stationary states, delocalized or not, related to a presence or absence of notion of ergodicity. It is natural to wonder whether the very different natures of the quasi-stationary long time states in different parts of the phase diagram are also present for the corresponding eigenstates. Besides, ergodicity is often discussed in relation with chaos. We now turn to the study of the eigenstates and spectrum, from the perspective of quantum signatures of chaos.

## 6.3 Eigenstates and spectrum

### 6.3.1 Two families of eigenstates

The two examples of long time quasi-stationary states, originating from a preparation inside or outside the topological region (see Fig. 6.5(a,c)), have the same average energy $E \simeq 10.7$. We show on Fig. 6.5(b) an eigenstate of similar energy whose average number of quanta is located inside the topological region. It has the same qualitative feature as the long time quasi-stationary state of Fig. 6.5(a): it is delocalized (approximately) inside the entire topological region, constrained by the energy boundaries of the classical dynamics. On the other hand, on Fig. 6.5(d), we represent an eigenstate at approximately the same energy located outside the topological region: it is localized in $\boldsymbol{N}$-space and lies only within one of the two adiabatic regions (in this case the ground-space).

Let us describe more quantitatively these two families of eigenstates. On Fig. 6.6(a), every point corresponds to the average value of $\hat{\boldsymbol{N}}$ in one eigenstate. The color is the spreading $\Delta n_\perp$ in the direction of pumping $n_\perp = (-\omega_2 n_1 + \omega_1 n_2)/|\boldsymbol{\omega}|$ (see Fig. 6.5(b,d)). Every eigenstate located outside the topological sector is localized in the pumping direction, corresponding to a small $\Delta n_\perp$, whereas every eigenstate located inside the topological domain is extended in the pumping direction, with a large $\Delta n_\perp$ of the order of magnitude of the width of the topological domain. Note that we consider only the eigenstates of energies not affected by the numerical truncation of Hilbert space, see appendix 6.C for details.

On Fig. 6.6(b), we represent in color the relative weight $W_+ - W_-$ of each eigenstate in the two adiabatic subspaces. The weight $W_\pm$ of an eigenstate of energy $E$ is computed by summing the photon number probability $P_{n_1 n_2}$ of the eigenstate for $(n_1, n_2)$ lying in the blue or red region of Fig. 6.3(b) associated to its eigenenergy $E$. The eigenstates located outside the topological region have a relative weight of approximately $\pm 1$, corresponding to a localization on one of the two adiabatic subspaces only. On the other hand, the eigenstates located inside the topological domain are delocalized in both adiabatic subspaces, with approximately $W_+ - W_- \simeq -0.3$ (due to the larger extension of ground-space region, see Fig. 6.5(b)). We identify a third family of eigenstates, whose average value of $\hat{\boldsymbol{N}}$ lies near the topological boundaries, which have different repartition between the ground and excited spaces. We interpret them as a signature of the dynamical mechanism of successive Landau-Zener transitions occurring in this region of breakdown of adiabaticity.

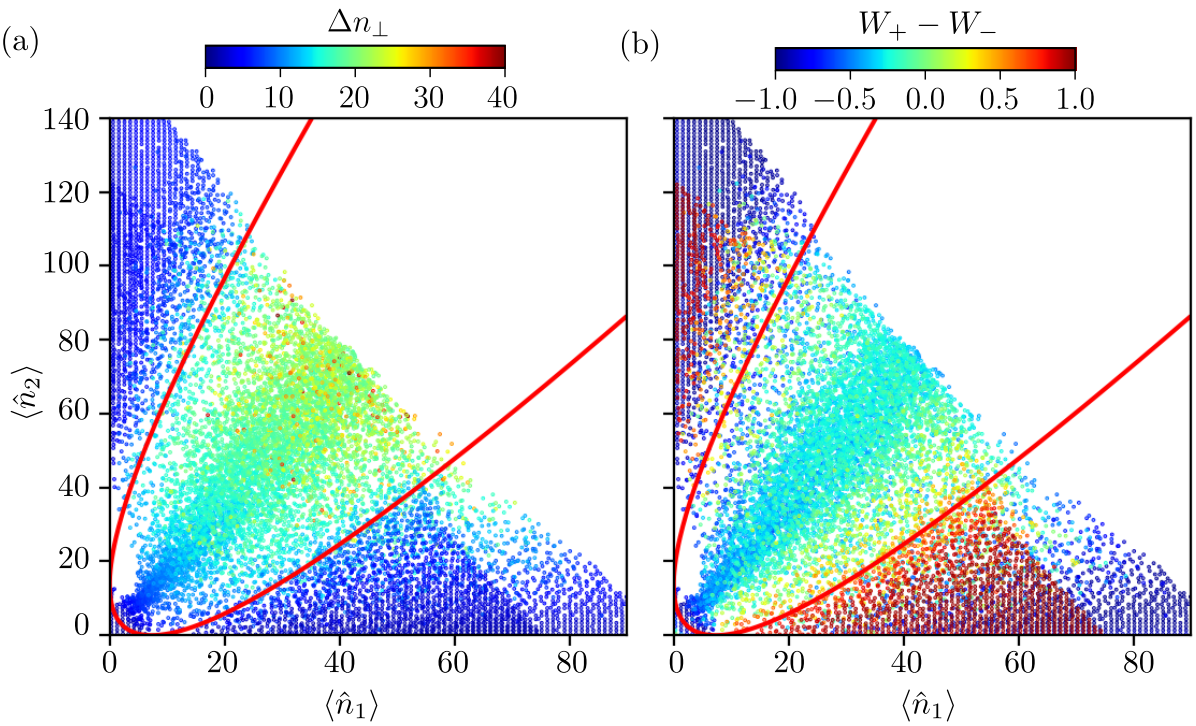


Figure 6.6: Two families of eigenstates. Every point corresponds to the average value of $\hat{\boldsymbol{N}}$ in an eigenstate. (a) In color: spreading $\Delta n_\perp = \sqrt{\langle \hat{n}_\perp^2 \rangle - \langle \hat{n}_\perp \rangle^2}$ of the eigenstate in the pumping direction (see Fig. 6.5(b,d)). Eigenstates outside the topological domain are localized, with small $\Delta n_\perp$. Eigenstates inside the topological region are delocalized in the pumping direction, in between the two topological boundaries. (b) Distribution of the eigenstates between the two adiabatic subspaces. In color: difference of weights $W_+ - W_-$ between the two subspaces. In the topologically trivial domain (and far from the topological boundaries), the eigenstates are localized within one adiabatic subspace. Inside the topological domain, the eigenstates are distributed between the two subspaces.

We recover properties related to the Eigenstate Thermalization Hypothesis (ETH) [222] for eigenstates located within the topological region. This hypothesis states in particular that the average value of an observable $\hat{O}$ in an eigenstate varies very little with respect to the energy, *i.e.*, neighboring eigenstates in energy have similar average values of observables. We observe this behavior for the eigenstates within the topological region on Fig. 6.6: their average value of $\hat{\boldsymbol{N}}$ forms a dense cloud localized at mid-distance of the two topological boundaries (illustrating their almost uniform delocalization between the boundaries). On the other hand, the average value of eigenstates outside the topological region fills almost uniformly the $\boldsymbol{N}$-space, illustrating that eigenstates with similar eigenenergies have very different average value of $\hat{\boldsymbol{N}}$ in this region, thereby violating ETH. This is explicitly shown on Fig. 6.7(a), where we display the average value of the pumping coordinate $\hat{n}_\perp$ with respect to the energy eigenstate. The dense cloud of eigenstates between the orange dotted lines corresponds to the dense cloud of eigenstates within the topological region of Fig. 6.6: their average value of $\hat{n}_\perp$ varies little with respect to the energy, satisfying ETH. On the other hand, the eigenstates above and below the dotted lines are the eigenstates localized in the topologically trivial domains, with average values varying erratically with respect to the energy. In the following, we denote "topological family" the eigenstates contained in between the orange dotted lines of Fig. 6.7(a), and "trivial family" the eigenstates above and below the orange dotted lines. Note that in the trivial family of eigenstates, we also consider the little amount of "Landau-Zener" eigenstates located near the topological boundaries inside the topological domain on Fig. 6.6. The low energy eigenstates in grey on Fig. 6.7(a) correspond to eigenstates localized in the region of small $\langle \hat{n}_1 \rangle$ (below 15 on Fig 6.6). In this region, the adiabatic dynamics does not apply, so we do not take them into account in the analysis.

A family of eigenstates satisfying ETH is often considered as a quantum signature of chaos [222]. A striking feature here is the coexistence of these two families of eigenstates at similar energies. Usually, an entire range of energy has either chaotic or non-chaotic signatures. Here, a model of topological coupling exhibits mixed spectrum, with the topological family of eigenstates carrying signature of chaos, and a family of eigenstates carrying signature of absence of chaos. Other common signatures of chaos lie in spectral statistics [223], which we consider in the following.

### 6.3.2 Spectral statistics

For quantum systems having a classical correspondence, it is understood that the distributions of energy level spacings differ radically whether the classical analog of the system is chaotic or integrable [223]. The quantization of a chaotic classical Hamiltonian displays a level repulsion, *i.e.* quasi-degenerate energies are very rare, whereas for a classically integrable system, quasi-degenerate energies occur. Due to the presence of the two-level quantum subsystem, our total system has no immediate classical correspondence. Nevertheless, let us examine if the spectra of the two families of eigenstates have similar properties.

We represent the level spacing distribution $P(\delta)$ of the two families of eigenstates on Fig. 6.7(b). More precisely, we consider the ordered eigenstates $E_k$ of each family, $E_{k+1} \geq E_k$, and show the histogram of energy differences between two successive eigenstates $\delta_k = E_{k+1} - E_k$. We observe a clear level repulsion for the topological family (in orange), *i.e.*

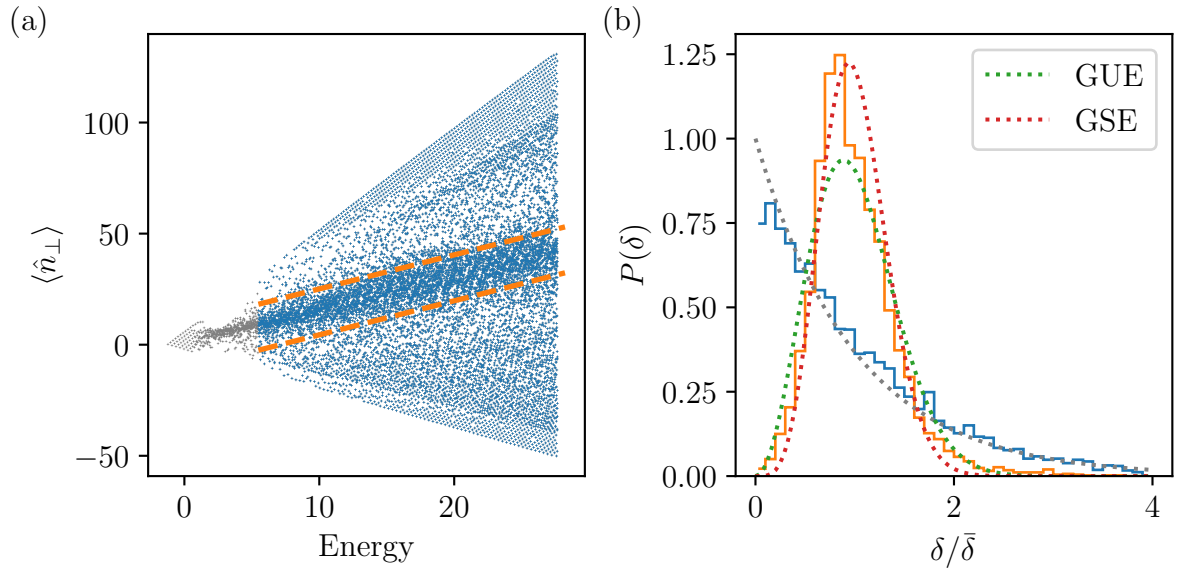


Figure 6.7: (a) Average value in eigenstates of the pumping coordinate $\hat{n}_\perp = (-\omega_2 n_1 + \omega_1 n_2)/|\boldsymbol{\omega}|$ depending on the eigenenergy. Between the orange dotted lines: "topological family" of eigenstates, forming the dense cloud inside the topological domain of Fig. 6.6. Above and below the orange dotted line: "trivial family" of eigenstates filling (almost) uniformly the trivial domains in Fig. 6.6 and violating ETH. We do not consider the low energy eigenstates (in grey). Note that in the trivial family, we also consider the little amount of "Landau-Zener" eigenstates located near the topological boundaries inside the topological domain on Fig. 6.6. (b) Level spacing statistics. Histogram of the level spacing $\delta_k = E_{k+1} - E_k$ between two successive eigenstates of the trivial family (in blue, without level repulsion), and for the topological family (in orange, with level repulsion). The trivial family follows the Poisson exponential distribution. The topological family does not follow exactly the Wigner distributions of the Gaussian unitary (dotted green line) or symplectic (dotted red line) random matrices ensembles. Spectra have been unfolded following the procedure detailed in appendix 6.D.

the distribution satisfies $P(\delta) \to 0$ as $\delta \to 0$, in contrast to the distribution of the trivial family (in blue).

A success of the Random Matrix Theory (RMT) for the study of quantum chaotic systems lies in the justification that, in many situations, the level spacing distribution follows a universal law determined by symmetry classes of the Hamiltonian [223, 224]. Integrable systems typically display Poisson distribution of level spacings, leading to the exponential decay in grey dotted line of Fig. 6.7(b). The trivial family of eigenstates follows this law. The most common ensemble of random matrices are Gaussian ensembles, leading to the Wigner distributions of level spacings [223]. We represent in dotted green and red lines respectively the laws obtained from Gaussian unitary (GUE) and symplectic (GSE) ensembles, corresponding respectively to a breaking of time reversal symmetry, or to time reversal symmetry with $\mathcal{T}^2 = -\mathbb{1}$. The level spacing distribution of the topological states does not follow these two laws. The topological family does not carry any standard signatures of chaos.

These universal laws describe statistical variations of the level spacing. To compare a spectrum to these universal laws, we have to unfold it in order to evaluate the statistical variation of the level spacing $\delta_k$ with respect to the mean level spacing $\bar{\delta}$. We describe the unfolding procedure in appendix 6.D. In the following, we estimate the Thouless energy of the topological family of eigenstates, in order to show that it lies at the limit of validity of random matrix theory. As such, this family displays signatures of chaos which are not accurately described by the most canonical ensembles of RMT.

### 6.3.3 Thouless energy and Random Matrix Theory

#### Thouless energy

The Thouless energy $E_{\mathrm{Th}}$ was historically introduced in the context of the Anderson localization of an electron in a mesoscopic disordered sample [225], as an energy scale associated with the sensitivity to boundary conditions. For a diffusive system, it is defined by $E_{\mathrm{Th}} = \hbar D/L^2 = \hbar t_d^{-1}$, with $D$ the diffusion constant, $L$ the sample size, and $t_d$ the classical diffusion time through the sample. It was then extended for ballistic systems [226], as an inverse time of flight between scattering events. In our model, Landau-Zener scattering occurs on the boundaries of the topological region. We note $N_{\mathrm{topo}}$ the length of the topological domain in the pumping direction $n_\perp$, represented on Fig. 6.8(a). We define the Thouless energy as $E_{\mathrm{Th}} = \hbar t_{\mathrm{pump}}^{-1}$ with the pumping time between the topological boundaries $t_{\mathrm{pump}} = N_{\mathrm{topo}}/\dot{n}_\perp = 2\pi N_{\mathrm{topo}}/(|\boldsymbol{\omega}|\mathcal{C})$, with $\mathcal{C} = |\mathcal{C}_\pm|$.

When looking for a quantum signature of chaos, the Thouless energy is understood as the maximum energy range on which random matrix theory accurately describes spectral correlations [224, 226]. Namely, statistical correlations between eigenergies lying in range $[E, E + E_{\mathrm{Th}}]$ (where statistical averages are taken with respect to the position $E$ of the range) are accurately described by statistical correlations of a random matrix ensemble. In particular, RMT applies when $E_{\mathrm{Th}}$ is large compared to the mean level spacing $\bar{\delta}$.

Let us estimate the Thouless energy from the spectral properties of the model. To do so, we consider the variance of the number of states $\mathrm{Var}N(\Delta E)$ in a strip of width $\Delta E$. Noting $N(E, \Delta E)$ the number of states whose energy lies in $[E, E + \Delta E]$, this variance is defined by

$$\mathrm{Var}N(\Delta E) = \left\langle N(E, \Delta E)^2 \right\rangle_E - \langle N(E, \Delta E) \rangle_E^2 , \tag{6.20}$$

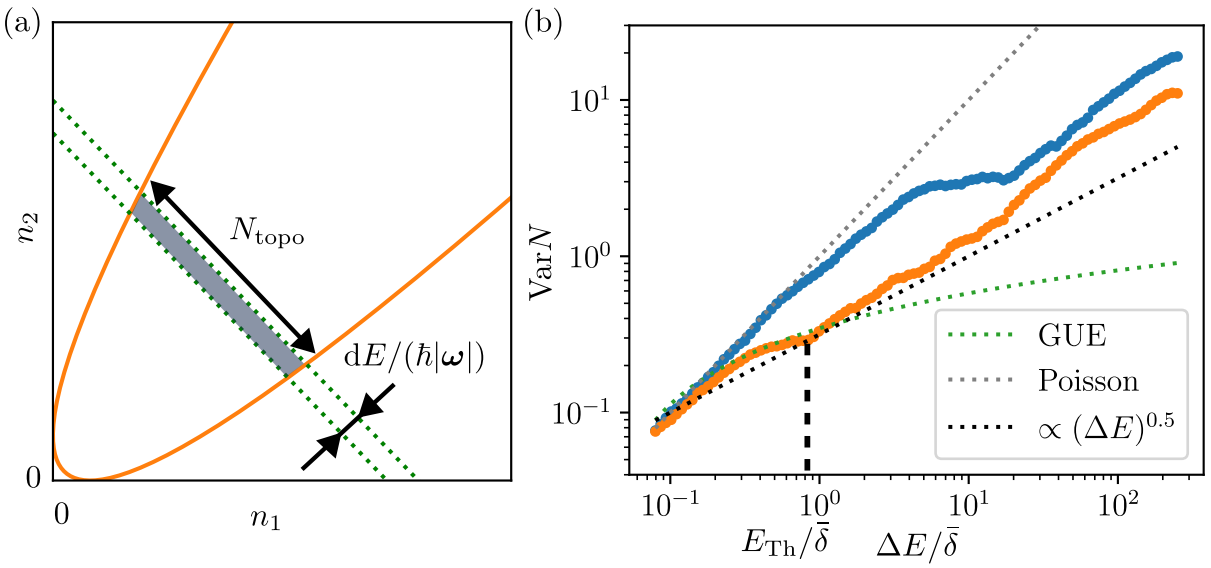


Figure 6.8: (a) Estimation of the mean energy level spacing $\bar{\delta}$ of topological family of eigenstates. The number of topological eigenstates of energy lying in a range $\mathrm{d}E$ is equal to the number of quantum state in the grey domain. (b) Variance of number of states in an energy range $[E, E + \Delta E]$. In blue, topologically trivial family of eigenstates: the variance follows at low energy the result of a Poisson distribution of energy levels (grey dotted line). In orange, topological family of eigenstates: the variance growths logarithmically at small $\Delta E$, following approximately the GUE random matrix result, and follows a power law above $\Delta E \gtrsim \bar{\delta}$ providing an estimation of the Thouless energy.

where $\langle . \rangle_E$ denotes average[4] with respect to $E$. We represent the variance of number of states for the trivial and topological families of eigenstates in respectively blue and orange on Fig. 6.8. For a random matrix model, this variance increases logarithmically for $\Delta E$ large compared to the mean level spacing $\bar{\delta}$ [224] (green dotted line in Fig. 6.8(b) for GUE). In the study of the motion of an electron in a mesoscopic disordered system, it was shown that for energy range $\Delta E$ larger than $E_{\rm Th}$, the number variance is proportional to $(\Delta E)^{d/2}$, with $d$ the space dimension [224, 227]. This enables to estimate the Thouless energy from a spectrum, as the energy scale of crossover between logarithmic and polynomial growth of the number variance [228].

The number variance of the topological family (in orange on Fig. 6.8(b)) follows approximately the GUE law at small $\Delta E$, up to $\Delta E \lesssim \bar{\delta}$, above which it increases as a power law. As a result, we estimate the Thouless energy to be of the order of the magnitude of the mean level spacing. This is a regime at the limit of validity of random matrix theory, thereby we expect the signatures of chaos of the topological family of eigenstates to be non-standard. For $\bar{\delta} \lesssim \Delta E \lesssim 20\ \bar{\delta}$, the number variance scales approximately as $(\Delta E)^{0.5}$ (black dotted line on Fig. 6.8(b)). We interpret this as a signature of an almost one dimensional transport between scattering events, corresponding to the topological pumping dynamics between Landau-Zener scatterings. A more precise fit of the variance on this range of energy provides a scaling of approximately $(\Delta E)^{0.57}$. On the other hand, the number variance of the trivial family (in blue on Fig 6.8(b)) increases linearly with $\Delta E$ for small $\Delta E$ (dotted grey line). This is characteristic of Poisson spectra without correlations obtained for non-chaotic systems [224, 228].

We observe on Fig. 6.8(b) another break point in the number variance near $\Delta E \simeq 10\ \bar{\delta}$, for both the topological and trivial families of states. This can be explained considering that an increase of the energy translates the energy domain of the eigenstates (blue and red in Fig. 6.3(b)) along the direction of the frequency vector $\boldsymbol{\omega}$ (see Fig. 6.8(a)). We therefore expect a transition when the energy difference between two eigenstates is large enough such that they have small overlaps.

### Mean level spacing

Considering spectral statistics, we observed above that the Thouless energy $E_{\rm Th}$ of the topological family of eigenstates is of the order of the magnitude of their mean level spacing $\bar{\delta}$. Let us precise this relation by estimating the mean level spacing $\bar{\delta}$ of this family of eigenstates.

We consider the number of eigenstates $\mathrm{d}N(E)$ inside the topological domain of energy lying in $[E, E + \mathrm{d}E]$, such that $\bar{\delta} = (\mathrm{d}N/\mathrm{d}E)^{-1}$. As discussed in Sec. 6.3.1, a topological eigenstate of energy $E$ is delocalized in the $n_\perp$ direction inside the topological region, inside the blue and red energy domains displayed in Fig. 6.3(b). These two energy domains are approximately symmetric with respect to the line of constant energy of the modes $\hbar\omega_1 n_1 + \hbar\omega_2 n_2 = E$ (green dotted line in 6.8(a)). Hence, when the energy $E$ is increased by $\mathrm{d}E$, these domains are slightly translated in the direction of the frequency vector $|\boldsymbol{\omega}|$ by $\mathrm{d}E/(\hbar|\boldsymbol{\omega}|)$. The number of extra states corresponds then to the number of states in the grey area of Fig. 6.8(a): $\mathrm{d}N \simeq 2N_{\rm topo}\mathrm{d}E/(\hbar|\boldsymbol{\omega}|)$, where the factor 2 accounts

[4]The spectrum $E_k$ of each family of eigenstates is first unfolded to remove macroscopic variation of the density of states $\bar{\delta}$ with respect to $E$, see appendix 6.D.

for the qubit degree of freedom. Hence, we estimate $\bar{\delta} \simeq \hbar|\boldsymbol{\omega}|/(2N_{\text{topo}})$.

Moreover, we estimated above the Thouless energy as the inverse pumping time between the topological boundaries: $E_{\text{Th}} = \hbar|\boldsymbol{\omega}|\mathcal{C}/(2\pi N_{\text{topo}})$. We thus obtain

$$E_{\text{Th}} \simeq \frac{\mathcal{C}}{\pi}\bar{\delta}. \tag{6.21}$$

The above argument is independent of the model-dependent shape of the topological domain. As a result, we expect it to be valid for any model of topological coupling between two harmonic oscillators and a qubit. The topological family of eigenstates has a Thouless energy of the order of magnitude of their mean level spacing. As such, this family lies at the limit of validity of RMT. It is expected to display signatures of chaos which are not accurately described by the canonical ensembles of RMT.

**Role of Landau-Zener scattering matrix**

The Thouless energy was historically introduced as a measure of the sensitivity of a diffusive system to boundary conditions. In our situation, we have semiclassical trajectories of wavepackets drifting towards a topological boundary due to topological pumping. A Landau-Zener tunnelling event can be viewed as a scattering process between these classical trajectories. As such, the spectral properties of the topological family of eigenstates, and their possible universality class, should depend on the associated scattering matrix. More precisely, let us note $\left|\pm, \bar{\boldsymbol{N}}, \bar{\boldsymbol{\Phi}}\right\rangle$ an adiabatic wavepacket within the adiabatic subspace $\mathcal{H}_\pm$ and localized in phase space around $(\bar{\boldsymbol{N}}, \bar{\boldsymbol{\Phi}})$. A Landau-Zener tunnelling event is a scattering process between an input adiabatic wavepacket $\left|-, \bar{\boldsymbol{N}}^{\text{in}}, \bar{\boldsymbol{\Phi}}^{\text{in}}\right\rangle$ (Fig. 6.4(b)) into a superposition of two output wavepackets in the two adiabatic subspaces $\hat{S}\left|-, \bar{\boldsymbol{N}}^{\text{in}}, \bar{\boldsymbol{\Phi}}^{\text{in}}\right\rangle = \left|-, \bar{\boldsymbol{N}}^{\text{out}}_-, \bar{\boldsymbol{\Phi}}^{\text{out}}_-\right\rangle + \left|+, \bar{\boldsymbol{N}}^{\text{out}}_+, \bar{\boldsymbol{\Phi}}^{\text{out}}_+\right\rangle$ (Fig. 6.4(d)). The relative weight of the + component, namely $\left|\left\langle +, \bar{\boldsymbol{N}}^{\text{out}}_+, \bar{\boldsymbol{\Phi}}^{\text{out}}_+\right| \hat{S} \left|-, \bar{\boldsymbol{N}}^{\text{in}}, \bar{\boldsymbol{\Phi}}^{\text{in}}\right\rangle\right|^2$, can be estimated using the Landau-Zener transition probability (which rely on a hybrid classical-quantum description of the system). However, the phase space positions of the output states $(\bar{\boldsymbol{N}}^{\text{out}}_\pm, \bar{\boldsymbol{\Phi}}^{\text{out}}_\pm)$ cannot be estimated by a Landau-Zener analysis as described in Chap. 1, which involves a classical description of the slow degrees of freedom. A full quantum mechanical description of the Landau-Zener tunnelling process is required. A possible origin of the signatures of chaos of the topological family of eigenstates can be an extreme sensitivity of the output phase space position $(\bar{\boldsymbol{N}}^{\text{out}}_\pm, \bar{\boldsymbol{\Phi}}^{\text{out}}_\pm)$ on the input phase space position $(\bar{\boldsymbol{N}}^{\text{in}}_-, \bar{\boldsymbol{\Phi}}^{\text{in}}_-)$.

We illustrate in appendix 6.E the dependence of the spectral properties of the topological eigenstates on a numerical example, by considering another set of parameters of the Hamiltonian leading to quantitatively different spectral statistics of the topological family, while displaying the same level repulsion and order of magnitude of Thouless energy.

## 6.4 Conclusion of chapter

We extended the model of quantum rotors topologically coupled to a two level system to the case of two quantum harmonic oscillators topologically coupled to a qubit. A classical limit of the harmonic oscillators enables to define the topological coupling between the qubit and the two modes following the result of Chap. 3. The topological or trivial

nature of the coupling depends on the number of quanta of the two harmonic oscillators. The quanta number plane is then split in topologically distinct domains. Far from the transitions lines between these domains, the adiabatic dynamics is valid.

The adiabatic dynamics of a wavepacket prepared inside the topological domain is characterized by topological pumping leading to a drift of the wavepacket towards a topological transition line, where adiabaticity breaks-down. This leads to a Landau-Zener scattering mechanism from one adiabatic subspace to another, and to a reverse direction of pumping. After a succession of adiabatic drifts and Landau-Zener scattering events, the wavepacket reaches a quasi-stationary state delocalized within a domain delimited by the topological and energy conservation boundaries. This provides a notion of ergodicity for initial states prepared within the topological domain. On the other hand, initial states prepared in the topologically trivial domain remain localized during the dynamics, without any notion of ergodicity.

These two families of long time quasi-stationary states translate into two families of eigenstates, the trivial and the topological family. The topological family of eigenstates satisfies an ETH feature, characteristic of chaotic systems, while the trivial does not. The striking property of the system is the coexistence of two family of eigenstates lying at similar energies. The topological family carries quantum signatures of chaos, whereas the trivial family does not.

We precised the quantum signatures of chaos of the topological family of eigenstates by considering spectral statistics. The topological family of eigenstates displays a clear level repulsion, in contrast to the trivial family. Interestingly, the level spacing distribution of topological states does not follow precisely universal laws of canonical classes of random matrix theory. We explained this by estimating their Thouless energy, which sets the domain of application of random matrix theory. From spectral statistics, we deduce this energy to be of the same order of magnitude as the mean level spacing, corresponding to the limit of validity of RMT. By estimating the Thouless energy as an inverse of topological pumping time, we argued that this behavior is expected for any model of topological coupling between two quantum harmonic oscillators and a qubit. A characterization of the non-adiabatic Landau-Zener scattering matrix would precise the origin of the chaotic behavior.

## 6.A Phase and number of quanta of the harmonic oscillator

The adimensionalized quadratures of the modes are defined by

$$\hat{x}_i = \frac{\hat{a}_i + \hat{a}_i^\dagger}{\sqrt{2}} \tag{6.22}$$

$$\hat{p}_i = \frac{\hat{a}_i - \hat{a}_i^\dagger}{i\sqrt{2}} \tag{6.23}$$

satisfying $[\hat{x}_i, \hat{p}_j] = i\delta_{ij}\mathbf{1}$, *i.e.* in the classical limit the quadratures satisfy the Poisson bracket relations $\{\sqrt{\hbar}x_i, \sqrt{\hbar}p_j\} = \delta_{ij}$. The following change of variable is symplectic

$$x_i = \sqrt{2n_i}\cos(\phi_i), \tag{6.24}$$

$$p_i = \sqrt{2n_i}\sin(\phi_i), \tag{6.25}$$

meaning that the photon number and phase satisfy the classical Poisson bracket $\{\hbar n_i, \phi_j\} = \delta_{ij}$. The classical limit of $\hat{a}$ and $\hat{a}^\dagger$ is then $\sqrt{n_i}e^{\pm i\phi_i}$.

## 6.B Scaling of energies and Berry curvature

To express the scaling relations of the Berry curvature and the quantum metric, we write them in terms of the Hamiltonian. We consider the quantum geometric tensor

$$T_{\nu,\alpha\beta} = \langle\partial_\alpha\psi_\nu|\left(1 - |\psi_\nu\rangle\langle\psi_\nu|\right)|\partial_\beta\psi_\nu\rangle \tag{6.26}$$

$$= \sum_{\mu\neq\nu} \frac{\langle\psi_\nu|\partial_\alpha H|\psi_\mu\rangle\langle\psi_\mu|\partial_\beta H|\psi_\nu\rangle}{(E_\mu - E_\nu)^2} \tag{6.27}$$

where the last expression is obtained using $\langle\psi_\mu|\partial_\alpha\psi_\nu\rangle = i\langle\psi_\mu|\partial_\alpha H|\psi_\nu\rangle/(E_\nu - E_\mu)$ for $\mu \neq \nu$.

We consider a linear coupling between the bosonic operators $\hat{a}_i, \hat{a}_i^\dagger$ and the qubit, *i.e.* $\hat{H}$ does not involve products of annihilation or creation operators. As such, its symbol $H(\boldsymbol{\Phi}, \boldsymbol{N})$ scales as $\sqrt{n_i}$. Its eigenvalues have the same scaling $E_\nu(\boldsymbol{\Phi}, \boldsymbol{N}) = \mathcal{O}(\sqrt{n_i})$, and the matrix elements of $\partial_{\phi_i}H$ scale as $\sqrt{n_i}$ whereas those of $\partial_{n_i}H$ scale as $1/\sqrt{n_i}$. We deduce from (6.27)

$$T_{\pm,\phi_i\phi_j} = \mathcal{O}(1) \quad ; \quad T_{\pm,\phi_i n_j} = \mathcal{O}\left(\frac{1}{n_j}\right) \quad ; \quad T_{\pm,n_i n_j} = \mathcal{O}\left(\frac{1}{n_i n_j}\right). \tag{6.28}$$

We have $F_{\nu,\alpha\beta} = -2\,\mathrm{Im}\,T_{\nu,\alpha\beta}$ and $g_{\nu,\alpha\beta} = \mathrm{Re}\,T_{\nu,\alpha\beta}$, such that the components of the Berry curvature and quantum metric satisfy the same scaling.

The energy correction reads

$$M_\nu = \sum_{i=1}^{2} \mathrm{Im}\,\langle\partial_{n_i}\psi_\nu|\left(H - E_\nu\right)|\partial_{\phi_i}\psi_\nu\rangle, \tag{6.29}$$

$$= \sum_{i=1}^{2} \mathrm{Im}\,\frac{\langle\psi_\nu|\partial_{n_i}H|\psi_\mu\rangle\langle\psi_\mu|\partial_{\phi_i}H|\psi_\nu\rangle}{E_\mu - E_\nu}, \tag{6.30}$$

such that, according to the above scaling relations, $M_\nu = \mathcal{O}(1/\sqrt{n_i})$.

## 6.C Numerical Truncation

Let us first provide the analytical expressions of the topological and energy boundaries of Fig. 6.3(b). The orange lines are the topological boundaries, corresponding to the values of $\boldsymbol{N}$ for which the gap of the qubit $|\boldsymbol{h}|(\boldsymbol{\Phi}, \boldsymbol{N})$ closes for some value of phase $\boldsymbol{\Phi}$. From (6.5), we obtain gap closing if $\boldsymbol{\Phi}$ is $(0,0)$, $(0,\pi)$, or $(\pi,0)$ and $\boldsymbol{N}$ satisfies

$$\frac{\omega_q}{2} \pm 2g_1\sqrt{n_1} \pm 2g_2\sqrt{n_2} = 0. \tag{6.31}$$

The above condition leads to the tilted orange parabola on 6.3(b) delimitating the topological domain.

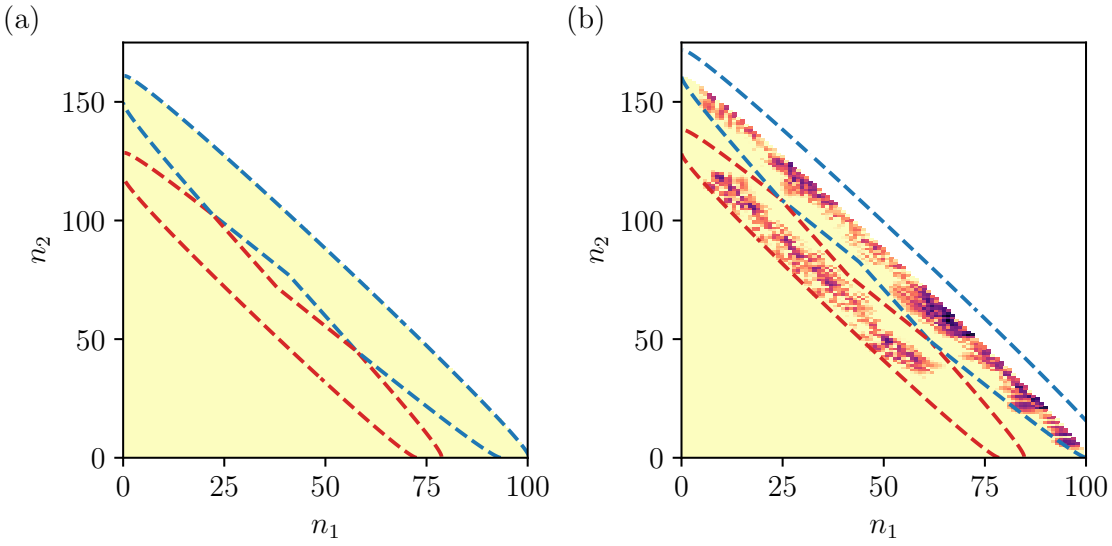


Figure 6.9: Numerical truncation of the Hilbert space. (a) We first consider a box in $\boldsymbol{N}$-space $0 \leq n_1 \leq n_1^{\max}$, $0 \leq n_2 \leq n_2^{\max}$. Here $(n_1^{\max}, n_2^{\max}) = (100, 175)$. We then consider the domain of maximum energy $E^{\max}$ which lies in this box (dotted lines). We ignore the points $\boldsymbol{N}$ above this domain (white region) in the diagonalization. (b) Example of (photon number distribution of) eigenstates of energy $E > E^{\max}$, affected by the finite size numerical truncation. In the spectral analysis, we keep only the eigenstates of energy $E < E^{\max}$, unaffected by the numerical truncation.

The blue and red energy domains on 6.3(b) are the values of $\boldsymbol{N}$ such that it exists $\boldsymbol{\Phi} \in [0, 2\pi]^2$ for which $\hbar\omega_1 n_1 + \hbar\omega_2 n_2 \pm |\boldsymbol{h}(\boldsymbol{\Phi}, \boldsymbol{N})| = E$. We define

$$|\boldsymbol{h}(\boldsymbol{N})|_{\max}/\hbar = \max_{\boldsymbol{\Phi}\in[0,2\pi]^2} |\boldsymbol{h}(\boldsymbol{\Phi}, \boldsymbol{N})|/\hbar = \frac{\omega_q}{2} + 2g_1\sqrt{n_1} + 2g_2\sqrt{n_2}, \tag{6.32}$$

$$|\boldsymbol{h}(\boldsymbol{N})|_{\min}/\hbar = \min_{\boldsymbol{\Phi}\in[0,2\pi]^2} |\boldsymbol{h}(\boldsymbol{\Phi}, \boldsymbol{N})|/\hbar = \min \begin{cases} \frac{\omega_q}{2} - 2g_1\sqrt{n_1} + 2g_2\sqrt{n_2} \\ \frac{\omega_q}{2} + 2g_1\sqrt{n_1} - 2g_2\sqrt{n_2} \\ -\frac{\omega_q}{2} + 2g_1\sqrt{n_1} + 2g_2\sqrt{n_2} \end{cases}, \tag{6.33}$$

such that the blue ground domain of Fig. 6.3(b) corresponds to the values of $\boldsymbol{N}$ such that

$$E + |\boldsymbol{h}(\boldsymbol{N})|_{\min} \leq \hbar\omega_1 n_1 + \hbar\omega_2 n_2 \leq E + |\boldsymbol{h}(\boldsymbol{N})|_{\max}, \tag{6.34}$$

and the red excited domain to the values of $\boldsymbol{N}$ such that

$$E - |\boldsymbol{h}(\boldsymbol{N})|_{\max} \leq \hbar\omega_1 n_1 + \hbar\omega_2 n_2 \leq E - |\boldsymbol{h}(\boldsymbol{N})|_{\min}. \tag{6.35}$$

Let us now detail the truncation of Hilbert space and the selection of eigenstates of low enough energy. We diagonalize the Hamiltonian in the basis $|n_1\rangle\otimes|n_2\rangle\otimes|\uparrow / \downarrow\rangle$. We expect the eigenstates to be contained in the energy domains of Fig. 6.3(b), whose boundaries are defined above. We first consider a rectangle, $0 \leq n_1 \leq n_1^{\max}$, $0 \leq n_2 \leq n_2^{\max}$. For the numerical simulation of main text, we use $n_1^{\max} = 100$ and $n_2^{\max} = 175$ (see Fig. 6.9(a)). We then keep only the values $(n_1, n_2)$ lying in energy domains fully contained in this rectangle. The corresponding maximum energy is

$$E^{\max}/\hbar = \max \begin{cases} \omega_1 n_1^{\max} + \omega_2 n_2^{\max} - \frac{\omega_q}{2} - 2g_1\sqrt{n_1^{\max}} \\ \omega_1 n_1^{\max} + \omega_2 n_2^{\max} - \frac{\omega_q}{2} - 2g_2\sqrt{n_2^{\max}} \end{cases} . \tag{6.36}$$

The domain of energy $E^{\max}$ is represented in dotted lines on Fig. 6.9(a). We then keep only the $(n_1, n_2)$ values satisfying

$$\omega_1 n_1 + \omega_2 n_2 - \frac{\omega_q}{2} - 2g_1\sqrt{n_1} - 2g_2\sqrt{n_2} \leq E^{\max}/\hbar, \tag{6.37}$$

which amounts to truncate the white domain on Fig. 6.9(a). We thus expect all the eigenstates of the untruncated Hamiltonian of energy $E \leq E^{\max}$ to be localized in our truncation of Hilbert space.

We diagonalize the Hamiltonian within this truncation. The eigenstates of energy greater than $E^{\max}$ are expected to be affected by the finite size effects of the truncation, because their energy domain is outside the Hilbert space truncation, see for example such an eigenstate on Fig. 6.9(b). We ignore them in our analysis, keeping only the eigenstates of energy $E < E^{\max}$ (which, for our parameters, amounts to consider the 12397 eigenstates of lowest energies among the 17600 eigenstates of the truncated Hamiltonian).

## 6.D Spectrum unfolding

In order to compare the statistics of a spectrum to laws provided by random matrix theory, the mean level spacing has to be uniform, *i.e.* to be independent of the energy range. In other words, random matrix theory describes fluctuations of energy level spacings of a spectrum around its mean level spacing. To do so, the spectrum is "unfolded". We note $E_k$ the original spectrum of a family of eigenstates, ordered such that $E_k \leq E_{k+1}$. Let us insist on the fact that $E_k$ is not the entire spectrum, but only a selected family of eigenstates (in our case, the topological or trivial family of eigenstates). We represent the original spectrum of the trivial and topological families of eigenstates respectively in blue and orange on Fig. 6.10(a). The energy is almost linear with respect to $k$ for the topological family, illustrating that the mean density of state of this family is almost independent of the energy. On the other hand, the mean density of states of the trivial family clearly varies with the energy, such that unfolding is required.

The unfolding is a transformation of a spectrum $e_k = f(E_k)$, such that the unfolded spectrum $e_k$ has a mean level spacing equal to 1. There exist different unfolding procedures, *i.e.* transformation function $f$ [223]. A common choice is the following. We

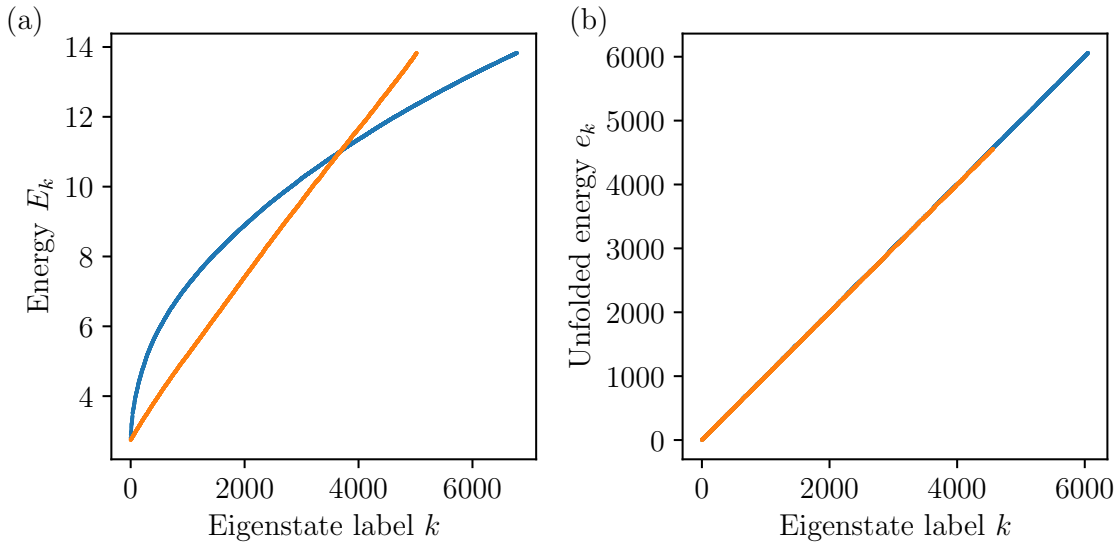


Figure 6.10: Spectrum unfolding. (a) Energy spectrum $E_k$ of the trivial family of eigenstates (in blue) and the topological family of eigenstates (in orange). In order to compare the spectral correlations to results of random matrix theory, the spectra have to be unfolded, in order to have a uniform mean level spacing. (b) Unfolded spectrum $e_k = f(E_k)$, increasing linearly with respect to $k$ up to fluctuations which can be compared to those of a random matrix.

require $e_{k+1} - e_k = \frac{\mathrm{d}f}{\mathrm{d}E}\frac{\mathrm{d}E}{\mathrm{d}k} = 1$ in average, such that $f$ is the integrated mean density of states

$$f(E) = \int_{-\infty}^{E} \frac{\Delta N}{\Delta E}(E')\mathrm{d}E' \tag{6.38}$$

with the mean density of states obtained by computing the number $\Delta N$ of eigenstates whose energy lie in $[E', E' + \Delta E]$, where $\Delta E$ has to be large compared to the mean level spacing and small compared to the scale of macroscopic variation of the density (which, as seen on Fig. 6.10, is of order 1 in units of $\hbar\omega_q$). We take $\Delta E = 1$ in the numerical analysis. This provides the unfolded spectrum on Fig. 6.10(b). The unfolded energy $e_k$ is linear with respect to $k$, up to fluctuations which can be compared to the fluctuations of a random matrix.

## 6.E Role of topological boundary position

Let us illustrate the dependence of the spectral properties of the topological eigenstates on a numerical example, by considering another set of parameters of the Hamiltonian. We diagonalize the Hamiltonian with $g_1/\omega_q = 0.035$, $g_2/\omega_q = 0.0575$, $\omega_2/\omega_q = 0.05$, and the same ratio between the frequencies of the modes. This set of parameters leads to the topological boundary in red on Fig. 6.11(a). The difference between this example and the one of main text is the right part of the topological boundary, which here lie almost along the $n_2 = 0$ axis for the energy scales we consider. This leads to an almost gap closing of the qubit $|\boldsymbol{h}(\boldsymbol{\Phi}, \boldsymbol{N})| \simeq 0$ for $n_2 \simeq 0$, $n_1 \simeq 50$ on the entire line $\phi_1 = 0$ on the torus (see Fig. 6.11(b)), rather than a local gap closing on $\boldsymbol{\Phi} = (0, \pi)$ as on Fig. 6.4(c). We thus

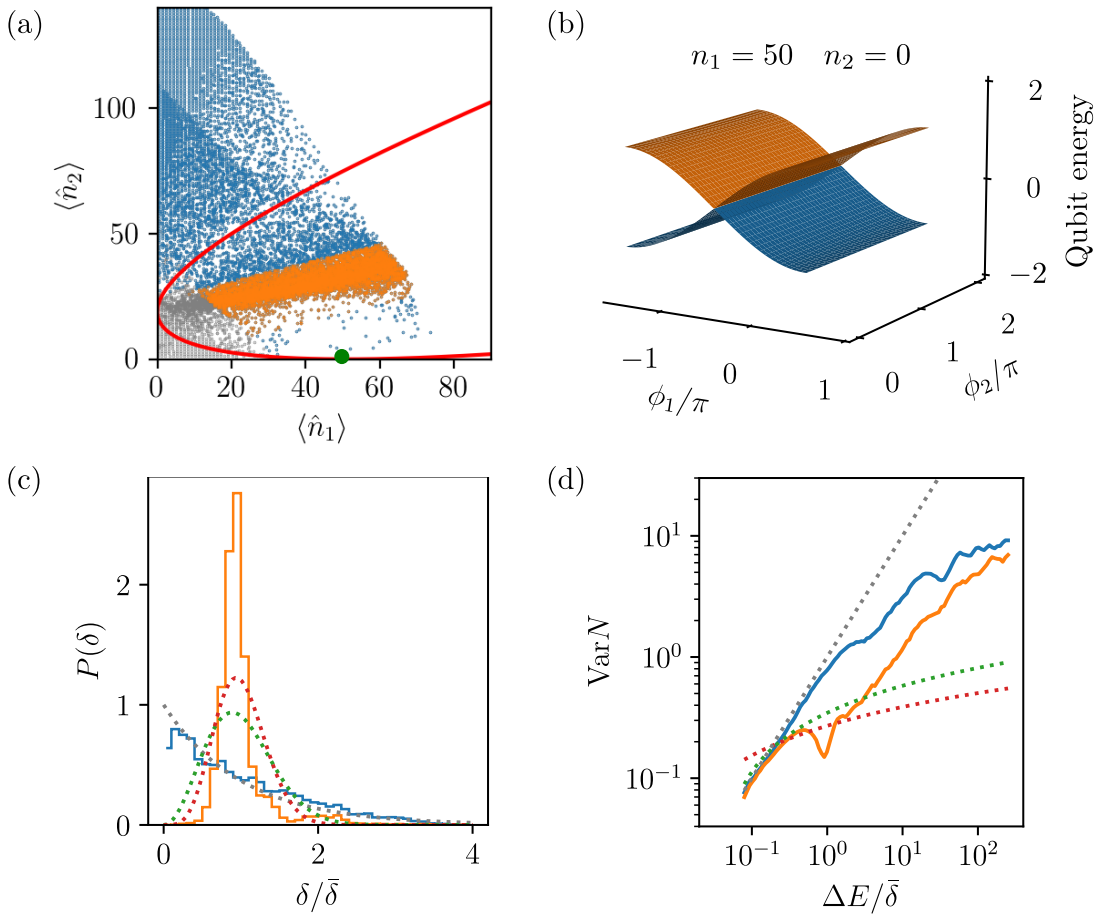


Figure 6.11: Spectral analysis of the Hamiltonian for another set of parameters $g_1/\omega_q = 0.035$, $g_2/\omega_q = 0.0575$, $\omega_2/\omega_q = 0.05$. (a) Average value of $\hat{\boldsymbol{N}}$ of each eigenstate. In orange, the dense family of topological eigenstates. (b) The bottom part of the topological boundary (in red on (a)) lie almost on the $n_2 = 0$ axis, where the qubit gap almost closes on the entire line $\phi_1 = 0$ on the torus for $\boldsymbol{N} \simeq (50, 0)$ (green point), in contrast with the local gap closing at $\boldsymbol{\Phi} = (0, \pi)$ for $\boldsymbol{N}$ on the topological boundary of the model considered in main text (Fig. 6.4(c)). We thus expect a qualitatively different Landau-Zener scattering matrix inducing qualitatively different spectral statistics of the topological eigenstates. (c) The level spacing distribution of the topological eigenstates (in orange) still displays a clear level repulsion but differs more radically from the GUE and GSE laws (respectively green and red dotted lines). The distribution of topologically trivial states follows the Poisson (non-chaotic) distribution (grey dotted line). (d) Variance of number of eigenstates for topological (orange) and trivial (blue) families of eigenstates. Green (respective red) dotted lines: GUE (respectively GSE) laws. The topological family still displays a crossover between logarithmic and polynomial scaling around $\Delta E \simeq \bar{\delta}$, such that $E_{\mathrm{Th}} \simeq \bar{\delta}$.

expect different features of the Landau-Zener scattering matrix, translating into different spectral statistics of topological states.

The dense cloud of selected topological eigenstates is shown in orange on Fig. 6.11(a). Their level spacing distribution is represented in orange on Fig. 6.11(c). It displays a clear level repulsion, but deviates more from the GUE and GSE laws (respectively dotted green and red lines) than the level spacing distribution of topological eigenstates of the Hamiltonian considered in main text (Fig. 6.7(b)). The level distribution of the topologically trivial family of eigenstates (in blue on Fig. 6.11(c)) follows the Poisson distribution characteristic of non-chaotic systems, as for the example of main text.

The number variance is represented on Fig. 6.11(d) (respectively in blue and orange for the trivial and topological families of eigenstates). They have the same qualitative dependence as the case considered in main text (Fig. 6.8(b)). The number variance of the topological family of eigenstates displays a crossover between the GUE logarithmic scaling (green dotted line) and a polynomial scaling around $\Delta E \sim \bar{\delta}$, such that we estimate the same Thouless energy $E_{\mathrm{Th}} \simeq \bar{\delta}$.

# Conclusion

## 1 Results

Reinterpreting topological pumps within the context of slow-fast quantum systems allowed us to define a notion of topological coupling between slow and fast quantum degrees of freedom. Topological pumps were historically described as a response of a slowly driven quantum system. The purpose of this thesis was to consider these drives as dynamical quantum degrees of freedom topologically coupled to the quantum system. The topological nature of the couplings leads to a transfer of charge or energy between the slow degrees of freedom. We payed special attention to the nature of the quantum states leading to the pumping dynamics, the adiabatic states, *i.e.* the states for which the effective adiabatic dynamics accurately describes the evolution of the slow degrees of freedom. We called them the adiabatic states, in close analogy with the notion of slow manifold.

In the chapter 1, we introduced the adiabatic evolution of a slowly driven quantum system, where we defined in particular the adiabatic states as those leading to the slowest time evolution of physical observables. Here no backaction of the quantum system onto the slow drives was considered. These slow drives were described in chapter 2 as slow quantum degrees of freedom coupled to a fast quantum system, allowing to consider the backaction of the fast subsystem onto the slow one. Our main contribution in this chapter was to precise the conditions of validity of the adiabatic approximation, providing quantitative conditions of existence of the adiabatic states. The description of the effective slow dynamics of these adiabatic states involves a geometric object, the Berry curvature, which carries the topological invariant.

This enabled us to define a notion of topological coupling between slow and fast quantum systems in chapter 3, reinterpreting examples of topological pumps within this framework. We illustrated the virtues of this formalism in chapter 4 with an experimental proposal of topological coupling between microwave modes and a superconducting quantum circuit, with a detailed measurement protocol for the topological redistribution of energy between the modes.

Considering the simplest example of topological coupling between two quantum rotors and a qubit, we showed in chapter 5 that adiabatic states are not naturally prepared experimentally, but any initial state decomposes into a pair of those. The topological pumping dynamics splits apart the two adiabatic components in the phase space of the modes, leading generically to a cat state. We described the weights of the cat as well as the entanglement between the modes and the qubit in terms of the geometry of the adiabatic

states, quantified by their quantum metric tensor. Finally, in chapter 6, we considered quantum harmonic oscillators topologically coupled to a qubit, with more common type of coupling encountered in quantum optics. The topological nature of the couplings depends on the number of quanta of the oscillators, leading to two families of initial states lying at the same energy scales, the topological and the trivial ones. The dynamics on short timescales is accurately described by the rotor model of chapter 5. On long timescales, the topological family of initial states leads to quasi-stationary states with a notion of ergodicity constrained by topological transition lines. The two families of quasi-stationary states translate into two families of eigenstates lying at similar energies. The trivial family of eigenstates carries no signature of chaos, whereas the topological family carries non-standard signatures of chaos. A more precise characterization of the chaotic behavior of the topological eigenstates is a stimulating perspective. In particular, the origin of chaos is suspected to arise from features of the Landau-Zener scattering matrix, more precisely from the sensitivity of the phase-space output position of scattered wave-packets to initial conditions.

# 2 Perspectives

### Other topological invariants

We defined a topological coupling between two slow quantum degrees of freedom and a fast quantum system characterized by a non-trivial first Chern number. A natural perspective is to translate topological pumps based on other topological invariants into an extended notion of topological coupling between slow-fast quantum systems, which could lead to new types of long-time dynamics and spectral statistics as those discussed in Chap. 6.

For example, a gapped quantum system depending on four, six, and in general an even number of periodic parameters allows to define higher Chern numbers. Higher dimensional topological pumps [26, 45, 229–234], corresponding to quantum Hall effect in higher dimensions could then be translated into a topological coupling between an even number of slow quantum degrees of freedom and a fast quantum system. Similarly, other types of topological coupling could be defined, considering the classification of topological pumps based on symmetry [235, 236], higher-order symmetry protected topological invariants [26, 237, 238], or non-abelian generalizations for a degenerate fast quantum system [26, 239–241]. It would also be interesting to extend the recent Floquet energy pumps [242–246], characterized by a topological winding number, into a coupling between quantum modes and a quantum system. This would correspond to a different type of slow-fast system since some of the modes are not slower than the quantum system, such that they have to be included as part of the fast subsystem.

### Open slow-fast quantum systems

We studied the dynamics of closed quantum system with a slow-fast separation. Considering dissipation and decoherence is a natural and experimentally very relevant perspective. As we saw in chapter 5, the adiabatic states are the only ones whose dynamics does not lead to cat states of the modes, such that they may correspond to pointer states [247] when considering the environment coupled to the qubit - two modes system.

Besides, in the experimental proposal of chapter 4, we modeled each microwave mode at a given frequency by a pair of conjugated phase and number of photons. Transmission lines having finite bandwidth, a continuous family of modes is actually present. In order to take into account the continuous family of slow degrees of freedom, we could extend as a first step the model introduced in chapter 3, where we expect the pumping equation (3.10) to be replaced by an integral over the mode frequencies, with a continuous number of Berry curvature components. Wether the presence of these Berry curvature components would affect the topological dynamics is a natural question. An interesting alternative description would be to formulate the reflection of microwave pulses on the superconducting qubit using an input-output approach [248]. Such a formulation may share similarities with the scattering formulation of parametric pumping [192, 249, 250], which is another form of (non necessarily quantized) pumping.

In order to consider dissipation in topologically coupled slow-fast quantum system, we could also build on the description of pumping in open systems described by a slowly time-dependent master equation [251–253], where the pumped observables are not related to a topological Chern number – obtained by integrating a Berry curvature – but to a circulation of a Landsberg connection (an open system analog of the Berry connection). The strategy would be to promote the drive parameters as dynamical slow quantum degrees of freedom and look at their effective slow dynamics. Moreover, other notions of adiabatic elimination exist in open systems, where the slow and fast time-scales do not correspond to inner dynamical timescales but to ratios between dissipative terms in a master equation [254]. Combining these different ideas of adiabatic eliminations of closed and open systems, with their geometric and topological features, is a stimulating perspective.

# Bibliography


[1] K. V. Klitzing, G. Dorda, and M. Pepper, "New method for high-accuracy determination of the fine-structure constant based on quantized hall resistance," *Physical Review Letters*, vol. 45, no. 6, pp. 494–497, 1980.

[2] D. J. Thouless, M. Kohmoto, M. P. Nightingale, and M. den Nijs, "Quantized Hall conductance in a two-dimensional periodic potential," *Physical Review Letters*, vol. 49, no. 6, p. 405, 1982.

[3] J. E. Avron, R. Seiler, and B. Simon, "Homotopy and quantization in condensed matter physics," *Physical Review Letters*, vol. 51, no. 1, p. 51, 1983.

[4] B. Simon, "Holonomy, the quantum adiabatic theorem, and Berry's phase," *Physical Review Letters*, vol. 51, no. 24, pp. 2167–2170, 1983.

[5] S.-s. Chern, "Characteristic Classes of Hermitian Manifolds," *The Annals of Mathematics*, vol. 47, no. 1, p. 85, 1946.

[6] R. B. Laughlin, "Quantized Hall conductivity in two dimensions," *Physical Review B*, vol. 23, no. 10, pp. 5632–5633, 1981.

[7] B. I. Halperin, "Quantized Hall conductance, current-carrying edge states, and the existence of extended states in a two-dimensional disordered potential," *Physical Review B*, vol. 25, no. 4, pp. 2185–2190, 1982.

[8] C. L. Kane, "Topological band theory and the $\mathbb{Z}_2$ invariant," in *Contemporary Concepts of Condensed Matter Science*, vol. 6, pp. 3–34, Elsevier, 2013.

[9] S. H. Simon, "Proposal for a quantum Hall pump," *Physical Review B*, vol. 61, no. 24, p. R16327, 2000.

[10] A. Fabre, J.-B. Bouhiron, T. Satoor, R. Lopes, and S. Nascimbene, "Laughlin's topological charge pump in an atomic hall cylinder," *Physical Review Letters*, vol. 128, no. 17, p. 173202, 2022.

[11] D. Thouless, "Quantization of particle transport," *Physical Review B*, vol. 27, no. 10, p. 6083, 1983.

[12] M. J. Rice and E. J. Mele, "Elementary excitations of a linearly conjugated diatomic polymer," *Physical Review Letters*, vol. 49, no. 19, p. 1455, 1982.

[13] D. Xiao, M.-C. Chang, and Q. Niu, "Berry phase effects on electronic properties," *Reviews of Modern Physics*, vol. 82, no. 3, p. 1959, 2010.

[14] M. Lohse, C. Schweizer, O. Zilberberg, M. Aidelsburger, and I. Bloch, "A Thouless quantum pump with ultracold bosonic atoms in an optical superlattice," *Nature Physics*, vol. 12, no. 4, pp. 350–354, 2016.

[15] S. Nakajima, T. Tomita, S. Taie, T. Ichinose, H. Ozawa, L. Wang, M. Troyer, and Y. Takahashi, "Topological Thouless pumping of ultracold fermions," *Nature Physics*, vol. 12, no. 4, pp. 296–300, 2016.

[16] J. Minguzzi, Z. Zhu, K. Sandholzer, A.-S. Walter, K. Viebahn, and T. Esslinger, "Topological Pumping in a Floquet-Bloch Band," *Physical Review Letters*, vol. 129, no. 5, p. 053201, 2022.

[17] D. Dreon, A. Baumgärtner, X. Li, S. Hertlein, T. Esslinger, and T. Donner, "Self-oscillating pump in a topological dissipative atom–cavity system," *Nature*, vol. 608, no. 7923, pp. 494–498, 2022.

[18] Y. E. Kraus, Y. Lahini, Z. Ringel, M. Verbin, and O. Zilberberg, "Topological states and adiabatic pumping in quasicrystals," *Physical Review Letters*, vol. 109, no. 10, p. 106402, 2012.

[19] M. Verbin, O. Zilberberg, Y. Lahini, Y. E. Kraus, and Y. Silberberg, "Topological pumping over a photonic fibonacci quasicrystal," *Physical Review B*, vol. 91, no. 6, p. 064201, 2015.

[20] Y. Ke, X. Qin, F. Mei, H. Zhong, Y. S. Kivshar, and C. Lee, "Topological phase transitions and Thouless pumping of light in photonic waveguide arrays," *Laser & Photonics Reviews*, vol. 10, no. 6, pp. 995–1001, 2016.

[21] A. Cerjan, M. Wang, S. Huang, K. P. Chen, and M. C. Rechtsman, "Thouless pumping in disordered photonic systems," *Light: Science & Applications*, vol. 9, no. 1, p. 178, 2020.

[22] M. Jürgensen, S. Mukherjee, and M. C. Rechtsman, "Quantized nonlinear Thouless pumping," *Nature*, vol. 596, no. 7870, pp. 63–67, 2021.

[23] I. H. Grinberg, M. Lin, C. Harris, W. A. Benalcazar, C. W. Peterson, T. L. Hughes, and G. Bahl, "Robust temporal pumping in a magneto-mechanical topological insulator," *Nature Communications*, vol. 11, no. 1, p. 974, 2020.

[24] E. Riva, M. I. N. Rosa, and M. Ruzzene, "Edge states and topological pumping in stiffness-modulated elastic plates," *Physical Review B*, vol. 101, no. 9, p. 094307, 2020.

[25] Y. Xia, E. Riva, M. I. Rosa, G. Cazzulani, A. Erturk, F. Braghin, and M. Ruzzene, "Experimental observation of temporal pumping in electromechanical waveguides," *Physical Review Letters*, vol. 126, no. 9, p. 095501, 2021.

[26] R. Citro and M. Aidelsburger, "Thouless pumping and topology," *Nature Reviews Physics*, vol. 5, no. 2, pp. 87–101, 2023.

[27] Q. Niu, D. J. Thouless, and Y.-S. Wu, "Quantized Hall conductance as a topological invariant," *Physical Review B*, vol. 31, p. 3372, 1985.

[28] Q. Niu and D. J. Thouless, "Quantised adiabatic charge transport in the presence of substrate disorder and many-body interaction," *Journal of Physics A: General Physics*, vol. 17, no. 12, pp. 2453–2462, 1984.

[29] J. Avron, R. Seiler, and L. Yaffe, "Adiabatic theorems and applications to the quantum Hall effect," *Communications in Mathematical Physics*, vol. 110, no. 1, pp. 33–49, 1987.

[30] J. E. Avron, A. Raveh, and B. Zur, "Adiabatic quantum transport in multiply connected systems," *Reviews of Modern Physics*, vol. 60, no. 4, pp. 873–915, 1988.

[31] L. J. Geerligs, S. M. Verbrugh, P. Hadley, J. E. Mooij, H. Pothier, P. Lafarge, C. Urbina, D. Estève, and M. H. Devoret, "Single Cooper pair pump," *Zeitschrift für Physik B Condensed Matter*, vol. 85, no. 3, pp. 349–355, 1991.

[32] R. Leone, L. P. Lévy, and P. Lafarge, "Cooper-Pair Pump as a Quantized Current Source," *Physical Review Letters*, vol. 100, no. 11, p. 117001, 2008.

[33] R. Leone and L. Lévy, "Topological quantization by controlled paths : Application to Cooper pairs pumps," *Physical Review B*, vol. 77, no. 6, p. 064524, 2008.

[34] R.-P. Riwar, M. Houzet, J. S. Meyer, and Y. V. Nazarov, "Multi-terminal Josephson junctions as topological matter," *Nature Communications*, vol. 7, no. 1, p. 11167, 2016.

[35] E. Eriksson, R.-P. Riwar, M. Houzet, J. S. Meyer, and Y. V. Nazarov, "Topological transconductance quantization in a four-terminal Josephson junction," *Physical Review B*, vol. 95, no. 7, p. 075417, 2017.

[36] P. A. Erdman, F. Taddei, J. T. Peltonen, R. Fazio, and J. P. Pekola, "Fast and accurate Cooper pair pump," *Physical Review B*, vol. 100, no. 23, p. 235428, 2019.

[37] T. Herrig and R.-P. Riwar, "A" minimal" topological quantum circuit," *arXiv preprint arXiv:2012.10655*, 2020.

[38] J. S. Meyer and M. Houzet, "Conductance quantization in topological Josephson trijunctions," *Physical Review B*, vol. 103, no. 17, p. 174504, 2021.

[39] V. Fatemi, A. R. Akhmerov, and L. Bretheau, "Weyl josephson circuits," *Physical Review Research*, vol. 3, no. 1, p. 013288, 2021.

[40] L. Peyruchat, J. Griesmar, J.-D. Pillet, and Ç. Ö. Girit, "Transconductance quantization in a topological Josephson tunnel junction circuit," *Physical Review Research*, vol. 3, no. 1, p. 013289, 2021.

[41] T. Herrig and R.-P. Riwar, "Cooper-pair transistor as a minimal topological quantum circuit," *Physical Review Research*, vol. 4, no. 1, p. 013038, 2022.

[42] H. Weisbrich, R. L. Klees, O. Zilberberg, and W. Belzig, "Fractional transconductance via non-adiabatic topological Cooper pair pumping," no. arXiv:2212.11757, 2022.

[43] L. Peralta Gavensky, G. Usaj, and C. A. Balseiro, "Multi-terminal Josephson junctions: A road to topological flux networks," *Europhysics Letters*, vol. 141, no. 3, p. 36001, 2023.

[44] I. Martin, G. Refael, and B. Halperin, "Topological frequency conversion in strongly driven quantum systems," *Physical Review X*, vol. 7, no. 4, p. 041008, 2017.

[45] Y. Peng and G. Refael, "Topological energy conversion through the bulk or the boundary of driven systems," *Physical Review B*, vol. 97, no. 13, p. 134303, 2018.

[46] W. Ma, L. Zhou, Q. Zhang, M. Li, C. Cheng, J. Geng, X. Rong, F. Shi, J. Gong, and J. Du, "Experimental Observation of a Generalized Thouless Pump with a Single Spin," *Physical Review Letters*, vol. 120, no. 12, p. 120501, 2018.

[47] S. Körber, L. Privitera, J. C. Budich, and B. Trauzettel, "Interacting topological frequency converter," *Physical Review Research*, vol. 2, no. 2, p. 022023, 2020.

[48] Q. Chen, H. Liu, M. Yu, S. Zhang, and J. Cai, "Dynamical decoupling for realization of topological frequency conversion," *Physical Review A*, vol. 102, no. 5, p. 052606, 2020.

[49] P. J. Crowley, I. Martin, and A. Chandran, "Half-integer quantized topological response in quasiperiodically driven quantum systems," *Physical Review Letters*, vol. 125, no. 10, p. 100601, 2020.

[50] Z. Qi, G. Refael, and Y. Peng, "Universal nonadiabatic energy pumping in a quasiperiodically driven extended system," *Physical Review B*, vol. 104, no. 22, p. 224301, 2021.

[51] D. Malz and A. Smith, "Topological Two-Dimensional Floquet Lattice on a Single Superconducting Qubit," *Physical Review Letters*, vol. 126, no. 16, p. 163602, 2021.

[52] S. Körber, L. Privitera, J. C. Budich, and B. Trauzettel, "Topological burning glass effect," *Physical Review B*, vol. 106, no. 14, p. L140304, 2022.

[53] K. Schwennicke and J. Yuen-Zhou, "Enantioselective topological frequency conversion," *The Journal of Physical Chemistry Letters*, vol. 13, no. 10, pp. 2434–2441, 2022.

[54] V. Gritsev and A. Polkovnikov, "Dynamical quantum Hall effect in the parameter space," *Proc. Natl. Acad. Sci.*, vol. 109, no. 17, pp. 6457–6462, 2012.

[55] M. Kolodrubetz, D. Sels, P. Mehta, and A. Polkovnikov, "Geometry and non-adiabatic response in quantum and classical systems," *Physics Reports*, vol. 697, pp. 1–87, 2017.

[56] J. Luneau, C. Dutreix, Q. Ficheux, P. Delplace, B. Douçot, B. Huard, and D. Carpentier, "Topological power pumping in quantum circuits," *Physical Review Research*, vol. 4, no. 1, p. 013169, 2022.

[57] J. Luneau, B. Douçot, and D. Carpentier, "Topological dynamics of adiabatic cat states," no. arXiv:2211.13502, 2022.

[58] P. Ehrenfest, "Adiabatische Invarianten und Quantentheorie," *Annalen der Physik*, vol. 356, no. 19, pp. 327–352, 1916.

[59] M. Born and V. Fock, "Beweis des Adiabatensatzes," *Zeitschrift für Physik*, vol. 51, no. 3-4, pp. 165–180, 1928.

[60] T. Kato, "On the Adiabatic Theorem of Quantum Mechanics," *Journal of the Physical Society of Japan*, vol. 5, no. 6, pp. 435–439, 1950.

[61] M. Nakahara, *Geometry, Topology, and Physics*. Graduate Student Series in Physics, Bristol ; Philadelphia: Institute of Physics Publishing, 2nd ed ed., 2003.

[62] M. Fruchart, D. Carpentier, and K. Gawedzki, "Parallel transport and band theory in crystals," *Europhysics Letters*, vol. 106, no. 6, p. 60002, 2014.

[63] D. Vanderbilt, *Berry Phases in Electronic Structure Theory: Electric Polarization, Orbital Magnetization and Topological Insulators*. Cambridge University Press, first ed., 2018.

[64] M. V. Berry, "Quantal phase factors accompanying adiabatic changes," *Proceedings of the Royal Society of London. A. Mathematical and Physical Sciences*, vol. 392, no. 1802, pp. 45–57, 1984.

[65] M. Le Bellac, *Physique quantique tome 2*. Savoirs actuels, Les Ulis Paris: EDP sciences CNRS éd, 3e éd ed., 2013.

[66] J. J. Sakurai and J. Napolitano, *Modern Quantum Mechanics*. Boston: Addison-Wesley, 2nd ed ed., 2011.

[67] G. Rigolin, G. Ortiz, and V. H. Ponce, "Beyond the quantum adiabatic approximation: Adiabatic perturbation theory," *Physical Review A*, vol. 78, no. 5, pp. 1–24, 2008.

[68] A. Messiah, *Quantum mechanics: volume II*. North-Holland Publishing Company Amsterdam, 1962.

[69] D. Guéry-Odelin, A. Ruschhaupt, A. Kiely, E. Torrontegui, S. Martínez-Garaot, and J. G. Muga, "Shortcuts to adiabaticity: Concepts, methods, and applications," *Reviews of Modern Physics*, vol. 91, no. 4, pp. 1–54, 2019.

[70] L. Garrido and F. Sancho, "Degree of approximate validity of the adiabatic invariance in quantum mechanics," *Physica*, vol. 28, no. 6, pp. 553–560, 1962.

[71] S. Teufel, *Adiabatic Perturbation Theory in Quantum Dynamics*. No. 1821 in Lecture Notes in Mathematics, Berlin ; New York: Springer, 2003.

[72] A. Lenard, "Adiabatic invariance to all orders," *Annals of Physics*, vol. 6, no. 3, pp. 261–276, 1959.

[73] M. V. Berry and J. Robbins, "Chaotic classical and half-classical adiabatic reactions: geometric magnetism and deterministic friction," *Proceedings of the Royal Society of London. Series A: Mathematical and Physical Sciences*, vol. 442, no. 1916, pp. 659–672, 1993.

[74] C. Emmrich and A. Weinstein, "Geometry of the transport equation in multicomponent WKB approximations," *Communications in mathematical physics*, vol. 176, no. 3, pp. 701–711, 1996.

[75] C. Zener, "Non-adiabatic crossing of energy levels," *Proceedings of the Royal Society of London. Series A, Containing Papers of a Mathematical and Physical Character*, vol. 137, no. 833, pp. 696–702, 1932.

[76] L. Landau, "On the theory of transfer of energy at collisions ii," *Phys. Z. Sowjetunion*, vol. 2, no. 46, p. 118, 1932.

[77] S. N. Shevchenko, S. Ashhab, and F. Nori, "Landau–Zener–Stückelberg interferometry," *Physics Reports*, vol. 492, no. 1, pp. 1–30, 2010.

[78] M. Born and R. Oppenheimer, "Zur quantentheorie der molekeln," *Annalen der Physik*, vol. 389, no. 20, pp. 457–484, 1927.

[79] M. Born and K. Huang, *Dynamical Theory of Crystal Lattices*. Clarendon Press, 1954.

[80] M. V. Berry, "The quantum phase, five years after," in *Geometric Phases in Physics*, vol. 5 of *Advanced Series in Mathematical Physics*, pp. 7–28, World Scientific, 1989.

[81] A. Bohm, A. Mostafazadeh, H. Koizumi, Q. Niu, and J. Zwanziger, *The Geometric Phase in Quantum Systems*. Berlin, Heidelberg: Springer Berlin Heidelberg, 2003.

[82] F. Faure and B. Zhilinskii, "Topological Chern Indices in Molecular Spectra," *Physical Review Letters*, vol. 85, no. 5, pp. 960–963, 2000.

[83] F. Faure and B. Zhilinskii, "Topological Properties of the Born-Oppenheimer Approximation and Implications for the Exact Spectrum," *Letters in Mathematical Physics*, vol. 55, pp. 219–238, 2001.

[84] F. Faure and B. Zhilinskii, "Topologically coupled energy bands in molecules," *Physics Letters A*, vol. 302, no. 5-6, pp. 242–252, 2002.

[85] G. Herzberg and H. C. Longuet-Higgins, "Intersection of potential energy surfaces in polyatomic molecules," *Discussions of the Faraday Society*, vol. 35, p. 77, 1963.

[86] C. A. Mead and D. G. Truhlar, "On the determination of Born-Oppenheimer nuclear motion wave functions including complications due to conical intersections and identical nuclei," *The Journal of Chemical Physics*, vol. 70, no. 5, pp. 2284–2296, 1979.

[87] C. A. Mead, "The geometric phase in molecular systems," *Reviews of Modern Physics*, vol. 64, no. 1, pp. 51–85, 1992.

[88] R. Jackiw, "Three elaborations on Berry's connection, curvature and phase," *International Journal of Modern Physics A*, vol. 03, no. 02, pp. 285–297, 1988.

[89] E. Deumens, A. Diz, R. Longo, and Y. Öhrn, "Time-dependent theoretical treatments of the dynamics of electrons and nuclei in molecular systems," *Reviews of Modern Physics*, vol. 66, no. 3, pp. 917–983, 1994.

[90] P. Carruthers and M. M. Nieto, "Phase and angle variables in quantum mechanics," *Reviews of Modern Physics*, vol. 40, no. 2, p. 411, 1968.

[91] E. I. Blount, "Formalisms of Band Theory," *Solid State Physics*, vol. 13, no. C, pp. 305–373, 1962.

[92] R. D. King-Smith and D. Vanderbilt, "Theory of polarization of crystalline solids," *Physical Review B*, vol. 47, no. 3, pp. 1651–1654, 1993.

[93] S. H. Simon and M. S. Rudner, "Contrasting lattice geometry dependent versus independent quantities: Ramifications for berry curvature, energy gaps, and dynamics," *Physical Review B*, vol. 102, no. 16, p. 165148, 2020.

[94] G. Nenciu, "Dynamics of band electrons in electric and magnetic fields: Rigorous justification of the effective Hamiltonians," *Reviews of Modern Physics*, vol. 63, no. 1, pp. 91–127, 1991.

[95] M.-C. Chang and Q. Niu, "Berry Phase, Hyperorbits, and the Hofstadter Spectrum," *Physical Review Letters*, vol. 75, no. 7, pp. 1348–1351, 1995.

[96] M.-C. Chang and Q. Niu, "Berry phase, hyperorbits, and the Hofstadter spectrum: Semiclassical dynamics in magnetic Bloch bands," *Physical Review B*, vol. 53, no. 11, pp. 7010–7023, 1996.

[97] G. Sundaram and Q. Niu, "Wave-packet dynamics in slowly perturbed crystals: Gradient corrections and Berry-phase effects," *Physical Review B*, vol. 59, no. 23, pp. 14915–14925, 1999.

[98] N. W. Ashcroft and N. D. Mermin, *Solid State Physics*. New York: Holt, Rinehart and Winston, 1976.

[99] F. Bloch, "Uber die Quantenmechanik der Elekronen in Kristallgittern.," *Zeitschrift für Physik*, vol. 52, pp. 555–600, 1929.

[100] C. Zener, "A theory of the electrical breakdown of solid dielectrics," *Proceedings of the Royal Society of London. Series A, Containing Papers of a Mathematical and Physical Character*, vol. 145, no. 855, pp. 523–529, 1934.

[101] R. Karplus and J. Luttinger, "Hall effect in ferromagnetics," *Physical Review*, vol. 95, no. 5, p. 1154, 1954.

[102] E. Mendez and G. Bastard, "Wannier-Stark Ladders and Bloch Oscillations in Superlattices," *Physics Today*, vol. 46, no. 6, p. 34, 1993.

[103] H. M. Price and N. R. Cooper, "Mapping the Berry curvature from semiclassical dynamics in optical lattices," *Physical Review A*, vol. 85, no. 3, p. 033620, 2012.

[104] A. Dauphin and N. Goldman, "Extracting the Chern Number from the Dynamics of a Fermi Gas: Implementing a Quantum Hall Bar for Cold Atoms," *Physical Review Letters*, vol. 111, no. 13, p. 135302, 2013.

[105] G. Jotzu, M. Messer, R. Desbuquois, M. Lebrat, T. Uehlinger, D. Greif, and T. Esslinger, "Experimental realization of the topological Haldane model with ultracold fermions," *Nature*, vol. 515, no. 7526, pp. 237–240, 2014.

[106] M. Aidelsburger, M. Lohse, C. Schweizer, M. Atala, J. T. Barreiro, S. Nascimbène, N. R. Cooper, I. Bloch, and N. Goldman, "Measuring the Chern number of Hofstadter bands with ultracold bosonic atoms," *Nature Physics*, vol. 11, no. 2, pp. 162–166, 2015.

[107] N. Fläschner, B. S. Rem, M. Tarnowski, D. Vogel, D.-S. Lühmann, K. Sengstock, and C. Weitenberg, "Experimental reconstruction of the Berry curvature in a Floquet Bloch band," *Science*, vol. 352, no. 6289, pp. 1091–1094, 2016.

[108] K. Wintersperger, C. Braun, F. N. Ünal, A. Eckardt, M. D. Liberto, N. Goldman, I. Bloch, and M. Aidelsburger, "Realization of an anomalous Floquet topological system with ultracold atoms," *Nature Physics*, vol. 16, no. 10, pp. 1058–1063, 2020.

[109] J. Zhou, W.-Y. Shan, W. Yao, and D. Xiao, "Berry Phase Modification to the Energy Spectrum of Excitons," *Physical Review Letters*, vol. 115, no. 16, p. 166803, 2015.

[110] M. Onga, Y. Zhang, T. Ideue, and Y. Iwasa, "Exciton Hall effect in monolayer MoS2," *Nature Materials*, vol. 16, no. 12, pp. 1193–1197, 2017.

[111] M. Wimmer, H. M. Price, I. Carusotto, and U. Peschel, "Experimental measurement of the Berry curvature from anomalous transport," *Nature Physics*, vol. 13, no. 6, pp. 545–550, 2017.

[112] A. Gianfrate, O. Bleu, L. Dominici, V. Ardizzone, M. De Giorgi, D. Ballarini, G. Lerario, K. W. West, L. N. Pfeiffer, D. D. Solnyshkov, D. Sanvitto, and G. Malpuech, "Measurement of the quantum geometric tensor and of the anomalous Hall drift," *Nature*, vol. 578, no. 7795, pp. 381–385, 2020.

[113] T. Chalopin, T. Satoor, A. Evrard, V. Makhalov, J. Dalibard, R. Lopes, and S. Nascimbene, "Probing chiral edge dynamics and bulk topology of a synthetic Hall system," *Nature Physics*, vol. 16, no. 10, pp. 1017–1021, 2020.

[114] E. Wigner, "On the quantum correction for thermodynamic equilibrium," *Physical Review*, vol. 40, no. 5, pp. 749–759, 1932.

[115] H. Weyl, *The Theory of Groups and Quantum Mechanics*. Dover Books on Advanced Mathematics, New York: Dover publ, facsim. ed ed., 1950.

[116] G. A. Baker, "Formulation of quantum mechanics based on the quasi-probability distribution induced on phase space," *Physical Review*, vol. 109, no. 6, pp. 2198–2206, 1958.

[117] J. E. Moyal, "Quantum mechanics as a statistical theory," *Mathematical Proceedings of the Cambridge Philosophical Society*, vol. 45, no. 1, pp. 99–124, 1949.

[118] F. Bopp, "La mécanique quantique est-elle une mécanique statistique classique particulière?," *Annales de l'Institut Henri Poincaré*, vol. 15, no. 2, pp. 81–112, 1956.

[119] W. B. Case, "Wigner functions and Weyl transforms for pedestrians," *American Journal of Physics*, vol. 76, no. 10, pp. 937–946, 2008.

[120] T. L. Curtright and C. K. Zachos, "Quantum Mechanics in Phase Space," *Asia Pacific Physics Newsletter*, vol. 01, no. 01, pp. 37–46, 2012.

[121] A. Polkovnikov, "Phase space representation of quantum dynamics," *Annals of Physics*, vol. 325, no. 8, pp. 1790–1852, 2010.

[122] E. I. Blount, "Bloch Electrons in a Magnetic Field," *Physical Review*, vol. 126, no. 5, pp. 1636–1653, 1962.

[123] I. Fialkovsky and M. Zubkov, "Precise Wigner-Weyl calculus for lattice models," *Nuclear Physics B*, vol. 954, p. 114999, 2020.

[124] H.-M. Stiepan and S. Teufel, "Semiclassical approximations for hamiltonians with operator-valued symbols," *Communications in Mathematical Physics*, vol. 320, no. 3, pp. 821–849, 2013.

[125] M. V. Karasev, "New global asymptotics and anomalies for the problem of quantization of the adiabatic invariant," *Functional Analysis and Its Applications*, vol. 24, no. 2, pp. 104–114, 1990.

[126] R. G. Littlejohn and W. G. Flynn, "Geometric phases in the asymptotic theory of coupled wave equations," *Physical Review A*, vol. 44, no. 8, p. 5239, 1991.

[127] N. Perez, *Topological Waves in Geophysical and Astrophysical Fluids*. PhD thesis, Ecole Normale Supérieure de Lyon, 2022.

[128] H. Kuratsuji and S. Iida, "Effective Action for Adiabatic Process: Dynamical Meaning of Berry and Simon's Phase," *Progress of Theoretical Physics*, vol. 74, no. 3, pp. 439–445, 1985.

[129] H. Kuratsuji and S. Iida, "Semiclassical quantization with a quantum adiabatic phase," *Physics Letters A*, vol. 111, no. 5, pp. 220–222, 1985.

[130] H. Kuratsuji and S. Iida, "Dynamical Meaning of Quantum Adiabatic Phase: The Case of a Noncanonical System," *Physical Review Letters*, vol. 56, no. 10, pp. 1003–1006, 1986.

[131] S. Iida and H. Kuratsuji, "Adiabatic theorem and anomalous commutators," *Physics Letters B*, vol. 184, no. 2-3, pp. 242–246, 1987.

[132] H. Kuratsuji and S. Iida, "Deformation of symplectic structure and anomalous commutators in field theories," *Physical Review D*, vol. 37, no. 2, pp. 441–447, 1988.

[133] J. Moody, A. Shapere, and F. Wilczek, "Adiabatic Effective Lagrangians," in *Geometric Phases in Physics*, vol. 5 of *Advanced Series in Mathematical Physics*, pp. 160–181, World Scientific, 1989.

[134] P. Gosselin, F. Ménas, A. Bérard, and H. Mohrbach, "Semiclassical dynamics of electrons in magnetic Bloch bands: A Hamiltonian approach," *Europhysics Letters*, vol. 76, no. 4, pp. 651–656, 2006.

[135] P. Gosselin, A. Bérard, and H. Mohrbach, "Semiclassical diagonalization of quantum Hamiltonian and equations of motion with Berry phase corrections," *The European Physical Journal B*, vol. 58, no. 2, pp. 137–148, 2007.

[136] P. Gosselin, J. Hanssen, and H. Mohrbach, "Recursive diagonalization of quantum Hamiltonians to all orders in $\hbar$," *Physical Review D*, vol. 77, no. 8, p. 085008, 2008.

[137] P. Gosselin, A. Bérard, and H. Mohrbach, *Quantum Hamiltonian Diagonalization and Equations of Motion with Berry Phase Corrections*, vol. 9, pp. 253–266. World Scientific, 2009.

[138] R. G. Littlejohn and S. Weigert, "Adiabatic motion of a neutral spinning particle in an inhomogeneous magnetic field," *Physical Review A*, vol. 48, no. 2, pp. 924–940, 1993.

[139] V. I. Arnold, *Mathematical Methods of Classical Mechanics*, vol. 60 of *Graduate Texts in Mathematics*. New York, NY: Springer New York, 1978.

[140] D. Xiao, J. Shi, and Q. Niu, "Berry Phase Correction to Electron Density of States in Solids," *Physical Review Letters*, vol. 95, no. 13, p. 137204, 2005.

[141] R. Resta, "Geometry and topology in many-body physics," no. arXiv:2006.15567, 2020.

[142] L. Friedland and A. N. Kaufman, "Congruent reduction in geometric optics and mode conversion," *Physics of Fluids*, vol. 30, no. 10, p. 3050, 1987.

[143] D. N. Page and C. D. Geilker, "Indirect evidence for quantum gravity," *Physical Review Letters*, vol. 47, no. 14, pp. 979–982, 1981.

[144] J. Oppenheim and Z. Weller-Davies, "The constraints of post-quantum classical gravity," *Journal of High Energy Physics*, vol. 2022, no. 2, p. 80, 2022.

[145] A. Anderson, "Quantum backreaction on "classical" variables," *Physical Review Letters*, vol. 74, no. 5, pp. 621–625, 1995.

[146] J. Maddox, "Classical and quantum physics mix," *Nature*, vol. 373, no. 6514, pp. 469–469, 1995.

[147] Q. Zhang and B. Wu, "General approach to quantum-classical hybrid systems and geometric forces," *Physical Review Letters*, vol. 97, no. 19, p. 190401, 2006.

[148] H. D. Liu, S. L. Wu, and X. X. Yi, "Berry phase and Hannay's angle in a quantum-classical hybrid system," *Physical Review A*, vol. 83, no. 6, pp. 1–8, 2011.

[149] L. Landau and E. Lifshitz, *Course of Theoretical Physics: Mechanics*. Butterworth-Heinemann, 1976.

[150] P. Kramer and M. Saraceno, *Geometry of the Time-Dependent Variational Principle in Quantum Mechanics*, vol. 140 of *Lecture Notes in Physics*. Berlin, Heidelberg: Springer Berlin Heidelberg, 1981.

[151] A. Heslot, "Quantum mechanics as a classical theory," *Physical Review D*, vol. 31, no. 6, p. 1341, 1985.

[152] M. H. Devoret, "Quantum fluctuations in electrical circuits," in *Quantum Fluctuations: Les Houches Session LXIII*, pp. 351–386, Elsevier, 1995.

[153] H.-I. Lu, M. Schemmer, L. M. Aycock, D. Genkina, S. Sugawa, and I. B. Spielman, "Geometrical pumping with a bose-einstein condensate," *Physical Review Letters*, vol. 116, no. 20, p. 200402, 2016.

[154] Y. Ke, S. Hu, B. Zhu, J. Gong, Y. Kivshar, and C. Lee, "Topological pumping assisted by Bloch oscillations," *Physical Review Research*, vol. 2, p. 033143, 2020.

[155] W. Liu, S. Hu, L. Zhang, Y. Ke, and C. Lee, "Correlated topological pumping of interacting bosons assisted by Bloch oscillations," *Physical Review Research*, vol. 5, no. 1, p. 013020, 2023.

[156] A. M. Zagoskin, *Quantum Engineering: Theory and Design of Quantum Coherent Structures*. Cambridge ; New York: Cambridge University Press, 2011.

[157] U. Vool and M. Devoret, "Introduction to quantum electromagnetic circuits," *International Journal of Circuit Theory and Applications*, vol. 45, no. 7, pp. 897–934, 2017.

[158] A. Blais, A. L. Grimsmo, S. M. Girvin, and A. Wallraff, "Circuit quantum electrodynamics," *Reviews of Modern Physics*, vol. 93, no. 2, p. 025005, 2021.

[159] P. J. Leek, J. M. Fink, A. Blais, R. Bianchetti, M. Göppl, J. M. Gambetta, D. I. Schuster, L. Frunzio, R. J. Schoelkopf, and A. Wallraff, "Observation of Berry's Phase in a Solid-State Qubit," *Science*, vol. 318, no. 5858, pp. 1889–1892, 2007.

[160] M. D. Schroer, M. H. Kolodrubetz, W. F. Kindel, M. Sandberg, J. Gao, M. R. Vissers, D. P. Pappas, A. Polkovnikov, and K. W. Lehnert, "Measuring a Topological Transition in an Artificial Spin-1/2 System," *Physical Review Letters*, vol. 113, no. 5, p. 050402, 2014.

[161] P. Roushan, C. Neill, Y. Chen, M. Kolodrubetz, C. Quintana, N. Leung, M. Fang, R. Barends, B. Campbell, Z. Chen, B. Chiaro, A. Dunsworth, E. Jeffrey, J. Kelly, A. Megrant, J. Mutus, P. J. J. O'Malley, D. Sank, A. Vainsencher, J. Wenner, T. White, A. Polkovnikov, A. N. Cleland, and J. M. Martinis, "Observation of topological transitions in interacting quantum circuits," *Nature*, vol. 515, no. 7526, pp. 241–244, 2014.

[162] S. Berger, M. Pechal, P. Kurpiers, A. A. Abdumalikov, C. Eichler, J. A. Mlynek, A. Shnirman, Y. Gefen, A. Wallraff, and S. Filipp, "Measurement of geometric dephasing using a superconducting qubit," *Nature Communications*, vol. 6, no. 1, p. 8757, 2015.

[163] X. Tan, D. W. Zhang, Z. Yang, J. Chu, Y. Q. Zhu, D. Li, X. Yang, S. Song, Z. Han, Z. Li, Y. Dong, H. F. Yu, H. Yan, S. L. Zhu, and Y. Yu, "Experimental Measurement of the Quantum Metric Tensor and Related Topological Phase Transition with a Superconducting Qubit," *Physical Review Letters*, vol. 122, no. 21, p. 210401, 2019.

[164] D. Malz and A. Smith, "Topological two-dimensional Floquet lattice on a single superconducting qubit," *Physical Review Letters*, vol. 126, no. 16, p. 163602, 2021.

[165] E. Boyers, P. J. D. Crowley, A. Chandran, and A. O. Sushkov, "Exploring 2d synthetic quantum Hall physics with a quasiperiodically driven qubit," *Physical Review Letters*, vol. 125, no. 16, p. 160505, 2020.

[166] A. Somoroff, Q. Ficheux, R. A. Mencia, H. Xiong, R. V. Kuzmin, and V. E. Manucharyan, "Millisecond coherence in a superconducting qubit," *arXiv preprint arXiv:2103.08578*, 2021.

[167] H. Zhang, S. Chakram, T. Roy, N. Earnest, Y. Lu, Z. Huang, D. K. Weiss, J. Koch, and D. I. Schuster, "Universal fast-flux control of a coherent, low-frequency qubit," *Physical Review X*, vol. 11, no. 1, p. 011010, 2021.

[168] L. B. Nguyen, Y.-H. Lin, A. Somoroff, R. Mencia, N. Grabon, and V. E. Manucharyan, "High-coherence fluxonium qubit," *Physical Review X*, vol. 9, no. 4, p. 041041, 2019.

[169] G. Zhu, D. G. Ferguson, V. E. Manucharyan, and J. Koch, "Circuit QED with fluxonium qubits: Theory of the dispersive regime," *Physical Review B*, vol. 87, no. 2, p. 024510, 2013.

[170] V. E. Manucharyan, J. Koch, L. I. Glazman, and M. H. Devoret, "Fluxonium: Single cooper-pair circuit free of charge offsets," *Science*, vol. 326, no. 5949, pp. 113–116, 2009.

[171] F. D. M. Haldane, "Model for a Quantum Hall Effect without landau levels: Condensed-matter realization of the "parity anomaly"," *Physical Review Letters*, vol. 61, pp. 2015–2018, 1988.

[172] A. Vepsäläinen and G. S. Paraoanu, "Simulating spin chains using a superconducting circuit: Gauge invariance, superadiabatic transport, and broken time-reversal symmetry," *Advanced Quantum Technologies*, vol. 3, no. 4, p. 1900121, 2020.

[173] J. Cano, B. Bradlyn, Z. Wang, L. Elcoro, M. G. Vergniory, C. Felser, M. I. Aroyo, and B. A. Bernevig, "Building blocks of topological quantum chemistry: Elementary band representations," *Physical Review B*, vol. 97, p. 035139, 2018.

[174] J. Zak, "Symmetry specification of bands in solids," *Physical Review Letters*, vol. 45, no. 12, p. 1025, 1980.

[175] J. Zak, "Band representations and symmetry types of bands in solids," *Physical Review B*, vol. 23, no. 6, p. 2824, 1981.

[176] J. Zak, "Band representations of space groups," *Physical Review B*, vol. 26, no. 6, p. 3010, 1982.

[177] L. Michel and J. Zak, "Elementary energy bands in crystals are connected," *Physics Reports*, vol. 341, no. 1-6, pp. 377–395, 2001.

[178] B. Bradlyn, L. Elcoro, J. Cano, M. G. Vergniory, Z. Wang, C. Felser, M. I. Aroyo, and B. A. Bernevig, "Topological quantum chemistry," *Nature*, vol. 547, no. 7663, pp. 298–305, 2017.

[179] H. C. Po, A. Vishwanath, and H. Watanabe, "Symmetry-based indicators of band topology in the 230 space groups," *Nature Communications*, vol. 8, no. 1, pp. 1–9, 2017.

[180] M. G. Vergniory, L. Elcoro, C. Felser, N. Regnault, B. A. Bernevig, and Z. Wang, "A complete catalogue of high-quality topological materials," *Nature*, vol. 566, no. 7745, pp. 480–485, 2019.

[181] F. Tang, H. C. Po, A. Vishwanath, and X. Wan, "Comprehensive search for topological materials using symmetry indicators," *Nature*, vol. 566, no. 7745, pp. 486–489, 2019.

[182] T. Zhang, Y. Jiang, Z. Song, H. Huang, Y. He, Z. Fang, H. Weng, and C. Fang, "Catalogue of topological electronic materials," *Nature*, vol. 566, no. 7745, pp. 475–479, 2019.

[183] J. Cano and B. Bradlyn, "Band representations and topological quantum chemistry," *Annual Review of Condensed Matter Physics*, vol. 12, no. 1, pp. 225–246, 2021.

[184] T. L. Hughes, E. Prodan, and B. A. Bernevig, "Inversion-symmetric topological insulators," *Physical Review B*, vol. 83, p. 245132, 2011.

[185] C. Fang, M. J. Gilbert, and B. A. Bernevig, "Bulk topological invariants in noninteracting point group symmetric insulators," *Physical Review B*, vol. 86, p. 115112, 2012.

[186] R. Bianchetti, S. Filipp, M. Baur, J. M. Fink, C. Lang, L. Steffen, M. Boissonneault, A. Blais, and A. Wallraff, "Control and tomography of a three level superconducting artificial atom," *Physical Review Letters*, vol. 105, no. 22, p. 223601, 2010.

[187] M. J. Peterer, S. J. Bader, X. Jin, F. Yan, A. Kamal, T. J. Gudmundsen, P. J. Leek, T. P. Orlando, W. D. Oliver, and S. Gustavsson, "Coherence and decay of higher energy levels of a superconducting transmon qubit," *Physical Review Letters*, vol. 114, no. 1, p. 010501, 2015.

[188] Q. Ficheux, *Quantum Trajectories with Incompatible Decoherence Channels*. Theses, École normale supérieure - ENS PARIS, Dec. 2018.

[189] N. Cottet, S. Jezouin, L. Bretheau, P. Campagne-Ibarcq, Q. Ficheux, J. Anders, A. Auffèves, R. Azouit, P. Rouchon, and B. Huard, "Observing a quantum maxwell demon at work," *Proceedings of the National Academy of Sciences*, vol. 114, no. 29, pp. 7561–7564, 2017.

[190] A. Ronzani, B. Karimi, J. Senior, Y.-C. Chang, J. T. Peltonen, C. Chen, and J. P. Pekola, "Tunable photonic heat transport in a quantum heat valve," *Nature Physics*, vol. 14, no. 10, pp. 991–995, 2018.

[191] R. Kokkoniemi, J.-P. Girard, D. Hazra, A. Laitinen, J. Govenius, R. Lake, I. Sallinen, V. Vesterinen, M. Partanen, J. Tan, *et al.*, "Bolometer operating at the threshold for circuit quantum electrodynamics," *Nature*, vol. 586, no. 7827, pp. 47–51, 2020.

[192] D. Meidan, T. Micklitz, and P. W. Brouwer, "Topological classification of adiabatic processes," *Physical Review B*, vol. 84, no. 19, p. 195410, 2011.

[193] F. Nathan, I. Martin, and G. Refael, "Topological frequency conversion in a driven dissipative quantum cavity," *Physical Review B*, vol. 99, p. 094311, 2019.

[194] C. Psaroudaki and G. Refael, "Photon pumping in a weakly-driven quantum cavity–spin system," *Annals of Physics*, vol. 435, p. 168553, 2021.

[195] D. M. Long, P. J. Crowley, A. J. Kollár, and A. Chandran, "Boosting the quantum state of a cavity with floquet driving," *Physical Review Letters*, vol. 128, no. 18, p. 183602, 2022.

[196] D.-W. Wang, H. Cai, R.-B. Liu, and M. O. Scully, "Mesoscopic Superposition States Generated by Synthetic Spin-Orbit Interaction in Fock-State Lattices," *Physical Review Letters*, vol. 116, no. 22, p. 220502, 2016.

[197] J. Deng, H. Dong, C. Zhang, Y. Wu, J. Yuan, X. Zhu, F. Jin, H. Li, Z. Wang, H. Cai, C. Song, H. Wang, J. Q. You, and D.-W. Wang, "Coherent control of quantum topological states of light in Fock-state lattices," no. arXiv:2208.03452, 2022.

[198] H. Cai and D.-W. Wang, "Topological phases of quantized light," *National Science Review*, vol. 8, no. 1, p. nwaa196, 2021.

[199] J. Yuan, C. Xu, H. Cai, and D.-W. Wang, "Gap-protected transfer of topological defect states in photonic lattices," *APL Photonics*, vol. 6, no. 3, p. 030803, 2021.

[200] P. Saugmann and J. Larson, "A Fock state lattice approach to quantum optics," no. arXiv:2203.13813, 2022.

[201] B. A. Bernevig, T. L. Hughes, and S.-C. Zhang, "Quantum spin hall effect and topological phase transition in hgte quantum wells," *Science*, vol. 314, no. 5806, pp. 1757–1761, 2006.

[202] Y. Aharonov and J. Anandan, "Phase change during a cyclic quantum evolution," *Physical Review Letters*, vol. 58, no. 16, p. 1593, 1987.

[203] J. Provost and G. Vallee, "Riemannian structure on manifolds of quantum states," *Communications in Mathematical Physics*, vol. 76, no. 3, pp. 289–301, 1980.

[204] F. Piéchon, A. Raoux, J.-N. Fuchs, and G. Montambaux, "Geometric orbital susceptibility: Quantum metric without berry curvature," *Physical Review B*, vol. 94, no. 13, p. 134423, 2016.

[205] A. Graf and F. Piéchon, "Berry curvature and quantum metric in n-band systems: An eigenprojector approach," *Physical Review B*, vol. 104, no. 8, p. 085114, 2021.

[206] S. Peotta and P. Törmä, "Superfluidity in topologically nontrivial flat bands," *Nature Communications*, vol. 6, no. 1, p. 8944, 2015.

[207] D. Witthaut, F. Keck, H. J. Korsch, and S. Mossmann, "Bloch oscillations in two-dimensional lattices," *New Journal of Physics*, vol. 6, pp. 41–41, 2004.

[208] A. R. Kolovsky and H. J. Korsch, "Bloch oscillations of cold atoms in two-dimensional optical lattices," *Physical Review A*, vol. 67, no. 6, p. 063601, 2003.

[209] S. Mossmann, A. Schulze, D. Witthaut, and H. J. Korsch, "Two-dimensional Bloch oscillations: A Lie-algebraic approach," *Journal of Physics A: Mathematical and General*, vol. 38, no. 15, pp. 3381–3395, 2005.

[210] J. M. Zhang and W. M. Liu, "Directed coherent transport due to the Bloch oscillation in two dimensions," *Physical Review A*, vol. 82, no. 2, p. 025602, 2010.

[211] N. Marzari, A. A. Mostofi, J. R. Yates, I. Souza, and D. Vanderbilt, "Maximally localized wannier functions: Theory and applications," *Reviews of Modern Physics*, vol. 84, no. 4, p. 1419, 2012.

[212] D. Thouless, "Wannier functions for magnetic sub-bands," *Journal of Physics C: Solid State Physics*, vol. 17, no. 12, p. L325, 1984.

[213] D. Monaco, G. Panati, A. Pisante, and S. Teufel, "Optimal decay of wannier functions in chern and quantum hall insulators," *Communications in Mathematical Physics*, vol. 359, no. 1, pp. 61–100, 2018.

[214] N. Ng, S. Wenderoth, R. R. Seelam, E. Rabani, H.-D. Meyer, M. Thoss, and M. Kolodrubetz, "Localization dynamics in a centrally coupled system," *Physical Review B*, vol. 103, no. 13, p. 134201, 2021.

[215] G. Engelhardt, S. Choudhury, and W. V. Liu, "Unified Light-Matter Floquet Theory and its Application to Quantum Communication," no. arXiv:2207.08558, 2022.

[216] Z. Leghtas, G. Kirchmair, B. Vlastakis, M. H. Devoret, R. J. Schoelkopf, and M. Mirrahimi, "Deterministic protocol for mapping a qubit to coherent state superpositions in a cavity," *Physical Review A*, vol. 87, no. 4, p. 042315, 2013.

[217] D. I. Schuster, A. A. Houck, J. A. Schreier, A. Wallraff, J. M. Gambetta, A. Blais, L. Frunzio, J. Majer, B. Johnson, M. H. Devoret, S. M. Girvin, and R. J. Schoelkopf, "Resolving photon number states in a superconducting circuit," *Nature*, vol. 445, no. 7127, pp. 515–518, 2007.

[218] I. I. Rabi, "On the Process of Space Quantization," *Physical Review*, vol. 49, no. 4, pp. 324–328, 1936.

[219] I. I. Rabi, "Space Quantization in a Gyrating Magnetic Field," *Physical Review*, vol. 51, no. 8, pp. 652–654, 1937.

[220] P. Forn-Díaz, L. Lamata, E. Rico, J. Kono, and E. Solano, "Ultrastrong coupling regimes of light-matter interaction," *Reviews of Modern Physics*, vol. 91, p. 025005, June 2019.

[221] A. Frisk Kockum, A. Miranowicz, S. De Liberato, S. Savasta, and F. Nori, "Ultrastrong coupling between light and matter," *Nature Reviews Physics*, vol. 1, pp. 19–40, Jan. 2019.

[222] J. M. Deutsch, "Eigenstate thermalization hypothesis," *Reports on Progress in Physics*, vol. 81, no. 8, p. 082001, 2018.

[223] F. Haake, *Quantum Signatures of Chaos*, vol. 54 of *Springer Series in Synergetics*. Berlin, Heidelberg: Springer Berlin Heidelberg, 2010.

[224] T. Guhr, A. Müller–Groeling, and H. A. Weidenmüller, "Random-matrix theories in quantum physics: Common concepts," *Physics Reports*, vol. 299, pp. 189–425, June 1998.

[225] D. Thouless, "Electrons in disordered systems and the theory of localization," *Physics Reports*, vol. 13, no. 3, pp. 93–142, 1974.

[226] A. Altland, Y. Gefen, and G. Montambaux, "What is the Thouless Energy for Ballistic Systems?," *Physical Review Letters*, vol. 76, no. 7, pp. 1130–1133, 1996.

[227] B. L. Al'tshuler and B. I. Shklovskii, "Repulsion of energy levels and conductivity of small metal samples," *Sov. Phys. JETP*, vol. 64, no. 1, p. 127, 1986.

[228] D. Braun and G. Montambaux, "Spectral correlations from the metal to the mobility edge," *Physical Review B*, vol. 52, no. 19, pp. 13903–13909, 1995.

[229] H. M. Price, O. Zilberberg, T. Ozawa, I. Carusotto, and N. Goldman, "Four-Dimensional Quantum Hall Effect with Ultracold Atoms," *Physical Review Letters*, vol. 115, no. 19, p. 195303, 2015.

[230] T. Ozawa, H. M. Price, N. Goldman, O. Zilberberg, and I. Carusotto, "Synthetic dimensions in integrated photonics: From optical isolation to four-dimensional quantum Hall physics," *Physical Review A*, vol. 93, no. 4, pp. 1–17, 2016.

[231] M. Lohse, C. Schweizer, H. M. Price, O. Zilberberg, and I. Bloch, "Exploring 4D quantum Hall physics with a 2D topological charge pump," *Nature*, vol. 553, no. 7686, pp. 55–58, 2018.

[232] O. Zilberberg, S. Huang, J. Guglielmon, M. Wang, K. P. Chen, Y. E. Kraus, and M. C. Rechtsman, "Photonic topological boundary pumping as a probe of 4D quantum Hall physics," *Nature*, vol. 553, no. 7686, pp. 59–62, 2018.

[233] O. Zilberberg, H. M. Price, and I. Petrides, "Six-dimensional quantum Hall effect and three-dimensional topological pumps," *Physical Review B*, vol. 98, no. 12, p. 125431, 2018.

[234] H. Weisbrich, R. Klees, G. Rastelli, and W. Belzig, "Second Chern Number and Non-Abelian Berry Phase in Topological Superconducting Systems," *PRX Quantum*, vol. 2, no. 1, p. 1, 2021.

[235] J. C. Y. Teo and C. L. Kane, "Topological defects and gapless modes in insulators and superconductors," *Physical Review B*, vol. 82, no. 11, p. 115120, 2010.

[236] F. Zhang and C. L. Kane, "Anomalous topological pumps and fractional Josephson effects," *Physical Review B*, vol. 90, no. 2, pp. 1–4, 2014.

[237] W. A. Benalcazar, J. Noh, M. Wang, S. Huang, K. P. Chen, and M. C. Rechtsman, "Higher-order topological pumping and its observation in photonic lattices," *Physical Review B*, vol. 105, no. 19, p. 195129, 2022.

[238] J. F. Wienand, F. Horn, M. Aidelsburger, J. Bibo, and F. Grusdt, "Thouless Pumps and Bulk-Boundary Correspondence in Higher-Order Symmetry-Protected Topological Phases," *Physical Review Letters*, vol. 128, no. 24, p. 246602, 2022.

[239] V. Brosco, L. Pilozzi, R. Fazio, and C. Conti, "Non-abelian Thouless pumping in a photonic lattice," *Physical Review A*, vol. 103, p. 063518, 2021.

[240] O. You, S. Liang, B. Xie, W. Gao, W. Ye, J. Zhu, and S. Zhang, "Observation of Non-Abelian Thouless Pump," *Physical Review Letters*, vol. 128, no. 24, p. 244302, 2022.

[241] Y.-K. Sun, X.-L. Zhang, F. Yu, Z.-N. Tian, Q.-D. Chen, and H.-B. Sun, "Non-Abelian Thouless pumping in photonic waveguides," *Nature Physics*, vol. 18, no. 9, pp. 1080–1085, 2022.

[242] P. Titum, E. Berg, M. S. Rudner, G. Refael, and N. H. Lindner, "Anomalous floquet-anderson insulator as a nonadiabatic quantized charge pump," *Physical Review X*, vol. 6, no. 2, p. 021013, 2016.

[243] M. H. Kolodrubetz, F. Nathan, S. Gazit, T. Morimoto, and J. E. Moore, "Topological floquet-thouless energy pump," *Physical Review Letters*, vol. 120, no. 15, p. 150601, 2018.

[244] P. J. Crowley, I. Martin, and A. Chandran, "Topological classification of quasiperiodically driven quantum systems," *Physical Review B*, vol. 99, no. 6, p. 064306, 2019.

[245] D. M. Long, P. J. Crowley, and A. Chandran, "Nonadiabatic topological energy pumps with quasiperiodic driving," *Physical Review Letters*, vol. 126, no. 10, p. 106805, 2021.

[246] F. Nathan, R. Ge, S. Gazit, M. Rudner, and M. Kolodrubetz, "Quasiperiodic floquet-thouless energy pump," *Physical Review Letters*, vol. 127, no. 16, p. 166804, 2021.

[247] S. Haroche and J.-M. Raimond, *Exploring the Quantum: Atoms, Cavities, and Photons*. Oxford Graduate Texts, Oxford: Oxford University Press, first published in paperback ed., 2013.

[248] C. W. Gardiner and P. Zoller, *Quantum Noise: A Handbook of Markovian and Non-Markovian Quantum Stochastic Methods with Applications to Quantum Optics*. Springer Series in Synergetics, Berlin ; New York: Springer, 3rd ed ed., 2004.

[249] P. W. Brouwer, "Scattering approach to parametric pumping," *Physical Review B*, vol. 58, no. 16, p. R10135, 1998.

[250] I. C. Fulga, F. Hassler, and A. R. Akhmerov, "Scattering theory of topological insulators and superconductors," *Physical Review B*, vol. 85, no. 16, p. 165409, 2012.

[251] N. A. Sinitsyn, "The stochastic pump effect and geometric phases in dissipative and stochastic systems," *Journal of Physics A: Mathematical and Theoretical*, vol. 42, no. 19, p. 193001, 2009.

[252] J. E. Avron, M. Fraas, and G. M. Graf, "Adiabatic Response for Lindblad Dynamics," *Journal of Statistical Physics*, vol. 148, no. 5, pp. 800–823, 2012.

[253] T. Pluecker, M. R. Wegewijs, and J. Splettstoesser, "Gauge freedom in observables and Landsberg's nonadiabatic geometric phase: Pumping spectroscopy of interacting open quantum systems," *Physical Review B*, vol. 95, no. 15, pp. 1–38, 2017.

[254] A. Sarlette, P. Rouchon, A. Essig, Q. Ficheux, and B. Huard, "Quantum adiabatic elimination at arbitrary order for photon number measurement," no. arXiv:2001.02550, 2020.

**Abstract:**

This thesis introduces a notion of topological coupling between quantum systems with a slow-fast decomposition. I study the dynamics of the slow degrees of freedom, showing that the topological nature of coupling induces a quantized transfer of charge or energy between them. Considering the slow degrees of freedom as classical parameters imposing a time-dependence to the fast quantum system, we recover the appearance of a permanent current through this quantum system, discussed previously in the context of topological pumps. Guided by the goal of a direct measure of this transfer, I propose an experimental realization of such coupling between microwave electromagnetic modes and a superconducting quantum circuit.

I study then the nature of the quantum states of the total system, showing that the topological nature of coupling imposes an entanglement between the slow and fast subsystems. Generically, any initial state decomposes into a superposition of states which are separated in phase space by the topological dynamics, thereby creating a cat state.

In a last part, I identify two families of initial states of such a system, leading or not to a topological dynamics. This separation in two families of initial states translates into two families of eigenstates of the total system at the same energies. The family of eigenstates associated to a non-trivial topology carries signatures of a non-standard quantum chaos, whereas the one associated to a trivial topology does not.

**Résumé :**

Cette thèse introduit une notion de couplage topologique entre des systèmes quantiques ayant une séparation lent-rapide. J'étudie la dynamique des degrés de libertés lents, montrant que la nature topologique du couplage induit un transfert quantifié d'énergie ou de charge entre ceux-ci. En considérant les degrés de libertés lents comme des paramètres classiques qui imposent une dépendance temporelle au système quantique rapide, nous retrouvons l'apparition d'un courant permanent au sein de ce système quantique discuté précédemment dans le contexte des pompes topologiques. Guidé par l'objectif d'une mesure directe de ce transfert, je propose une réalisation expérimentale d'un tel couplage entre des modes électromagnétiques micro-ondes et un circuit quantique supraconducteur.

J'étudie ensuite la nature des états quantiques du système complet, montrant que la nature topologique du couplage impose une intrication entre les sous-systèmes lents et rapides. De façon générique, tout état initial se décompose en une superposition d'états que la dynamique topologique sépare dans l'espace des phases, créant un état de chat.

Dans une dernière partie, j'identifie deux familles d'états initiaux d'un tel système, qui mènent ou non à une dynamique topologique. Cette séparation en deux familles d'états initiaux se traduit en deux familles d'états propres du système total aux mêmes échelles d'énergies. La famille d'états propres associée à une topologie non triviale porte des signatures d'un chaos quantique non standard, tandis que celle associée à une topologie triviale n'en porte pas.